UNIVERSIDADE FEDERAL DE PERNAMBUCO
CENTRO DE TECNOLOGIA E GEOCIÊNCIAS
DEPARTAMENTO DE GEOLOGIA
PROGRAMA DE PÓS-GRADUAÇÃO EM GEOCIÊNCIAS

JOSÉ FERREIRA DE ARAÚJO NETO

O DEPÓSITO ESMERALDÍFERO DO TIPO "TECTONIC MAGMATIC-RELATED" DE PARANÁ (RIO GRANDE DO NORTE): dos controles geológicos aos modelos genético e prospectivo

Recife
2023

JOSÉ FERREIRA DE ARAÚJO NETO

O DEPÓSITO ESMERALDÍFERO DO TIPO "TECTONIC MAGMATIC-RELATED" DE PARANÁ (RIO GRANDE DO NORTE): dos controles geológicos aos modelos genético e prospectivo

Tese apresentada ao Programa de Pós-Graduação em Geociências do Centro de Tecnologia e Geociências da Universidade Federal de Pernambuco, como requisito parcial para a obtenção do grau de Doutor em Geociências.

Área de concentração: Geoquímica, Geofísica e Evolução Crustal

Orientador: Prof. Dr. Lauro Cézar Montefalco de Lira Santos
Coorientadora: Profa. Dra. Thais Andressa Carrino

Recife

2023

Catalogação na fonte
Bibliotecário Gabriel Luz CRB-4 / 2222

A663d Araújo Neto, José Ferreira de.
O depósito esmeraldífero do tipo “tectonic magmatic-related” de Paraná (Rio Grande do Norte): dos controles geológicos aos modelos genético e prospectivo / José Ferreira de Araújo Neto. 2023.
145 f: il.

Orientador: Prof. Dr. Lauro Cézar Montefalco de Lira Santos.
Coorientadora: Profa. Dra. Thais Andressa Carrino.
Tese (Doutorado) – Universidade Federal de Pernambuco. CTG. Programa de Pós-Graduação em Geociências, Recife, 2023.
Inclui referências e anexo.

1. Geociências. 2. Esmeralda. 3. Geneses de depósitos minerais. 4. Modelo prospectivo. 5. Província Borborema. I. Santos, Lauro Cézar Montefalco de Lira (Orientador). II. Carrino, Thais Andressa (Coorientadora). III. Título.

UFPE

551 CDD (22. ed.) BCTG / 2023 - 57

JOSÉ FERREIRA DE ARAÚJO NETO

O DEPÓSITO ESMERALDÍFERO DO TIPO "TECTONIC MAGMATIC-RELATED" DE PARANÁ (RIO GRANDE DO NORTE): dos controles geológicos aos modelos genético e prospectivo

Tese apresentada ao Programa de Pós-Graduação em Geociências do Centro de Tecnologia e Geociências da Universidade Federal de Pernambuco, como requisito parcial para a obtenção do grau de Doutor em Geociências.

Área de concentração: Geoquímica, Geofísica e Evolução Crustal

Aprovada em: 06/02/2023

BANCA EXAMINADORA

_____

Prof. Dr. Haroldo Monteiro Lima (Examinador Externo)
Universidade Federal de Pernambuco

_____

Prof. Dr. Alvaro Penteado Crósta (Examinador Externo)
Universidade Estadual de Campinas

_____

Prof. Dr. Luís Gustavo Ferreira Viegas (Examinador Externo)
Universidade de Brasília

_____

Prof. Dr. Ricardo Augusto Scholz Cipriano (Examinador Externo)
Universidade Federal de Ouro Preto

_____

Dr. Vladimir Cruz de Medeiros (Examinador Externo)
Serviço Geológico do Brasil

A Diego de Araújo Lindoso (*in memorian*)

Por me ensinar a buscar com intensidade meus objetivos, sem deixar de ver a beleza das pequenas conquistas realizadas ao longo do caminho. Sua confiança em meu sucesso foi, e continua sendo, uma força motriz para a minha jornada acadêmica.

AGRADECIMENTOS

Os anos de desenvolvimento dessa tese foram marcados por situações contrastantes. Se de um lado nunca se discutiu tanto a anticiência e o negacionismo ao método científico, do outro, nunca dantes a ciência foi tão necessária para a manutenção da nossa existência. Dentre vários desafios, alguns conflitos internos e diversas pedras pelo caminho (perdão pelo trocadilho), esse volume foi se desenhando e ganhando corpo com o incentivo e a colaboração dos vários motivadores a quem dedico esta seção.

Agradeço aos meus pais, Maria da Conceição e Fábio Glei, pelo esforço investido em minha educação e pelo apoio à minha dedicação à carreira acadêmica. Também agradeço à minha esposa, Daiane Araújo, pelo apoio, suporte emocional e paciência ao longo desses onze anos de estudos geológicos. Essa pré-tese é a culminação de uma etapa de um projeto de vida sonhado por mim, mas construído para nós dois.

Agradeço aos professores Lauro Montefalco e Thais Carrino pela orientação, pela amizade e pelo apoio científico e logístico que permitiram a realização desta pesquisa. Estendo esse agradecimento à professora Sandra de Brito Barreto, que foi o arco que me lançou no estudo de minerais gemológicos e que tem me acompanhado desde então nessa trajetória.

O estudo do depósito de esmeralda de Paraná não seria possível se não fosse pelo apoio do Sr. Luís Amorim e de todos que fazem parte da Mineração Limeira, Comércio, Exportação e Importação. Deixo aqui minha profunda gratidão pelo suporte logístico e financeiro prestado pelo Sr. Luís e pela Mineração Limeira, que sempre se demonstraram grandes incentivadores do conhecimento científico. Agradeço a todos os trabalhadores que me auxiliaram nas etapas de campo e durante as investidas em subsuperfície para coleta de amostras: Júnior, Adilson, Zé Paulo, Samuca, Joaquitan (Novo) e Maria.

Agradeço à CAPES (Coordenação de Aperfeiçoamento de Pessoal de Nível Superior), fundação do Ministério da Educação (MEC), pelo apoio financeiro através da concessão da bolsa de doutorado.

Agradeço a todos(as) os(as) cientistas que colaboraram direta ou indiretamente à realização desta pesquisa: Carolina de Souza, Charles Henrique, Daniel Miggins, Elder Yokoyama, Elton Dantas, Gustavo Viegas, Igor Manoel, Ingrid Hoyer, Glenda Santos, Peter Cawood, Rosa Pabón e Valmir Souza. E por fim, dedico agradecimento especial aos membros da banca examinadora pela contribuição ao refinamento e à qualidade deste volume.

RESUMO

O Brasil figura entre os maiores produtores de esmeralda do mundo. Cristais de qualidade gemológica ocorrem sobretudo nos estados de Minas Gerais, Goiás e Bahia. Na Província Borborema, nordeste do Brasil, mineralizações pontuais de esmeralda vêm ganhando cada vez mais destaque nas últimas décadas, seja sob olhar científico ou do ponto de vista econômico. A presença de diversos pegmatitos berilíferos e exposições de rochas máficas/ultramáficas, especialmente na Subprovíncia Setentrional, associados a estruturas tectônicas que servem como meio de transporte aos fluidos mineralizantes, fazem dessa região uma área promissora para estudo da gênese de esmeralda em ambientes intensamente deformados. Este trabalho apresenta uma investigação integrada, em diferentes escalas de análise, sobre a caracterização, origem e prospecção do depósito de esmeralda de Paraná, no extremo sudoeste do estado do Rio Grande do Norte. Para a construção de um modelo genético, foram utilizadas imagens geofísicas de aeromagnetometria, dados estruturais nas escalas meso- e microscópicas, geocronologia U-Pb e $^{40}Ar/^{39}Ar$. As esmeraldas de Paraná estão hospedadas em lentes irregulares de flogopita- e actinolita-flogopita xistos intercalados a vênulas quartzo-feldspáticas e corpos pegmatíticos. Os xistos hospedeiros ocorrem de forma concordante em gnaisses riacianos do embasamento (Complexo Caicó) e estão dispostos ao longo da zona de cisalhamento Portalegre, estrutura com forte contraste magnético e movimentação dextral na direção NE-SW. Deformação dúctil coeva à mineralização é indicada pela foliação milonítica verticalizada, presença de *boudins* assimétricos, porfiroclastos do tipo σ, estruturas do tipo *mica-fish*, além de formação de bandas de cisalhamento S-C e S-C-C'. A formação do xisto esmeraldífero durante deformação Brasiliana é suportada por idades $^{40}Ar/^{39}Ar$ em cristais de flogopita de 524 ± 1 e 528 ± 1 Ma. Corpos graníticos deformados, encontrados no interior do xisto, apresentaram idades concordia de U-Pb em zircão de 2210 ± 8 Ma e 2201 ± 6 Ma, sugerindo um retrabalhamento do gnaisse encaixante do Complexo Caicó durante a formação do depósito. A integração desses dados sugere que metassomatismo de pegmatitos graníticos injetados ao longo da zona de cisalhamento Portalegre concomitantes ao tectonismo brasiliano foi o principal responsável pela formação de esmeralda em Paraná. Nesse processo, Be, K, Al e Si provenientes do fluido pegmatítico, e Cr, Fe e Mg contidos em rochas máficas do embasamento reagiram dando origem a pegmatitos dessilicados e ao xisto mineralizado. Do ponto de vista prospectivo, a presença de flogopita e actinolita no xisto hospedeiro permitiu a individualização da sua assinatura espectral em relação às demais rochas do depósito.

Utilizando espectroscopia de refletância pontual é possível distinguir a presença de cristais de esmeralda mesmo em situação de mistura com a matriz de flogopita xisto. Três índices espectrais para identificação automatizada de esmeralda (EI1, EI2 e EI3) e três índices para identificação do xisto hospedeiro (MI_{depth}, MI_{ratio} e ACI) foram propostos e representam uma ferramenta valiosa para estudos de rotina em grande quantidade de amostras. Adicionalmente, imageamento hiperespectral de alta resolução permite a identificação de cristais de esmeralda em pixels de ~1 mm e a confecção de mapas mineralógicos/espectrais em amostras de mão e de furo de sonda.

Palavras-chave: esmeralda; gênese de depósitos minerais; modelo prospectivo; Província Borborema.

ABSTRACT

Brazil is one of the largest emerald producers in the world. Gem-quality crystals occur mainly in the states of Minas Gerais, Goiás, and Bahia. In the Borborema Province, northeastern Brazil, punctual emerald mineralizations have been gaining the spotlights of scientific and economic interests in recent decades. The presence of several beryl-bearing pegmatites and exposures of mafic/ultramafic rocks, especially in the Northern Subprovince, associated with tectonic structures that work as a means of transport for mineralizing fluids, make this region a promising area for the study of emerald genesis in intensely deformed environments. This work presents an integrated investigation, at different scales of analysis, on the characterization, origin, and prospecting of the Paraná emerald deposit, southwestern Rio Grande do Norte state. To build a genetic model, aeromagnetometry images, meso- and microscopic structural data, U-Pb and $^{40}Ar/^{39}Ar$ geochronology were used. The Paraná emeralds are hosted in irregular lenses of phlogopite- and actinolite-phlogopite schists interleaved with quartz-feldspathic veinlets and pegmatite bodies. The host schists are concordant with Rhyacian basement gneisses (Caico Complex) along the Portalegre shear zone, a structure with strong magnetic contrast and dextral kinematics in the NE-SW direction. Ductile deformation coeval to the mineralization is indicated by vertical mylonite foliation, asymmetric *boudins*, σ-type porphyroclasts, mica-fish structures and formation of S-C and S-C-C' shear bands. Origin of the emerald-bearing schist during Brasiliano deformation is supported by $^{40}Ar/^{39}Ar$ phlogopite ages of 524 ± 1 and 528 ± 1 Ma. Deformed granitic bodies, found within the schist showed U-Pb zircon ages of 2210 ± 8 Ma and 2201 ± 6 Ma, suggesting a reworking of the basement gneisses of the Caicó Complex during the deposit formation. The integration of these data suggests that metasomatism of granitic pegmatites injected along the Portalegre shear zone concomitant with Brasiliano tectonism was responsible for emerald mineralization in the Paraná region. In this process, Be, K, Al, and Si from the pegmatite fluid and Cr, Fe, and Mg from the mafic rocks have reacted, resulting in desilicated pegmatites and mineralized schists. From a prospective point of view, the presence of phlogopite and actinolite in the host schist allowed the individualization of its spectral signature relative to other rocks of the deposit. Using punctual reflectance spectroscopy, it is possible to distinguish the presence of emerald crystals even in a mixture with a phlogopite schist matrix. Three spectral indices for automated emerald identification (EI1, EI2, and EI3) and three indices for host schist identification (MI_{depth}, MI_{ratio} and ACI) have been proposed and represent a valuable tool for routine studies on large amounts

of samples. Additionally, high-resolution hyperspectral imaging allows the identification of emerald crystals in ~1 mm pixels and the production of mineralogical/spectral maps in handpicked and drill core samples.

Keywords: emerald; genesis of mineral deposits; prospective model; Borborema Province.

SUMÁRIO

1 INTRODUÇÃO

A esmeralda é uma variedade gemológica de berilo ($Be_3Al_2Si_6O_{18}$) na cor verde-grama e uma das pedras preciosas mais valiosas do mundo. Sua coloração rara se dá devido à presença de Cr^{3+} e/ou V^{3+} substituindo o Al^{3+} em seu retículo cristalino (Wood e Nassau, 1968). Essa raridade está relacionada às condições geológicas e geoquímicas específicas, necessárias para que haja o contato do berílio, de fonte usualmente pegmatítica, com o cromo e/ou vanádio, cujas fontes são comumente associadas às rochas máficas e ultramáficas (Groat et al., 2008).

A Província Borborema, nordeste do Brasil, é detentora de raros depósitos e/ou ocorrências de esmeralda que vem recebendo maior destaque, do ponto de vista científico e econômico, nas últimas décadas (*e.g.*, Scholz et al., 2010; Zwaan et al., 2012; Santiago et al., 2019; Araújo Neto et al., 2019, 2021). Descoberto em meados da década de 1980, o depósito de esmeralda de Paraná, localizado no extremo sudoeste do estado do Rio Grande do Norte, detém cristais de esmeralda de reconhecido potencial gemológico hospedados em flogopita xistos e/ou actinolita-flogopita xistos ao longo de faixas de rocha intensamente deformadas pela zona de cisalhamento Portalegre. Estudos geológicos pioneiros dessas mineralizações figuravam em relatórios técnicos ou trabalhos de mapeamento regional (*e.g.*, Moraes, 1999; Medeiros, 2008; Souza, 2017).

Recentemente, após reabertura dos serviços de pesquisa mineral, o depósito vem recebendo destaque de pesquisadores nacionais e internacionais, com publicação dos primeiros artigos científicos de caracterização mineralógica e geológica do depósito (*cf.* Araújo Neto et al., 2019, 2021). Entretanto, até o cenário atual, havia uma grande carência de estudos estruturais e geocronológicos que permitissem a compreensão da evolução genética da mineralização à luz dos eventos orogênicos que moldaram a Província Borborema. Dentre os vários aspectos que devem ser considerados para entender a origem do depósito, destacam-se a tipologia das rochas hospedeira e das fontes de berílio e elementos cromóforos, assembleia mineral, elementos estruturais, idade e temperatura de formação, dentre outros.

Por apresentar uma forte ligação com zonas intensamente deformadas por cisalhamento, o depósito de Paraná se caracteriza como um importante estudo de caso do papel de estruturas tectônicas e do metamorfismo regional na origem de mineralizações de esmeralda, um tópico constantemente debatido nos principais esquemas de classificação de depósitos (Giuliani et al., 1990, 1997, 2019; Schwarz e Giuliani, 2001; Zwaan, 2006). Se no passado buscava-se separar depósitos de esmeralda entre àqueles associados a pegmatitos graníticos e àquelas relacionados a estruturas tectônicas (Schwarz et al., 2001; Schwarz e Giuliani, 2001), hoje compreende-se

que essas estruturas são importantes canalizadoras dos fluidos mineralizantes na maioria das ocorrências, sejam elas de origem magmática e/ou metamórfica (Giuliani et al., 2019).

Nesse sentido, esta pesquisa apresenta um compilado de métodos analíticos aplicados ao entendimento da evolução genética do depósito de esmeralda de Paraná ao longo da zona de cisalhamento Portalegre. Adicionalmente, por tratar-se de um mineral gemológico chave para crescimento econômico local, há necessidade de se desenvolver técnicas prospectivas cada vez mais eficazes para identificação e/ou mapeamento de horizontes mineralizados. De forma pioneira, este trabalho traz um estudo de caso do uso de técnicas espectrais de alta resolução para a prospecção de esmeralda e determinação da assinatura espectral do depósito, incluindo acertos e limitações da metodologia.

1.1 OBJETIVOS

Esta pesquisa tem foco em dois grandes objetivos: o modelamento genético e a proposição de uma metodologia investigativa/prospectiva para o depósito de esmeralda de Paraná. O primeiro, tem por finalidade entender as condições genéticas que levaram a formação de esmeralda na região de Paraná. Para isto, pretende-se adotar diversas metodologias de estudos de depósitos de minerais gemológicos, em diferentes escalas. Evidências geofísicas, estruturais, petrográficas e geocronológicas serão integradas para caracterização da origem da esmeralda e proposição de um modelo esquemático de formação do depósito. Portanto, os seguintes objetivos específicos devem ser alcançados:

i. Detalhar, através de interpretações geofísicas e mapeamento geológico-estrutural, o comportamento do xisto hospedeiro e das demais litologias associadas ao longo da zona de cisalhamento Portalegre.
ii. Realizar datação do xisto hospedeiro através de $^{40}Ar/^{39}Ar$ em flogopita, bem como a datação U-Pb em zircão de rochas associadas à mineralização.
iii. Integrar estes e demais dados publicados acerca da mineralização para propor um esquema de evolução genética para formação de esmeralda.

O segundo objetivo visa o uso de técnicas de imageamento e caracterização espectral em amostras de mão e de furo de sonda do depósito de Paraná para propor as bases de um novo método automatizado de identificação e/ou mapeamento mineral. Estes dados serão balizados por petrografia e/ou geoquímica de rocha total para uma avaliação ainda mais precisa. Dentre outras observações, se almeja identificar a assinatura espectral da esmeralda, bem como do

xisto hospedeiro, buscando individualizar essas assinaturas em detrimento aos demais espectros de absorção de outras rochas associadas ao depósito.

1.2 ESTRUTURA DA TESE

O volume final desta tese é composto por três artigos científicos, sendo o primeiro deles um artigo de revisão (artigo científico I), equivalente a um capítulo de estado da arte de aspectos genéticos de depósitos de esmeralda, em especial àqueles associados a zonas de cisalhamento, e os outros dois, de resultados (artigos científicos II e III). Nesse sentido, o artigo científico II é voltado à gênese do depósito de esmeralda, enquanto o artigo científico III é dedicado ao uso de métodos espectrais para a exploração de esmeralda. Um breve resumo da disposição e abordagem de cada capítulo é apresentado a seguir:

- **Capítulo 2: Artigo científico I – Geologia e aspectos genéticos de depósitos de esmeralda em zonas de cisalhamento: um olhar sobre os depósitos esmeraldíferos da Província Borborema, NE do Brasil**. Neste artigo é revisado os principais modelos genéticos de esmeralda e esquemas de classificação, com destaque para aqueles associados a estruturas tectônicas. Um olhar mais profundo é apresentado, pela primeira vez, para os depósitos de esmeralda da Província Borborema como um todo, destacando a importância da Subprovíncia Setentrional para este tipo de mineralização.
- **Capítulo 3: Artigo científico II – Structural and geochronological constraints on the Portalegre shear zone: implications for emerald mineralization in the Borborema Province, Brazil**. Este trabalho apresenta uma integração de imagens geofísicas, análises estruturais na meso- e microescala, e os primeiros dados geocronológicos do depósito de esmeralda de Paraná. Um esquema idealizado para formação do depósito e um modelo com os principais elementos estruturais são propostos.
- **Capítulo 4: Artigo científico III – Advances for the exploration of tectonic-magmatic related emerald deposits using a high-resolution spectral approach: unraveling the spectral footprint of the Paraná deposit (NE Brazil).** Esse artigo apresenta o primeiro estudo de caso da obtenção de índices espectrais voltados para exploração de esmeralda, bem como de espectroscopia de imageamento para mapeamento de amostras contendo esmeralda. Estas técnicas foram aplicadas em amostras de mão e de furo de sonda, balizadas por petrografia e geoquímica de rocha total. Uma discussão sobre os acertos e limitações do método é apresentada.

- **Capítulo 5: Considerações Finais**. Síntese conclusiva dos principais resultados obtidos por esta pesquisa.

1.3 CONTEXTO GEOLÓGICO

A Província Borborema (PB) representa a porção nordeste da Plataforma Sulamericana (Almeida et al., 1981), cujos estágios finais de desenvolvimento se deram na transição entre o fim do Neoproterozoico e o início do Cambriano (Santos e Medeiros, 1999; Brito Neves et al., 2000, 2014; Caxito et al., 2020; Santos et al., 2023). Em reconstituições geodinâmicas pré-atlânticas, a PB é considerada parte central de Gondwana Oeste (Figura 1.1A), apresentando extensas zonas de cisalhamento que segmentam grandes blocos crustais, como resultado de sua estruturação ao fim do evento orogênico Brasiliano (Brito Neves et al., 2000; Santos et al., 2008; Van Schmus et al., 2008; Santos et al., 2010; Oliveira e Medeiros, 2018; Santos et al., 2021). Nesse contexto, as zonas de cisalhamento Patos e Pernambuco, de direção E-W e escala continental, subdividem a PB em três subprovíncias: Setentrional, Transversal e Meridional (*cf.* Van Schmus et al., 2011) (Figura 1.1B).

A Subprovíncia Setentrional – por vezes, também separada em três distintas subprovíncias ou domínios geotectônicos: Médio Coreaú, Ceará Central e Rio Grande do Norte (*cf.* Van Schmus et al., 2008; Santos et al., 2014) – é marcada por extensas exposições do embasamento gnáissico-migmatítico paleoproterozoico intercaladas com rochas supracrustais e/ou magmáticas de idade neoproterozoica a cambriana (Jardim de Sá et al., 1995; Brito Neves et al., 2000; Delgado et al., 2003). Esta subprovíncia contém os mais importantes campos e distritos pegmatíticos da Província Borborema (Baumgartner et al., 2006; Beurlen et al., 2009, 2011; Santos et al., 2014), sendo responsável por hospedar diversos depósitos de minerais gemológicos, tais como água-marinha, esmeralda, elbaíta, ametista, citrino, granada, dentre outros (Moraes, 1999; Barreto e Bittar, 2010).

Depósitos e ocorrências de esmeralda da Província Borborema são reportados exclusivamente na Subprovíncia Setentrional (*e.g.* Cassedanne et al., 1979; Castelo Branco et al., 1988; Zwaan et al., 2012; Santiago et al., 2019; Araújo Neto et al., 2019). O depósito de esmeralda de Paraná, objeto de estudo desta pesquisa, está localizado no centro da subprovíncia, em uma região dominada por exposições gnáissicas/migmatíticas de rochas do Complexo Caicó (Figura 1.1C). Essas rochas seguem um *trend* NE-SW impresso por diversas zonas de cisalhamento transcorrentes que cortam a região e controlam o alojamento de corpos pegmatíticos e a configuração lito-estrutural do depósito e das áreas adjacentes (Araújo Neto et

al., 2018). A esmeralda é encontrada em lentes de flogopita xisto encaixadas em gnaisses miloníticos do Complexo Caicó ao longo da zona de cisalhamento Portalegre. Cristais de qualidade gemológica podem ser encontrados inseridos nos planos de xistosidade ou em vênulas e veios quartzo-feldspáticos envelopados pelo xisto (Araújo Neto et al., 2019).

Figura 1.1 - Contexto geológico do depósito de esmeralda de Paraná.

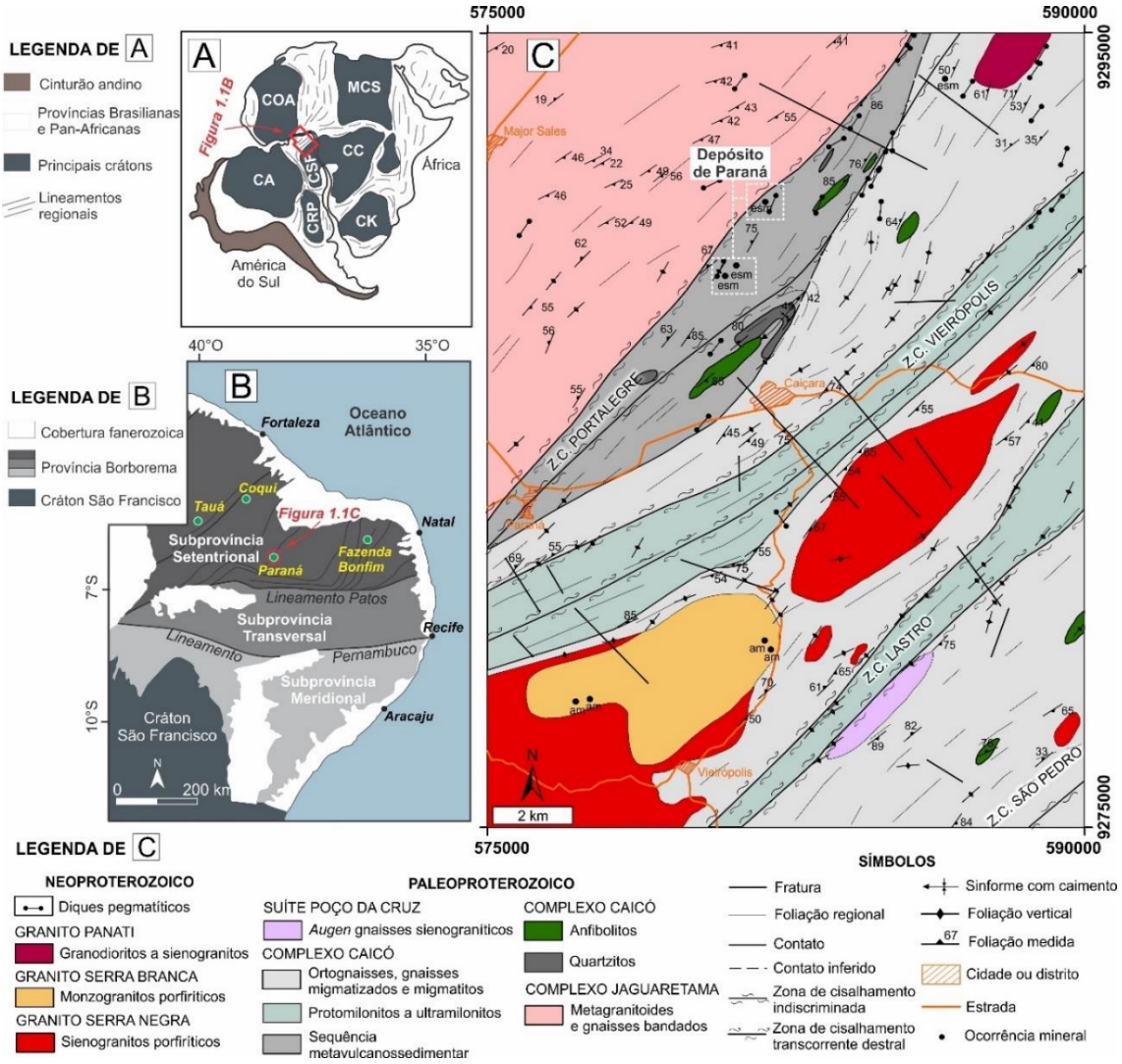

Fonte: O Autor (2023)

(A) Reconstituição geodinâmica das principais províncias Brasilianas e Pan-africanas e blocos cratônicos do oeste da África e leste da América do Sul no contexto de Gondwana Oeste. Adaptado de Santos et al. (2019). (B) Divisão esquemática da Província Borborema em três subprovíncias de acordo com Van Schmus et al. (2011), com localização dos principais depósitos e ocorrências de esmeralda (círculo fechado verde). Adaptado de Santos et al. (2014). (C) Mapa geológico do depósito de esmeralda de Paraná e regiões adjacentes. Adaptado de Araújo Neto et al. (2018). az = amazonita; esm = esmeralda.

2 ARTIGO CIENTÍFICO I – GEOLOGIA E ASPECTOS GENÉTICOS DE DEPÓSITOS DE ESMERALDA EM ZONAS DE CISALHAMENTO: UM OLHAR SOBRE OS DEPÓSITOS ESMERALDÍFEROS DA PROVÍNCIA BORBOREMA, NE DO BRASIL

Publicado em: *Geologia USP. Série Científica*
Recebido em 29 de dezembro de 2020; aceito em 14 de abril de 2021
DOI: https://doi.org/10.11606/issn.2316-9095.v21-180467

José Ferreira de Araújo Neto[1*], Lauro Cézar Montefalco de Lira Santos[1,2], Glenda Lira Santos[1]

[1]Programa de Pós-Graduação em Geociências, Centro de Tecnologia e Geociências, Universidade Federal de Pernambuco – UFPE, Brasil; [2]Departamento de Geologia, Universidade Federal de Pernambuco – UFPE, Brasil

*Autor correspondente: José Ferreira de Araújo Neto

RESUMO

Esmeralda é uma variedade de berilo na cor verde-grama, sendo uma das mais raras e valiosas gemas do mundo. Além das características magmáticas e metamórficas particulares de cada depósito, descontinuidades crustais sempre estão presentes, interpretadas como os meios físicos para canalização dos fluidos mineralizantes. Exemplos importantes são observados nos depósitos de Habachtal, na Áustria, e de Carnaíba e Santa Terezinha de Goiás, no Brasil. Na Província Borborema (NE do Brasil), a conexão entre zonas de cisalhamento e ocorrências de esmeralda tem despertado interesse científico e comercial, principalmente quanto às estruturas associadas a pegmatitos berilíferos. Neste trabalho apresentamos uma revisão sobre a evolução do conhecimento de mineralizações de esmeralda em zonas de cisalhamento, com esquemas de classificação recentes, principais modelos esquemáticos adaptados e com enfoque nos controles geológicos dos principais depósitos do nordeste brasileiro. Na região de Fazenda Bonfim (Rio Grande do Norte), o desenvolvimento de flogopititos esmeraldíferos se deu em zonas metassomáticas, enquanto nas ocorrências de Tauá e Coqui (Ceará), a mineralização está associada a corpos pegmatíticos em faixas de flogopita-xistos e tremolititos, ambos fortemente afetados por tectônica transcorrente. No depósito de Paraná (Rio Grande do Norte), tem-se

interpretado um componente extensional concomitante à transcorrência, que possibilitou a interação entre fluidos pegmatíticos contendo berílio e rochas metabásicas ricas em elementos cromóforos. Concluímos que o regime de deformação dúctil ligado as zonas de cisalhamento regionais representam um dos mais importantes metalotectos para prospecção de esmeralda na Província Borborema.

Palavras-chave*:* Depósitos controlados por zonas de cisalhamento; Esquemas de classificação; Modelos genéticos; Subprovíncia Setentrional.

ABSTRACT

Emerald is a grass-green beryl variety, and one of the rarest and most valuable gems in the world. Besides the magmatic and metamorphic characteristics of each deposit, crustal discontinuities are always present, being interpreted as the physical means for channeling mineralizing fluids. Important examples are seen in the Habachtal deposit in Austria, Carnaíba and Santa Terezinha de Goiás deposits in Brazil. In the Borborema Province (Northeastern Brazil), the connection between shear zones and emerald occurrences has aroused scientific and commercial interest, especially regarding structures associated with beryllium pegmatites. In this paper a review on the evolution of knowledge of shear zone-related emerald mineralizations is developed, with recent classification schemes and adapted main schematic models, with a focus on the geological controls of the main deposits in northeastern Brazil. In the Fazenda Bonfim region (Rio Grande do Norte State), the development of emerald-bearing phlogopitites occurred in metasomatic zones. In the occurrences of Tauá and Coqui (Ceará State), mineralization is associated with pegmatite veins in phlogopite-schist and tremolitite bands, both strongly affected by strike-slip tectonics. In the Paraná deposit (Rio Grande do Norte State), an extensional component has been interpreted to be concomitant to the transcurrent tectonics, allowing the interaction between beryllium-bearing pegmatitic fluids and metabasic rocks containing chromophore elements. In conclusion, the ductile deformation regime linked to the regional shear zones represents one of the most important controls for prospecting emerald in the Borborema Province.

Keywords*:* Shear-zone controlled deposits; Classification schemes; Genetic models; Northern Subprovince.

INTRODUÇÃO

O termo esmeralda deriva do grego *smaragdos*, que significa “gema verde”. Registros da sua exploração e comércio, bem como utilização em ornamentos pessoais, amuletos e joias datam desde a Antiguidade, por volta de 2000 a.C. nos antigos Egito e Índia (Sinkankas, 1989). No Brasil, as primeiras ocorrências foram oficialmente descobertas na região de Brumado, no estado da Bahia, em 1912, mas o país só passou a figurar entre os maiores produtores do mundo a partir da década de 1980, após o descobrimento de diversas jazidas com cristais de qualidade gemológica nos estados de Minas Gerais, Bahia e Goiás (Cornejo e Bartorelli, 2010).

Por tratar-se de um dos minerais gemológicos mais valiosos do mundo, estudos sistemáticos de depósitos de esmeralda e das condições sob as quais se formaram logo tornaram-se foco de geólogos e mineralogistas por todo o globo. Definida como uma variedade gemológica de berilo, cuja cor verde se dá pela presença de traços de cromo e/ou vanádio em sua estrutura cristalina, a esmeralda teve seus aspectos genéticos inicialmente estudados a partir das fontes de berílio e de cromo e/ou vanádio. A natureza das rochas hospedeiras e fornecedoras de Be e elementos cromóforos guiaram a criação dos primeiros esquemas de classificação genética para ocorrências de esmeralda (*cf.* Schwarz, 1987; Kazmi e Snee, 1989).

Apesar dos esforços válidos desses esquemas preliminares, diversas ambiguidades nas variáveis propostas e a introdução de novas teorias para formação de esmeralda levaram a modelos de classificação cada vez mais robustos. Schwarz e Giuliani (2001) e Schwarz et al. (2001) propuseram uma classificação em dois tipos principais de depósitos, tomando como base esquemas preliminares desenvolvidos para depósitos de esmeralda brasileiros: depósitos relacionados a intrusões graníticas e depósitos controlados por estruturas tectônicas.

Esse modelo, apesar de amplamente utilizado, não levava em consideração que as duas condições propostas não são excludentes, ou seja, mineralizações associadas a intrusões graníticas podem ser controladas por estruturas tectônicas e vice-versa, e dessa forma diversos depósitos poderiam ser classificados de forma imprecisa (Zwaan, 2006). Nos anos subsequentes, vários trabalhos demonstraram a importância das zonas de cisalhamento como mecanismo fundamental para o transporte de fluidos metassomáticos formadores de esmeralda, mesmo em mineralizações intimamente ligadas à granitos e pegmatitos (*cf.* Moraes, 2000; Zwaan, 2006; Zwaan et al., 2012; Santiago et al., 2019). Estes avanços no conhecimento geológico-genético levaram Giuliani et al. (2019) a propor uma classificação aperfeiçoada, que contempla atividade tectônica, ambiente geológico, tipo de rocha hospedeira, grau de metamorfismo, entre outras considerações.

Neste sentido, este trabalho tem como objetivo apresentar uma revisão das condições geológicas de formação de esmeralda e das classificações genéticas de depósitos, com destaque para o papel das zonas de cisalhamento na formação destas mineralizações. Para isso, tomamos como base diversos esquemas de classificação propostos e alguns dos principais exemplos de jazidas brasileiras e do mundo. Adicionalmente, buscamos trazer um olhar mais detalhado para os depósitos e ocorrências de esmeralda da Província Borborema, nordeste do Brasil, uma vez que as informações sobre estas são escassas e/ou temporalmente espaçadas, dificilmente figurando em trabalhos de revisão de alcance mais amplo. A Província Borborema se apresenta como um excelente estudo de caso, tendo em vista que sua configuração tectônica-estrutural ao final do evento de colagem orogênica brasiliana (800 – 500 Ma; Brito Neves et al., 2014) favoreceu uma série de mineralizações ao longo de zonas de cisalhamento que se desenvolveram durante este período.

EVOLUÇÃO DOS MODELOS GENÉTICOS

No modelo clássico de formação, também conhecido por tipo xisto (*schist-type*) ou hospedado em xisto (*schist hosted*), a esmeralda se cristaliza no interior de biotita ou flogopita xistos (biotititos e/ou flogopititos) desenvolvidos em zona metassomatizada por metamorfismo de contato, doravante referida como zona metassomática de contato (*blackwall zone)* entre pegmatitos contendo Be e rochas máficas e ultramáficas que contenham Cr e/ou V (Figura 2.1) (Fersmann, 1929; Schwarz, 1987). Neste modelo, o metassomatismo é responsável pela conversão da rocha máfica/ultramáfica em uma rocha micácea contendo esmeralda e pela transformação do pegmatito granítico em um pegmatito dessilicado, i.e., formado pela dissolução de sílica, resultando em composições tipicamente abundantes em plagioclásio e pobres em quartzo e K-feldspato (Walton, 2004).

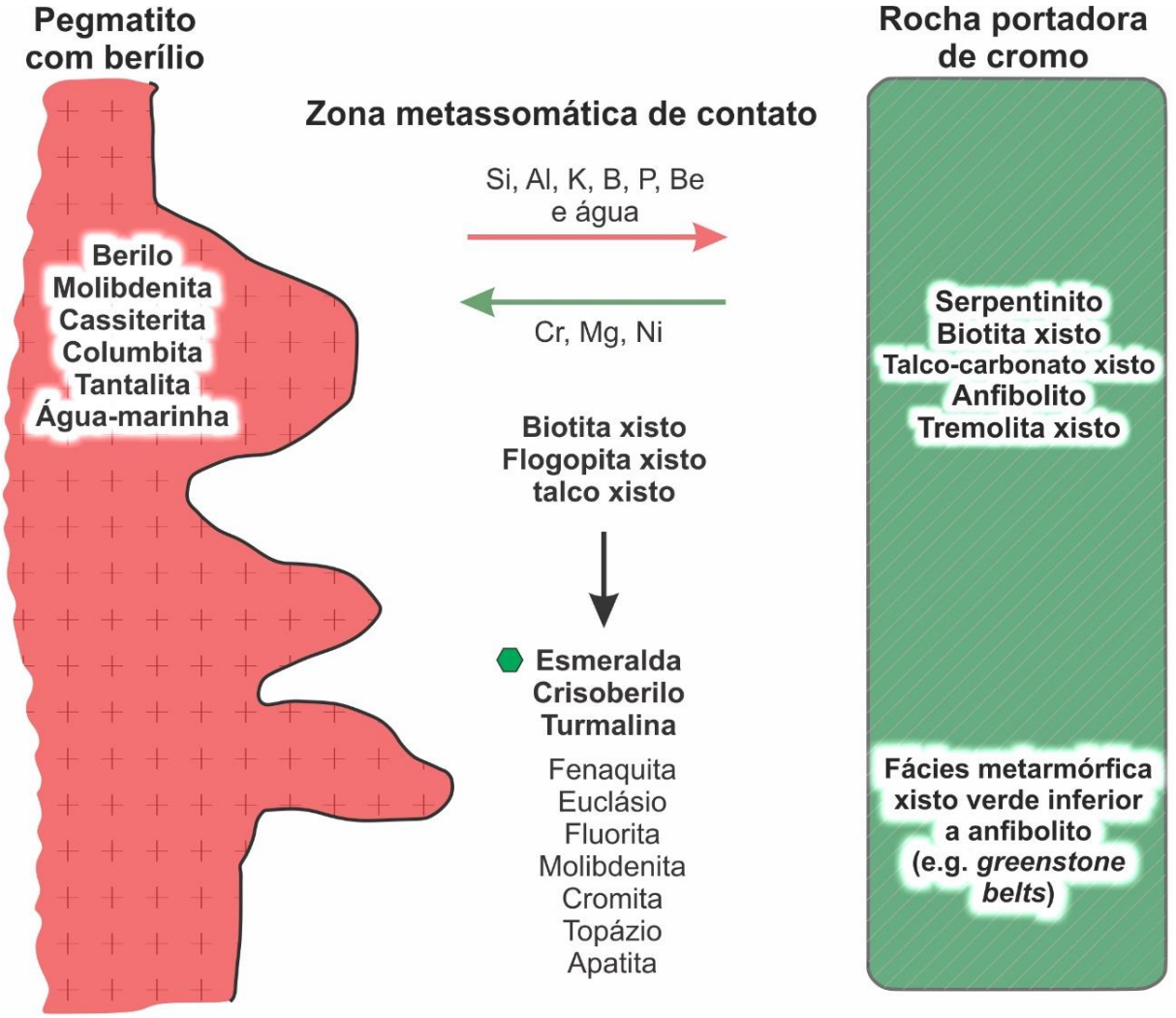

Figura 2.1. Modelo esquemático para formação de depósitos de esmeralda do "tipo xisto" segundo Walton (2004).

A mais conhecida exceção a esse modelo é a esmeralda colombiana, uma vez que ocorre em veios e bolsões ricos em carbonatos, silicatos e pirita alojados em sucessões de folhelhos negros e calcários. Essa mineralização se deu devido a processos de circulação hidrotermal sem evidências claras de magmatismo associado, caracterizando um tipo de depósito denominado de "hidrotermal" ou "sedimentar" (Schwarz, 1987; Giuliani et al., 1995; Schwarz et al., 2002; Groat et al., 2008). Neste caso, tanto Be quanto Cr e V estariam aprisionados como elementos traço em folhelhos negros, sendo apenas liberados para formação de esmeralda após reações entre a matéria orgânica dos folhelhos com o enxofre resultante da interação entre H_2S e salmouras hidrotermais ricas em sulfatos (Ottaway et al., 1994).

Grundmann e Morteani (1989) constataram que a formação de esmeralda nos depósitos de Habachtal (Áustria) e Leydsdorp (África do Sul) não se encaixava em nenhum dos tipos

anteriormente descritos. Nestes depósitos, a esmeralda é encontrada em zonas metassomatizadas associadas a rochas ultramáficas formadas por reações sin- a pós-tectônicas durante metamorfismo de baixo grau sem contribuição de fusões magmáticas.

Ao longo dos anos, diversos autores buscaram, diversos autores buscaram ao longo dos anos agrupar os depósitos de esmeralda em diferentes classificações com base em parâmetros físicos, aspectos mineralógicos, geoquímicos ou até mesmo combinando esses dados com idade de formação e composição isotópica (*e.g.* Schwarz, 1987; Kazmi e Snee, 1989; Giuliani et al., 1990; Dereppe et al., 2000; Schwarz e Giuliani, 2001; Schwarz et al., 2001; Barton e Young, 2002 e outros). Destaca-se aqui a classificação de Giuliani et al. (1990) para depósitos brasileiros, atualizada em Giuliani et al. (1997), que caracteriza os depósitos de esmeralda em dois tipos principais: tipo I, correspondente ao modelo clássico "hospedado em xisto", em zonas metassomáticas associadas a rochas máfica-ultramáficas e pegmatitos (*e.g.* Carnaíba e Socotó, Bahia); e tipo II, estratiforme, onde a infiltração de fluidos hidrotermais se deu a partir estruturas tectônicas como zonas de cisalhamento (*e.g.* Santa Terezinha de Goiás, Goiás).

Essa classificação binária foi expandida por Schwarz e Giuliani (2001) e Schwarz et al. (2001), incluindo diversos depósitos de esmeralda do mundo e caracterizando subdivisões do tipo I com base na presença ou ausência de xisto em contato com pegmatitos, bem como subdividindo o tipo II em xistos na ausência de pegmatitos e folhelhos negros com veios e brechas.

Nesse contexto, diversos depósitos magmáticos associados a atividade tectônica não poderiam ser classificados corretamente sem gerar ambiguidades, pois, assim como depósitos do tipo I podem apresentar fluidos canalizados por estruturas tectônicas, os depósitos do tipo II não necessariamente descartam a conexão com intrusões ígneas mais profundas (Zwaan, 2006; Groat et al., 2008, 2014). Zwaan (2006) aponta uma série de inconsistências nas diversas classificações propostas até então, assinalando que cristais de esmeralda de boa qualidade podem ocorrer em diferentes ambientes geológicos, contanto que algumas condições básicas sejam atendidas:

- disponibilidade de berílio, cromo (e/ou vanádio);
- meio de transporte para junção desses elementos;
- condições de temperatura em que a esmeralda seja estável, usualmente entre 600° e 300°;
- espaço suficiente para crescimento de cristais bem formados e transparentes.

A necessidade de uma classificação cada vez mais precisa, as diversas controvérsias nos modelos usuais e o entendimento da importância da atividade tectônica para formação de esmeralda levaram Giuliani et al. (2019) a proporem uma classificação revisada para depósitos de esmeralda (Tabela 2.1), que divide as ocorrências em dois tipos principais:

- Tipo I: Tectono-magmático, com subtipos hospedados em: (IA) rochas máfica-ultramáficas, (IB) rochas sedimentares e (IC) rochas graníticas;
- Tipo II: Tectono-metamórfico, com subtipos hospedados em: (IIA) rochas máfica-ultramáficas, (IIB) rochas sedimentares, (IIC) rochas metamórficas e (IID) depósitos do tipo I metamorfizados ou relacionados a intrusões graníticas ocultas e alguns depósitos não classificados.

Do ponto de vista econômico, os depósitos tectono-magmáticos do tipo IA e tectono-metamórficos do tipo IIB e IIC correspondem aos mais importantes em termos de volume e qualidade do material produzido. Os depósitos tectono-metamórficos do tipo IIA, são, por vezes, considerados de menor importância econômica devido ao tamanho reduzido e disseminação dos cristais de esmeralda, além de maiores custos para mineração artesanal. No entanto, devem ser considerados na prospecção em *greenstone belts* e sequências metavulcanossedimentares arqueanas e pré-cambrianas.

Tabela 2.1. Alguns dos principais esquemas de classificação tipológica para depósitos de esmeralda

Giuliani et al. (1990)	Tipos de depósito	Tipo I	Tipo II	Tipo III	
		Associados a rochas máfica-ultramáficas, granitos proximais e pegmatitos	Biotita xistos esmeraldíferos desenvolvidos em zonas de cisalhamento na ausência de pegmatitos	Depósitos de origem incerta, relacionados à presença de pegmatitos com berilo, água-marinha e/ou Nb-Ta-cassiterita	
	Exemplos	Carnaíba e Socotó (Brasil)	Santa Terezinha de Goiás (Brasil)	Itabira, Tauá e Coqui (Brasil)	
Giuliani et al. (1997)	Tipos de Depósito	Tipo I	Tipo II		
		Tipo xisto, associado a pegmatitos e rochas básicas e/ou ultrabásicas	Estratiforme, na ausência de pegmatitos, formado por infiltração de fluidos hidrotermais controlados por estruturas tectônicas		
	Exemplos	Carnaíba, Socotó, Itabira, Tauá e Coqui (Brasil)	Itaberaí, Santa Terezinha de Goiás (Brasil)		
Schwarz e Giuliani (2001); Schwarz	Tipos de depósito	Tipo I		Tipo II	
		Relacionado a intrusões graníticas		Controlado por estruturas tectônicas	
	Subtipos	Pegmatito com xisto na zona de contato	Pegmatito sem xisto na zona de contato	Xistos na ausência de pegmatitos	Folhelhos negros com

et al. (2001)					veios e brechas
	Exemplos	Carnaíba, Itabira, Tauá, Coqui (Brasil), Sandawana (Zimbábue)	Emmaville–Torrington (Austrália); Eidsvoll (Noruega)	Habachtal (Áustria), Santa Terezinha de Goiás (Brasil)	Colômbia
Giuliani et al. 2019	Tipos de depósito	Tipo I Tectono-magmático		Tipo II Tectono-metamórfico	
	Subtipos	Hospedado em rochas máfica-ultramáficas (IA), rochas sedimentares (IB), rochas graníticas (IC)		Hospedado em rochas máfica-ultramáficas (IIA), rochas sedimentares (IIB), rochas metamórficas (IIC). Depósitos do tipo I metamorfizados ou relacionados a fontes graníticas ocultas e depósitos não classificados são considerados do subtipo IID.	
	Exemplos	IA: Carnaíba, Socotó, Fazenda Bonfim (Brasil), Sandawana (Zimbábue); IB: Emmaville (Austrália); IC: Kaduna (Nigéria)		IIA: Habachtal (Áustria), Santa Terezinha de Goiás (Brasil); IIB: Cinturões Oriental e Ocidental (Colômbia); IIC: Hiddenite (EUA); IID: Poona (Austrália)	

DEPÓSITOS DE ESMERALDA E ZONAS DE CISALHAMENTO

O papel das zonas de cisalhamento na formação de esmeralda, bem como sua contribuição em depósitos magmáticos, vem sendo cada vez mais abordado em âmbito internacional e nacional (Zwaan, 2006; Zwaan et al., 2012; Araújo Neto et al., 2019; Santiago et al., 2019). Em sua classificação de depósitos de esmeralda, Giuliani et al. (2019) reconhecem que todos os modelos genéticos requerem algum nível de atividade tectônica. A continuidade dessa atividade pode resultar em metamorfismo de depósitos magmáticos e sedimentares existentes, e, em níveis crustais mais profundos, fusão parcial pode dificultar a distinção entre depósitos tipicamente metamórficos ou magmáticos. Dessa forma, para cada situação faz-se necessária uma avaliação criteriosa da extensão do tectonismo na formação da mineralização, balizada por evidências estruturais, metamórficas, geocronológicas etc. Formação em múltiplos estágios e remobilização de elementos durante eventos deformacionais também devem ser levados em consideração.

A ação do metamorfismo regional na formação de rochas mineralizadas em esmeralda é reconhecida desde os trabalhos pioneiros nos depósitos de Habachtal e Leydsdorp (Grundmann e Morteani, 1989 e referências nele contidas), onde a mineralização ocorre predominantemente em biotita, clorita, actinolita e talco xistos (Figura 2.2). De acordo com Grundmann e Morteani (op. cit.), diversas evidências apontam para uma origem metamórfica regional:

- textura *augen* nos metagranitos e metapegmatitos do embasamento;

- crescimento polifásico com deformação simultânea indicada em traços de inclusão sigmoidais em cristais de esmeralda intensamente zonados;
- ausência de evidências de metamorfismo de contato nos minérios de esmeralda ou nas rochas encaixantes imediatas;
- padrões de fracionamento de elementos terras raras e razões Yb/Ca versus Tb/Ca de cristais de fluorita coexistentes com esmeralda que indicam a existência de um fluido abundante não-pegmatítico durante a formação da esmeralda, provavelmente ligado a exalações vulcânicas submarinas.

Por outro lado, Zwaan (2006) assinala que interpretações nos casos em que as fontes pegmatíticas de berílio não estejam expostas devem ser tomadas com precaução. Fluidos provenientes de pegmatitos (ocultos em superfície) podem percorrer um longo caminho, especialmente ao longo de rochas intensamente cisalhadas. A hipótese de uma influência magmática em Habachtal é suportada pela presença de pegmatitos em regiões próximas ao depósito (Satir, 1974; Schulz et al., 2001) e pelos altos teores de Cs nos cristais de esmeralda (Calligaro et al., 2000), o apontando como depósito tipo IID (Giuliani et al., 2019), resultado de uma provável remobilização metamórfica de um depósito tipo IA.

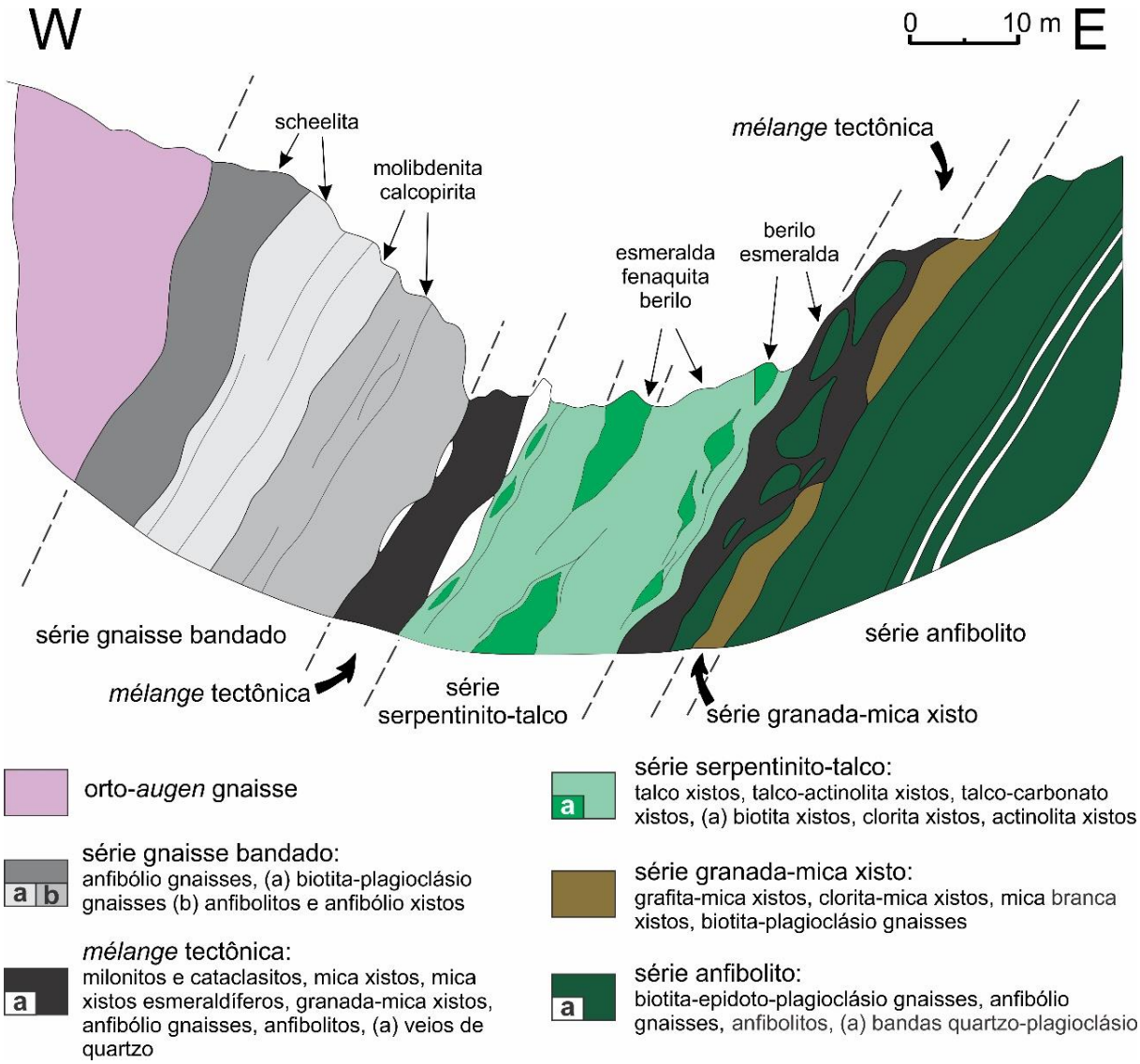

Figura 2.2. Seção geológica simplificada do depósito de Habachtal (Áustria). Modificada de Grundmann e Morteani (1989).

Em Sandawana, Zimbábue, a esmeralda ocorre em zonas metassomáticas no contato entre rochas ultramáficas e pegmatitos graníticos. Estes pegmatitos intrudiram rochas do *greenstone belt* Mweza antes e/ou durante um grande evento deformacional neoarqueano (2,6 Ga; Zwaan, 2006), caracterizando este depósito como tectono-magmático do tipo IA (Giuliani et al., 2019). De acordo com Zwaan (2006), metassomatismo potássico e sódico se deram de forma sin-tectônica, com fluidos ricos em Na, contendo F, P, Li, Be e Cr, canalizados e injetados através de zonas de cisalhamento levando tanto à albitização dos pegmatitos pré-existentes quanto à flogopitização das rochas ultramáficas encaixantes (Figura 2.3). Evidências de deformação dúctil coeva são registradas pela presença de microzonas de cisalhamento, bandas diferenciadas de anfibólio-flogopita xisto e pegmatitos com estruturas dobradas, *boudinage* e *pinch and swell*.

Domínios de baixa pressão nessas estruturas favoreceram, inclusive, o crescimento de cristais de esmeralda de qualidade gemológica.

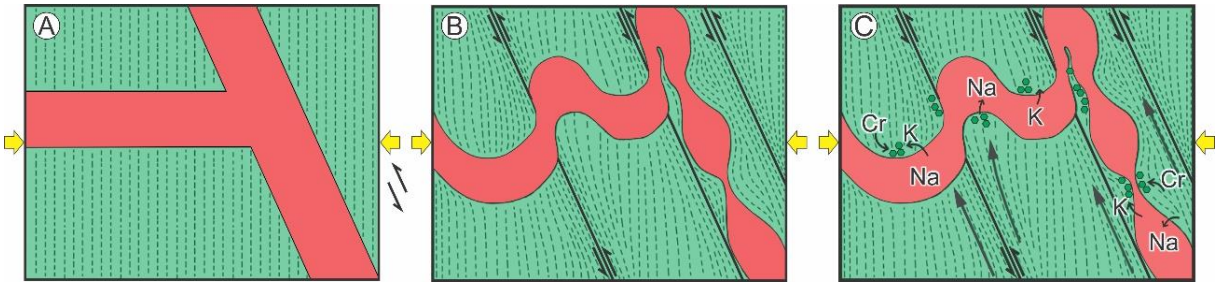

Figura 2.3. Processo de formação de esmeralda no depósito de Sandawana envolvendo atividades magmáticas e tectônicas. Em (A) há intrusão de pegmatito (em vermelho) contendo elementos raros imediatamente antes e/ou durante o principal estágio de deformação; (B) compressão e cisalhamento ocorrem de forma simultânea causando dobramento e estruturas boundinadas e do tipo pinch-and-swell; (C) infiltração de fundidos tardios ricos em Na ao longo das zonas de cisalhamento causando metassomatismo de pegmatitos e alterações no contato com rochas ultramáficas (em verde) resultando na formação de cristais de esmeralda em zonas de baixa pressão. Adaptado de Zwaan (2006).

Principais depósitos do Brasil

No Brasil, os depósitos de esmeralda caracteristicamente magmáticos, com origem do fluido metassomática-hidrotermal, tais como os da região de Itabira-Nova Era (MG) e de Carnaíba (BA), possuem uma forte associação com estruturas tectônicas (depósitos tectono-magmáticos; Giuliani et al., 2019). As mineralizações de esmeralda no distrito mineiro Itabira-Nova Era em Minas Gerais, responsável pela maior parte da produção de esmeralda no Brasil, se dão em uma extensão de aproximadamente 5 km entre as minas de Capoeirana, Piteiras e Belmont e ocorrem alojadas em zonas de cavalgamento na borda sudoeste do Cráton São Francisco. Estas zonas proporcionaram a circulação de fluidos hidrotermais durante a Orogênese Brasiliana (508 Ma; Giuliani et al., 1997; Giuliani et al., 2019). Os fluidos interagiram com granitos deformados (Granito Borrachudos) e pegmatitos ricos em Be, bem como rochas metabásicas e/ou metaultrabásicas contendo Cr e V (Rondeau et al., 2003) (Figura 2.4).

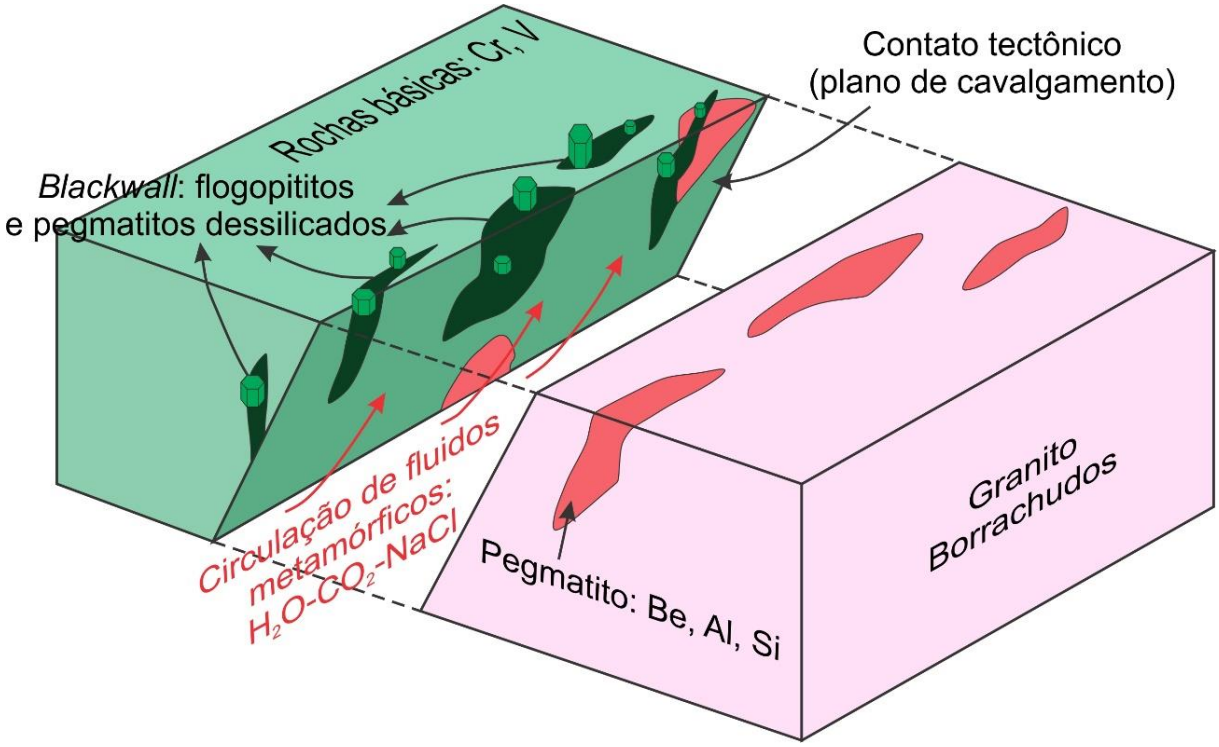

Figura 2.4. Diagrama esquemático para formação de esmeralda na região de Capoeirana, Piteiras e Belmont. O fluido hidrotermal de origem metamórfica (seta vermelha) percolou durante a Orogênese Brasiliana (508 Ma) na interface tectônica entre o granito deformado contendo pegmatitos berilíferos e rochas básicas contendo cromo e vanádio. A esmeralda cristalizou em flogopita xistos e pegmatitos dessilicados. Adaptado de Rondeau et al. (2003).

A mineralização de esmeralda em Carnaíba, Bahia, ocorre nas proximidades do Granito de Carnaíba, em uma zona de alteração metassomática (flogopititos) desenvolvida entre pegmatitos dessilicados e rochas básicas encaixantes do cinturão metavulcanossedimentar de Jacobina (Giuliani et al., 1990). Griffon et al. (1967) apontam para a importância de várias fases tectônicas superpostas tanto ligadas à ascensão do Granito de Carnaíba quanto à tectônica regional da Serra da Jacobina para o desenvolvimento da jazida em Carnaíba (Figura 2.5). De acordo com Schwarz (1987), a formação de esmeralda nesta região estaria associada a fase tardi-tectônica, com mineralizações encontradas em zonas de maior influência tectônica contendo faixas frequentemente milonitizadas. Rudowski (1989) enfatiza que o Granito de Carnaíba não era previamente enriquecido em berílio (5 a 11 ppm de Be) e, portanto, o desenvolvimento de esmeralda nas rochas encaixantes estaria relacionado, sobretudo, à eficácia dos flogopititos como armadilha metassomática ideal para as mineralizações.

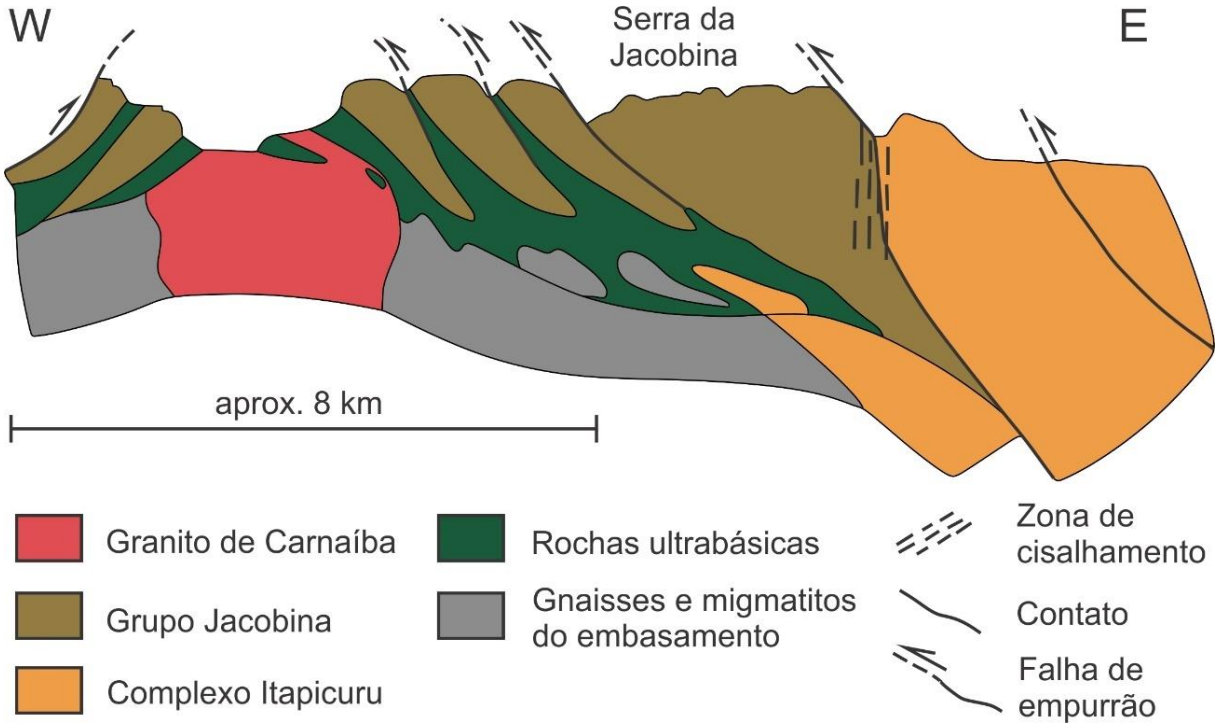

Figura 2.5. Seção geológica esquemática da região de Carnaíba, na Serra da Jacobina. Adaptado de Santana et al. (1995). Unidades litológicas segundo Couto (2000).

Na região central do estado de Goiás, o depósito de esmeralda de Santa Terezinha de Goiás corresponde ao melhor exemplo de depósito tectono-metamórfico do Brasil. A ausência de veios pegmatíticos e o desenvolvimento da esmeralda em xistos ao longo de zonas de cisalhamento destacaram a necessidade de separar o depósito de Santa Terezinha dos demais depósitos brasileiros desde os trabalhos pioneiros de classificação tipológica de Schwarz (1987) e Giuliani et al. (1990). No modelo mais recente, é considerado um depósito do tipo IIA (tectono-metamórfico hospedado em rochas máfica-ultramáficas; Giuliani et al., 2019). A esmeralda é encontrada na sequência metavulcanossedimentar Santa Terezinha (Figura 2.6), em vênulas de quartzo hidrotermal, no interior de massas carbonatadas que podem conter talco e clorita, ou inserida em flogopititos, talco xistos e/ou clorita flogopititos que envolvem núcleos carbonatados (Biondi, 1990).

O início do processo hidrotermal e consequente mineralização em Santa Terezinha de Goiás se deu de forma sin-tectônica ao cisalhamento gerado durante a Orogênese Brasiliana. O minério está associado às camadas confinadas a dobras recumbentes e em bainha, superpostas por dobras isoclinais e normais, seguidas por deslocamentos e fraturas de alto ângulo (Biondi, 1990; Fuck et al., 2007). A migração de fluidos hidrotermais foi proporcionada pela deformação

dúctil-frágil através de planos de fratura e foliação, lineação de estiramento e quaisquer outros canais formados por contatos litológicos mais permeáveis (Giuliani et al., 1997).

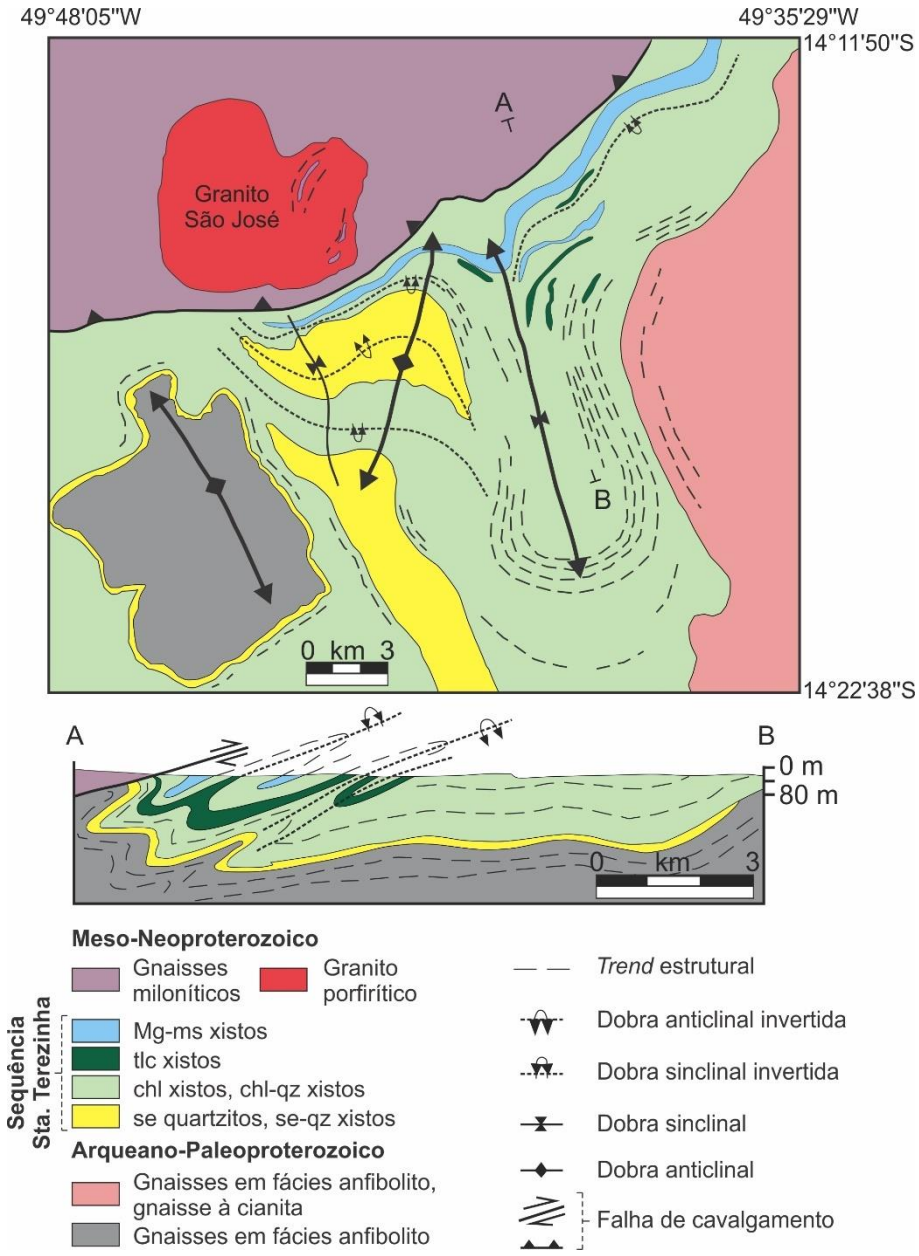

Figura 2.6. Mapa geológico e perfil geológico simplificados do distrito esmeraldífero de Santa Terezinha de Goiás. Adaptado de D'el-Rey Silva e Barros Neto (2002). chl: clorita; Mg-ms: muscovita magnesiana; qz: quartzo; tlc: talco; se: sericita.

Análise da composição isotópica de δD em esmeralda e flogopita apontam tanto para origem metamórfica quanto magmática do fluido mineralizante em Santa Terezinha (Giuliani et al., 1997); entretanto, uma origem metamórfica tem sido apresentada devido à ausência de granitos e pegmatitos, à baixa concentração de berílio na sequência vulcanossedimentar (Be <

2 ppm) e o forte controle estrutural por zonas de cisalhamento (Giuliani et al., 2019). Além disso, cristais de flogopita do flogopitito mineralizado forneceram idades $^{40}Ar/^{39}Ar$ de 520 ± 2 Ma intimamente ligadas a deformação brasiliana (Ribeiro-Althoff et al., 1997). Em contrapartida, Aurisicchio et al. (2018) apontam que o elevado conteúdo de Cs suporta a hipótese de que fluidos magmáticos possam ter se misturado com fluidos de origem metamórfica durante a cristalização de esmeralda, corroborando com diversos trabalhos que sugerem que o granito porfirítico sin-tectônico São José, localizado a poucos mais de 5 km a noroeste do depósito, seja a possível fonte de Be para esmeralda (D'el-Rey Silva e Giuliani, 1988; Giuliani et al., 1990; D'el-Rey Silva e Barros Neto, 2002; Fuck et al., 2007).

DEPÓSITOS DE ESMERALDA NA PROVÍNCIA BORBOREMA

A Província Borborema (Almeida et al., 1981) é caracterizada por domínios gnáissico-migmatíticos com idades que variam do Arqueano ao Paleoproterozoico e que ocorrem sotopostos ou em contato tectônico com domínios cedo a tarde neoproterozoicos, englobando sequências de rochas supracrustais intrudidas por vasto magmatismo granítico, sendo fortemente deformada durante a Orogênese Brasiliana-Panafricana (Brito Neves et al., 2000, 2014).

Diversos autores, com base em dados estruturais, geofísicos e geocronológicos, dividem a Borborema em domínios ou subprovíncias limitadas por lineamentos e/ou zonas de cisalhamento de escala regional a continental (*e.g.* Brito Neves et al., 2000; Van Schmus et al., 2008; Santos et al., 2010; Santos et al., 2017, 2018). De acordo com a revisão realizada por Santos et al. (2014) e referências ali contidas, podem ser reconhecidas:

- três subprovíncias ao norte da Zona de Cisalhamento Patos, denominadas Médio Coreaú, Ceará Central e Rio Grande do Norte (juntas convencionalmente conhecidas como Subprovíncia Norte ou Setentrional);
- a Subprovíncia Transversal, situada entre as zonas de cisalhamento Patos e Pernambuco;
- a Subprovíncia Meridional que se encontra ao sul da Zona de Cisalhamento Pernambuco (Figura 2.7).

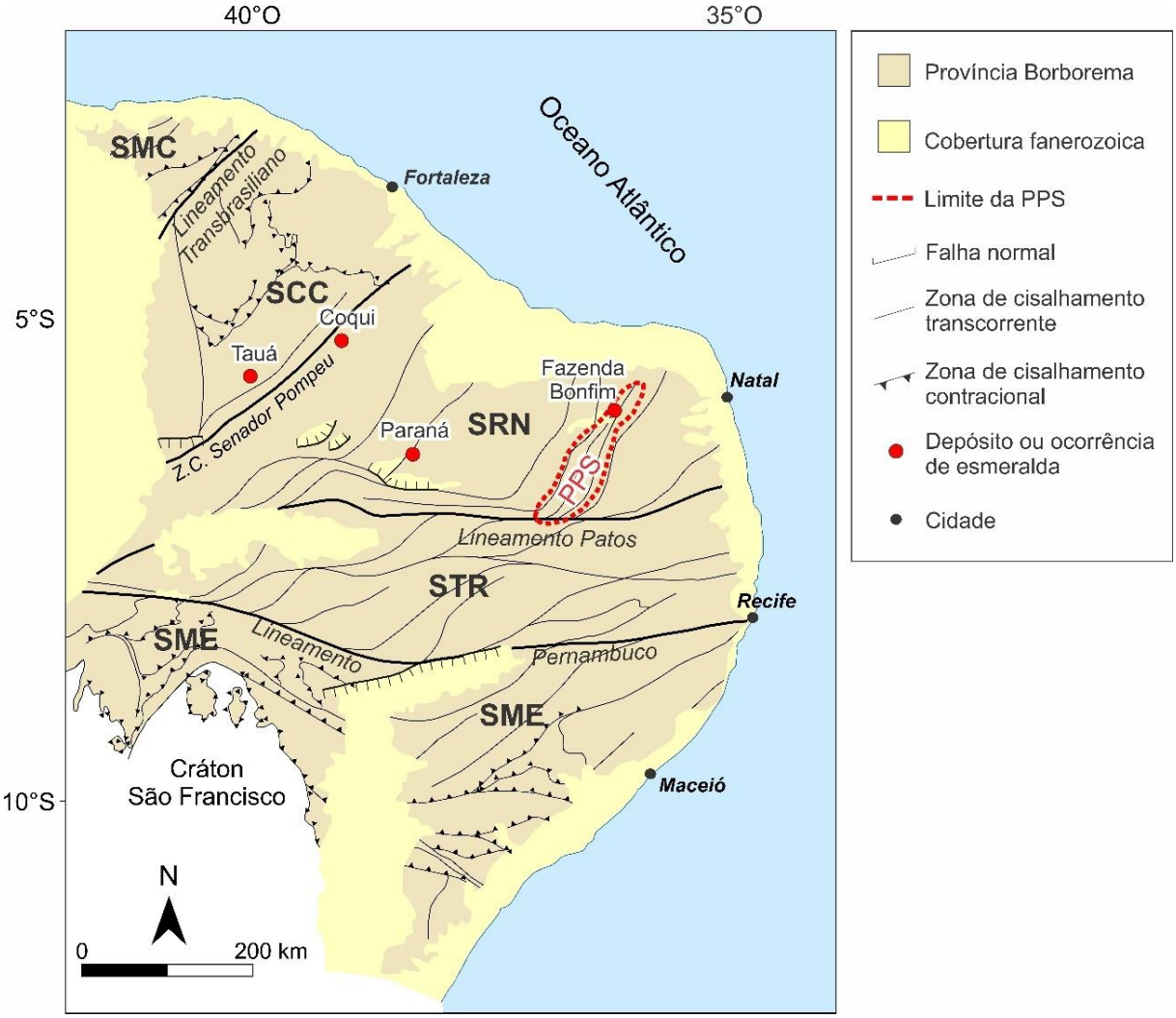

Figura 2.7. Localização dos principais depósitos e ocorrências de esmeralda da Província Borborema. PPS: Província Pegmatítica do Seridó; SMC: Subprovíncia Médio Coreaú; SCC: Subprovíncia Ceará Central; SRN: Subprovíncia Rio Grande do Norte; STR: Subprovíncia Transversal; SME: Subprovíncia Meridional. Modificado de Santos et al. (2014).

Considerada o maior evento tectônico que moldou as províncias neoproterozoicas sul-americanas, a Orogênese Brasiliana-Panafricana apresenta grande representatividade não só na Província Borborema como em todos os cinturões orogênicos que compõem o Gondwana Ocidental, concebendo importantes evidências para a reconstrução desse supercontinente, especialmente ao conectar o nordeste do Brasil ao centro-oeste da África (Caxito et al., 2020 e referências ali contidas). Segundo Brito Neves et al. (2014), a colagem orogênica crustal brasiliana se deu em quatro intervalos distintos:

- eocriogeniano (ca. 800-750 Ma);
- tardicriogeniano-eoediacarano (ca. 660 – 610 Ma);

- eo-médio ediacarano (ca. 590 – 560 Ma);
- tardicambriano (520 – 500 Ma).

Os estágios finais dessa colagem orogênica são marcados por uma rede complexa de zonas de cisalhamento dúctil transcorrentes de natureza transcontinental (600 – 500 Ma; Vauchez et al., 1995; Archanjo et al., 2008; Ganade de Araújo et al., 2014).

A estruturação final da Província Borborema ao fim da era Neoproterozoica e início do período Cambriano favoreceu a formação de diversos depósitos e/ou ocorrências minerais (*e.g.* Araújo et al., 2005; Pereira et al., 2019), incluindo ocorrências de esmeralda confinadas ao longo de zonas de cisalhamento transcorrentes, cujo pico metamórfico foi estimado em 566 ± 6 Ma (Viegas et al., 2014).

Os principais depósitos e/ou ocorrências aqui abordados são: Fazenda Bonfim (RN), Tauá e Coqui (CE) e Paraná (RN) (Figura 2.7).

Fazenda Bonfim

O depósito de Fazenda Bonfim, no centro-leste da Subprovíncia Rio Grande do Norte, é o mais recém-descoberto da Província Borborema. A esmeralda de Lajes, Caiçara do Rio dos Ventos e São Tomé, como foi inicialmente chamada, teve seu descobrimento de forma inesperada durante pesquisas de rochas ultrabásicas anômalas em Cr e Ni na região (Cavalcanti Neto e Barbosa, 2007). O depósito de esmeralda está situado na Faixa Seridó, região amplamente reconhecida pela presença de mais de 700 pegmatitos graníticos mineralizados em elementos raros (berílio, tântalo, nióbio, estanho) da Província Pegmatítica do Seridó, classicamente denominada Província Pegmatítica da Borborema (Da Silva et al., 1995; Beurlen et al., 2009; Santos et al., 2014).

Estes pegmatitos constituem fases tardias da atividade magmática brasiliana-panafricana (Souza Neto et al., 2008) e tiveram suas idades entre 480 e 510 Ma (U-Pb em uraninita; Ebert, 1970), em 523,1 ± 1,1 Ma ($^{40}Ar/^{39}Ar$ em biotita; Araújo et al., 2005) e entre 509,5 ± 2,9 Ma e 514,9 ± 1,1 Ma (U-Pb em columbita; Baumgartner et al., 2006). Nesse contexto, as mineralizações de esmeralda em Fazenda Bonfim ocorrem em corpos pegmatíticos recristalizados que ocorrem intercalados a talco-, talco-anfibólio-, biotita±anfibólio- e biotita xistos encaixados em gnaisses graníticos sob influência da Zona de Cisalhamento Santa Mônica (Zwaan et al., 2012) (Figura 2.8).

Scholz et al. (2010) conduziram trabalhos de mapeamento geológico e prospecção geoquímica de solos em 1.351 amostras, que revelaram áreas anômalas em berílio e cromo ao

longo da Zona de Cisalhamento Santa Mônica, de direção NNE-SSW. Santiago et al. (2019) apontam que os controles estruturais e contrastes litológicos foram fundamentais para percolação de fluidos e desenvolvimento dos flogopititos na zona metassomática de contato (*blackwall*). A mineralização de esmeralda foi fortemente controlada pela transcorrência brasiliana seguida de alojamento sin-cinemático de albita granitos ricos em Be, favorecendo processos hidrotermais/metassomáticos, serpentinização e talcificação de rochas metamáficas e/ou metaultramáficas e albitização de granitos e/ou pegmatitos preexistentes (Santiago et al., 2019).

Análises geocronológicas de amostras do albita granito forneceram idades de cristalização U-Pb em zircão de 561 ± 4 Ma, enquanto análises de amostras do flogopita xisto metassomático resultaram em idades ^{40}Ar-^{39}Ar de 553 ± 4 Ma, sugerindo que a esmeralda de Fazenda Bonfim se formou ao final da Orogênese Brasiliana, em um regime metassomático intenso mas de relativa curta duração, possivelmente devido ao baixo volume de magma intrusivo (Santiago et al., 2019). A combinação entre origem metassomática-hidrotermal, hospedagem em rocha máfica-ultramáfica, associação a granitos e pegmatitos berilíferos e um forte controle estrutural levaram Giuliani et al. (2019) a classificarem este depósito como tectono-magmático do tipo IA.

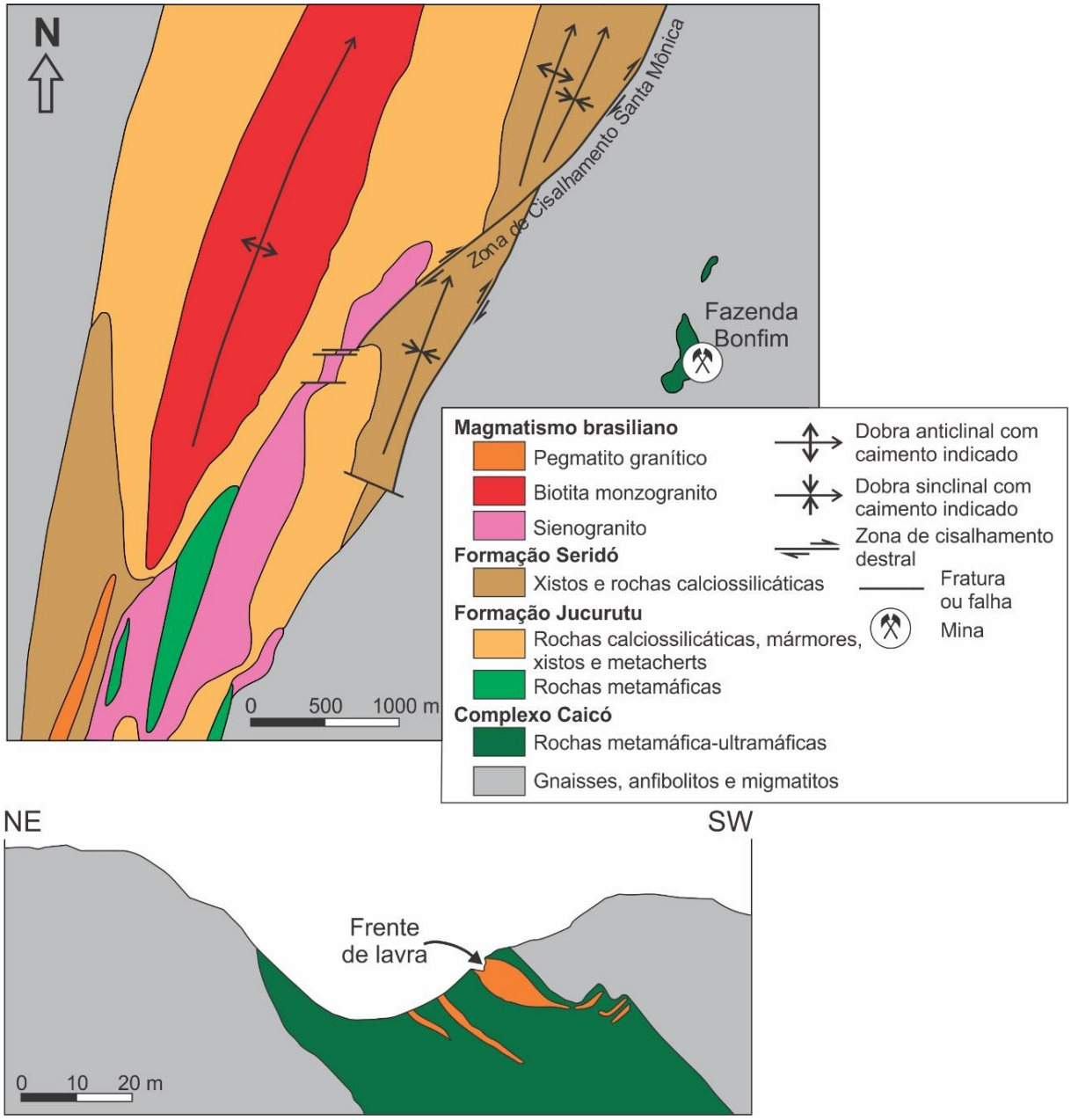

Figura 2.8. Mapa geológico simplificado da região de Fazenda Bonfim na Faixa de Dobramentos Seridó, com perfil esquemático da frente de lavra. Adaptado de Santiago et al. (2019).

Tauá e Coqui

A região de Tauá está inserida na porção sul da Subprovíncia Ceará Central. A ocorrência de Tauá, ou de Fazenda Boa Esperança, como era conhecida nas primeiras décadas de atividade garimpeira e de exploração mineral, é caracterizada pela presença de cristais de esmeralda de baixa qualidade (cor verde maçã) e em pouca quantidade, razão pela qual não são

explotadas atualmente. A extração de esmeralda por garimpeiros de forma esporádica teve início em 1954 e deu lugar, nos anos 1970, à exploração em maior escala pela empresa "Mineração São Pedro Ltda", que logo abandonou o projeto devido aos elevados custos de investimento (Korpershoek, 1983; Schwarz, 1987; Cavalcanti, 2015).

Segundo Schwarz (1987) e referências nele contidas, a esmeralda de Tauá está geologicamente inserida no Complexo Pedra Branca, uma unidade vulcanossedimentar de idade arqueana retrabalhada durante a Orogênese Brasiliana. Esta unidade compreende, localmente, rochas ultramáficas (transformadas em talco xistos, talco-tremolita xistos e tremolititos), metabasitos (anfibolitos e hornblenda gnaisses), biotita gnaisses e biotita xistos esmeraldíferos.

Diversos corpos pegmatíticos homogêneos, de composição quartzo-albítica, ocorrem sob forma alongada e irregular ou como intrusões concordantes, de granulação grossa a fina (aplitos, nas porções mais afetadas pela deformação tectônica), podendo conter cristais de berilo, columbita-tantalita, turmalina, apatita, molibdenita e bismutita (Cassedanne et al., 1979). Korpershoek (1983) propõe que estes são provavelmente pegmatitos anatéticos, mobilizados localmente durante metamorfismo regional através de fusão parcial. Os biotita xistos esmeraldíferos teriam se formado em uma zona metassomática de contato entre os pegmatitos e rochas básicas-ultrabásicas contendo cromo, ferro e vanádio.

Trabalhos recentes de mapeamento em escala 1:100.000, realizados pelo Serviço Geológico do Brasil, apresentam atualizações referentes ao conhecimento estratigráfico regional, porém pouco foi alterado com relação às ocorrências de esmeralda. Cavalcante et al. (2003) cunharam o termo Complexo Cruzeta, em substituição ao Complexo Pedra Branca, e o subdividiram nas unidades Tróia, Indiferenciado e Mombaça. Cavalcanti (2015) reconhece no Complexo Cruzeta as unidades Tróia, Pedra Branca e Mombaça e assinala que as ocorrências de esmeralda de Tauá estão inseridas na unidade Tróia, em pegmatitos associados a flogopita xistos encaixados em um conjunto de rochas miloníticas. Segundo Almeida et al. (2007), as rochas neoarqueanas da unidade Tróia foram afetadas pelo Evento Brasiliano, que verticalizou os planos de foliação e os reorientou para direção NE, formando milonitos a ultramilonitos e gnaisses migmatíticos. Entretanto, todo o Complexo Cruzeta e suas unidades teriam sidos pouco afetados pela granitogênese neoproterozoica, com granitos bordejando o núcleo arqueano, na medida em que esse se mantinha rígido e coeso. Ainda de acordo com Almeida et al. (2007), o único representante litológico do Evento Brasiliano nessa região são corpos métricos de pegmatitos, intrudidos em falhas extensionais tardi-transcorrência, o que sugere

que os xistos esmeraldíferos de origem metassomática tenham provavelmente se formado nos estágios finais da Orogênese Brasiliana.

Ainda no estado do Ceará, as ocorrências de esmeralda de Coqui (Figura 2.9), localidade do município de Quixeramobim, estão associadas a pequenos corpos pegmatíticos em faixas de biotita xisto e tremolititos intercalados com o embasamento gnáissico (Castelo Branco et al., 1988). A área encontra-se inserida na faixa de dobramentos Jaguaribeana, em uma região intensamente afetada por deformação dúctil, entre as zonas de cisalhamento Senador Pompeu (a oeste) e Orós (a leste). A mineralização em Coqui está diretamente relacionada às intrusões pegmatíticas pertencentes ao Distrito Pegmatítico Solonópole-Quixeramobim, reconhecida pela presença de água-marinha, columbita-tantalita, cassiterita e minerais de lítio. Reações metassomáticas entre pegmatitos berilíferos e rochas básicas metamorfizadas são os prováveis mecanismos de formação dos flogopititos esmeraldíferos (Castelo Branco et al., 1988). No entanto, assim como em Tauá, a esmeralda de Coqui não possui interesse econômico. Em ambos os casos, os cristais são por vezes chamados de “berilo verde”, um termo mais comercial do que científico, comumente utilizado para denominar “esmeralda” de cor menos saturada (Walton, 2004).

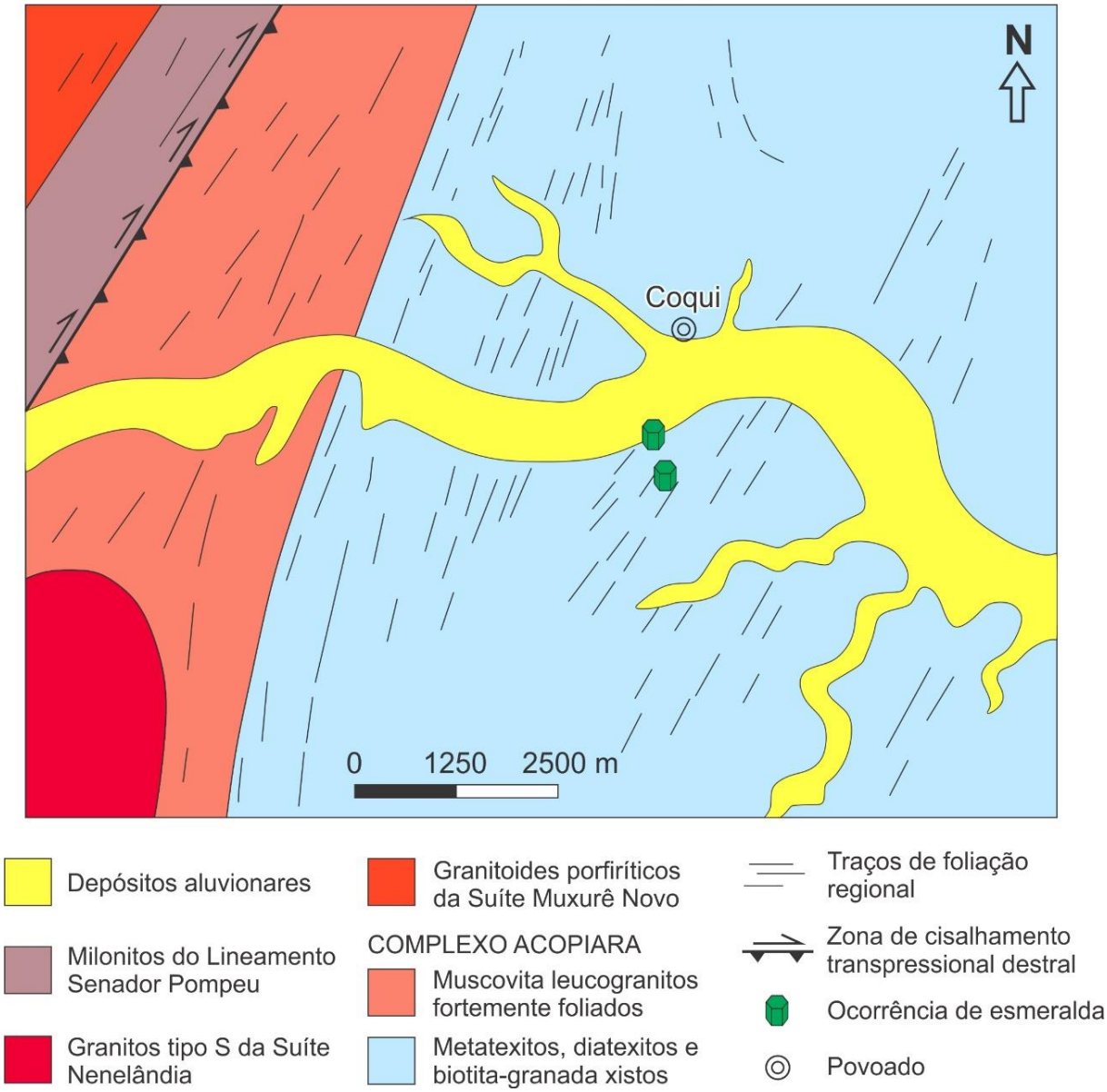

Figura 2.9. Mapa geológico simplificado da região de Coqui. Adaptado de Castelo Branco et al. (1988) e Almeida et al. (2007).

Na classificação de Giuliani et al. (1997) dos depósitos de esmeralda brasileiros entre depósitos do Tipo I (associado a pegmatitos) e do Tipo II (ligado a zonas de cisalhamento dúctil), as ocorrências de Tauá e Coqui foram consideradas como do Tipo I devido à evidente associação com pegmatitos graníticos contendo berilo. Entretanto, valores de $\delta^{18}O$ de +12,1‰ para esmeralda de Coqui já indicavam uma possível participação de fluidos metamórficos ($\delta^{18}O$ entre +12,0‰ e +12.4‰). Giuliani et al. (2019) reconhecem a participação de estruturas tectônicas na formação dessas mineralizações, reclassificando-as como do Tipo IA: tectono-magmático hospedados em rochas máficas/ultramáficas.

Paraná

Descobertas há cerca de 40 anos, as mineralizações de esmeralda no município de Paraná (RN) foram inicialmente descritas por Vasconcelos (1984), que descreveu cristais de esmeralda em veios de quartzo, diques aplíticos e pegmatoides intercalados em flogopita-xistos, que por sua vez, estão encaixados de forma concordante nos ortognaisses do Complexo Caicó (embasamento da região). Localizadas no centro-oeste da Subprovíncia Rio Grande do Norte, essas mineralizações foram incluídas por Moraes (1999) como parte do Distrito Gemológico do Extremo Sudoeste (DGSW) do estado do Rio Grande do Norte, que também abrange pegmatitos ricos em água-marinha da cidade de Tenente Ananias (RN).

Sete ocorrências do flogopita-xisto hospedeiro foram catalogadas por Moraes (1999). Essas rochas ocorrem de forma lenticular ao longo da Zona de Cisalhamento Portalegre (ZCPA) (Figura 2.10), em associação com pegmatitos graníticos. Devido a essa configuração, Moraes (2000) propõe que essa faixa esmeraldífera corresponde a um depósito de características mistas dentro da classificação tipológica de Giuliani et al. (1997). Esses dados geológico-estruturais foram corroborados em relatórios técnicos de mapeamento nas escalas 1:250.000 (SB.24-Z-A; Medeiros, 2008) e 1:100.000 (SB.24-Z-A-II; Souza, 2017) realizados pelo Serviço Geológico do Brasil.

Durante a década de 1990, os cristais de esmeralda em Paraná foram “exauridos” devido à extração garimpeira. As atividades de pesquisa na região apenas foram retomadas nos últimos 10 anos, após a aquisição dos direitos de pesquisa pela empresa Mineração Limeira Comércio, Exportação e Importação Ltda, que aperfeiçoou os antigos serviços garimpeiros e investiu em estratégias prospectivas.

Trabalhos mais recentes apontam para ocorrência de esmeralda tanto nos veios e vênulas de composição granítica/ácida (Figuras 2.11A, e 11B) como no interior dos planos de foliação em flogopita xistos (Figura 2.11C) e actinolita-flogopita xistos (Araújo Neto, 2018). De acordo com Araújo Neto et al. (2019), os diques pegmatíticos associados ao depósito de Paraná possuem composição simples, constituídos majoritariamente por feldspato potássico, com quartzo, muscovita e granada ocorrendo de forma subordinada. Diques métricos de albitito foram identificados em subsuperfície (Figura 2.11D), adjacentes aos gnaisses encaixantes e xistos esmeraldíferos. A presença de albititos (prováveis pegmatitos dessilicados) e a variação composicional dos xistos máficos, que inclui ainda ocorrências pontuais de flogopita-fengita xistos (até então estéreis), sugerem origem metassomática para essas mineralizações, com variações no processo metassomático (Araújo Neto, 2018). O evidente controle estrutural

condicionado pela ZCPA e a ligação com fontes magmáticas aponta para um depósito tectono-magmático do tipo IA, conforme classificação de Giuliani et al. (2019).

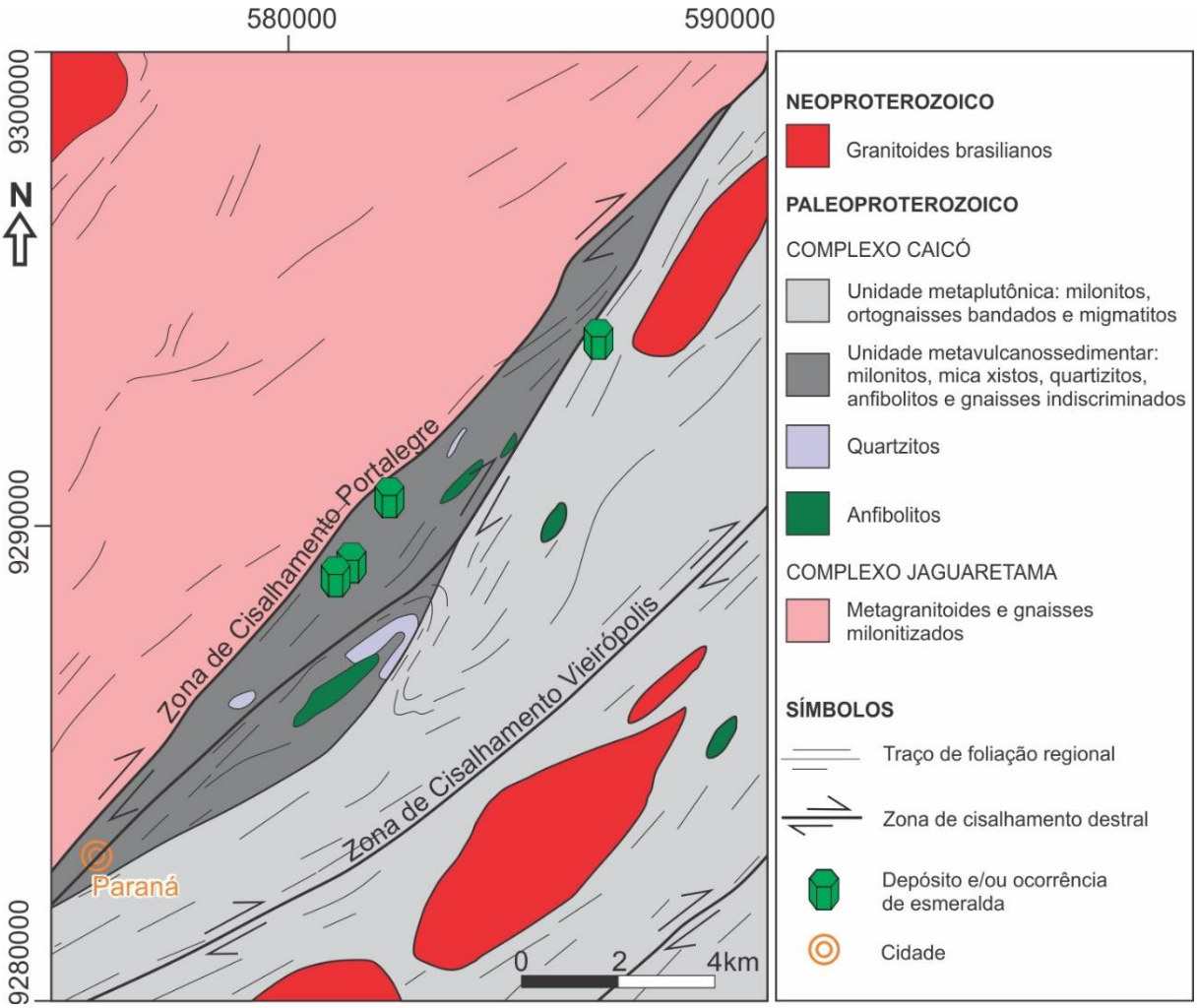

Figura 2.10. Mapa geológico simplificado da região de Paraná com localização das principais ocorrências de esmeralda ao longo da Zona de Cisalhamento Portalegre. Adaptado de Araújo Neto et al. (2018).

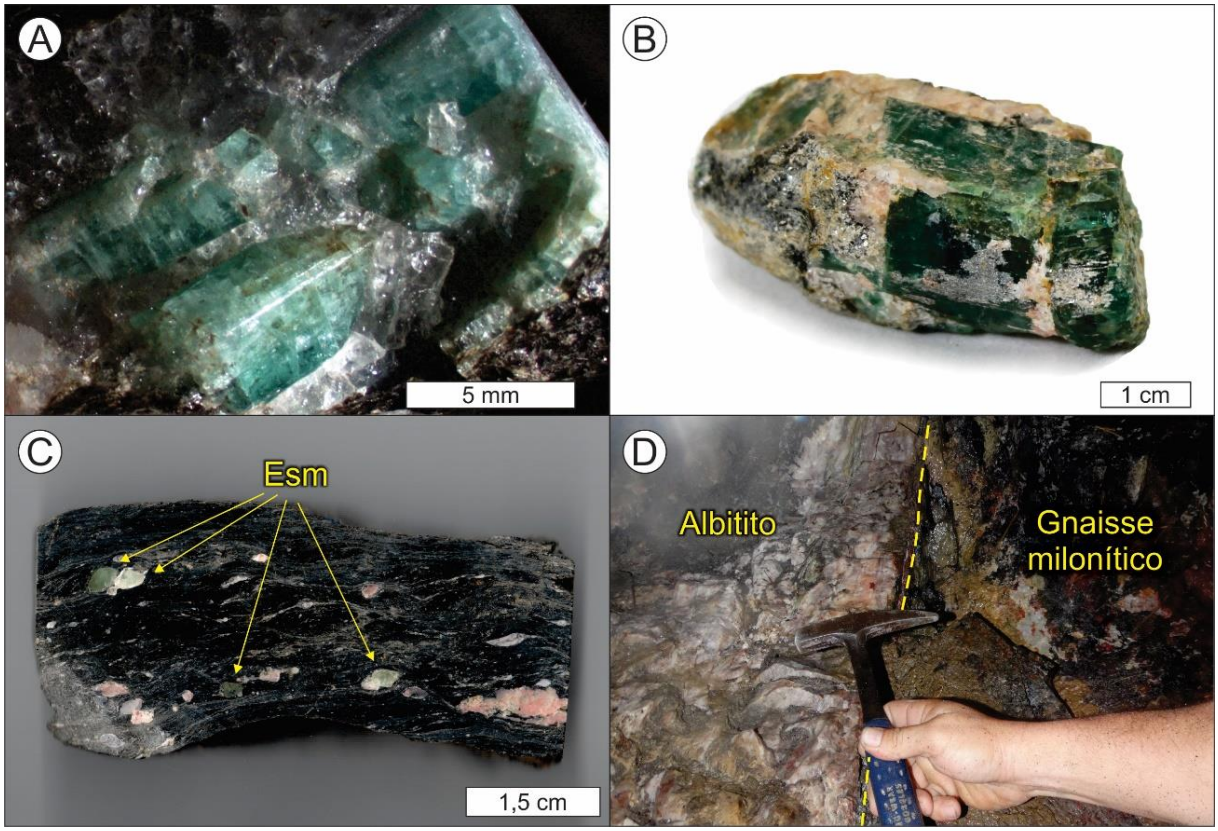

Figura 2.11. Aspectos do depósito de esmeralda de Paraná; (A) prismas de esmeralda em veio de quartzo no interior de flogopita xisto; (B) esmeralda em matriz granítica-pegmatítica; (C) cristais de esmeralda deformados ao longo da foliação do flogopita xisto; (D) dique de albitito no interior do shaft Pitombeiras no depósito de Paraná.

Estudos preliminares ao longo da ZCPA sugerem que um componente extensional concomitante à transcorrência (i.e., regime transtensional) tenha possibilitado a ascensão dos fluidos pegmatíticos contendo Be que viriam a interagir com o Cr das rochas metabásicas do Complexo Caicó para formar esmeralda durante a orogênese Brasiliana (Araújo Neto e Santos, 2019). Diversos corpos pegmatíticos de direção NE-SW, paralelos a subparalelos à foliação milonítica e a presença de pegmatitos mineralizados em água-marinha nas municipalidades vizinhas (*e.g.* água-marinha de Tenente Ananias e de Vieirópolis; Barreto, 1991 e Lira Santos et al., 2020, respectivamente) apoiam uma fonte pegmatítica para o Be. Por outro lado, a fonte de Cr ainda é motivo de discussão, uma vez que rochas ultramáficas/ultrabásicas não foram encontradas na região. Até então, lentes metabásicas de anfibolitos da unidade metavulcanossedimentar do Complexo Caicó, que ocorrem ao longo da ZCPA, são citadas como fortes candidatas a fonte de Cr e Fe para a esmeralda de Paraná (Souza, 2017; Araújo Neto et al., 2019). A possibilidade de uma fonte metabásica é suportada pelos baixos teores de

Cr e V e altos teores de Fe que tornam as esmeraldas de Paraná, até então, as mais proporcionalmente enriquecidas em Fe do Brasil (Araújo Neto et al., 2019). Outra hipótese é a de que o metassomatismo tenha se dado entre pegmatitos e xistos máficos preexistentes. Neste caso, elementos como Fe, Mg, Cr e V seriam apenas remobilizados durante alteração hidrotermal, enquanto o aporte de Be, Al, Si e Na se daria através das injeções pegmatíticas.

CONSIDERAÇÕES FINAIS

A importância do metamorfismo regional no desenvolvimento de mineralizações de esmeralda é reconhecida desde os primeiros esforços de classificação tipológica de depósitos. As classificações mais recentes que consideram a formação de esmeralda em múltiplos estágios e que refletem a possibilidade de mistura entre fatores magmáticos e metamórficos representam o futuro para estudos de gênese e de exploração mineral. Os principais depósitos brasileiros possuem uma relação tectono-magmática fundamental para formação de esmeralda. É o caso de Itabira-Nova Era (MG) e de Carnaíba (BA). Mesmo em depósitos tipificados como tectono-metamórficos, como o de Santa Terezinha (GO), não se descarta a participação de fluidos magmáticos.

Na região Nordeste do país, a configuração tectono-estrutural atual da Província Borborema, atingida nos estágios finais da colagem orogênica brasiliana (ca. 600 – 500 Ma) foi um importante agente catalizador para formação de mineralizações de esmeralda. Neste período, o desenvolvimento de diversas zonas de cisalhamento transcorrentes (Figura 2.12) espacialmente associadas a rochas básicas/ultrabásicas foram fundamentais tanto para alcançar o gradiente térmico necessário para estabilidade da esmeralda, quanto para permitir a percolação de fluidos e mobilização dos elementos cromóforos Cr, V e Fe.

Entretanto, apesar do Evento Brasiliano ter configurado a Província Borborema, com desenvolvimento de extensas zonas de cisalhamento transcorrentes em todas as três subprovíncias, as mineralizações de esmeralda parecem estar, até então, associadas exclusivamente à Subprovíncia Setentrional. Esta limitação pode estar ligada à presença restrita de fontes de berílio, essencial para formação de esmeralda. De fato, na Subprovíncia Setentrional estão localizadas as principais províncias, distritos e campos pegmatíticos com berílio da Borborema, a maioria deles contendo cristais de berilo na variação água-marinha. Vale ainda ressaltar a proximidade de poucos quilômetros entre essas regiões berilíferas e os depósitos e ocorrências de esmeralda. É o caso da Província Pegmatítica do Seridó e o depósito de esmeralda de Fazenda Bonfim, do Distrito Pegmatítico Solonópole-Quixeramobim e a

ocorrência de esmeralda de Coqui, e do Campo Pegmatítico de Vieirópolis e dos pegmatitos de Tenente Ananias e o depósito de esmeralda de Paraná. Isso implica que a presença de pegmatitos berilíferos, de rochas básicas/ultrabásicas e de estruturas tectônicas, especialmente de regime dúctil, são os mais importantes metalotectos para prospecção de jazidas de esmeralda na Província Borborema.

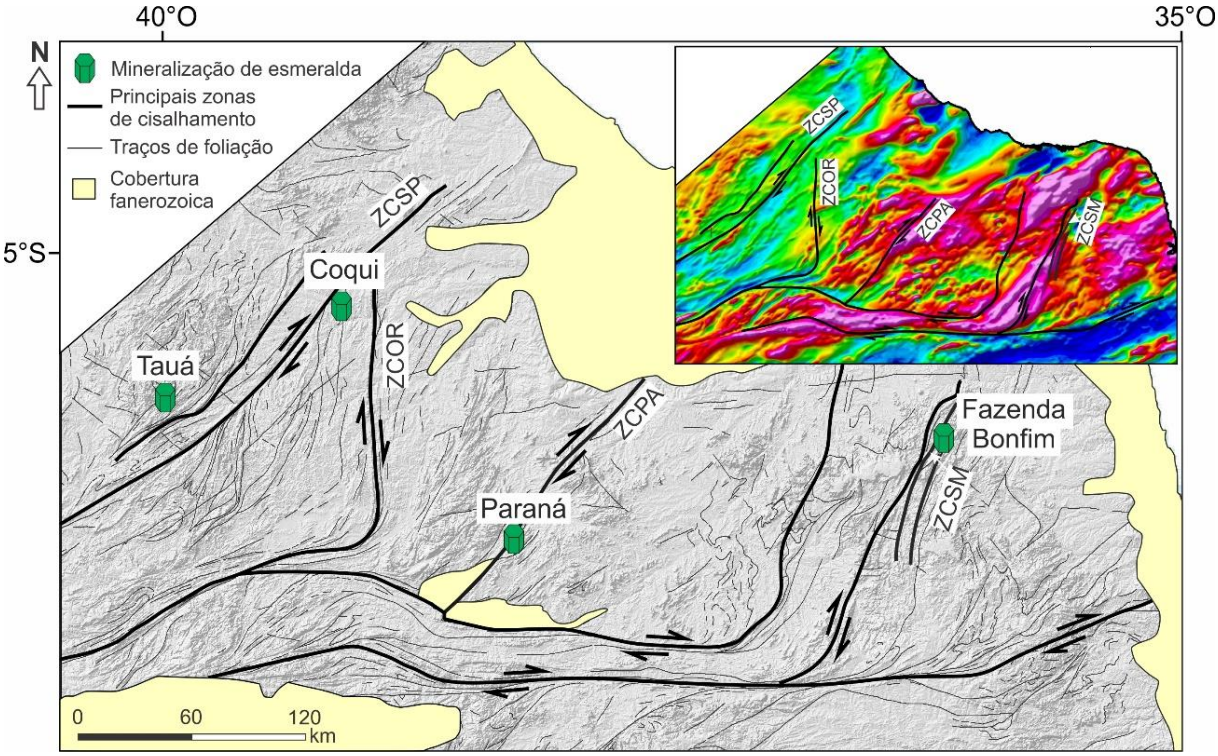

Figura 2.12. Mapa estrutural simplificado da Subprovíncia Setentrional com localização das mineralizações de esmeralda da Província Borborema ao longo de zonas de cisalhamento transcorrentes. Na margem superior direita, expressão dessas estruturas sobre mapa de anomalia magnética reduzida ao polo. ZCSP: Zona de Cisalhamento Senador Pompeu; ZCOR: Zona de Cisalhamento Orós; ZCPA: Zona de Cisalhamento Portalegre; ZCSM: Zona de Cisalhamento Santa Mônica.

Depósitos tectono-magmáticos do tipo IA nos estados de Minas Gerais e Bahia correspondem aos mais importantes produtores de esmeralda em esfera nacional. Na Província Borborema, estes depósitos, ainda que possuam menor importância econômica, correspondem a uma fonte promissora desse mineral gemológico, tendo em vista que investigações controladas em subsuperfície tiveram início há pouco mais de uma década.

AGRADECIMENTOS

O presente trabalho foi realizado com apoio da Coordenação de Aperfeiçoamento de Pessoal de Nível Superior - Brasil (CAPES) - Código de Financiamento 001, e é parte integrante da pesquisa de doutorado do primeiro autor na Universidade Federal de Pernambuco. Os autores gostariam de expressar sua gratidão à Prof.ª Dr.ª Sandra de Brito Barreto pelo incentivo a esta pesquisa, bem como ao Sr. Luis Amorim e toda a equipe da Mineração Limeira Comércio, Exportação e Importação pelo suporte logístico dado aos estudos de campo em Paraná-RN.

REFERÊNCIAS

Almeida, A. F., Parente, C. V., Arthaud, M. H. (Eds.) (2007). *Quixeramobim - SB.24-V-D-III*. Escala 1:100.000: nota explicativa integrada com Boa Viagem e Itatira. Ceará: UFC/CPRM, 196 p.

Almeida, F. F. M., Hasui, Y., Brito Neves, B. B., Fuck, R. A. (1981). Brazilian structural provinces: an introduction. *Earth Science Reviews*, 17(1-2), 1-29. https://doi.org/10.1016/0012-8252(81)90003-9

Araújo, M. N. C., Vasconcelos, P. M., Alves da Silva, F. C., Jardim de Sá, E., Sá, J. M. (2005). $^{40}Ar/^{39}Ar$ geochronology of gold mineralization in Brasiliano strike-slip shear zone in the Borborema Province, NE Brazil. *Journal of South American Earth Sciences*, 19, 445-460. https://doi.org/10.1016/j.jsames.2005.06.009

Araújo Neto, J. F. (2018). *Caracterização da esmeralda do município de Paraná, estado do Rio Grande do Norte, Brasil*. Dissertação (Mestrado). Recife: Centro de Tecnologia e Geociências – UFPE.

Araújo Neto, J. F., Barreto, S. B., Carrino, T. A., Müller, A., Santos, L. C. M. L. (2019). Mineralogical and gemological characterization of emerald crystals from Paraná deposit, NE Brazil: a study of mineral chemistry, absorption and reflectance spectroscopy and thermal analysis. *Brazilian Journal of Geology*, 49(3), 1-15. https://doi.org/10.1590/2317-4889201920190014

Araújo Neto, J. F., Lira Santos, G., Souza, I. M. B. A., Barreto, S. B., Santos, L. C. M. L., Bezerra, J. P. S., Carrino, T. A. (2018). Integration of remote sensing, airborne geophysics and structural analysis to geological mapping: a case study of the Vieirópolis region, Borborema Province, NE Brazil. *Geologia USP. Série Científica*, 18(3), 89-103. https://doi.org/10.11606/issn.2316-9095.v18-140834

Araújo Neto, J. F., Santos, L. C. M. L. (2019). O papel da Zona de Cisalhamento Portalegre no controle das mineralizações de esmeralda do sudoeste do Rio Grande do Norte: considerações preliminares. *XXVIII Simpósio de Geologia do Nordeste*, 505. Aracajú: SBG - Núcleo Nordeste.

Archanjo, C. J., Hollanda, M. H. B. M., Rodrigues, S. W. O., Brito Neves, B. B., Armstrong, R. (2008). Fabrics of pre- and syntectonic granite plutons and chronology of shear zones in the Eastern Borborema Province, NE Brazil. *Journal of Structural Geology*, 30(3), 310-326. https://doi.org/10.1016/j.jsg.2007.11.011

Aurisicchio, C., Conte, A. M., Medeghini, L., Ottolini, L., De Vito, C. (2018) Major and trace element geochemistry of emerald from several deposits: Implications for genetic models and classification schemes. *Ore Geology Reviews*, 94, 351-366. https://doi.org/10.1016/j.oregeorev.2018.02.001

Barreto, S. B. (1991). *Caracterização químico-mineralógica dos berilos de Tenente Ananias – RN*. Dissertação (Mestrado). Recife: Instituto de Geociências - UFPE.

Barton, M. D., Young, S. (2002). Non-pegmatitic deposits of beryllium: mineralogy, geology, phase equilibria and origin. In: Grew, E.S. (Ed.). Beryllium: Mineralogy, Petrology, and Geochemistry. *Reviews in Mineralogy and Geochemistry*, 50(1), 591-691. https://doi.org/10.2138/rmg.2002.50.14

Baumgartner, R., Romer, R. L., Moritz, R., Sallet, R., Chiaradia, M. (2006). Columbite–tantalite-bearing granitic pegmatites from the Seridó Belt, northeastern Brazil: genetic constraints from U–Pb dating and Pb isotopes. *The Canadian Mineralogist*, 44(1), 69-86. https://doi.org/10.2113/gscanmin.44.1.69

Beurlen, H., Barreto, S. B., Martin, R., Melgarejo, J., Da Silva, M. R. R., Souza Neto, J. A. (2009) The Borborema Pegmatite Province, NE-Brazil revisited. *Estudos Geológicos*, 19(2), 62-66. http://dx.doi.org/10.18190/1980-8208/estudosgeologicos.v19n2p62-66

Biondi, J. C. (1990). Depósitos de esmeralda de Santa Terezinha (GO). *Revista Brasileira de Geociências*, 20, 7-24.

Brito Neves, B. B., Fuck, R. A., Pimentel, M. M. (2014). The Brasiliano collage in South America: a review. *Brazilian Journal of Geology*, 44(3), 493-518. https://doi.org/10.5327/Z2317-4889201400030010

Brito Neves, B. B., Santos, E. J., Van Schmus, W. R. Q. (2000). Tectonic history of the Borborema Province. In: Cordani, U.G., Milani E.J., Thomaz Filho A., Campos D.A. (Org.). Tectonic Evolution of South America. Rio de Janeiro, *31st International Geological Congress Special Publication*, 151-182.

Calligaro, T., Dran, J. C., Poirot, J. P., Querré, G., Salomon, J., Zwaan, J. C. (2000). PIXE/PIGE characterisation of emeralds using an external micro-beam. *Nuclear Instruments and Methods in Physics Research Section B*, 161-163, 769-774. https://doi.org/10.1016/S0168-583X(99)00974-X

Cassedanne, J. P., Cassedanne, J. O., Mello, Z. F. (1979). As esmeraldas de Tauá e Pilão Arcado. *Mineração Metalúrgica*, 43(410), 50-58.

Castelo Branco, R. M. G, Giuliani, G., Cheilletz, A., Clementeile, L. (1988). Os berilos verdes da região de Coqui, município de Quixeramobim: novas ocorrências de esmeraldas no estado do Ceará. *XXXV Congresso Brasileiro de Geologia*. Belém: SBG.

Cavalcante, J. C., Vasconcelos, A. M, Gomes, F. E. M., Medeiros, M. F., Paiva, I. G. (2003). *Atlas digital de geologia e recursos minerais do Ceará*. Escala 1:500.000. Fortaleza: CPRM.

Cavalcanti, J. A. D. (Ed.). (2015). *Geologia e recursos minerais da Folha Várzea do Boi SB.24-V-B-IV: estado do Ceará*. Fortaleza: CPRM.

Cavalcanti Neto, M. T. O., Barbosa, R. V. N. (2007). As esmeraldas de Lajes, Caiçara do Rio dos Ventos e São Tomé/RN. *Holos*, 2, 92-104. https://doi.org/10.15628/holos.2007.103

Caxito, F. A., Santos, L. C. M. L., Ganade, C. E., Bendaoud, A., Fettous, E-H., Bouyo, M. H. (2020). Toward an integrated model of geological evolution for NE Brazil-NW Africa: The Borborema Province and its connections to the Trans-Saharan (Benino-Nigerian and Tuareg shields) and Central African orogens. *Brazilian Journal of Geology*, 50(2), e20190122. https://doi.org/10.1590/2317-4889202020190122

Cornejo, C., Bartorelli, A. (2010). *Minerais e pedras preciosas do Brasil*. São Paulo: Solaris Edições Culturais.

Couto, P. A. A. (2000). *Mapa Gemológico do Estado da Bahia: Texto Explicativo*. Salvador: CPRM.

Da Silva, M. R. R., Höll, R. Beurlen, H. (1995). Borborema Pegmatitic Province: geological and geochemical characteristics. *Journal of South American Earth Sciences*, 8, 355-364. https://doi.org/10.1016/0895-9811(95)00019-C

D'el-Rey Silva, L. J. H., Giuliani, G. (1988). Controle estrutural da jazida de esmeraldas de Santa Terezinha de Goiás: Implicações na gênese, na têctonica regional e no planajamento de lavra. *XXXV Congresso Brasileiro de Geologia*, 1, 413-427. Belém: SBG.

D'el-Rey Silva, L. J. H., Barros Neto, L. S. (2002). The Santa Terezinha-Campos Verdes emerald district, central Brazil: structural and Sm-Nd data to constrain the tectonic evolution of the Neoproterozoic Brasília belt. *Journal of South American Earth Sciences*, 15(6), 693-708. https://doi.org/10.1016/S0895-9811(02)00087-1

Dereppe, J. M., Moreaux, C., Chauvaux, B., Schwarz, D. (2000). Classification of emeralds by artificial neural networks. *Journal of Gemmology*, 27, 93-105. https://doi.org/10.15506/JOG.2000.27.2.93

Ebert, H. (1970). The Precambrian geology of the Borborema Belt (State of Paraíba and Rio Grande do Norte, northeastern Brazil) and the origin of its mineral provinces. *Geologische Rundschau*, 59, 1299-1326.

Fersmann, A. (1929). Geochemische Migration der Elemente. *Abhandlungen zur praktishen Geologie und Bergwirtschaftslenhre*, 18, 74-118.

Fuck, R. A., Dantas, E. L., De Sordi, D. A., Chiarini, M. F. N., Oliveira, C. G. (2007). *Santa Terezinha de Goiás - SD.22-Z-A-III*. Escala 1:100.000: nota explicativa. Goiás: UnB/CPRM.

Ganade de Araújo, C., Rubatto, D., Hermann, J., Cordani, U. G., Caby, R., Basei, M. A. S. (2014). Ediacaran 2,500-km-long synchronous deep continental subduction in the West Gondwana Orogen. *Nature Communications*, 5, 5198. https://doi.org/10.1038/ncomms6198

Giuliani, G., Cheilletz, A., Arboleda, C., Carrillo, V., Rueda, F., Baker, J. H. (1995). An evaporitic origin of the parent brines of Colombian emeralds: fluid inclusion and sulphur isotope evidence. *European Journal of Mineralogy*, 7, 151-165.

Giuliani, G., France-Lanord, C., Zimmermann, J. L., Cheilletz, A., Arboleda, C., Charoy, B., Coget, P., Fontan, F., Giard, D. (1997). Fluid composition, δD of channel H_2O, and $\delta^{18}O$ of lattice oxygen in beryls: genetic implications for Brazilian, Colombian, and Afghanistani emerald deposits. *International Geology Reviews*, 39, 400-424. https://doi.org/10.1080/00206819709465280

Giuliani, G., Groat, L.A., Marshall, D., Fallick, A.E., Branquet, Y. (2019). Emerald Deposits: A Review and Enhanced Classification. *Minerals*, 9(2), 105. https://doi.org/10.3390/min9020105

Giuliani, G., Silva, L. J. H. D., Couto, P. (1990). Origin of emerald deposits of Brazil. *Mineralium Deposita*, 25, 57-64. https://doi.org/10.1007/BF03326384

Griffon, J. C., Kremer, M. R., Misi, A. (1967). Estudo estrutural e genético da Jazida de Esmeralda de Carnaíba-BA. *Anais da Academia Brasileira de Ciências*, 39, 150-161.

Groat, L. A., Giuliani, G., Marshall, D. D., Turner, D. (2008). Emerald deposits and occurrences: A review. *Ore Geology Reviews*, 34:87-112. https://doi.org/10.1016/j.oregeorev.2007.09.003

Groat, L., Giuliani, G., Marshall, D., Turner, D. (2014). Emerald. In: Raeside, E.R. (Ed.). Geology of Gem Deposits, *Mineralogical Association of Canada, Short Course Series*, 44, 135-174.

Grundmann, G., Morteani, G. (1989). Emerald mineralisation during regional metamorphism: the Habachtal (Austria) and Leydsdorp (Transvaal, South Africa) deposits. *Economic Geology*, 84, 1835-1849. https://doi.org/10.2113/gsecongeo.84.7.1835

Kazmi, A. H., Snee, L. W. (1989). Geology of the world emerald deposits: a brief review. In: Kazmi, A.H.; Snee, L.W. (Eds.) *Emeralds of Pakistan – Geology, Gemology and Genesis, Geological Survey of Pakistan*. 13-38. New York: Elite Publishers Limited, Karachi, Pakistan and Van Nostrand Reinhold Company.

Korpershoek, H. R. (1983). *Report on the Boa Esperança emerald showing, Tauá, State of Ceará, Northeast Brazil*. Relatório Interno. Mineração São Pedro Ltda./MBL - Mineração Brasileira Ltda.

Lira Santos, G., Souza, I. M. B. A., Barreto, S. B., Araújo Neto, J. F., Müller, A. (2020). The Serra Branca amazonite pegmatite of the Vieirópolis pegmatite field, Paraíba, Brazil: a new and unusual megacrystic amazonite deposit. *The Canadian Mineralogist*, canmin.1900095. https://doi.org/10.3749/canmin.1900095

Medeiros, V. C. (Ed.). (2008). *Geologia e Recursos Minerais da Folha Sousa SB.24-Z-A*. Escala 1:250.000. Recife: CPRM – Serviço Geológico do Brasil.

Moraes, J. F. S. (1999). *Gemas do Estado do Rio Grande do Norte. Recife*. Relatório Técnico. CPRM – Serviço Geológico do Brasil.

Moraes, J. F. S. (2000). As ocorrências de esmeraldas do Estado do Rio Grande do Norte: uma nova tipologia de depósito. *XVIII Simpósio de Geologia do Nordeste*. Recife: SBG: Núcleo Nordeste.

Ottaway, T. L., Wicks, F. J., Bryndzia, L. T., Keyser, T. K., Spooner, E. T. C. (1994). Formation of the Muzo hydrothermal emerald deposit in Colombia. *Nature* 369, 552-554. https://doi.org/10.1038/369552a0

Pereira, L. C. L., Santos, L. C. M. L., Carrino, T. A. (2019). The role of airborne geophysics in the investigation of gold occurrences in the Itapetim Region, Borborema Province, Northeast Brazil. *Brazilian Journal of Geology*, 49(3), e20190028. https://doi.org/10.1590/2317-4889201920190028

Ribeiro-Althoff, A. M., Cheilletz, A., Giuliani, G., Féraud, G., Barbosa Camacho, G., Zimmermann, J. L. (1997). $^{40}Ar/^{39}Ar$ and K-Ar Geochronological Evidence for Two Periods (~2 Ga and 650 to 500 Ma) of Emerald Formation in Brazil. *International Geology Review*, 39(10), 924-937. https://doi.org/10.1080/00206819709465310

Rondeau, B., Notari, F., Giuliani, G., Michelou, J.-C., Martins, S., Fritsch, E., Respinger, A. (2003). La mine de Piteiras, Minas Gerais, nouvelle source d'émeraude de belle qualité au Brésil. *Revue de Gemmologie*, 148, 9-25.

Rudowski, L. (1989). *Pétrologie et géochimie des granites transamazoniens de Campo Formoso et Carnaíba (Bahia, Brésil) et des phlogopitites à émeraude associées*. Tese (Doutorado). Paris: Université Paris.

Santana, A. J., Moreira, M. D., Couto, P. A. A. (1995). *Esmeralda de Carnaíba e Socotó, Bahia: geologia e potencialidade econômica*. Salvador: CBPM.

Santiago, J. S., Souza, V. S., Dantas, E. L., Oliveira, C. G. (2019). Ediacaran emerald mineralization in Northeastern Brazil: the case of the Fazenda Bonfim Deposit. *Brazilian Journal of Geology*, 49(4), 1-14. https://doi.org/10.1590/2317-4889201920190081

Santos, E. J., Souza Neto, J. A., Silva, M. R. R., Beurlen, H., Cavalcanti, J. A. D., Silva, M. G., Dias, V. M., Costa, A. F., Santos, L. C. M. L., Santos, R. B. (2014). Metalogênese das porções norte e central da Província Borborema. In: Silva, M.G., Rocha Neto, M.B., Jost, H., Kuyumijan, R.M. *Metalogênese das províncias tectônicas brasileiras*. 343-388. Belo Horizonte: CPRM.

Santos, E. J., Van Schmus, W. R., Kozuch, M., Brito Neves, B. B. (2010). The Cariris Velhos tectonic event in northeast Brazil. *Journal of South American Earth Sciences*, 29(1), 61-76. https://doi.org/10.1016/j.jsames.2009.07.003

Santos, L. C. M. L., Dantas, E. L., Cawood, P. A., Lages, G. A., Lima, H. M., Santos, E. J. (2018). Accretion tectonics in western Gondwana deduced from Sm-Nd isotope mapping of terranes in the Borborema Province, NE Brazil. *Tectonics*, 37, 2727-2743. https://doi.org/10.1029/2018TC005130

Santos, L. C. M. L., Dantas, E. L., Vidotti, R. M., Cawood, P. A., Santos, E. J., Fuck, R. A., Lima, H. M. (2017). Two-stage terrane assembly in Western Gondwana: Insights from structural geology and geophysical data of central Borborema Province, NE Brazil. *Journal of Structural Geology*, 103, 167-184. https://doi.org/10.1016/j.jsg.2017.09.012

Satir, M. (1974). Rb-Sr-Altersbestimmungen and Glimmern der westlichen Hohen Tauern: interpretation und geologische Bedeutung. *Schweizerische Mineralogische und Petrographische Mitteilungen*, 54, 214-228.

Scholz, R., Romano, A. W., Belotti, F. M., Chaves, M. L. S. C. (2010). Prospecção geoquímica de berilo variedade esmeralda na região da Fazenda Bonfim (Lajes, RN). *Geociências*, 29(4), 613-621.

Schulz, B., Siegesmund, S., Steenken, A., Schoenhofer, R. Heinrichs, T. (2001). Geologie des ostalpinen Kristallins südlich des Tauernfensters zwischen Virgental und Pustertal. *Zeitschrift der Deutschen Geologischen Gesellschaft*, 152, 261-307. https://doi.org/10.1127/zdgg/152/2001/261

Schwarz, D. (1987). *Esmeraldas: inclusões em gemas*. Ouro Preto: Universidade Federal de Ouro Preto (UFOP), Imprensa Universitária.

Schwarz, D., Giuliani, G. (2001). Emerald deposits a review. *Australian Gemmologist*, 21, 17-23.

Schwarz, D., Giuliani, G., Grundmann, G., Glas, M. (2001). Die Entstehung der Smaragde, ein vieldisskutiertes Thema. In: Schwarz, D., Hochlitner, R. (Eds.) Smaragd, der kostbarste Beryll, der teuerste Edelstein. *Extra Lapis*, 21, 68-73.

Schwarz, D., Giuliani, G., Grundmann, G., Glas, M. (2002). The origin of emerald - A controversial topic. *Extra Lapis English*, 2, 18-21.

Sinkankas, J. (1989). *Emerald and other beryls*. Prescott: Geoscience Press. 665p.

Souza, L. C. (Ed.). (2017). *Geologia e Recursos Minerais da Folha Pau dos Ferros SB.24-Z-A-II*. Escala 1:100.000. Recife: CPRM - Serviço Geológico do Brasil / Universidade Federal do Rio Grande do Norte.

Souza Neto, J. A., Legrand, J. M., Volfinger, M., Pascal, M.-L., Sonnet, P. (2008). W–Au skarns in the Neo-Proterozoic Seridó Belt, Borborema Province in northeastern Brazil: an overview with emphasis on the Bonfim deposit. *Mineralium Deposita*, 43, 185-205. https://doi.org/10.1007/s00126-007-0155-1

Van Schmus, W. R., Oliveira, E. P., Silva Filho, A. F., Toteu, F., Penaye, J., Guimarães, I. P. (2008). Proterozoic Links between the Borborema Province, NE Brazil, and the Central African

Fold Belt. Geological Society, London, *Special Publications*, 294(1), 69-99. https://doi.org/10.1144/SP294.5

Vasconcelos, F. J. C. (1984). *Ocorrência de esmeralda em Pitombeiras, município de Paraná, Estado do Rio Grande do Norte*. Especialização em Gemologia. Belo Horizonte: Instituto de Geociências - UFMG.

Vauchez, A., Neves, S. P., Caby, R., Corsini, M., Egydio-Silva, M., Arthaud, M. H., Amaro, V. (1995). The Borborema shear zone system, NE Brazil. *Journal of South American Earth Sciences*, 8, 247-266. https://doi.org/10.1016/0895-9811(95)00012-5

Viegas, L. G. F., Archanjo, C. J., Hollanda, M. H. B. M., Vauchez, A. (2014). Microfabrics and zircon U–Pb (SHRIMP) chronology of mylonites from the Patos shear zone (Borborema Province, NE Brazil). *Precambrian Research*, 243, 1-17. https://doi.org/10.1016/j.precamres.2013.12.020

Walton, L. (2004). *Exploration criteria for coloured gemstone deposits in the Yukon*. Yukon: Yukon Geological Survey.

Zwaan, J. C. (2006). Gemmology, geology and origin of the Sandawana emerald deposits, Zimbabwe. Scripta Geologica, 131, 1-211.

Zwaan, J. C., Jacob, D. E., Haeger, T., Cavalcanti Neto, M. T. O., Kanis, J. (2012). Emeralds from the Fazenda Bonfim Region, Rio Grande do Norte, Brazil. *Gems & Gemology*, 48(1), 2-17.

3 ARTIGO CIENTÍFICO II – STRUCTURAL AND GEOCHRONOLOGICAL CONSTRAINTS ON THE PORTALEGRE SHEAR ZONE: IMPLICATIONS FOR EMERALD MINERALIZATION IN THE BORBOREMA PROVINCE, BRAZIL

Submitted in: *Journal of Structural Geology*
Submission date: January 23, 2023

José Ferreira de Araújo Neto[1*], Lauro Cézar Montefalco de Lira Santos[1], Carolina P. de Souza[2], Daniel Miggins[3], Peter A. Cawood[4]

[1]Department of Geology, Federal University of Pernambuco, Brazil; [2]Institute of Geosciences, University of Brasilia, Brazil; [3]College of Earth, Ocean and Atmospheric Sciences, Oregon State University, USA; [4]School of Earth, Atmosphere and Environment, Monash University, Australia

*Corresponding author: José Ferreira de Araújo Neto

ABSTRACT

Shear zones are efficient channels to drive mineralizing fluids within the crust. In the northern Borborema Province, NE Brazil, emerald occurrences are linked to strike-slip deformation associated with the final stages of the Neoproterozoic-Cambrian Brasiliano orogeny. We present aeromagnetic, meso- and micro-scale structural, and geochronologic data across the Portalegre shear zone to understand emerald formation at the Paraná deposit. In this region, shear zones are marked by conspicuous aeromagnetic anomalies that coincide with mapped mylonitic gneisses and schists with vertical to subvertical foliation in association with horizontal mineral stretching lineation. A dextral movement of shearing is supported by deformed asymmetric *augens* and pegmatite boudins, as well as S-C and S-C-C' surfaces. Emerald is found in phlogopite- and actinolite-phlogopite schists, and prismatic crystals occur parallel to the schist foliation plane. Deformation temperatures in the range of 390-530 °C are supported by microstructural analysis as evidenced by quartz recrystallization controlled by subgrain rotation. Zircon U-Pb ages of veins and *boudins* of granitic composition interleaved with the schist yielded ages of ca. 2.20-2.21 Ga, suggesting an intense reworking of the orthogneissic basement (Caicó Complex) during ore formation. Phlogopite $^{40}Ar/^{39}Ar$ analysis

yielded ages of ca. 524-528 Ma for the mineralized phlogopite schist, the best estimation for the emerald mineralization at the Paraná deposit. These data were interpreted in the light of emerald genesis to propose a tectonic-magmatic-related origin for the deposit, implying that emerald-bearing phlogopite schists were formed after metasomatic interactions between Cambrian Be-bearing pegmatite dykes and amphibolite lenses of the Caicó Complex during the strike-slip stage of the Portalegre shear zone.

Keywords: emerald deposit, geophysical and structural mapping, $^{40}Ar/^{39}Ar$ dating, genetic modelling, Borborema Province

INTRODUCTION

Ductile shear zones are considered the major structural controls for hydrothermal flow percolation and mineralization trapping in orogenic belts of all ages (Hronsky and Groves 2008, Haldar 2013). Shear-controlled mineralized areas are commonly found in gold, copper, and iron deposits related to accretionary and collisional margins (*e.g.*, Talukdar et al. 2012, Cawood and Hawkesworth 2015, Kitt et al. 2016, Vitorino et al. 2020). Although less common, rare-elements and gemstone deposits might be strongly controlled by deep-seated strike-slip structures (*e.g.*, Araújo et al. 2001, Demartis et al. 2011), including several emerald deposits that require specific geological and geochemical conditions to bring beryllium and chromophore elements (*e.g.*, Cr, V, Fe) together (Zwaan 2006, Zwaan et al. 2012, Giuliani et al. 2019).

The role of lithospheric shear zones, magmatism, and regional metamorphism in emerald genesis has been extensively discussed (*e.g.*, Grundmann and Morteani 1989, Ribeiro-Althoff et al. 1997, Zwaan 2006, Giuliani et al. 2019). In favorable structural sites, syn-kinematic plutonism and fluid percolation are the prime factors that, in association with metasomatic reactions, lead to emerald crystallization and accumulation (Schwarz and Giuliani 2001, Zwaan 2006, Giuliani et al. 2019). Hence, ore formation can be driven by shear zone-controlled fluids originating from the mid- to lower crust and mantle (Vapnik et al. 2006). At deep crustal levels, emerald growth might be recorded in high-grade metamorphic conditions reaching granulite facies pressure and temperature values (Vapnik et al. 2005). Yet, most deposits form in the range of 200-600°C and 0.5-4.0 kbar, which fits with medium-grade metamorphic conditions (Grundmann and Morteani 1989, Schwarz and Giuliani 2001, Vapnik et al. 2005).

The Borborema Province developed during the assembly of the western portion of Gondwana in the late Neoproterozoic-Cambrian transition (Meert and Lieberman 2008, Brito Neves et al. 2014), the Borborema Province (Figure 3.1a), and preserves a complex continental-scale strike-slip shear zone system with important gold, tungsten, and other precious-metals mineralization (*e.g.*, Araújo et al. 2005, Souza Neto et al. 2008, Pereira et al. 2019). Such occurrences are mostly related to the final stages of the Brasiliano/Pan-African Orogeny (ca. 600-520 Ma; *e.g.*, Vauchez et al. 1995; Brito Neves et al. 2000, Viegas et al. 2014).

It has been argued that these structures acted as channels for the migration of rare element pegmatitic fluids and subsequent remobilization of mineralizing elements (Santos et al. 2014 and references therein). During the final stages of the Brasiliano Orogeny (*ca.* 590-510 Ma, Brito Neves et al. 2014), shear zone-controlled metasomatism, spatially related to post-collisional granite plutons, took place in several portions of the province, giving rise to W-Au skarns and local gemstone deposits (Souza Neto et al. 2008, Zwaan et al. 2012, Hollanda et al. 2017).

Emerald formation in the Borborema Province is rare and restricted to its northern portion (Figure 3.1b); the ore is frequently related to ductile, amphibolite facies-related shear zones that are spatially associated with mafic-ultramafic sequences as well as beryl-bearing pegmatite fields (Zwaan et al. 2012, Santiago et al. 2019, Araújo Neto et al. 2019). Well-known examples are the Fazenda Bonfim deposit within the Santa Monica shear zone in the region of the Seridó Pegmatite Province (Zwaan et al. 2012, Santiago et al. 2019), and the Coqui occurrence along the Senador Pompeu shear zone in the vicinities of the Solonópole-Quixeramobim Pegmatite District (Castelo Branco et al. 1988).

The Paraná emerald deposit, located in southwestern Rio Grande do Norte state of Brazil, is associated with the Portalegre shear zone (PASZ), a major structural control for several granitic aquamarine-bearing pegmatites (Barreto 1991, Santos et al. 2020). In this paper, we discuss the role of the Portalegre shear zone as the main structural control of emerald mineralization at the Paraná deposit through a combination of airborne geophysics, field structural mapping, microstructural analysis, and geochronology (zircon U-Pb and phlogopite $^{40}Ar/^{39}Ar$). Our goal is to unravel the structural and metamorphic conditions involved in ore formation, including host rock ages and the timing of strike-slip deformation. The aim of the study is to establish a comprehensive genetic model for the Paraná emerald deposit, as an example for deformed gem-bearing deposits in the Borborema Province and correlated orogenic belts.

GEOLOGICAL SETTING

The Borborema Province (BP) constitutes most of the northeastern portion of the Precambrian platform of South America and consists of a complex mosaic-like orogenic system assembled in late Neoproterozoic to Cambrian times (Caxito et al. 2020, Santos et al. 2023). The province comprises a large set of Paleoproterozoic gneiss-migmatite basement rocks alternating with Archean nuclei and domains of Meso- to Neoproterozoic supracrustal sequences, intruded by a vast number of early to late Neoproterozoic granitic plutons (*e.g.*, Van Schmus et al. 1995, 2011, Medeiros et al. 2012, Dantas et al. 2013, Nascimento et al. 2015, Sial and Ferreira 2016, Lima et al. 2018, Santos et al. 2022).

As a result of orogenic event during the Gondwana assembly, the BP presents several transcurrent structures that separate different crustal blocks (*e.g.*, Brito Neves et al. 2000, Almeida et al. 2021,2022, Santos et al. 2017, 2018, 2021, Oliveira and Medeiros 2018). For instance, the continental-scale, E-W strike-slip Patos and Pernambuco shear zones separate the BP into three tectonic subprovinces: Northern, Transversal/Central and Southern (Van Schmus et al. 2011, Brito Neves et al. 2016; Figure 3.1b).

The Northern Subprovince represents a dominant Paleoproterozoic gneissic-migmatitic block, also containing late Neoproterozoic to Cambrian supracrustal and granitic-pegmatitic sequences, that occurs between the Patos shear zone to the south and the São Luís Craton to the north (Jardim de Sá et al. 1995, Brito Neves et al. 2000, Delgado et al. 2003). It was formed by several accretionary episodes from Archean to Neoproterozoic, representing a strongly reworked continental block that extends to the *Benino*-Nigerian Shield in West Gondwana reconstructions (*e.g.*, Dantas et al. 2004, Ganade de Araújo et al. 2014, Caxito et al. 2020, Ferreira et al. 2020). It hosts all the currently known emerald mineralization of the BP, as well as several occurrences of industrial and gem-quality minerals (Santos et al. 2014), which are mostly related to granites and pegmatites that were emplaced along NE-trending shear zones (Baumgartner et al. 2006, Beurlen et al. 2009, 2011).

In southwestern Rio Grande do Norte State, emerald mineralization occurs in phlogopite and actinolite-phlogopite schists as well as in schist-hosted granitic lenses or veins. The ore is found as lens-shaped bodies within the Portalegre NE-trending shear zone (Figure 3.1c), which extends ~150 km from the border of intracontinental basins to the south, until disappearing under the Phanerozoic cover of coastal basins to the north (Hackspacher and Legrand 1989). The PASZ represents a subsidiary shear zone, splaying from the main E-W Patos shear system, developed during the final stages of the Brasiliano Orogeny between ca. 590-510 Ma (Vauchez

et al. 1995, Viegas et al. 2014). This shear zone was regarded as a boundary between different geotectonic and/or geophysical domains (Jardim de Sá et al. 1997, Campelo 1999), but more recent gravity and magnetic data suggests that the PASZ does not necessarily separate contrasting crustal compartments (Oliveira and Medeiros 2018). In the studied region, the shear zone occurs along basement mylonitic gneisses and phlogopite schists, locally referred to as the Caicó Complex (Hackspacher and Legrand 1989, Medeiros 2008). Some amphibolite lenses and quartzites with mylonitic textures has been recently reported (Araújo Neto et al. 2018).

Several syn-tectonic pegmatite lenses or *boudins* of granitic composition are found along the PASZ, as well as in its secondary structures (*e.g.*, the Vieirópolis shear zone). Due to the well-marked structural control of the emerald-bearing phlogopite schists, the PASZ is frequently evoked as the main channel for hydrothermal process involving basement mafic rocks and pegmatite injections that ultimately formed emerald (Souza 2017, Araújo Neto et al. 2019, 2021). The mineralization lies in a complex network of phlogopite schists, schist-hosted granitic lenses and veins within the mylonitic gneisses. These schists are narrow (up to 5 m wide) and poorly exposed at the surface, which makes them difficult to be tracked down by surface geological mapping. Some outcrops are connected in a NE-SW trend composing a hypothetical emerald belt, but the best expositions are found in trenches and mine shafts.

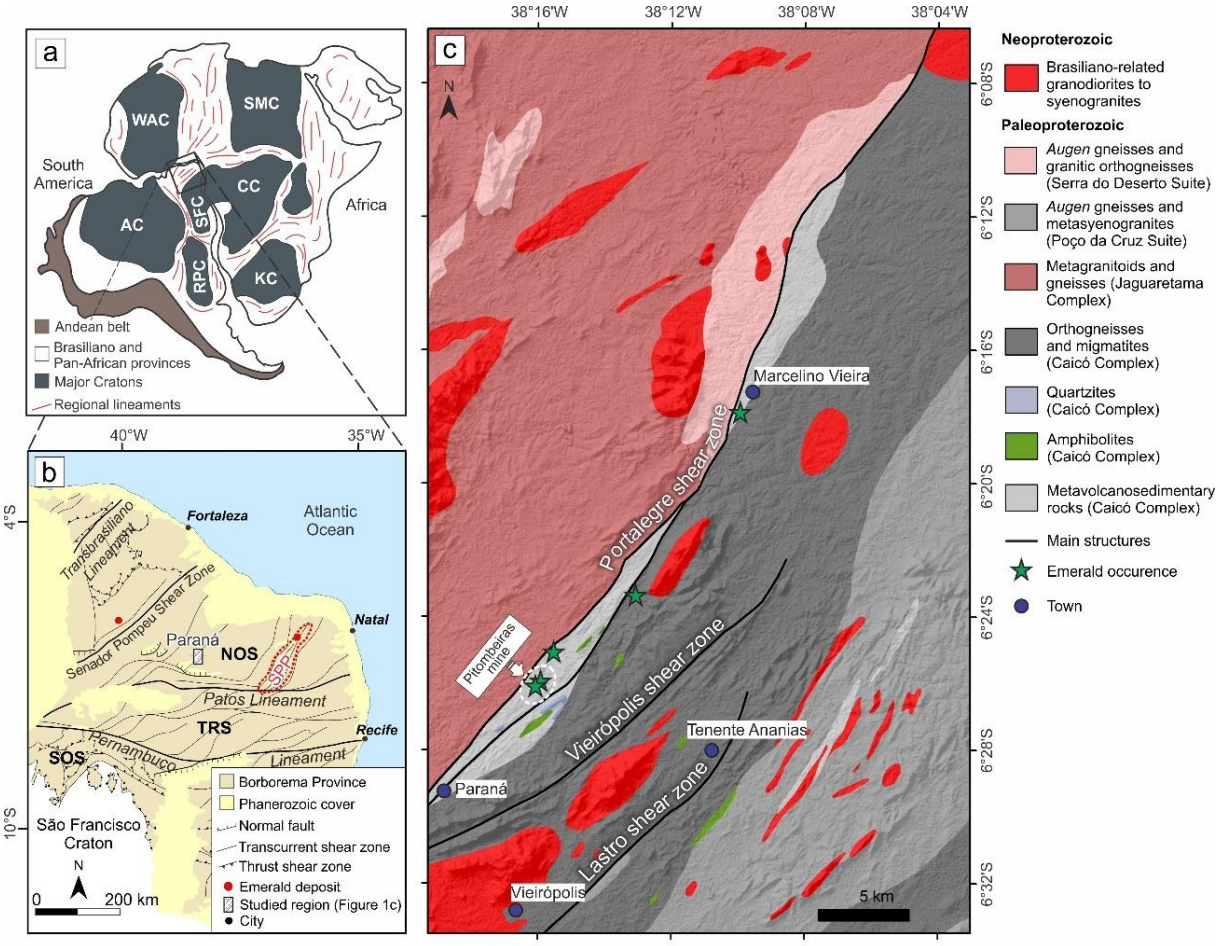

Figure 3.1. Regional setting of the Portalegre shear zone. (a) Tectonic configuration of the Borborema Province in pre-drift reconstruction of West Gondwana (extracted from Santos et al. 2019). (b) Simplified map of Borborema Province with main tectonic subdivisions (modified from Santos et al. 2014). (c) Geological map of the study area highlighting emerald occurrences along the Portalegre shear zone (adapted from Medeiros 2008 and Araújo Neto et al. 2018). Cratons: AC = Amazonian, CC = Congo, KC = Kalahari, RPC = Rio de la plata, SF = São Francisco, SMC = Sahara Metacraton, WAC = West Africa. Subprovinces: NOS = Northern, TRS = Transversal, SOS = Southern. SPP = Seridó Pegmatite Province.

MATERIAL AND METHODS

Geophysical data

Airborne magnetic data for the study area was obtained from the Paraíba-Rio Grande do Norte Airborne Geophysical Project managed by the Geological Survey of Brazil (CPRM) between 1/31/2009 and 9/10/2009. The survey was carried out with a nominal flight altitude of

100 m, and N-S-trending flight lines and E-W-trending tie lines spaced at 500 and 10,000 m, respectively. Bidirectional techniques were applied to the magnetic data for generating a grid of anomalous magnetic field with a cell size of 125 m (CPRM 2010).

For analysis of magnetic data, we used the total magnetic intensity (TMI) and the filtered images of 3D analytic signal amplitude (ASA), first vertical derivative (FD) and Tilt derivative (TD) for visual interpretation of magnetic lineaments, supporting the identification and delimitation of geological contacts and structural fabrics at a 1:150,000 viewed scale. Euler deconvolution technique was applied in order to obtain more accurate information of the residual magnetic sources. This semi-automatic interpretation method provides an estimation of location and depth of magnetic sources based on a given source type represented by a structural index (Reid et al. 1990). For this study, a structural index of 1 was used.

Structural analysis

The structural mapping was performed along the Portalegre shear zone in a NNE-SSW trend, accompanied by collection of representative samples. Detailed mesoscale structural observations were focused on local-scale emerald mines of the Paraná deposit, especially the Pitombeiras mine. These localities show the best expositions of the ore and associated rocks due to mining activities. Microstructural analysis was performed on the collected samples of the PASZ, including mylonitic basement rocks, phlogopite and actinolite-phlogopite schists and schist-hosted granitic lenses and veins. This study was carried out with polarized light microscopy in oriented thin sections cut in planes perpendicular to the foliation and parallel to the lineation.

Zircon U-Pb geochronology

Zircon crystals were extracted from two samples of schist-hosted granitic lenses (boudins and veins) for U-Pb dating at the Geochronology Laboratory of Universidade de Brasília, Brazil. Sample crushing, sieving, and heavy mineral separation through gravimetric and magnetic methods were performed at the Stable Isotope Laboratory – LABISE of Universidade de Pernambuco, Brazil. The remaining zircon grains were handpicked, using a binocular microscope, and mounted in epoxy resins for Laser Ablation Inductively Coupled Plasma Mass Spectrometry (LA-ICP-MS) isotope ratio acquisition. Cathodoluminescence and back-scattered

images were used to investigate the internal structure of each zircon crystal prior to isotopic analysis.

Geochronological U-Pb data was acquired using a Thermo Finnigan Neptune Multi Collector ICPMS equipped with a secondary electron multiplier-ion counter. Only coherent interval analyses were chosen to avoid signal mixed ages. Normalization was performed with the GJ-1 primary standard zircon ($^{207}Pb/^{206}Pb$ = 608.3 Ma, $^{206}Pb/^{238}U$ = 600.7 Ma and $^{207}Pb/^{235}U$ = 602.2 Ma, Jackson et al. 2004), whilst the 91500 zircon standard (ID-TIMS 1065.4 ± 0.3 Ma; Wiedenbeck et al. 2004) was analyzed as secondary reference material, and the obtained ages are 1042 ± 27 Ma ($^{207}Pb/^{206}Pb$ age), 1055 Ma ± 14 ($^{207}Pb/^{235}U$ age) and 1064 ± 10 Ma ($^{206}Pb/^{238}U$ age). Procedures for data reduction followed procedures stablished by Bühn et al. (2009) and Matteini et al. (2010) and the obtained ages were calculated using Isoplot version 4.1 (Ludwig 2012), avoiding high common Pb concentration spots.

Phlogopite $^{40}Ar/^{39}Ar$ geochronology

Hand samples for selected emerald-bearing phlogopite schists were collected for $^{40}Ar/^{39}Ar$ dating. Mineral separates of phlogopite were cleaned by rinsing each sample with cold water, then with 200 proof acetone, ethyl alcohol, then washed in triple distilled water (Milli-Q Water) then dried in a drying oven at 55°C. Final separates were obtained using a binocular microscope to obtain purities of > 99.9 %.

Age determinations for the phlogopite separates were obtained at the Oregon State University (OSU) Argon Laboratory in Corvallis, Oregon, using incremental CO_2 laser heating and/or Total Fusion Methods and analyzed on a multi-collector noble gas mass spectrometer. Phlogopite separates, along with sanidine flux monitors FCT-2-NM with a calibrated age of 28.201 ± 0.023 Ma, 1σ; after Kuiper et al., 2008), were placed in irradiation package 20-OSU-04 and irradiated for 6 Megawatt hours in the CLICIT position at the TRIGA nuclear reactor at Oregon State University (OSU). Irradiated samples were loaded into Cu-planchettes in an ultra-high vacuum sample chamber and incrementally heated by scanning a defocused 30W Synrad CO_2 laser beam at increasing laser powers in pre-set patterns across the sample, in order to evenly release the argon from the samples. It must be noted that the laser system has not been calibrated for knowing exact temperatures. After each heating step or total fusion run, and prior to analysis, reactive gases were cleaned for 3 minutes using a set of AP10 Zr-Al getters; 2 hot getters operated at 450 °C and 2 at room temperature (21 °C). Argon isotopic measurements were performed using a ThermoFisher Scientific TM multi-collector ARGUS-VI noble gas

mass spectrometer (spectrometer "F" at the OSU lab) that has 5 faraday collectors (fitted with a 10^{12} Ohm resistors for measurement of masses ^{41}Ar and ^{40}Ar, and 10^{13} Ohm resistors for masses ^{39}Ar, ^{38}Ar, and ^{37}Ar) and 1 ion-counting Cu-Be electron multiplier. This configuration allows to simultaneously measure all argon isotopes, with mass 36 on the multiplier and masses 37 through 40 on the four adjacent faradays. This configuration also provides the advantage of running in a full multi-collector mode while measuring the lowest peak (on mass 36) on the highly sensitive electron multiplier (CDD) located in a position next to the lowest mass faraday collector which, in turn, has an extremely low dark-noise and a very high peak/noise ratio.

All ages were calculated using the corrected value for the original constant of Steiger and Jäger (1977) constant for total ^{40}K decay to ^{40}Ar with a new value of 5.530 ± 0.097 x 10-10/yr (2σ) as reported by Min et al. (2000). For all other constants used in the age calculations we refer to Table 2 in Koppers et al. (2003). Individual J-values for each sample were calculated by parabolic extrapolation of the measured flux gradient against irradiation height and typically give 0.06–0.13% uncertainties (1σ). Calculated ages used the assumed trapped $^{40}Ar/^{36}Ar$ ratio of 295.5. Incremental heating plateau ages and isochron ages were calculated as either plateau, mini-plateau or weighted mean with 1/σ2 as weighting factor (Taylor, 1997) and as YORK2 least-square fits with correlated errors (York, 1968) using the ArArCALC v2.7.0 software from Koppers (2002) available from the following website http://earthref.org/ArArCALC/. All age uncertainties presented are 2-sigma. Samples are presented in Tables 3.2 and 3.3 and shown in age plateau diagrams in Fig. 3.11.

RESULTS

Aeromagnetic data analysis

The plotting of emerald mineralization on the TMI and ASA maps (Figure 3.2a and 3.2b) shows a strong correlation between the NE-trending emerald belt (N20E-N45E) and major magnetic alignments. The first order structures are extensive lineaments that can delimit four main magnetic domains (Figure 3.2c). Based on the total magnetic intensity map, domain 1 presents medium magnitude, dominated by negative values of -50 to -10 nT, whereas domain 2 presents medium to high magnitudes, varying approximately from -50 to 60 nT; domain 3 comprises the lowest magnitudes of the study area, usually between -50 and -300 nT, except for the very strong southwestern positive anomaly (~50-200 nT); on the other hand, domain 4 covers the most extensive area with high positive magnitudes, commonly between 5 and 50 nT.

Although these domains are not a direct representation of the vertical position of the magnetic sources (due to the bipolar nature of the magnetic anomalies at low latitudes, as is the case of northeastern Brazil), their boundaries relate to lithological and/or structural contrasts as seen in the similar magnetic lineaments interpreted from the 3D analytic signal amplitude filter (Figure 3.2d). First and second order magnetic lineaments were best interpreted based on relief and magnetic gradients from the first- and tilt derivative maps (Figure 3.2e and 3.2f) at a 1:150,000 viewed scale. First order lineaments are NE-trending long structures (≥ 15 km) and/or boundaries of magnetic domains whereas second order lineaments are structures of minor extent (< 15 km) with a main ENE-WSW trend usually within the magnetic domains (Figure 3.2g and 3.2h).

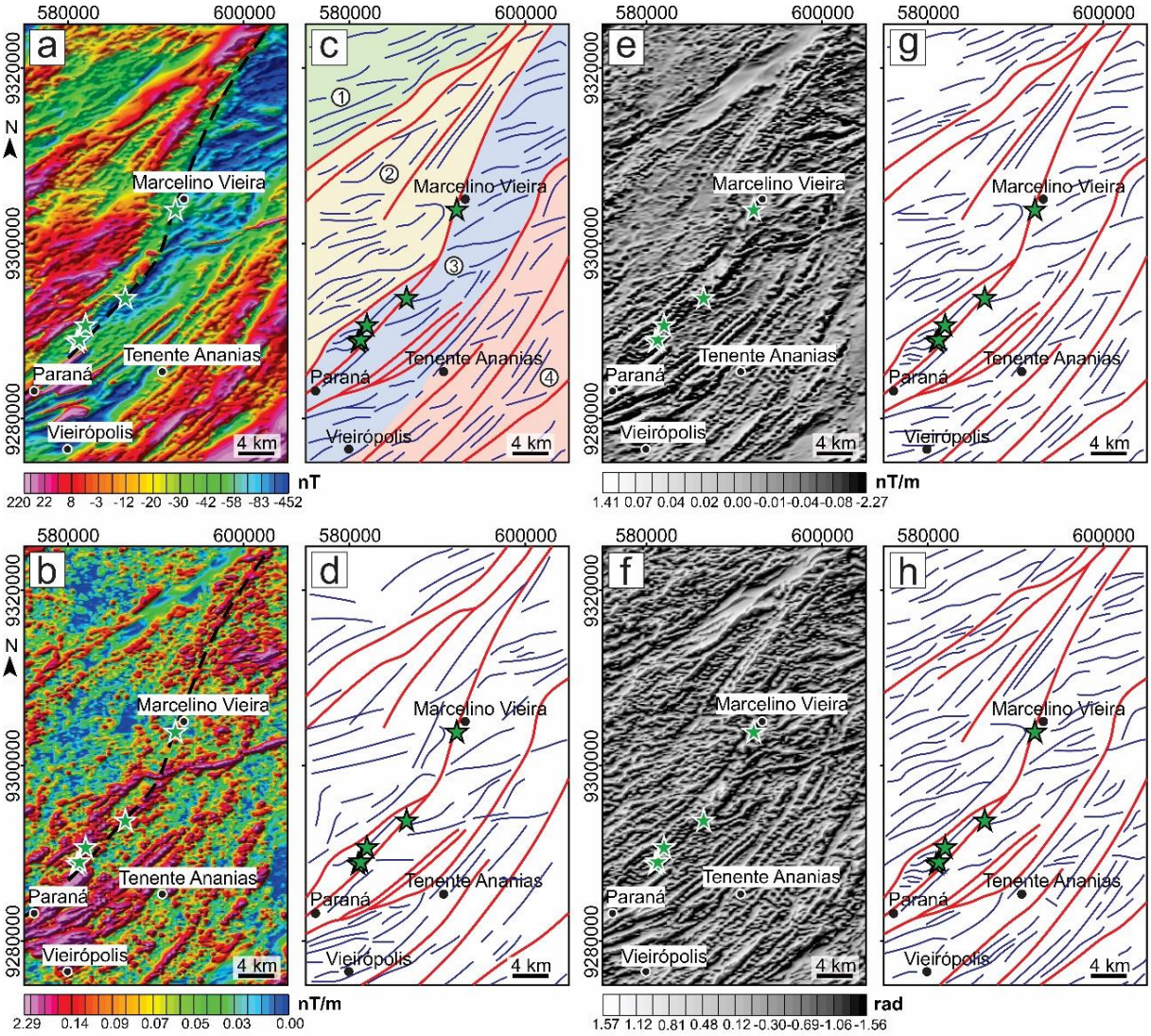

Figure 3.2. Magnetic maps and interpreted products for the study area. (a) Total magnetic intensity map. (b) 3D analytic signal amplitude map. (c) Magnetic domains and lineaments interpreted from TMI (see the text for descriptions of domains 1 to 4). (d) Magnetic lineaments

interpreted from ASA. (e) First derivative map. (f) Tilt derivative map. (g) Magnetic lineaments interpreted from FD. (h) Magnetic lineaments interpreted from TD. Black dashed line = hypothetical main emerald belt; green star = emerald occurrence; black dot = city or district; red continuous line = first order lineaments; blue continuous line = second order lineaments.

Euler deconvolution

Depth of magnetic sources was obtained by Euler deconvolution, choosing a structural index of 1 (see Reid et al. 1990) and an 1875 m wide window. Euler solutions were categorized in four depth intervals (Figure 3.3). Shallowest values (less than 70 m) are found scattered across the study area and commonly in an ENE-WSW direction. Most depths are in the 70-200 m interval, defining both NE-SW and ENE-WSW trends, whereas deeper solutions (200-400 m interval) are mainly associated with the regional NE-SW direction, displaying a consistent correlation with major magnetic lineaments. Deepest values (more than 400 m) are scarce, but always clustered within NE-trending first order structures.

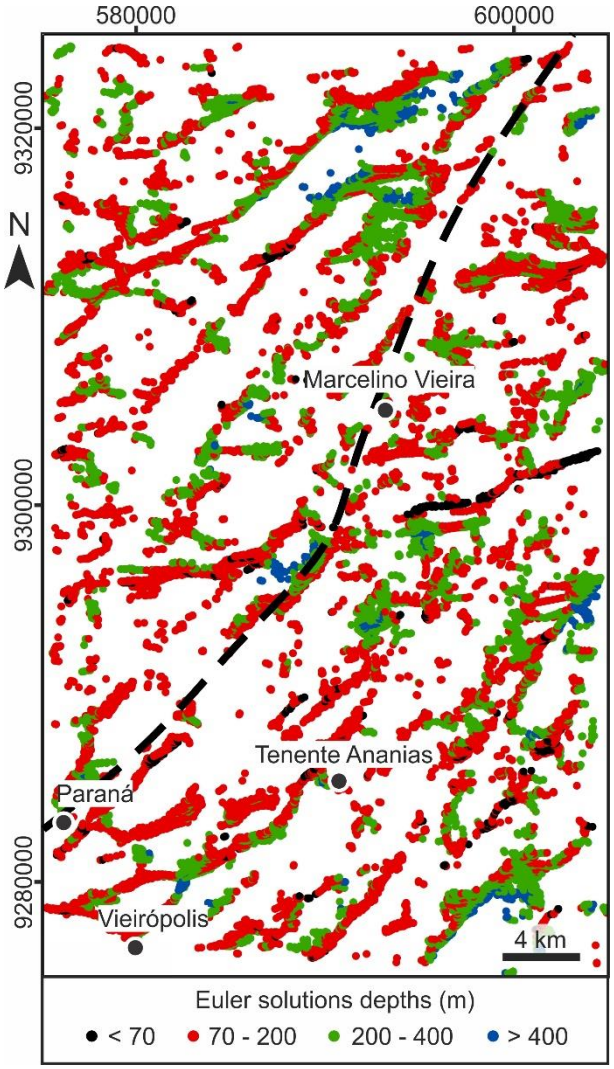

Figure 3.3. Categorized Euler solutions depths for the study area, using a structural index of 1. Black dashed line = hypothetical main emerald belt.

Structures and fabrics

Mesoscale structural data

Typical pre-Brasiliano structures (e.g., gneissic layering) are progressively overprinted by strike-slip deformation. This process is evidenced by the development of a medium- to coarse-grained foliation, defined by the preferred orientation of flattened quartz, feldspar and biotite grains.

The most common rocks within the PASZ are mylonitic gneisses with a vertical to sub-vertical (ca. 90-80°) mylonitic foliation that has an average N30E trend (Figure 3.4). Horizontal to sub-horizontal (ca. 7°) NE-SW-trending mineral stretching lineations are common, being

usually defined by oriented biotite and elongated quartz and feldspar crystals (Figure 3.5a). However, in the central portion of the shear zone, the mylonitic foliation has a moderate dip (35-65°) with oblique mineral stretching lineation (20-35°) (Figure 3.5b).

The mylonitic gneisses are mostly medium-grained (usually between 50-70 µm), granitic in composition, and typically layered: quartz-feldspar-rich bands alternate with biotite-quartz-feldspar ± magnetite and hornblende-rich layers. These rocks exhibit intrafolial and other shear-related folds, such as sheath folds with axial plane foliation sub-parallel to the plane of shearing (Figure 3.5c) and synthetic asymmetric folds with thinned short limbs – Z-folds – indicative of a dextral sense of shear (Figure 3.5d).

Coarser-grained (100-500 µm) samples are characterized by centimetric K-feldspar porphyroclasts surrounded by elongated biotite (and locally muscovite) flakes and quartz ribbons. The porphyroclasts are usually deformed and asymmetric, developing *augen* textures and S-C surfaces coherent with the overall dextral kinematics (Figure 3.5e). This dextral shear sense is reinforced by a sigmoidal penetrative mylonitic foliation in biotite schists (Figure 3.5f) and asymmetric boudins (Figure 3.5g) locally defining bookshelf geometries (Figure 3.5h).

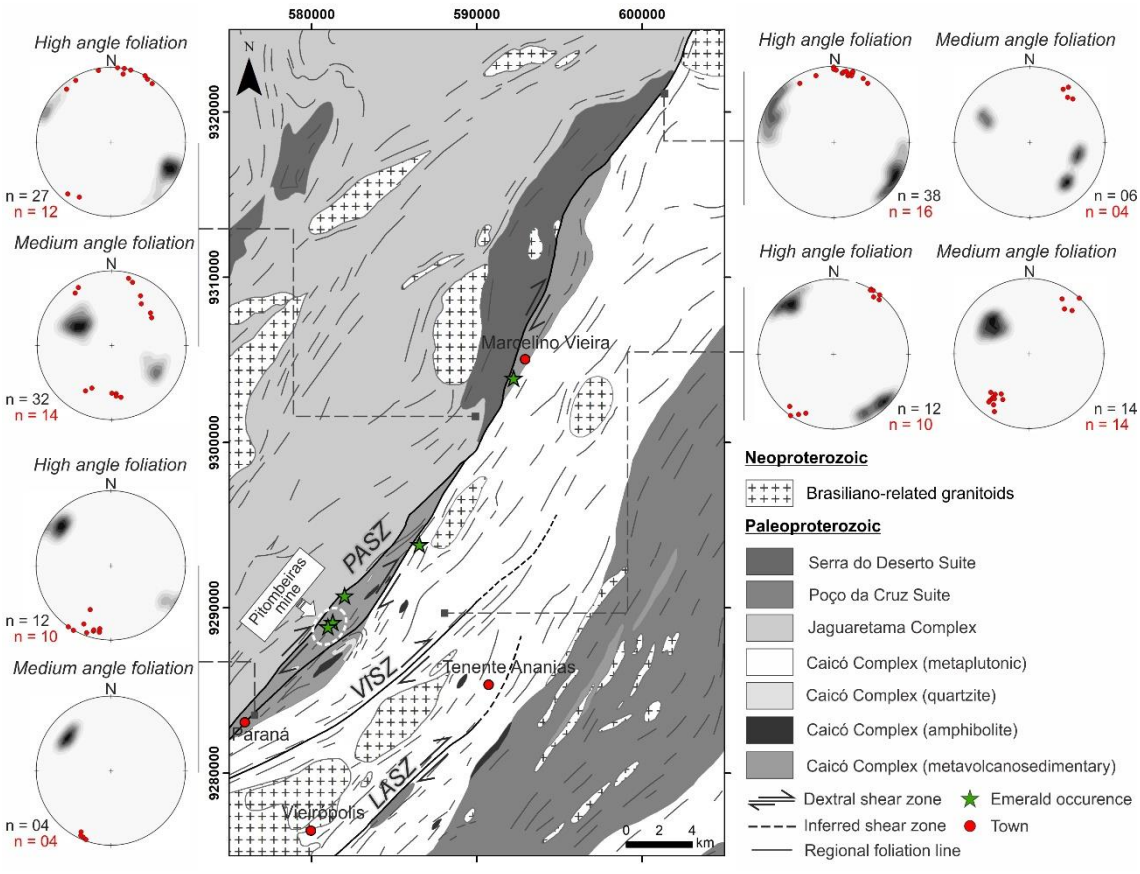

Figure 3.4. Main lithological units and structures of the Portalegre shear zone. The low-hemisphere, equal area Schmidt stereograms show the variation in planar and linear fabrics

along the Portalegre shear zone. Gray-scale contours denote foliation measurements (n_{total} = 145). Red dots represent the stretching lineation (n_{total} = 84). PASZ = Portalegre shear zone; VISZ = Vieirópolis shear zone; LASZ = Lastro shear zone. Pitombeiras mine indicated in white square.

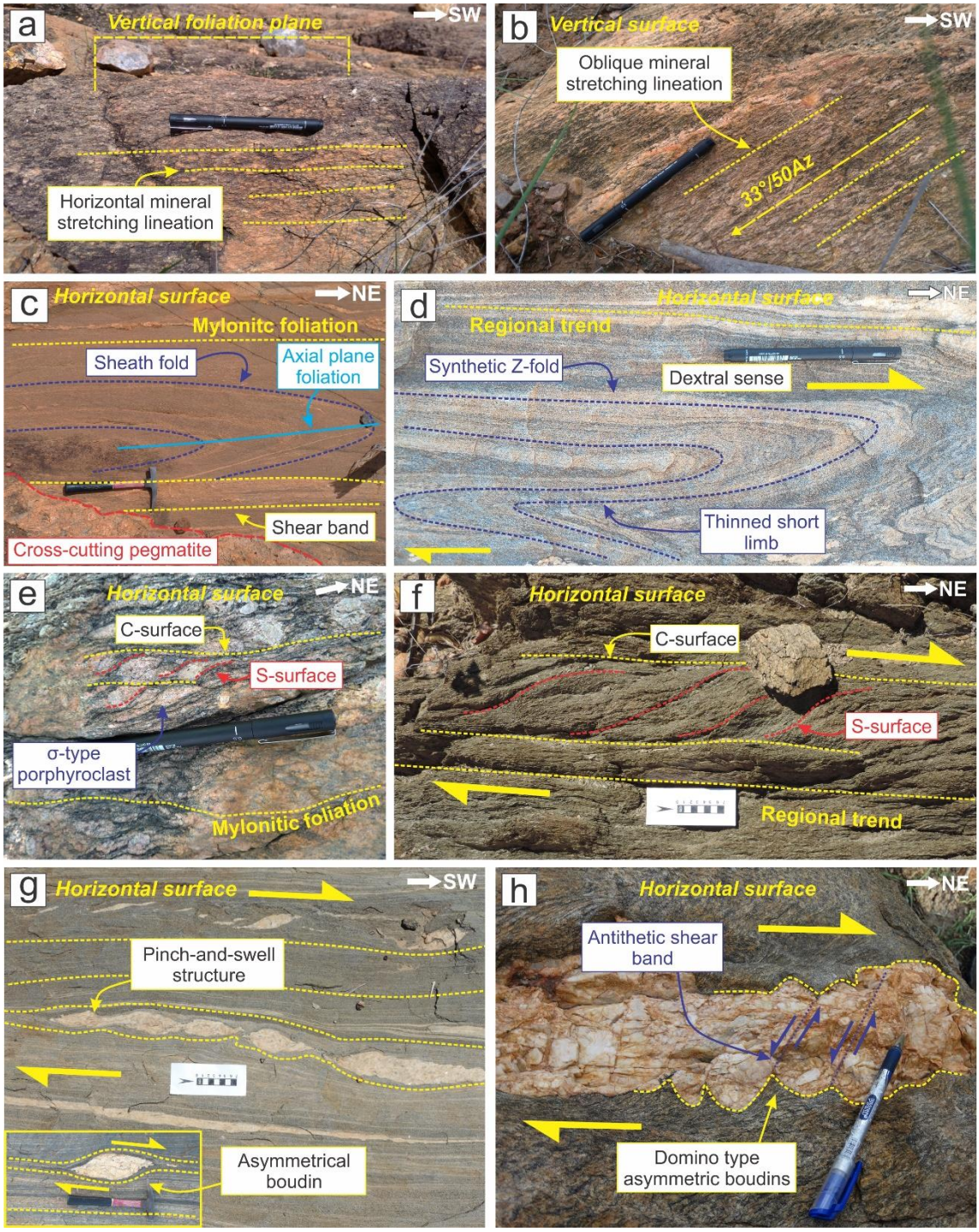

Figure 3.5. Structures of the Portalegre shear zone and associated Vieirópolis shear zone. (a) Horizontal lineation marked by elongated feldspar crystals. (b) Mylonitic gneiss with oblique mineral stretching lineation. (c) Sheath folds with axial plane foliation sub-parallel to the main

mylonitic foliation. All structures are cross-cut by irregular-shaped homogenous pegmatite. (d) Synthetic Z-fold with thinned short limb and clockwise vergence indicating dextral shear sense. (e) *Augen-g*neiss with σ-type porphyroclasts defining a dextral S-C fabric. (f) Biotite-schist with well-developed S-C surfaces with dextral shear sense. (g) Asymmetric pegmatite boudins exhibiting pinch-and-swell structures with dextral shear sense at the VISZ. (h) Domino type asymmetric pegmatite boudins with antithetic shear bands developed under dextral strike-slip deformation.

Structures at the emerald deposit

At the Pitombeiras emerald mine (location in Figure 3.4), phengite-phlogopite-, actinolite-phlogopite-, and phlogopite schists occur as metric-sized coarse-grained lenses along the PASZ. The schists have vertical to sub-vertical foliation oriented between N20E and N45E (Figure 3.6a). Elongated NE-trending mica flakes define a horizontal mineral stretching lineation (Figure 3.6b). Subsurface analysis indicates that some of these dispersed lenses are connected, forming an anastomosed sigmoidal system of schists with a dextral shear sense at the deposit-scale (see Figure 3.6a). At the outcrop-scale, this dextral shear sense is recorded by S-C fabrics on phlogopite schists (Figure 3.6c). Still, such fabrics are heterogenous, with development of C' extensional shear bands and rotation of the S-surfaces until a higher level of parallelism with C-surfaces in areas with increased shear strain components (Figure 3.6d).

Asymmetric and boudinaged granitic lenses within the schists are common and provide reliable kinematic criteria (Figure 3.6e). These lenses are variable in composition but are frequently deformed, with growth of recrystallized quartz-feldspar tails in the boudinaged cores. The emerald crystals are often found in the granitic veins and veinlets or within the schistosity (Figure 3.6f), with its crystallographic *c*-axis usually parallel to the foliation plane, being parallel or perpendicular to the correspondent lineation.

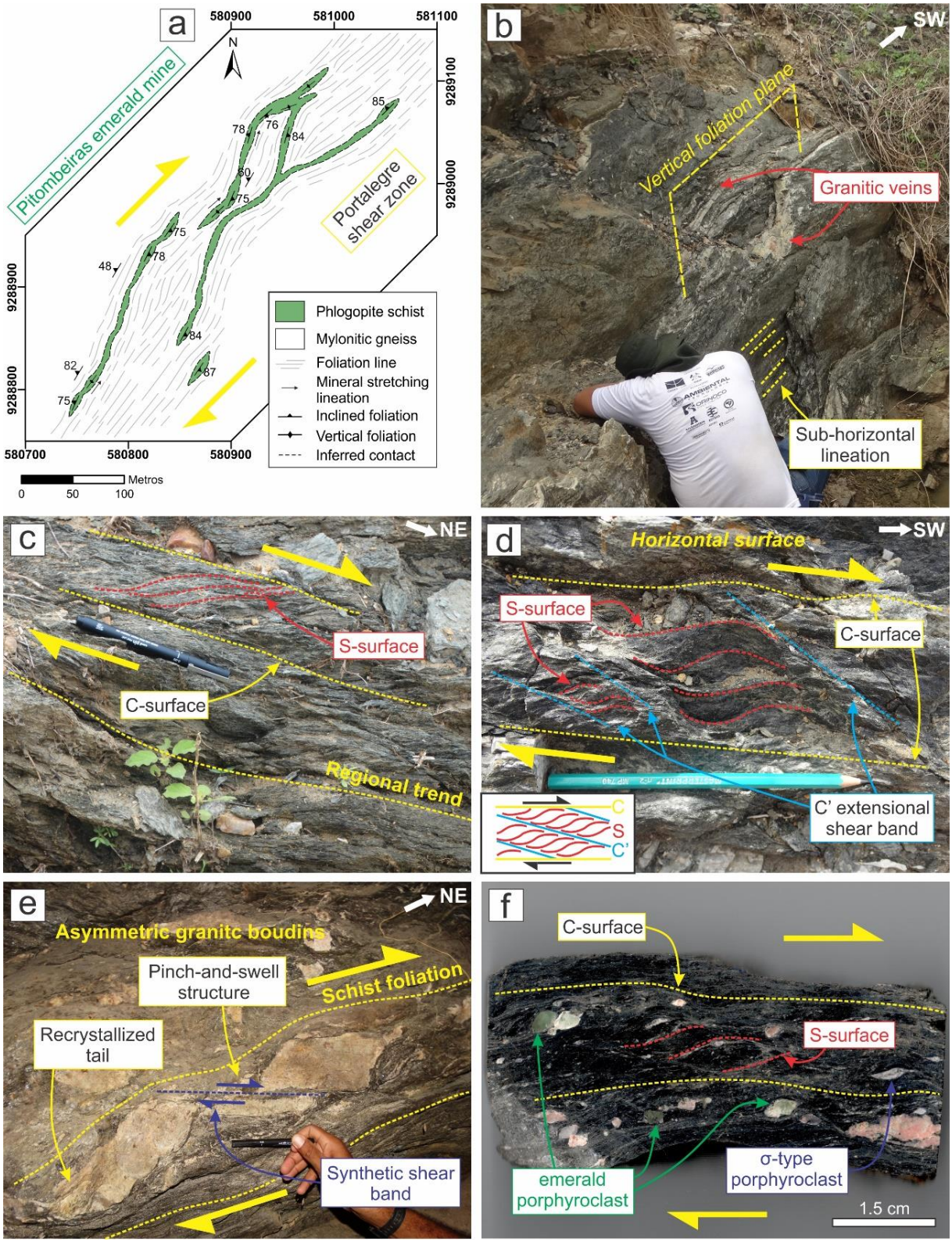

Figure 3.6. Structural features of the Pitombeiras mine. (a) Schematic geological map of the Pitombeiras region, showing the anastomosed sigmoidal distribution of the schist along the Portalegre shear zone. (b) High angle foliation with sub-horizontal mineral stretching lineation and centimetric granitic veins in the phlogopite schist. (c) S-C fabric showing clockwise rotation of S-surfaces due to dextral strike-slip deformation. (d) Development of C' extensional

bands in phlogopite schist after progressive deformation. The distribution of S-C-C' structures indicate dextral shear sense. Schematic S-C-C' fabric diagram adapted from Blenkinsop and Treloar (1995). (e) Asymmetric granitic boudins with former pinch-and-swell structures disrupted after brittle deformation in an inclined gallery wall of the Pitombeiras mine. (f) Emerald porphyroclast with the crystallographic *c*-axis subparallel to the foliation plane. A dextral shear sense is indicated by σ-type porphyroclasts of K-feldspar and the asymmetry of the S-C fabric.

Microstructures

Mylonitic gneiss

The mineralogical composition of the gneissic rocks of the Caicó Complex within the PASZ consists of quartz (25-40 %) + K-feldspar (15-30 %) + plagioclase (10-30 %) and biotite (5-20 %) as the main Fe-silicate. Some magnetite (< 8 %) and hornblende (< 5 %) can be present. Apatite, muscovite, titanite and zircon occur as accessory minerals (< 5 %). Accessory epidote and allanite are also locally observed.

Biotite-rich layers are composed of elongated biotite ± muscovite flakes with grain sizes usually greater than 100 μm and a shape-preferred orientation (SPO) parallel to the mylonitic foliation. Quartz-feldspar bands present equigranular texture with an oblique orientation (~30°) in relation to the main mylonitic foliation (Figures 3.7a and b).

The quartz crystals have grain sizes ranging from 50 to 100 μm, sub-elliptical shape and straight to curvilinear boundaries. They have undulose extinction and show subgrain boundaries commonly oriented at oblique angles in relation to the mean SPO. K-feldspar and plagioclase crystals are variable in size. In the quartz-feldspar aggregates, minor sub-elliptical crystals have mean grain size of 70 μm. However, K-feldspar relicts can form millimetric porphyroclasts (1-4 mm) that show tartan twinning or flame perthites; these porphyroclasts have undulose extinction and often exhibit incipient core-mantle structures. Plagioclase locally records deformation as mechanical twinning (Figure 3.7c).

In coarser-grained mylonitic gneiss, the porphyroclasts (~1cm) are elliptical and elongated parallel to the mylonitic foliation; they are fractured and fragmented, with small (~20 μm) rounded quartz-feldspar crystals filling the fracture and at the borders of the crystals, forming recrystallized tails (Figure 3.7d). The matrix has variable grain size (100-500 μm) comprising plagioclase grains with mechanical twinning, thin elongated biotite lamellae and

quartz ribbons. The quartz ribbons have undulose extinction and oblique subgrains boundaries; they are elongated parallel to the mylonitic foliation (Figure 3.7d), with local deflections around K-feldspar porphyroclasts. In some quartz-rich layers, straight contacts between quartz crystals are replaced by lobate contacts (Figure 3.7e). Lobate and serrated contacts are common in coarse-grained (200-400 µm) feldspar crystals with development of myrmekite and rounded fine grained (~20 µm) bulges at the serrated boundaries (Figure 3.7f).

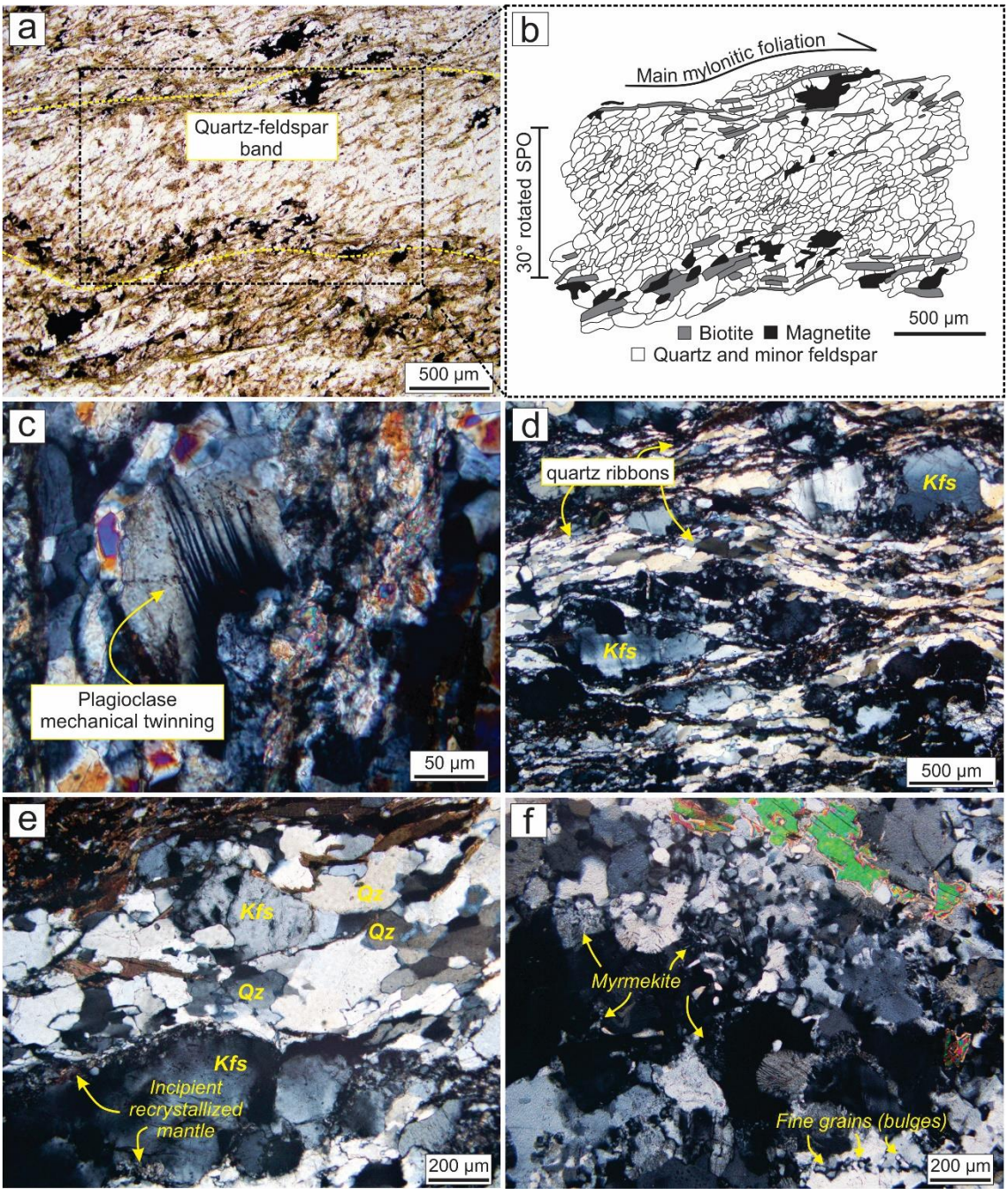

Figure 3.7. Microstructures of the Portalegre shear zone. (a) Equigranular quartz-feldspar ± biotite grains in the quartz-feldspar band with SPO oblique (~30°) to the main regional

mylonitic foliation. (b) Detailed sketch of the quartz-feldspar SPO in relation to the mylonitic foliation. (c) Deformed plagioclase crystal exhibiting mechanical twinning. (d) Elongated quartz ribbons and K-feldspar porphyroclasts showing recrystallization. (e) Mylonitic fabric with K-feldspar porphyroclasts showing recrystallized mantle and quartz grains with straight contacts and some lobate contacts. (f) Feldspar crystals exhibiting myrmekitization and serrated boundaries with fine grained crystals at the edges. Kfs = K-feldspar; Qz = quartz.

Phlogopite schist and granitic lenses

The phlogopite schist shows a heterogenous grain size distribution with coarse grained domains (millimetric elongated mica and amphibole) associated with fine grained quartz and feldspar (~20 μm). Its composition is dominated by phlogopite and variable concentration of felsic minerals (quartz, K-feldspar and plagioclase). Accessory minerals are apatite, titanite, allanite and emerald. Actinolite and phengite are observed in some samples and can represent 20-30 % of the total modal composition in actinolite-phlogopite and phengite-phlogopite schists. Typical microstructures are intrafolial folds and crenulation cleavages with *chevron* folds marked by elongated phlogopite and actinolite (Figure 3.8a). Dextral shear sense indicators are found as S-C surfaces, σ-type porphyroclasts and mica fish, the latter defined by millimetric phlogopite grains with its longest dimension at an angle of 35° to the mylonitic foliation (Figure 3.8b). The felsic minerals are usually fine-grained (~20 μm) and dispersed within the schistosity or concentrated around K-feldspar porphyroclasts as recrystallized mantles or tails (Figure 3.8c). Coarse-grained emerald crystals (> 500 μm) can be found (i) as porphyroclasts along the schistosity (Figure 3.8d), (ii) associated with quartz-feldspar lenses, or (iii) at the contact zone between schist and gneiss (Figure 3.8e).

Several granitic lenses found within the schists are characterized by fractured, centimetric K-feldspar porphyroclasts with tartan twinning and a coarse-grained domain (usually 0.3-1.0 mm) composed by feldspar and quartz. The later shows undulose extinction and serrated to lobate contacts (Figure 3.8f).

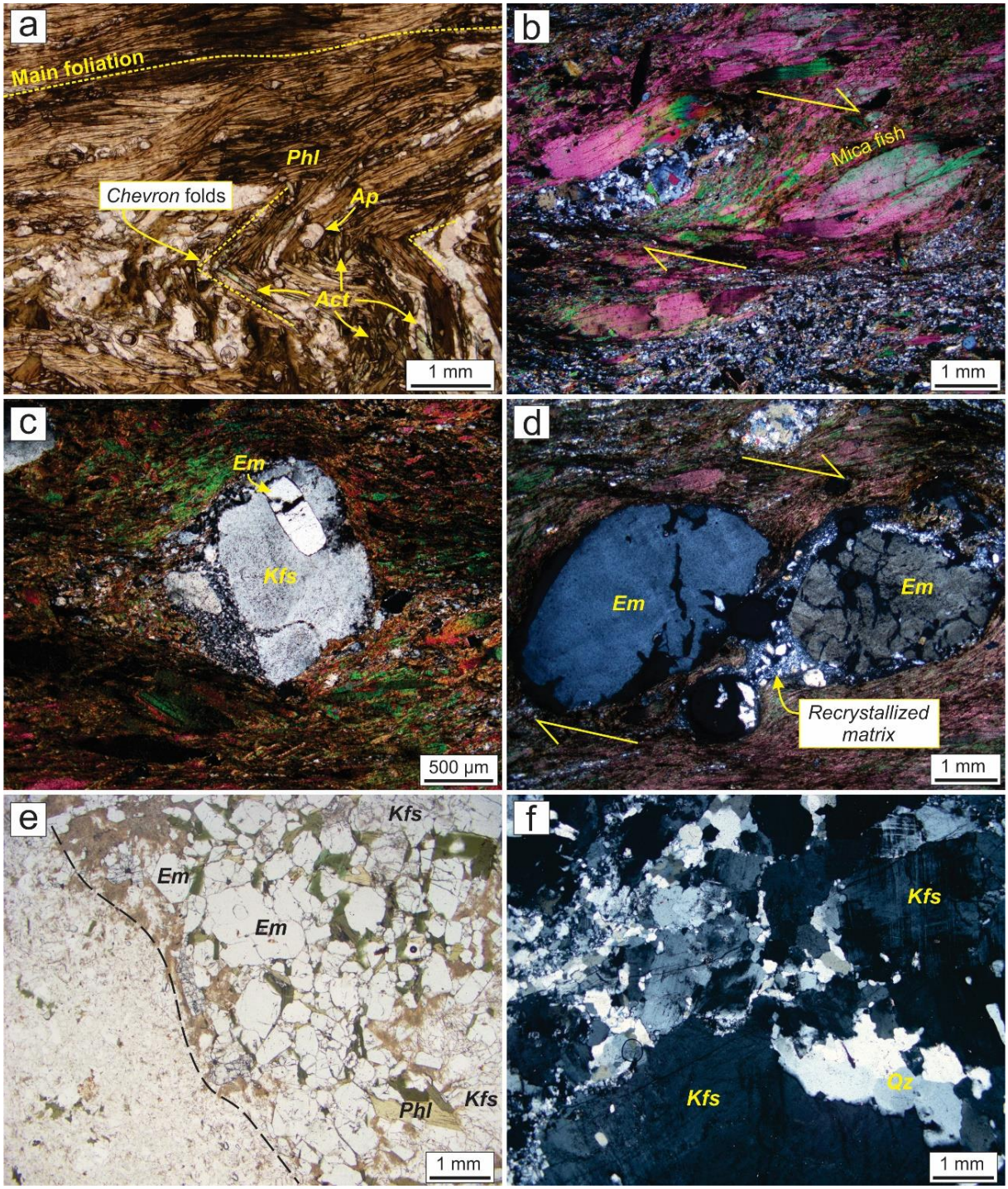

Figure 3.8. Microstructures of the phlogopite schist and granitic lenses at the emerald deposit. (a) Actinolite-phlogopite schist exhibiting *chevron* folds with axial plane parallel to regional foliation. (b) Mica fish with dextral shear sense, defined by millimetric sigmoidal phlogopite crystal oblique to the main mylonitic foliation. (c) K-feldspar and emerald porphyroclasts with fine-grained recrystallized tail. (d) Fractured and rotated emerald porphyroclasts oblique to the C-surface, exhibiting clockwise movement. (e) Idiomorphic and subidiomorphic emerald crystals formed at the contact zone (right) between gneiss (left) and schist. (f) Mylonitized

granitic lens with K-feldspar porphyroclasts surrounded by coarse-grained quartz crystals with lobate contacts. Act = actinolite; Ap = apatite; Em = emerald; Phl = phlogopite; Kfs = K-feldspar; Qz = quartz.

U-Pb geochronology

Sample ARO-SH01 is a coarse-grained metamonzogranite from a centimeter-thick vein (~50 cm) interleaved within the phlogopite schist and obtained inside a mine shaft. Both schist and veins are folded and can have narrow K-feldspar-rich veins (1-5 cm) with translucent emerald crystals close to the contact zone. The recovered zircon crystals were colorless to pale brown euhedral prisms (Figure 3.9a). They range in size from 110 to 260 µm with axial ratios between 1:2 and 1:3. Crystal morphology, symmetrical oscillatory zoning and a Th/U ratio ranging from 0.62 to 2.42 are indicative of an igneous origin (Table 3.1). The concordia diagram for a cluster of thirteen analyzed spots yields an upper intercept age of 2210 ± 8 Ma (MSWD = 3.7), which is interpreted as the protolith age of the metamonzogranite, whereas the lower intercept yields an age of 202 ± 230 Ma, which is not considered for interpretations due to high error (Figure 3.9b).

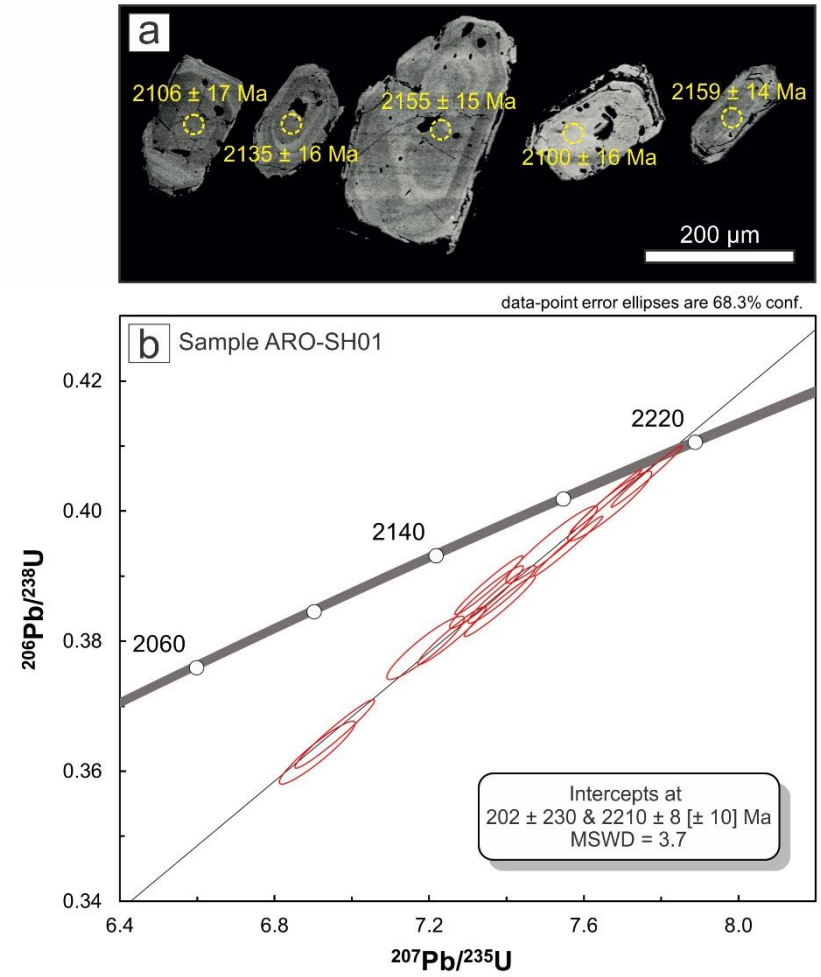

Figure 3.9. Zircon U-Pb geochronological data for sample ARO-SH01. (a) Back-scattered electrons images of selected zircons for the studied sample. Spot position represented by yellow dashed circles. Quoted ages are $^{207}Pb/^{235}U$. (b) U-Pb concordia diagram obtained for thirteen analyzed spots.

Sample PAR-89 is a leucocratic boudin inserted within the phlogopite schist, obtained from a mine gallery at the Pitombeiras region (see Figure 3.6e). The boudin consist of a coarse-grained metamonzogranite with approximately 30 cm in length. Collected zircon crystals were slightly brown euhedral prims with axial ratio of 1:2 to 1:3 and size raging from 100 to 310 µm (Figure 3.10a). Oscillatory zoning is quite common but poorly developed. The Th/U ratio ranges from 1.10 to 2.20, which is consistent with values for igneous zircon (Table 3.1). Nine analyzed spots were selected for creating the concordia diagram with an upper intercept age of 2201 ± 6 Ma (MSWD = 2.4) interpreted as the protolith age of the metamonzogranite, whereas 233 ± 81 Ma marks the lower intercept, which can be, despite the large error, interpreted as the result of Pb loss during Mesozoic reactivations of the PASZ (Figure 3.10b).

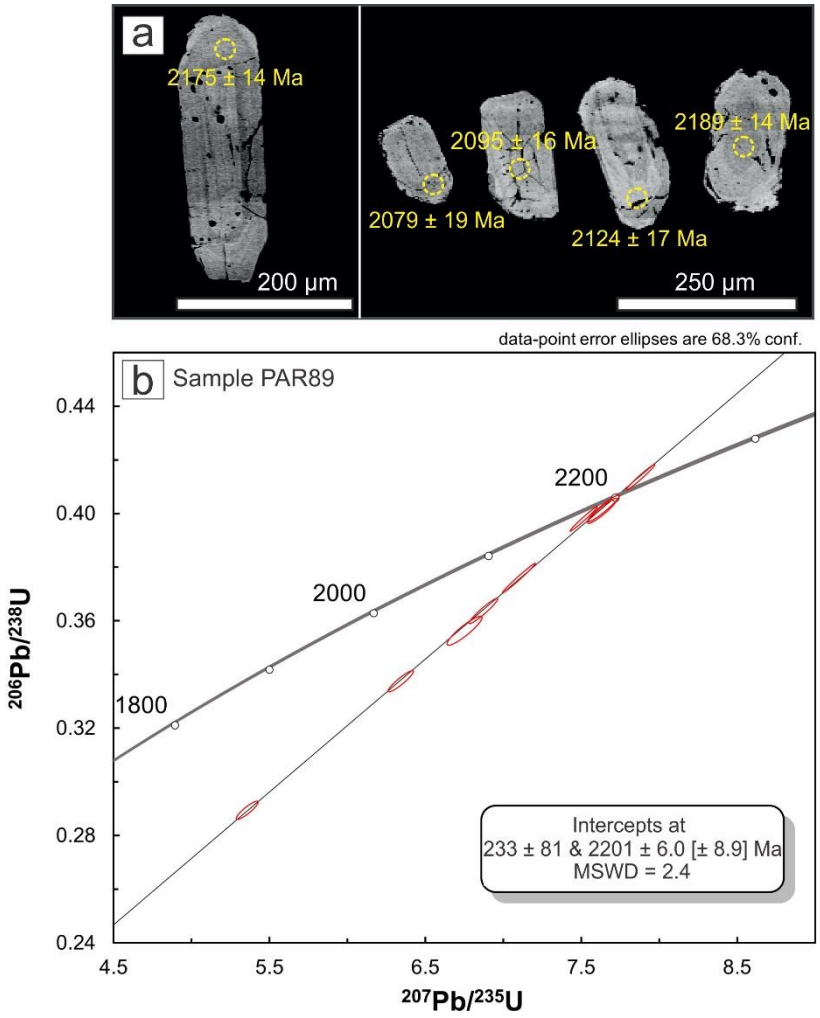

Figure 3.10**.** Zircon U-Pb geochronological data for sample PAR-89. (a) Back-scattered electrons images of selected zircons for the studied sample. Spot position represented by yellow dashed circles. Quoted ages are $^{207}Pb/^{235}U$. (b) U-Pb concordia diagram obtained for thirteen analyzed spots.

Table 3.1. Summary of LA-ICP-MS data for the recovered zircons from samples ARO-SH01 and PAR89.

Grain spot	Isotope ratio						Age (Ma)								
	$^{207}Pb/^{206}Pb$	±1σ	$^{207}Pb/^{235}U$	±1σ	$^{206}Pb/^{238}U$	±1σ	$^{207}/Pb/^{206}Pb$	±2σ	$^{207}Pb/^{235}U$	±2σ	$^{206}Pb/^{238}U$	±2σ	Rho	Th/U	Conc. (%)
ARO05	0.138	0.24	6.955	0.98	0.366	0.95	2202	28	2106	17	2010	33	0.97	2.42	95.45
ARO06	0.138	0.32	7.517	1.04	0.395	0.99	2204	29	2175	18	2146	36	0.95	1.05	98.65
ARO10	0.137	0.36	7.190	0.92	0.379	0.85	2191	30	2135	16	2072	30	0.92	1.54	97.03
ARO12	0.138	0.22	7.259	0.80	0.381	0.77	2207	28	2144	14	2081	28	0.96	1.20	97.06
ARO14	0.137	0.18	7.354	0.79	0.389	0.77	2190	28	2155	14	2117	28	0.98	1.55	98.21
ARO19	0.138	0.25	7.348	0.86	0.387	0.82	2197	29	2155	15	2108	30	0.96	0.62	97.85
ARO21	0.139	0.31	7.668	0.94	0.401	0.88	2214	29	2193	16	2173	33	0.94	1.21	99.10
ARO26	0.138	0.33	6.910	0.94	0.363	0.88	2197	30	2100	16	1996	30	0.94	2.31	95.06

ARO33	0.139	0.19	7.383	0.83	0.385	0.80	2209	28	2159	14	2102	29	0.97	1.35	97.36
ARO37	0.139	0.12	7.763	0.78	0.405	0.77	2216	27	2204	14	2194	29	0.99	1.11	99.55
ARO51	0.138	0.13	7.560	0.78	0.395	0.77	2198	28	2180	14	2145	28	0.99	1.35	98.37
ARO54	0.138	0.23	7.388	0.79	0.387	0.75	2201	28	2159	14	2110	27	1.47	0.96	97.72
ARO55	0.137	0.09	7.657	0.79	0.402	0.79	2191	27	2192	14	2177	29	1.47	0.99	99.31
PAR07	0.138	0.26	6.871	0.89	0.364	0.85	2200	29	2095	16	2001	29	0.96	2.03	95.50
PAR09	0.138	0.14	7.101	0.97	0.376	0.96	2198	28	2124	17	2059	34	0.99	1.10	96.91
PAR10	0.138	0.29	7.636	0.82	0.401	0.77	2205	29	2189	14	2175	28	0.93	1.65	99.34
PAR11	0.134	0.39	5.355	0.88	0.290	0.79	2153	31	1878	15	1640	23	0.89	1.34	87.32
PAR20	0.138	0.13	7.516	0.77	0.398	0.76	2197	27	2175	14	2161	28	0.99	1.14	99.35
PAR26	0.137	0.27	7.644	0.86	0.402	0.82	2193	29	2190	15	2179	30	0.95	1.61	99.50
PAR33	0.138	0.15	7.880	0.77	0.414	0.76	2204	28	2217	14	2232	29	0.98	1.72	100.66
PAR37	0.137	0.47	6.752	1.11	0.357	1.00	2188	32	2079	19	1966	34	0.91	2.20	94.54
PAR48	0.136	0.32	6.341	0.84	0.338	0.78	2181	30	2024	15	1876	25	0.92	1.24	92.67

$^{40}Ar/^{39}Ar$ geochronology

Sample PAR-EM01 is a coarse-grained emerald-bearing phlogopite schist obtained from the inner portion of the hosting schist in a mine gallery. The phlogopite flakes yielded a plateau age of 524.04 ± 1.23 Ma (MSWD = 1.99; P = 0.04 %) including 98.66 % of the ^{39}Ar released in 36 incremental heating steps (Figure 3.11a). The sample displays a flat age containing 98.6 % of the ^{39}Ar released. The analytical data and apparent ages are reported in Table 3.2.

The phlogopite of sample PAR-EM02 was collected from an emerald-bearing contact zone between the gneiss and the phlogopite schist. Incremental heating results are similar to those of PAR-EM01. A plateau age of 527.93 ± 1.25 Ma (MSWD = 1.06; P = 38 %) was obtained consisting of 84.87% of the ^{39}Ar released in 32 steps (Figure 3.11b). Summary of incremental heating data is registered in Table 3.3.

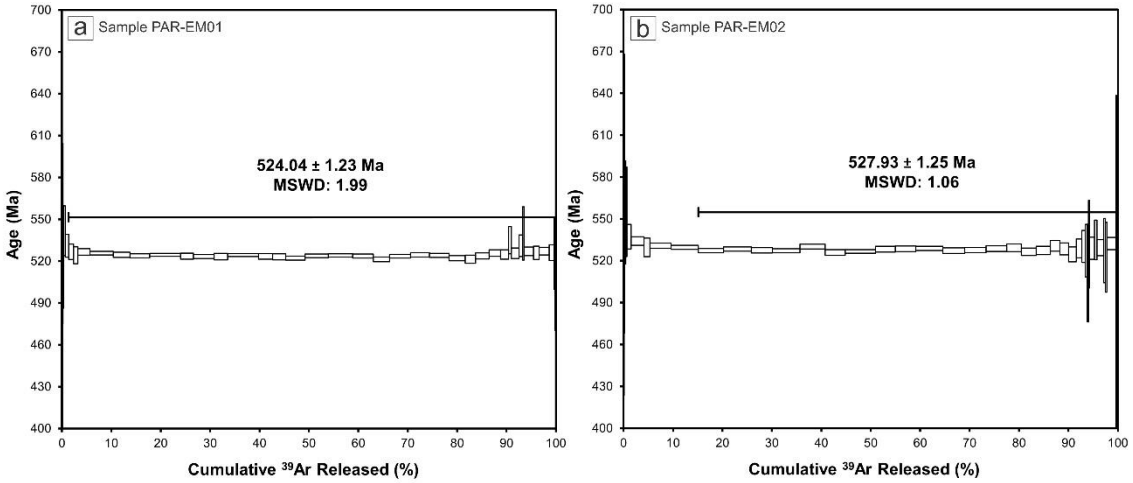

Figure 3.11. Incremental heating $^{40}Ar/^{39}Ar$ plateau age spectra for phlogopite from samples (a) PAR-EM01 and (b) PAR-EM02 of the Paraná emerald deposit.

Table 3.2. Summary of $^{40}Ar/^{39}Ar$ step heating data for phlogopite flakes from sample PAR-EM-01 in the Paraná emerald deposit.

Measurements	Relative Abundance	^{36}Ar (fA)	%1σ	^{37}Ar (fA)	%1σ	^{38}Ar (fA)	%1σ	^{39}Ar (fA)	%1σ	^{40}Ar (fA)	%1σ	40(r)/39(k)	± 2σ	Age (Ma)	± 2σ	$^{40}Ar(r)$ (%)	$^{39}Ar(k)$ (%)	K/Ca	± 2σ
20F30665	0.1 %	0.0299	2.25	0.0141	133.36	0.0017	646.24	0.1803	4.75	37.23	0.53	157.01	± 15.24	403.16	± 35.11	76.06	0.12	5	± 15
20F30667	0.2 %	0.0055	11.35	0.0079	219.37	0.0094	113.22	0.1307	6.86	30.21	0.65	218.54	± 30.28	539.73	± 64.76	94.55	0.09	7	± 31
20F30668	0.3 %	0.0086	7.12	0.0005	3743.98	0.0022	464.18	0.2167	4.00	48.27	0.41	210.82	± 17.03	523.14	± 36.77	94.66	0.15	189	± 14118
20F30670	0.4 %	0.0155	4.15	0.0123	148.89	0.0061	164.99	0.4562	1.88	104.77	0.19	219.49	± 8.34	541.75	± 17.83	95.58	0.31	16	± 47
20F30671	0.6 %	0.0295	2.26	0.0017	1021.74	0.0131	78.79	0.9872	0.89	220.54	0.09	214.49	± 3.85	531.05	± 8.27	96.01	0.67	251	± 5124
20F30672*	0.8 %	0.0255	2.56	0.0044	391.26	0.0252	40.88	1.4671	0.59	319.34	0.06	212.48	± 2.53	526.71	± 5.45	97.62	1.00	143	± 1122
20F30674*	1.0 %	0.0192	3.50	0.0101	171.11	0.0300	32.19	1.3227	0.66	285.26	0.07	211.32	± 2.82	524.22	± 6.09	97.99	0.90	56	± 192
20F30675*	1.5 %	0.0222	2.92	0.0008	2242.88	0.0424	23.94	3.5084	0.25	751.90	0.03	212.42	± 1.06	526.59	± 2.29	99.12	2.39	1893	± 84929
20F30676*	1.9 %	0.0394	1.76	0.0140	120.32	0.0844	12.36	6.9715	0.14	1490.03	0.01	212.04	± 0.59	525.78	± 1.27	99.21	4.75	213	± 514
20F30678*	2.3 %	0.0078	7.94	0.0024	736.62	0.0620	16.69	4.9035	0.20	1039.11	0.02	211.44	± 0.85	524.47	± 1.84	99.77	3.34	865	± 12745
20F30679*	2.7 %	0.0119	5.57	0.0161	106.27	0.0735	14.36	5.8934	0.16	1247.59	0.02	211.09	± 0.68	523.72	± 1.46	99.71	4.02	158	± 335
20F30680*	3.1 %	0.0217	3.15	0.0072	243.37	0.1082	9.45	9.1496	0.11	1941.52	0.01	211.49	± 0.49	524.58	± 1.05	99.67	6.24	547	± 2661
20F30682*	3.4 %	0.0050	12.57	0.0039	464.23	0.0595	17.33	3.8485	0.24	813.57	0.02	211.01	± 1.01	523.55	± 2.18	99.82	2.62	421	± 3909
20F30683*	3.7 %	0.0122	5.32	0.0251	77.07	0.0567	17.88	6.1543	0.15	1301.66	0.02	210.91	± 0.65	523.33	± 1.40	99.72	4.20	105	± 162
20F30684*	4.0 %	0.0049	12.58	0.0144	120.58	0.0419	24.67	3.9910	0.25	842.98	0.02	210.85	± 1.06	523.21	± 2.28	99.83	2.72	119	± 287
20F30686*	4.3 %	0.0184	3.63	0.0076	241.25	0.1159	8.76	9.1784	0.11	1945.44	0.01	211.36	± 0.49	524.30	± 1.05	99.72	6.26	522	± 2521
20F30687*	4.6 %	0.0043	14.33	0.0113	154.94	0.0475	22.64	4.1817	0.22	883.31	0.02	210.92	± 0.95	523.36	± 2.05	99.85	2.85	159	± 492
20F30688*	4.9 %	0.0046	13.49	0.0135	130.91	0.0426	22.90	3.8921	0.24	821.80	0.02	210.79	± 1.00	523.07	± 2.16	99.83	2.65	124	± 326
20F30690*	5.3 %	0.0083	8.05	0.0083	211.19	0.0620	17.00	5.7723	0.17	1216.84	0.02	210.38	± 0.70	522.18	± 1.52	99.80	3.94	299	± 1264
20F30691*	5.6 %	0.0080	8.20	0.0121	149.19	0.0761	13.02	6.8567	0.14	1450.00	0.01	211.12	± 0.60	523.79	± 1.29	99.83	4.68	245	± 730
20F30692*	5.9 %	0.0103	6.22	0.0090	197.13	0.0921	10.81	7.2330	0.12	1531.17	0.01	211.27	± 0.52	524.10	± 1.13	99.80	4.93	345	± 1359
20F30694*	6.3 %	0.0115	5.82	0.0041	448.32	0.0686	15.23	6.1517	0.16	1301.89	0.02	211.07	± 0.68	523.68	± 1.47	99.74	4.20	638	± 5725
20F30695*	6.6 %	0.0075	8.84	0.0021	878.39	0.0543	18.30	4.8233	0.19	1014.95	0.02	209.96	± 0.81	521.28	± 1.75	99.78	3.29	997	± 17518
20F30696*	7.0 %	0.0080	8.22	0.0029	594.89	0.0740	14.07	6.2252	0.15	1316.01	0.02	211.02	± 0.66	523.56	± 1.42	99.82	4.25	914	± 10869
20F30698*	7.4 %	0.0074	8.96	0.0114	157.61	0.0648	16.91	5.5772	0.17	1181.56	0.02	211.46	± 0.72	524.52	± 1.55	99.81	3.80	210	± 662
20F30699*	7.8 %	0.0078	8.16	0.0136	133.39	0.0707	14.56	5.8195	0.15	1231.82	0.02	211.27	± 0.66	524.11	± 1.42	99.81	3.97	183	± 489
20F30700*	8.2 %	0.0078	8.23	0.0469	37.85	0.0650	15.69	4.8178	0.20	1015.76	0.02	210.35	± 0.85	522.13	± 1.83	99.77	3.29	44	± 33
20F30702*	8.7 %	0.0032	20.14	0.0052	337.44	0.0364	29.68	3.0754	0.32	646.82	0.03	210.01	± 1.34	521.38	± 2.90	99.85	2.10	256	± 1729
20F30703*	9.1 %	0.0039	15.96	0.0247	73.47	0.0506	20.87	4.0070	0.24	846.90	0.02	211.07	± 1.01	523.67	± 2.18	99.86	2.73	70	± 102

20F30704*	9.6 %	0.0013	49.71	0.0175	100.60	0.0386	26.64	3.4372	0.25	729.27	0.03	212.06	± 1.07	525.81	± 2.31	99.95	2.34	85	± 170
20F30706*	10.1 %	0.0024	25.45	0.0176	104.36	0.0235	41.95	2.3609	0.36	500.20	0.04	211.57	± 1.55	524.75	± 3.34	99.86	1.61	58	± 120
20F30707*	10.5 %	0.0021	28.08	0.0219	81.65	0.0056	189.05	0.8537	1.05	184.06	0.11	216.34	± 4.57	535.02	± 9.79	100.34	0.58	17	± 27
20F30708*	11.0 %	0.0009	71.31	0.0026	685.41	0.0340	30.43	2.2352	0.41	474.05	0.04	211.97	± 1.74	525.61	± 3.76	99.95	1.52	371	± 5087
20F30710*	11.5 %	0.0018	33.76	0.0144	127.52	0.0137	77.10	1.0571	0.83	226.21	0.09	214.51	± 3.60	531.08	± 7.74	100.24	0.72	32	± 81
20F30711*	12.0 %	0.0016	36.40	0.0060	304.43	0.0031	331.14	0.4452	2.02	96.84	0.20	218.61	± 8.92	539.88	± 19.08	100.50	0.30	32	± 194
20F30712*	12.5 %	0.0046	13.60	0.0111	162.77	0.0341	30.91	2.8214	0.33	601.26	0.03	212.62	± 1.44	527.02	± 3.09	99.77	1.92	109	± 356
20F30714*	13.0 %	0.0020	31.03	0.0200	84.43	0.0178	56.76	1.6605	0.51	352.87	0.06	212.15	± 2.20	526.01	± 4.74	99.83	1.13	36	± 60
20F30715*	13.5 %	0.0007	95.48	0.0420	43.31	0.0361	29.76	2.9641	0.30	630.65	0.03	212.70	± 1.30	527.18	± 2.79	99.97	2.02	30	± 26
20F30717*	14.0 %	0.0010	59.07	0.0115	150.67	0.0173	60.41	1.4286	0.61	303.40	0.06	212.16	± 2.62	526.03	± 5.65	99.90	0.97	54	± 161
20F30718*	14.5 %	0.0009	64.25	0.0129	141.44	0.0016	638.72	0.3279	2.81	69.27	0.28	212.07	± 12.02	525.83	± 25.91	100.40	0.22	11	± 31
20F30720*	15.0 %	0.0003	216.94	0.0016	1127.24	0.0134	76.46	0.2508	3.43	50.21	0.39	200.49	± 13.92	500.71	± 30.41	100.17	0.17	68	± 1530

J value = 0.00156921 ± 0.00000198; total fusion age = 524.18 ± 1.21 Ma; *steps chosen for weighted mean age calculation; negative values in red.

Table 3.3. Summary of $^{40}Ar/^{39}Ar$ step heating data for phlogopite flakes from sample PAR-EM-02 in the Paraná emerald deposit.

Measurements	Relative Abundance	^{36}Ar (fA)	%1σ	^{37}Ar (fA)	%1σ	^{38}Ar (fA)	%1σ	^{39}Ar (fA)	%1σ	^{40}Ar (fA)	%1σ	40(r)/39(k)	± 2σ	Age (Ma)	± 2σ	$^{40}Ar(r)$ (%)	$^{39}Ar(k)$ (%)	K/Ca	± 2σ
20F30578	0.1 %	0.0598	0.92	0.0467	37.27	0.0107	92.74	0.1283	6.83	42.42	0.25	191.58	± 26.36	482.07	± 58.30	57.92	0.13	1	± 1
20F30580	0.2 %	0.0100	4.32	0.0239	73.62	0.0049	206.91	0.0837	10.18	22.34	0.48	231.41	± 47.31	568.12	± 99.86	86.64	0.08	2	± 2
20F30581	0.3 %	0.0230	2.12	0.0069	265.88	0.0090	111.80	0.2239	3.83	57.26	0.19	225.07	± 17.33	554.68	± 36.84	88.00	0.22	14	± 74
20F30583	0.4 %	0.0224	2.03	0.0296	56.07	0.0026	396.74	0.2444	3.33	61.74	0.18	225.22	± 15.08	555.00	± 32.06	89.15	0.24	4	± 4
20F30584	0.6 %	0.0414	1.20	0.0105	176.25	0.0304	32.98	0.9159	0.94	211.05	0.05	216.93	± 4.08	537.30	± 8.75	94.15	0.90	38	± 132
20F30585	0.8 %	0.0540	0.97	0.0185	96.25	0.0428	23.44	2.6476	0.34	586.53	0.02	215.45	± 1.46	534.12	± 3.14	97.25	2.59	62	± 118
20F30587	1.0 %	0.0239	2.03	0.0018	929.14	0.0179	55.07	1.1886	0.71	260.69	0.04	213.34	± 3.06	529.56	± 6.59	97.27	1.16	280	± 5202
20F30588	1.5 %	0.0299	1.58	0.0033	543.72	0.0552	18.54	4.3922	0.20	948.38	0.01	213.89	± 0.87	530.76	± 1.87	99.06	4.29	568	± 6173
20F30589	1.9 %	0.0791	0.77	0.0079	221.19	0.0786	12.63	5.6571	0.16	1230.44	0.01	213.33	± 0.68	529.55	± 1.47	98.08	5.53	309	± 1367
20F30591*	2.3 %	0.0792	0.74	0.0062	289.84	0.0793	13.14	5.2085	0.17	1129.22	0.01	212.26	± 0.74	527.25	± 1.60	97.90	5.09	363	± 2104
20F30592*	2.7 %	0.0583	1.05	0.0017	1065.61	0.0762	13.39	5.7442	0.16	1239.65	0.01	212.78	± 0.69	528.36	± 1.50	98.60	5.61	1458	± 31063
20F30593*	3.1 %	0.0270	2.03	0.0058	301.31	0.0542	19.31	4.3208	0.21	925.73	0.01	212.38	± 0.90	527.51	± 1.95	99.13	4.22	320	± 1928
20F30595*	3.4 %	0.0217	2.16	0.0033	523.59	0.0662	15.08	5.7638	0.15	1229.78	0.01	212.24	± 0.65	527.20	± 1.40	99.47	5.63	752	± 7875
20F30596*	3.7 %	0.0157	3.00	0.0160	107.39	0.0636	17.21	5.2164	0.18	1119.05	0.01	213.63	± 0.79	530.19	± 1.70	99.58	5.10	140	± 301
20F30597*	4.0 %	0.3309	0.30	0.0150	115.22	0.0973	10.75	4.1669	0.22	980.87	0.01	211.68	± 0.95	526.00	± 2.06	89.93	4.07	119	± 275
20F30599*	4.3 %	0.0193	2.57	0.0120	146.26	0.0697	14.45	6.2484	0.15	1330.43	0.01	212.00	± 0.62	526.68	± 1.35	99.57	6.11	225	± 658
20F30600*	4.6 %	0.0122	3.83	0.0340	52.03	0.0480	21.18	4.0781	0.23	871.31	0.01	212.77	± 0.97	528.33	± 2.10	99.58	3.99	52	± 54
20F30601*	4.9 %	0.0089	5.39	0.0208	88.91	0.0436	22.31	4.2566	0.22	908.71	0.01	212.86	± 0.92	528.53	± 1.99	99.71	4.16	88	± 157
20F30603*	5.3 %	0.0115	4.01	0.0116	155.42	0.0644	16.15	5.5817	0.17	1192.38	0.01	213.01	± 0.72	528.85	± 1.55	99.71	5.46	207	± 644
20F30604*	5.6 %	0.0139	3.50	0.0328	52.84	0.0529	20.33	4.5345	0.22	966.56	0.01	212.24	± 0.94	527.20	± 2.03	99.57	4.43	59	± 63
20F30605*	5.9 %	0.0126	3.68	0.0071	252.10	0.0485	21.83	4.4533	0.20	949.97	0.01	212.47	± 0.86	527.70	± 1.85	99.60	4.35	268	± 1354
20F30607*	6.3 %	0.0085	5.59	0.0297	58.86	0.0557	18.58	4.2747	0.22	912.77	0.01	212.93	± 0.93	528.70	± 2.01	99.72	4.18	62	± 73
20F30608*	6.6 %	0.0072	6.15	0.0278	63.56	0.0274	35.14	3.0052	0.30	642.82	0.02	213.18	± 1.27	529.22	± 2.73	99.66	2.94	46	± 59
20F30609*	7.0 %	0.0072	6.56	0.0076	226.88	0.0348	29.79	3.0548	0.29	649.45	0.02	211.89	± 1.22	526.45	± 2.63	99.67	2.99	174	± 789
20F30611*	7.4 %	0.0056	7.87	0.0060	302.66	0.0338	29.85	2.9203	0.32	621.74	0.02	212.33	± 1.38	527.40	± 2.97	99.73	2.85	211	± 1277
20F30612*	7.8 %	0.0030	14.24	0.0137	128.19	0.0145	72.82	1.9908	0.41	426.69	0.03	213.87	± 1.78	530.72	± 3.83	99.79	1.95	62	± 160
20F30613*	8.2 %	0.0042	10.15	0.0002	6898.19	0.0113	89.85	1.8001	0.47	384.42	0.03	212.85	± 2.00	528.52	± 4.31	99.67	1.76	3150	± 434612
20F30615*	8.7 %	0.0027	16.12	0.0293	59.44	0.0118	87.86	1.6059	0.58	339.65	0.03	211.01	± 2.45	524.54	± 5.30	99.77	1.57	24	± 28
20F30616*	9.1 %	0.0011	37.91	0.0040	453.23	0.0032	315.79	1.1610	0.73	247.67	0.04	213.03	± 3.12	528.91	± 6.73	99.86	1.13	125	± 1137

20F30617*	9.6 %	0.0001	430.77	0.0179	104.89	0.0132	77.22	0.6954	1.24	148.54	0.07	213.64	± 5.33	530.22	± 11.48	100.02	0.68	17	± 35
20F30619*	10.1 %	0.0005	88.84	0.0132	135.83	0.0029	350.68	0.4178	2.05	88.82	0.12	212.25	± 8.73	527.22	± 18.83	99.84	0.41	14	± 37
20F30620*	10.5 %	0.0000	38089.78	0.0204	87.68	0.0025	403.44	0.2192	3.91	44.90	0.24	204.85	± 16.10	511.17	± 35.04	100.00	0.21	5	± 8
20F30621*	11.0 %	0.0015	29.54	0.0106	159.50	0.0068	155.02	0.2453	3.38	53.02	0.20	214.38	± 14.55	531.82	± 31.32	99.18	0.24	10	± 32
20F30623*	11.5 %	0.0019	22.81	0.0428	38.00	0.0114	87.95	1.0118	0.85	216.14	0.05	213.06	± 3.66	528.96	± 7.88	99.73	0.99	10	± 8
20F30624*	12.0 %	0.0030	13.28	0.0190	94.86	0.0082	123.32	0.5357	1.53	116.50	0.09	215.80	± 6.62	534.88	± 14.23	99.23	0.52	12	± 23
20F30625*	12.5 %	0.0024	17.78	0.0141	126.44	0.0178	57.45	1.3855	0.62	296.18	0.04	213.25	± 2.64	529.38	± 5.68	99.76	1.35	42	± 107
20F30627*	13.0 %	0.0016	24.33	0.0085	210.87	0.0026	413.27	0.3473	2.50	74.22	0.15	212.27	± 10.64	527.26	± 22.97	99.34	0.34	18	± 74
20F30628*	13.5 %	0.0021	19.79	0.0163	108.69	0.0083	124.45	0.3030	2.74	64.30	0.17	210.06	± 11.58	522.50	± 25.07	99.01	0.30	8	± 17
20F30630*	14.0 %	0.0021	20.04	0.0260	65.70	0.0143	73.45	1.8893	0.47	406.09	0.03	214.62	± 2.04	532.32	± 4.39	99.85	1.85	31	± 41
20F30631*	14.5 %	0.0008	55.02	0.0072	252.36	0.0015	654.21	0.0569	15.03	11.74	0.92	202.10	± 61.03	505.19	± 133.32	98.02	0.06	3	± 17
20F30633*	15.0 %	0.0025	16.91	0.0303	57.91	0.0054	195.30	0.3326	2.70	70.14	0.15	208.61	± 11.31	519.35	± 24.52	98.93	0.33	5	± 5

J value = 0.00157265 ± 0.00000200; total fusion age = 528.55 ± 1.27 Ma; *steps chosen for weighted mean age calculation; negative values in red.

DISCUSSION

Shear zone kinematics and deformation mechanisms

The disposition of all interpreted magnetic domains in the NE-SW direction reflects the strong influence of strike-slip shear zones (*e.g.*, PASZ, VISZ, LASZ) in the geometric framework of the study area. Major magnetic lineaments are found in agreement with deeper Euler solutions depths (200 to > 400 m) around these structures. Most important for emerald mineralization, the PASZ is marked by a high magnetic contrast in the area of the Paraná emerald deposit, as observed in the total magnetic intensity map (Figure 3.2a). First order high magnetic lineaments after 3D analytic signal amplitude filtering are associated with this structure, representing the main structural control for the emerald occurrences.

At a mesoscopic scale, emerald host rocks (*i.e.*, phlogopite- and actinolite-phlogopite schists) are found within a mylonitic corridor with vertical to sub-vertical foliation imprinted in both host schists and enclosing gneisses. Horizontal mineral stretching lineation marked by oriented phlogopite lamellae in the schists and deformed quartz and feldspar in gneisses suggest that transcurrent shear is the main component associated with emerald formation. A dextral movement during shearing is supported by deformed asymmetric *augens* and pegmatite *boudins*, as well as S-C and S-C-C' surfaces (Figures 3.5f, g and 6a, d, e, f).

Microstructural analysis on the mylonitic rocks of the PASZ points to dynamic recrystallization of the quartz crystals, which is mainly dominated by subgrain rotation (SGR). This is evidenced by the presence of ribbon grains and equigranular quartz bands with recrystallized grains (50 to 100 µm) oriented oblique to the main mylonitic foliation (Figure 3.7a, b, d). In a few samples, where quartz may have coarser grain sizes (> 300 µm), lobate and interfingering grain boundaries are present suggesting recrystallization through grain boundary migration (GBM). Feldspar shows core-mantle structures that are typical for mid-crustal conditions (*e.g.*, Tullis 2002; Figure 3.7e). Theses microstructures are consistent with deformation at moderate temperatures in the quartz SGR zone (Stipp et al. 2002, Faleiros et al. 2010). A temperature range of 390-550 °C is considered, including the bulging (BLG)-SGR and SGR-GBM transition zones of Stipp et al. (2002), and the dynamic recrystallization at the margins of feldspar clasts (Fitz Gerald and Stünitz 1993). GBM domains may be restricted to localized portions with increased strain.

Age constraints on emerald mineralization

Zircon U-Pb geochronology of granitic veins and boudins interleaved with the schist yielded ages of 2210 ± 8 Ma and 2201 ± 6 Ma close to those reported for the Caicó basement dated at ca. 2150-2200 Ma (Hackspacher et al. 1990, Fetter et al. 2000, Hollanda et al. 2011). Theses ages suggest that basement rocks were intensely reworked by ductile strike-slip deformation during ore development. Gneiss fragments were probably enclosed by the metasomatic schist as the latter was formed during shear stress of the PASZ in the last stages of the Brasiliano Orogeny, as suggested by meso- and microscale structural analysis.

Formation of the emerald-bearing phlogopite schist during the PASZ deformation is evidenced by the phlogopite ^{40}Ar-^{39}Ar ages of 524 ± 1 Ma and 528 ± 1 Ma. These ages are similar to biotite $^{40}Ar/^{39}Ar$ ages registered in pegmatites of the northern Borborema Province (523.1 ± 1.1 Ma; Araújo et al. 2005) suggesting that pegmatite intrusion and subsequent metasomatic modification may have occurred contemporaneously. Thus, emerald mineralization is directly related to the ductile evolution of the Portalegre shear zone in the late Neoproterozoic-early Cambrian (Hackspacher and Legrand 1989), rather than to latter brittle reactivations in the Cretaceous period (apatite fission track ages of 90-125 Ma, da Nóbrega et al. 2005). The continuous process of pegmatite intrusion and metasomatism during ductile deformation is also proposed by Zwaan (2006) for the Sandawana emerald deposit (Zimbabwe), formed around 2.6 Ga, depicting the importance of tectonism in bringing together the necessary elements and conditions to form emerald.

Towards a genetic model for the Paraná Deposit

The classic schist-hosted model for emerald formation involves metasomatism between beryllium-rich granites/pegmatites and chromium- or vanadium-bearing mafic/ultramafic rocks or their metamorphic equivalent (Walton 2004 and references therein). Whether these schist-hosted emerald deposits were connected to magmatic intrusions or to tectonic structures, represented the main subdivisions in older classifications (*e.g.*, Schwarz and Giuliani 2001, Schwarz et al. 2001). Modern classification schemes, on the other hand, recognize the role of tectonism in most emerald deposits (Giuliani et al. 2019). Even when mineralizing fluids have a metasomatic-hydrothermal origin from interactions between pegmatite and mafic/ultramafic rocks, brittle and ductile structures may participate as fluid channels determining ore geometry

and litho-structural controls (see Abdalla and Mohamed 1999, Zwaan 2006, Zwaan et al. 2012, Santiago et al. 2019).

In the Paraná emerald deposit, ore body geometry is directly related to the strike-slip geometry and dextral kinematics of the PASZ. The emerald occurrences are roughly aligned in a trend that extends for, at least, 20 km between the Pitombeiras mine and Marcelino Vieira occurrences (see Figure 3.1c). Deformation temperatures at 390-550 °C are in consonance with most emerald formation temperature ranges (Barton and Young 2002, Zwaan 2006, Groat et al. 2008).

A syn-kinematic formation of emerald is proposed based on (i) the host rock geometry, (ii) σ-type porphyroclasts of syngenetic K-feldspar, (iii) rotated emerald crystals enveloped by the phlogopite schist foliation, and (iv) prismatic emerald crystals grown parallel to foliation planes. Therefore, a tectonic-magmatic-related type of deposit is proposed, following the classification scheme of Giuliani et al. (2019). Be-bearing pegmatites might have been emplaced coeval to the strike-slip deformation of the PASZ, accompanied and/or followed by hydrothermal/metasomatic activity. The presence of albitite or desilicated pegmatites dykes parallel to the schist foliation (see Araújo Neto et al. 2021) are suggestive of a metasomatic modification of the granitic pegmatites after interaction with mafic/ultramafic rocks, a common setting in other Brazilian emerald deposits (Giuliani et al. 1990, 1997, Santiago et al. 2019). Moreover, unaltered beryl-bearing pegmatites can be found a few kilometers (10-15 km) from the Paraná deposit (Barreto 1991, Santos et al. 2020).

The formation of emerald requires the presence of a chromophore source, *i.e.*, Cr and V suppliers that gives the emerald its color. In metasomatic emerald deposits, the phlogopite schist is reportedly formed after modification of a mafic-ultramafic source by potassium metasomatism (Walton 2004, Zwaan 2006, Santiago et al. 2019, Giuliani et al. 2019). In the Paraná emerald deposit, Cr-bearing ultramafic rocks have not been reported. The best candidates for the chromophore source, as well as Fe and Mg suppliers – main constituents of the host schist – are amphibolite lenses of the Caicó Complex that occur along the PASZ (see Figure 3.1c). Thus, this Paleoproterozoic lithotype can be considered as the protolith of the phlogopite schist. The high Fe content and low Cr and V of the Paraná emeralds, in comparison with worldwide examples (see Araújo Neto et al. 2019), may be a result from this more mafic source instead of an ultramafic source, directly influencing the final emerald color (Fe is responsible for bluish green and/or yellowish green pleochroism in emerald).

Zircon U-Pb geochronology supports reworking of the Paleoproterozoic basement during the emerald-bearing phlogopite schist development, which ultimately formed between

ca. 530-520 Ma, at the final stages of the Brasiliano orogeny. Hence, intrusion of pegmatite and metasomatic modification of Be-bearing and chromophore-bearing sources should have occurred contemporaneously within the context of the Portalegre ductile deformation. A schematic genetic model summarizing the elements that led to emerald crystallization in the Paraná deposit is presented in Figure 3.12.

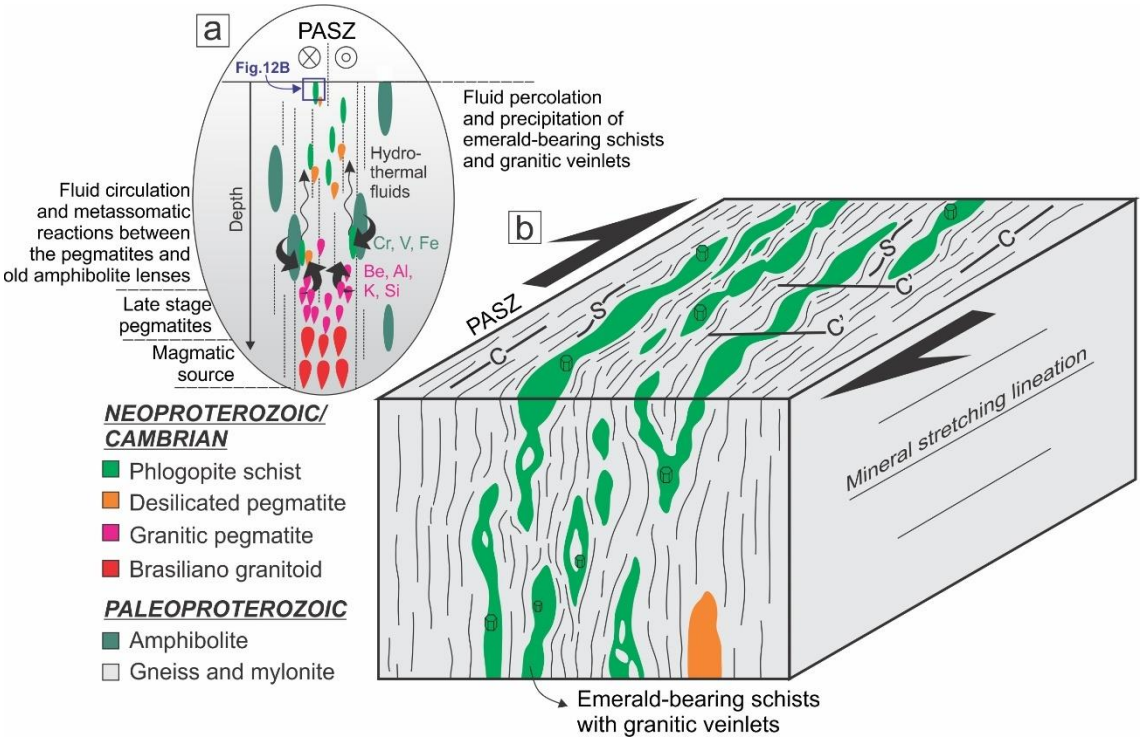

Figure 3.12. Schematic genetic model for emerald formation in the Paraná deposit. (a) Idealized interaction between pegmatites and amphibolite lenses through hydrothermal fluids along the Portalegre shear zone resulting in desilicated pegmatites and emerald bearing phlogopite schists. (b) Sketch of the current litho-structural setting of the Paraná emerald deposit.

CONCLUSIONS

In the southwestern part of the Portalegre shear zone, emerald mineralization occurs in phlogopite- and actinolite-phlogopite schists aligned into shear-controlled mylonitic corridors. Aeromagnetic images and Euler solution depths can be used to track down key magnetic lineaments and, consequently, important geological structures controlling the emerald-occurrence trend. The geophysical dataset shows that higher and deeper magnetic anomalies are associated with the main trend of the PASZ and other minor shear zones in the area.

A combination of geophysics, field structures and microstructural analysis evidence the importance of ductile shearing in the formation of the Paraná emerald deposit. Meso- and microfabrics suggest a syn-kinematic origin for the emerald-bearing schist in a dextral strike-slip regime. Microstructures suggest deformation at intermediate temperatures of 390-550 °C. Cambrian phlogopite $^{40}Ar/^{39}Ar$ ages (ca. 524-528 Ma) are presented to the phlogopite schist, and Rhyacian zircon U-Pb ages (ca. 2.20-2.21 Ga) are attributed to veins and *boudins* with granitic compositions interleaved with the schist, suggesting that both schist formation and reworking of the basement gneisses occurred during the Brasiliano orogeny.

The results presented here, coupled with other previous investigations on the Paraná emerald deposit, suggest a tectonic-magmatic-related type of deposit, with the development of an emerald-bearing phlogopite zone after metasomatic modification of Be-bearing pegmatites and amphibolite lenses of the Caicó Complex in a strike-slip setting. The Portalegre shear zone is regarded as the main structural control for the percolation of hydrothermal reactive fluids that ultimately led to emerald crystallization.

ACKNOWLEDGMENTS

We express our gratitude to Mr. Luis Amorim and the crew of Mineração Limeira Comércio, Exportação e Importação for providing access and fieldwork support in the emerald mines and for the financial support for geochronological $^{40}Ar/^{39}Ar$ analysis. J.F.A. Neto thanks the Coordenação de Aperfeiçoamento de Pessoal de Nível Superior (CAPES) for his doctoral scholarship. Gustavo Viegas acknowledges the Brazilian Research Council (CNPq) for a research grant (304478/2021–0) and Peter A. Cawood acknowledges support from the Australian Research Council grant FL160100168. We would also like to thank CPRM – Serviço Geológico do Brasil for providing access to the geophysical data for academic purposes.

REFERENCES

Abdalla, H.M., Mohamed, F.H. (1999). Mineralogical and geochemical investigations of beryl mineralizations, Pan-African belt of Egypt: Genetic and exploration aspects. *Journal of African Earth Sciences*, 28, 581–598. https://doi.org/10.1016/S0899-5362(99)00033-0

Almeida, G.M., Fuck, R.A., Dantas, E.L., Lima S.S. (2022). Oblique collision and accretionary processes in the South Borborema Province: Insights from structural geology and geophysical data. *Tectonophysics*, 844, 229607. https://doi.org/10.1016/j.tecto.2022.229607

Almeida, G.M., Fuck, R.A., Lima, D.P.D., Dantas, E.L. (2021). Accretion tectonics in Western Gondwana highlighted by the aeromagnetic signature of the Sergipano Belt, NE Brazil. *Tectonophysics*, 802, 228742. https://doi.org/10.1016/j.tecto.2021.228742

Araújo, M.N.C., Alves da Silva, F.C., Jardim de Sá, E.F. (2001). Pegmatite Emplacement in the Seridó Belt, Northeastern Brazil: Late Stage Kinematics of the Brasiliano Orogen. *Gondwana Research*, 4(1), 75-85. https://doi.org/10.1016/S1342-937X(05)70656-0

Araújo, M.N.C., Vasconcelos, P.M., Alves da Silva, F.C., Jardim de Sá, E.F., Sá, J.M. (2005). $^{40}Ar/^{39}Ar$ geochronology of gold mineralization in Brasiliano strike-slip shear zones in the Borborema province, NE Brazil. *Journal of South American Earth Sciences*, 19(4), 445-460. https://doi.org/10.1016/j.jsames.2005.06.009

Araújo Neto, J.F., Barreto, S.B., Carrino, T.A., Müller, A., Santos, L.C.M.L. (2019). Mineralogical and gemological characterization of emerald crystals from Paraná deposit, NE Brazil: a study of mineral chemistry, absorption and reflectance spectroscopy and thermal analysis. *Brazilian Journal of Geology*, 49(3), 1-15. https://doi.org/10.1590/2317-4889201920190014

Araújo Neto, J.F., Barreto, S.B., Carrino, T.A., Souza, I.M.B.A., Santos, G.L. (2021). Geochemical and reflectance spectroscopy data integration to characterize emerald deposits: the case of the Paraná deposit, Brazil. *Anais da Academia Brasileira de Ciências*, 93(1), e20200236. https://doi.org/10.1590/0001-3765202120200236

Araújo Neto, J.F., Lira Santos, G., Souza, I.M.B.A., Barreto, S.B., Santos, L.C.M.L., Bezerra, J.P.S., Carrino, T.A. (2018). Integration of remote sensing, airborne geophysics and structural analysis to geological mapping: a case study of the Vieirópolis region, Borborema Province, NE Brazil. *Geologia USP. Série Científica*, 18(3), 89-103. https://doi.org/10.11606/issn.2316-9095.v18-140834

Barreto, S.B. (1991). *Caracterização químico-mineralógica dos berilos de Tenente Ananias – RN*. Master thesis. Recife: Instituto de Geociências – UFPE.

Barton, M.D., Young, S. (2002). Non-pegmatitic deposits of beryllium: mineralogy, geology, phase equilibria and origin. In: Grew, E.S. (Ed.). Beryllium: Mineralogy, Petrology, and Geochemistry. *Reviews in Mineralogy and Geochemistry*, 50(1), 591–691. https://doi.org/10.2138/rmg.2002.50.14

Baumgartner, R., Romer, R.L., Moritz, R., Sallet, R., Chiaradia, M. (2006). Columbite–tantalite-bearing granitic pegmatites from the Seridó belt, northeastern Brazil: genetic constraints from U–Pb dating and Pb isotopes. *The Canadian Mineralogist*, 44(1), 69-86. https://doi.org/10.2113/gscanmin.44.1.69

Beurlen, H., Barreto, S.B., Martin, R., Melgarejo, J., Da Silva, M.R.R., Souza Neto, J.A. (2009) The Borborema Pegmatite Province, NE-Brazil revisited. *Estudos Geológicos*, 19(2), 62-66. http://dx.doi.org/10.18190/1980-8208/estudosgeologicos.v19n2p62-66

Beurlen, H., Moura, O.J.M., Soares, D.R., Da Silva, M.R.R., Rhede, D. (2011). Geochemical and geological controls on the genesis of gem-quality “Paraíba Tourmaline” in granitic

pegmatites from northeastern Brazil. *The Canadian Mineralogist*, 49(1), 277-300. https://doi.org/10.3749/canmin.49.1.277

Blenkinsop, T.G., Treloar, P.J. (1995). Geometry, classification and kinematics of S-C and S-C′ fabrics in the Mushandike area, Zimbabwe. *Journal of Structural Geology*, 17(3), 397-408. https://doi.org/10.1016/0191-8141(94)00063-6

Brito Neves, B.B., Fuck, R.A., Pimentel, M.M. (2014). The Brasiliano collage in South America: a review. *Brazilian Journal of Geology*, 44(3), 493-518. https://doi.org/10.5327/Z2317-4889201400030010

Brito Neves, B.B., Santos, E.J., Fuck, R.A., Santos, L.C.M.L. (2016). A preserved early Ediacaran magmatic arc at the northernmost portion of the Transversal Zone central subprovince of the Borborema Province, Northeastern South America. *Brazilian Journal of Geology*, 46(04), 491-508. https://doi.org/10.1590/2317-4889201620160004

Brito Neves, B.B., Santos, E.J., Van Schmus, W.R.Q. (2000). Tectonic history of the Borborema Province. In: Cordani, U.G., Milani E.J., Thomaz Filho A., Campos D.A. (Org.). Tectonic Evolution of South America. Rio de Janeiro, *31st International Geological Congress Special Publication*, 151-182.

Bühn, B.M., Pimentel, M.M., Matteini, M., Dantas, E.L. (2009). High spatial resolution analysis of Pb and U isotopes for geochronology by laser ablation multicollector inductively coupled plasma mass spectrometry (LA-MC-ICP-MS). *Anais da Academia Brasileira de Geociências* 81, 1–16. https://doi.org/10.1590/S0001-37652009000100011

Campelo, R.C. (1999). *Análise de terrenos na porção setentrional da Província Borborema, NE do Brasil: integração de dados geológicos e gravimétricos*. Dissertação (Mestrado). Natal: Centro de Ciências Exatas e da Terra – UFRN.

Castelo Branco, R.M.G, Giuliani, G., Cheilletz, A., Clementeile, L. (1988). Os berilos verdes da região de Coqui, município de Quixeramobim: novas ocorrências de esmeraldas no estado do Ceará. *XXXV Congresso Brasileiro de Geologia*. Belém: SBG.

Cawood, P.A., Hawkesworth, C.J. (2015). Temporal relations between mineral deposits and global tectonic cycles. *Geological Society, London, Special Publications*, 393 (1), 9-21. https://doi.org/10.1144/SP393.1

Caxito, F.A., Santos, L.C.M.L., Ganade, C.E., Bendaoud, A., Fettous, E-H., Bouyo, M.H. (2020). Toward an integrated model of geological evolution for NE Brazil-NW Africa: The Borborema Province and its connections to the Trans-Saharan (Benino-Nigerian and Tuareg shields) and Central African orogens. *Brazilian Journal of Geology*, 50(02), e20190122. https://doi.org/10.1590/2317-4889202020190122

CPRM – Serviço Geológico do Brasil. (2010). Projetos Aerogeofísicos: Paraíba - Rio Grande do Norte; Pernambuco - Paraíba. Relatório final do levantamento e processamento dos dados magnetométricos e gamaespectrométricos. Technical report. Lasa Engenharia e Prospecções, Prospectors Aerolevantamentos e Sistemas.

Da Nóbrega, M.A., Sá, J.M., Bezerra, F.H.R., Hadler Neto, J.C., Iunes, P.J., Guedes, S., Tello Saenz, C.A., Hackspacher, P.C., Lima-Filho, F.P. (2005). The use ofapatite fission track thermochronology to constrain fault movements and sedimentary basin evolution in northeastern Brazil. *Radiation Measurements*, 39, 627-633. https://doi.org/10.1016/j.radmeas.2004.12.006

Dantas, E.L., Souza, Z.S., Wernick, E., Hackspacher, P.C., Martin, H., Xiaodong, D., Li, J.-W. (2013). Crustal growth in the 3.4–2.7 Ga São José de Campestre Massif, Borborema Province, NE Brazil. Precambrian Research, 227, 120-156. https://doi.org/10.1016/j.precamres.2012.08.006

Dantas, E.L., Van Schmus, W.R., Hackspacher, P.C., Fetter, A.H., Brito Neves, B.B., Cordani, U., Nutman, A.P., Williams, I.S. (2004). The 3.4–3.5 Ga São José do Campestre massif, NE Brazil: remnants of the oldest crust in South America. *Precambrian Research*, 130(1-4), 113-137. https://doi.org/10.1016/j.precamres.2003.11.002

Delgado, I.M., Souza, J.D., Silva, L.C., Silveira Filho, N.C., Dos Santos, R.A., Pedreira, A.J., Guimarães, J.T., Angelim, L.A.A., Vasconcelos, A.M., Gomes, I.P., Lacerda Filho, J.V., Valente, C.R., Perotta, M.M., Heineck, C.A. (2003). Geotectônica do Escudo Atlântico. In: Bizzi, L.A. (ed.) et al. Geologia, tectônica e recursos minerais do Brasil: texto, mapas & SIG. *Geology, tectonics and mineral resources of Brazil: text, maps & GIS*. Brasília: CPRM, 227-334.

Demartis, M. Pinotti, L.P., Coniglio, J.E., D'Eramo, F.J., Tubía, J.M., Aragón, E., Insúa, L.A.A. (2011). Ascent and emplacement of pegmatitic melts in a major reverse shear zone (Sierras de Córdoba, Argentina). *Journal of Structural Geology*, 33(9), 1334-1346. https://doi.org/10.1016/j.jsg.2011.06.008

Faleiros, F.M., Campanha, G.A.C., Maria, R., Fuzikawa, K. (2010). Quartz recrystallizations regimes, c-axis texture transition and fluid inclusion reequilibration in a prograde greenschist to amphibolite facies mylonite zone (Ribeira Shear Zone, SE Brazil). *Tectonophysics*, 485, 193-214. https://doi.org/10.1016/j.tecto.2009.12.014

Ferreira, A.C.D., Dantas, E.L., Fuck, R.A., Nedel, I.M. (2020). Arc accretion and crustal reworking from late Archean to Neoproterozoic in Northeast Brazil. *Scientific Reports*, 10, 7855. https://doi.org/10.1038/s41598-020-64688-9

Fetter, A.H., Van Schmus, W.R., Santos, T.J.S., Nogueira Neto, J.A., Arthaud, M.H. (2000). U-Pb and Sm-Nd geochronological constraints on the crustal evolution and basement architecture of Ceará State, NW Borborema Province, NE Brazil: implications for the existence of the Paleoproterozoic supercontinent "Atlantica". *Revista Brasileira de Geociências*, 30, 102-106.

Fitz Gerald, J.D., Stünitz, H. (1993). Deformation of granitoids at low metamorphic grade. I: Reactions and grain size reduction. *Tectonophysics*, 221(3-4), 269-297. https://doi.org/10.1016/0040-1951(93)90163-E

Ganade de Araújo, C., Rubatto, D., Hermann, J., Cordani, U.G., Caby, R., Basei, M.A.S. (2014). Ediacaran 2,500-km-long synchronous deep continental subduction in the West Gondwana Orogen. *Nature Communications*, 5, 5198. https://doi.org/10.1038/ncomms6198

Giuliani, G., France-Lanord, C., Zimmermann, J.L., Cheilletz, A., Arboleda, C., Charoy, B., Coget, P., Fontan, F., Giard, D. (1997). Fluid composition, δD of channel H2O, and δ18O of lattice oxygen in beryls: genetic implications for Brazilian, Colombian, and Afghanistani emerald deposits. *International Geology Reviews*, 39, 400-424. https://doi.org/10.1080/00206819709465280

Giuliani, G., Groat, L.A., Marshall, D., Fallick, A.E., Branquet, Y. (2019). Emerald Deposits: A Review and Enhanced Classification. *Minerals*, 9(2), 105. https://doi.org/10.3390/min9020105

Giuliani, G., Silva, L.J.H.D. Couto, P. (1990). Origin of emerald deposits of Brazil. *Mineralium Deposita*, 25, 57–64. https://doi.org/10.1007/BF03326384

Groat, L.A., Giuliani, G., Marshall, D.D., Turner, D. (2008). Emerald deposits and occurrences: A review. *Ore Geology Reviews*, 34:87-112. https://doi.org/10.1016/j.oregeorev.2007.09.003

Grundmann, G., Morteani, G. (1989). Emerald mineralisation during regional metamorphism: the Habachtal (Austria) and Leydsdorp (Transvaal, South Africa) deposits. *Economic Geology*, 84, 1835–1849. https://doi.org/10.2113/gsecongeo.84.7.1835

Hackspacher P.C., Van Schmus W.R., Dantas E.L. 1990. Um embasamento Transamazônico na Provincia Borborema. *Congresso Brasileiro de Geologia*, 36, Natal, Anais, 6:2683-2696.

Hackspacher, P.C., Legrand, J.M. (1989). Microstructural and metamorphic evolution of the Portalegre shear zone, northeastern Brazil. *Revista Brasileira de Geociências*, 19, 63-75.

Haldar, S.K. (2013). Chapter 3 - Exploration Geology. In: *Mineral Exploration Principles and Applications*, 41-53. https://doi.org/10.1016/B978-0-12-416005-7.00003-9

Hollanda, M.H.B.M., Archanjo, C.J., Souza, L.C., Dunyi, L., Armstrong, R. (2011). Long-lived Paleoproterozoic granitic magmatism in the Seridó-Jaguaribe domain, Borborema Province–NE Brazil. *Journal of South American Earth Sciences*, 32(4), 287-300. https://doi.org/10.1016/j.jsames.2011.02.008

Hollanda, M.H.B.M., Souza Neto, J.A., Archanjo, C.J., Stein, H., Maia, A.C.S. (2017). Age of the granitic magmatism and the W-Mo mineralization in skarns of the Seridó belt (NE Brazil) based on zircon U-Pb (SHRIMP) and molybdenite Re-Os dating. *Journal of South American Earth Sciences*, 79, 1-11. https://doi.org/10.1016/j.jsames.2017.07.011

Hronsky, J.M.A., Groves, D.I. (2008). Science of targeting: definition, strategies,targeting and performance measurement. *Australian Journal of Earth Sciences*, 55(1), 3-12. http://dx.doi.org/10.1080/08120090701581356

Jackson, S.E., Pearson, N.J., Griffin, W.L., Belousova, E.A. (2004). The application of laser ablation-inductively coupled plasma-mass spectrometry to in situ U–Pb zircon geochronology. *Chemical Geology*, 211(1-2), 47-69. https://doi.org/10.1016/j.chemgeo.2004.06.017

Jardim de Sá, E.F., Fuck, R.A., Macedo, M.H.F., Peucat, J.J., Kawashita, K., Souza, Z.S., Bertrand, J.M. (1995). Pre-brasiliano orogenic evolution in the Seridó belt, NE Brazil:

Conflicting geochronological and structural data. *Revista Brasileira de Geociências*, 25(4), 307-314.

Jardim de Sá, E.F., Medeiros, W.E., Castro, D.L. 1997. Contribuição da gravimetria aos modelos de estruturação crustal da Província Borborema, Nordeste do Brasil. Atas XVII Simpósio de Geologia do Nordeste, 352-357, Fortaleza, CE.

Kitt, S., Kisters, A., Steven, N., Maiden, K., Hartmann, K. (2016). Shear-zone hosted copper mineralisation of the Omitiomire deposit — Structural controls of fluid flow and mineralisation during subduction accretion in the Pan-African Damara Belt of Namibia. *Ore Geology Reviews*, 75, 1-15. https://doi.org/10.1016/j.oregeorev.2015.10.035

Koppers, A.A. (2002). ArArCALC—Software for 40Ar/39Ar age calculations. *Computers & Geosciences*, 28(5), 605-619. https://doi.org/10.1016/S0098-3004(01)00095-4

Koppers, A.A.P., Staudigel, H., Duncan, R.A. (2003). High-resolution 40Ar/39Ar dating of the oldest oceanic basement basalts in the western Pacific basin. *Geochemistry Geophysics Geosystems*, 4(11), 1-20. https://doi.org/10.1029/2003GC000574

Kuiper, K., Deino, A., Hilgen, F., Krijgsman, W., Renne, P., Wijbrans, J. (2008). Synchronizing rock clocks of Earth history. *Science*, 320(5875), 500-504. https://doi.org/10.1126/science.1154339

Lima, H.M., Pimentel, M.M., Fuck, R.A., Santos, L.C.M.L., Dantas, E.L. (2018). Geochemical and detrital zircon geochronological investigation of the metavolcanosedimentary Araticum complex, sergipano fold belt: Implications for the evolution of the Borborema Province, NE Brazil. *Journal of South American Earth Sciences*, 86, 176-192. https://doi.org/10.1016/j.jsames.2018.06.013

Ludwig, K.R. (2012). User's manual for Isoplot 3.75. *Berkeley Geochronological Center Special Publication No. 5.*

Matteinni, M., Junges, S.L., Dantas, E.L., Pimentel, M.M., Bühn, B.M. (2010). *In situ* zircon U-Pb and Lu-Hf isotope systematic on magmatic rocks: Insights on the crustal evolution of the Neoproterozoic Goiás Magmatic Arc, Brasília belt, Central Brazil. *Gondwana Research* ,17(1), 1-12. https://doi.org/10.1016/j.gr.2009.05.008

Medeiros, V.C. (Ed.). (2008). *Geologia e Recursos Minerais da Folha Sousa SB.24-Z-A*. Escala 1:250.000. Recife: CPRM – Serviço Geológico do Brasil.

Medeiros, V.C., Nascimento, M.A.L., Galindo, A.C., Dantas, E.L. (2012). Augen gnaisses riacianos no Domínio Rio Piranhas-Seridó - Província Borborema, Nordeste do Brasil. *Geologia USP. Série Científica*, 12(2), 3-14. https://doi.org/10.5327/Z1519-874X2012000200001

Meert, J.G., Lieberman, B.S. (2008). The Neoproterozoic assembly of Gondwana and its relationship to the Ediacaran–Cambrian radiation. *Gondwana Research*, 14(1-2), 5-21. https://doi.org/10.1016/j.gr.2007.06.007

Min, K., Mundil, R., Renne, P. R., Ludwig, K. R. (2000). A test for systematic errors in 40Ar/39Ar geochronology through comparison with U/Pb analysis of a 1.1-Ga rhyolite. *Geochimica et Cosmochimica Acta*, 64(1), 73-98. https://doi.org/10.1016/S0016-7037(99)00204-5

Nascimento, M.A.L., Galindo, A.C., Medeiros, V.C. (2015). Ediacaran to Cambrian magmatic suites in the Rio Grande do Norte domain, extreme Northeastern Borborema Province (NE of Brazil): Current knowledge. *Journal of South American Earth Sciences*, 58, 281-299. https://doi.org/10.1016/j.jsames.2014.09.008

Oliveira, R.G., Medeiros, W.E. (2018). Deep crustal framework of the Borborema Province, NE Brazil, derived from gravity and magnetic data. *Precambrian Research*, 315, 45-65. https://doi.org/10.1016/j.precamres.2018.07.004

Pereira, L.C.L., Santos, L.C.M.L., Carrino, T.A. (2019). The role of airborne geophysics in the investigation of gold occurrences in the Itapetim Region, Borborema Province, Northeast Brazil. *Brazilian Journal of Geology*, 49(3), e20190028. https://doi.org/10.1590/2317-4889201920190028

Reid, A.B., Allson, J.M., Granser, H., Miett, A.J., Somerton, I.W. (1990). Magnetic interpretation in three dimensions using Euler deconvolution. *Geophysics*, 55, 80-91. https://doi.org/10.1190/1.1442774

Ribeiro-Althoff, A.M., Cheilletz, A., Giuliani, G., Féraud, G., Barbosa Camacho, G., Zimmermann, J.L. (1997). 40Ar/39Ar and K-Ar Geochronological Evidence for Two Periods (~2 Ga and 650 to 500 Ma) of Emerald Formation in Brazil. *International Geology Review*, 39(10), 924-937. https://doi.org/10.1080/00206819709465310

Santiago, J.S., Souza, V.S., Dantas, E.L., Oliveira, C.G. (2019). Ediacaran emerald mineralization in Northeastern Brazil: the case of the Fazenda Bonfim Deposit. *Brazilian Journal of Geology*, 49(4), 1-14. https://doi.org/10.1590/2317-4889201920190081

Santos, E.J., Souza Neto, J.A., Silva, M.R.R., Beurlen, H., Cavalcanti, J.A.D., Silva, M.G., Dias, V.M., Costa, A.F., Santos, L.C.M.L., Santos, R.B. (2014). Metalogênese das porções norte e central da Província Borborema. In: Silva, M.G., Rocha Neto, M.B., Jost, H., Kuyumijan, R.M. *Metalogênese das províncias tectônicas brasileiras*. 343-388. Belo Horizonte: CPRM.

Santos, G.L., Souza, I.M.B.A., Barreto, S.B., Araújo Neto, J.F., Müller, A. (2020). The Serra Branca amazonite pegmatite of the Vieirópolis pegmatite field, Paraíba, Brazil: A new and unusual megacrystic amazonite deposit. *The Canadian Mineralogist*, 58(6), 679-702. https://doi.org/10.3749/canmin.1900095

Santos, L.C.M.L., Caxito, F.A., Bouyo, M.H., Ouadahi, S., Araïbia, K., Lages, G.A., Santos, G.L., Pitombeira, J.P.A., Cawood, P.A. (2023). Relics of ophiolite-bearing accretionary wedges in NE Brazil and NW Africa: connecting threads of western Gondwana´s ocean during Neoproterozoic times. *Geosystems and Geoenvironment*, 100148. https://doi.org/10.1016/j.geogeo.2022.100148

Santos, L.C.M.L., Dantas, E.L., Cawood, P.A., Lages, G.A., Lima, H.M., Santos, E.J. (2018). Accretion tectonics in western Gondwana deduced from Sm-Nd isotope mapping of terranes in the Borborema Province, NE Brazil. *Tectonics*, 37, 2727-2743. https://doi.org/10.1029/2018TC005130

Santos, L.C.M.L., Dantas, E.L., Cawood., P.A., Lages, G.A., Lima., H.M., Santos, E.J., Caxito, F.A. (2019) Early to late Neoproterozoic subduction-accretion episodes in the Cariris Velhos Belt of the Borborema Province, Brazil: Insights from isotope and whole-rock geochemical data of supracrustal and granitic rocks. *Journal of South American Earth Sciences*, 96, 102384. https://doi.org/10.1016/j.jsames.2019.102384

Santos, L.C.M.L., Dantas, E.L., Vidotti, R.M., Cawood, P.A., Santos, E.J., Fuck, R.A., Lima, H.M. (2017). Two-stage terrane assembly in Western Gondwana: Insights from structural geology and geophysical data of central Borborema Province, NE Brazil. *Journal of Structural Geology*, 103, 167-184. https://doi.org/10.1016/j.jsg.2017.09.012

Santos, L.C.M.L., Lages, G.A., Lima, H.M., Araújo Neto, J.F., Santos, G.L., Paixão, M.S. (2022). An overview on the Rhyacian–Orosirian (ca. 2.1–2.0 Ga) granitic magmatism of the Alto Moxotó Terrane and its implications for the crustal evolution of the Borborema Province, NE Brazil. *Journal of Iberian Geology*, 48, 225-239. https://doi.org/10.1007/s41513-022-00191-6

Santos, L.C.M.L., Oliveira, R.G., Lages, G.A., Dantas, E.L., Caxito, F., Cawood, P.A., Fuck, R.A., Lima, H.M., Santos, G.L., Araújo Neto, J.F. (2021). Evidence for Neoproterozoic terrane accretion in the central Borborema Province, West Gondwana deduced by isotopic and geophysical data compilation. *International Geology Review*, 64(11), 1574-1593. https://doi.org/10.1080/00206814.2021.1944332

Schwarz, D., Giuliani, G. (2001). Emerald deposits: a review. *Australian Gemmologist*, 21, 17-23.

Schwarz, D., Giuliani, G., Grundmann, G., Glas, M. (2001). Die Entstehung der Smaragde, ein vieldisskutiertes Thema. In: Schwarz, D., Hochlitner, R. (Eds.) Smaragd, der kostbarste Beryll, der teuerste Edelstein. *Extra Lapis*, 21, 68–73.

Sial, A.N., Ferreira, V.P. (2016). Magma associations in Ediacaran granitoids of the Cachoeirinha–Salgueiro and Alto Pajeú terranes, northeastern Brazil: Forty years of studies. *Journal of South American Earth Sciences*, 68, 113-133. https://doi.org/10.1016/j.jsames.2015.10.005

Souza, L.C. (Ed.). (2017). *Geologia e Recursos Minerais da Folha Pau dos Ferros SB.24-Z-A-II*. Escala 1:100.000. Recife: CPRM - Serviço Geológico do Brasil / Universidade Federal do Rio Grande do Norte.

Souza Neto, J.A., Legrand, J.M., Volfinger, M., Pascal, M.-L., Sonnet, P. (2008). W–Au skarns in the Neo-Proterozoic Seridó Belt, Borborema Province in northeastern Brazil: an overview with emphasis on the Bonfim deposit. *Mineralium Deposita*, 43, 185-205. https://doi.org/10.1007/s00126-007-0155-1

Steiger, R.H., Jäger, E. (1977). Subcommission on geochronology: Convention on the use of decay constant in geo- and cosmochronology, Earth and Planetary Science Letters, 36(3), 359–362. https://doi.org/10.1016/0012-821X(77)90060-7

Stipp, M., Stünitz, H., Heilbronner, R., Schmid, S.M. (2002). The eastern Tonale fault zone: a "natural laboratory" for crystal plastic deformation of quartz over a temperature range from 250 to 700°C. *Journal of Structural Geology*, 24, 1861–1884. https://doi.org/10.1016/s0191-8141(02)00035-4

Talukdar, M., Chattopadhyay, N., Sanyal, S. (2012). Shear controlled Fe-mineralization from parts of South Purulia Shear Zone. *Journal of Applied Geochemistry*, 14(4), 496-508.

Taylor, J. R., 1997. An Introduction to Error Analysis: The Study of Uncertainties in Physical Measurements, 327 pp., University Science Books, Mill Valley, California.

Tullis, J. (2002). Deformation of granitic rocks: experimental studies and natural examples. In: Karato S-I, Wenk H-R (eds) Plastic deformation of minerals and rocks. *Reviews in Mineralogy and Geochemistry*, 51(1), 51–95. https://doi.org/10.2138/gsrmg.51.1.51

Van Schmus, W.R., Brito Neves, B.B., Hackspacher, P.C., Babinski, M. (1995). U-Pb and Sm-Nd geochronological studies of the Eastern Borborema Province, Northeastern Brazil, initial conclusions. *Journal of South American Earth Sciences*, 8(3-4), 267-288. https://doi.org/10.1016/0895-9811(95)00013-6

Van Schmus, W.R., Kozuch, M., Brito Neves, B.B. (2011). Precambrian history of the Zona Transversal of the Borborema Province, NE Brazil: Insights from Sm-Nd and U-Pb geochronology. *Journal of South American Earth Sciences*, 31(2-3), 227-252. https://doi.org/10.1016/j.jsames.2011.02.010

Vapnik, Y., Moroz, I., Eliezri, I. (2006). Formation of emeralds at pegmatite-ultramafic contacts based on fluid inclusions in Kianjavato emerald, Mananjary deposits, Madagascar. *Mineralogical Magazine*, 70(2), 141–158. https://doi.org/10.1180/0026461067020320

Vapnik, Y., Sabot, B., Moroz, I. (2005). Fluid inclusions in Ianapera emerald, Southern Madagascar. *International Geology Review*, 47, 647–662. https://doi.org/10.2747/0020-6814.47.6.647

Vauchez, A., Neves, S.P., Caby, R., Corsini, M., Egydio-Silva, M., Arthaud, M.H., Amaro, V. (1995). The Borborema shear zone system, NE Brazil. *Journal of South American Earth Sciences*, 8, 247–266. https://doi.org/10.1016/0895-9811(95)00012-5

Viegas, L.G.F., Archanjo, C.J., Hollanda, M.H.B.M., Vauchez, A. (2014). Microfabrics and zircon U–Pb (SHRIMP) chronology of mylonites from the Patos shear zone (Borborema Province, NE Brazil). *Precambrian Research*, 243, 1-17. https://doi.org/10.1016/j.precamres.2013.12.020

Vitorino, A.L.A., Figueiredo e Silva, R.C., Lobato, L.M. (2020). Shear-zone-related gold mineralization in quartz-carbonate veins from metamafic rocks of the BIF-hosted world-class Cuiabá deposit, Rio das Velhas greenstone belt, Quadrilátero Ferrífero, Brazil: Vein

classification and structural control. *Ore Geology Reviews*, 127, 103789. https://doi.org/10.1016/j.oregeorev.2020.103789

Walton, L. (2004). *Exploration criteria for coloured gemstone deposits in the Yukon*. Yukon: Yukon Geological Survey.

Wiedenbeck, M. et al. (2004). Further Characterisation of the 91500 Zircon Crystal. *Geostandards and Geoananalytical Research*, 28(1), 9-39.

York, D., 1968. Least squares fitting of a straight line with correlated errors. Earth and Planetary Science Letters, 5, 320–324. https://doi.org/10.1016/S0012-821X(68)80059-7

Zwaan, J.C. (2006). Gemmology, geology and origin of the Sandawana emerald deposits, Zimbabwe. *Scripta Geologica*, 131, 1-211.

Zwaan, J.C., Jacob, D.E., Haeger, T., Cavalcanti Neto, M.T.O., Kanis, J. (2012). Emeralds from the Fazenda Bonfim Region, Rio Grande do Norte, Brazil. *Gems & Gemology*, 48(1), 2–17.

4 ARTIGO CIENTÍFICO III – ADVANCES FOR THE EXPLORATION OF TECTONIC-MAGMATIC RELATED EMERALD DEPOSITS USING A HIGH-RESOLUTION SPECTRAL APPROACH: UNRAVELING THE SPECTRAL FOOTPRINT OF THE PARANÁ DEPOSIT (NE BRAZIL)

José Ferreira de Araújo Neto[1*], Thais Andressa Carrino[1], Lauro Cézar Montefalco de Lira Santos[1], Rosa Elvira Correa Pabón[2]

[1]Department of Geology, Federal University of Pernambuco, Brazil; [2]Instituto Tecnológico Vale

*Corresponding author: José Ferreira de Araújo Neto

ABSTRACT

This study provides the first strategies and basics for emerald exploration in a mafic/ultramafic-hosted deposit using point spectral data (ASD-FieldSpec) and hyperspectral imaging (HySpex). We reveal the spectral footprint of the Paraná emerald deposit, northeastern Brazil, by using spectral techniques in association with petrographic and/or geochemical studies on drill core and handpicked samples. Four main lithotypes were taken into count based on drill core descriptions: basement gneiss, pegmatite, mafic schist, and breccia. The schist is the most important target, as it represents the emerald host rock and was subdivided according to its paragenesis into phlogopite, actinolite-phlogopite, and phengite-phlogopite schists, with the latter being apparently sterile to emerald. Mylonitic rocks were also treated separately, as the presence of muscovite into these consistently changes their chemical and spectral behaviour. Chemical discriminating diagrams were suggested based on MgO versus Al_2O_3 content and using the technique of principal component analysis. The spectral signature of all lithotypes found in the deposit is presented in the range of 350-2500 nm. For the first time, spectral indices for emerald and host rock identification were provided and tested even in mixture spectra simulation. The emerald indices EI1, EI2, and EI3 were chosen based on the Paraná emerald diagnostic absorption features at ~1150, ~1460 and ~2155 nm. For the host schists, three indices were provided (MI_{depth}, MI_{ratio} and ACI) considering the Mg-OH diagnostic features of phlogopite and actinolite, allowing automatized distinction between potential mineralized rocks and other associated rocks of the Paraná deposit. In a high-resolution scale, imaging

spectroscopy can be applied for mineralogical mapping, highlighting the presence of emerald in pixels of ~1 mm in a given sample using chromium- and iron-derived absorption features in the visible-near infrared range.

INTRODUCTION

Emerald mineralization, *i.e.*., the dark-green variety of beryl and one of the most valuable gemstones in the world, constantly requires two distinct chemical suppliers to form: a beryllium source, usually associated with pegmatite and granite occurrences, and a chromium and/or vanadium source (emerald chromophore elements) concentrated in rocks of the oceanic crust and upper mantle and their metamorphic equivalents (Groat et al. 2008). Although emeralds can be formed in different geological settings (Walton 2004, Zwaan 2006), the most common mineralization style is the result of metasomatic changes between mafic-ultramafic rocks and beryllium-bearing granites/pegmatites (Simandl et al. 1999, Schwarz and Giuliani 2001, Giuliani et al. 2019), developing a phlogopite-rich zone where phlogopite schists encompass emerald crystals and quartz-feldspar veins and veinlets.

The geochemical contrast between the host schist and other associated rocks in an emerald deposit can be explored to track potential targets of mineralization. Therefore, indirect analysis, such as imaging and reflectance spectroscopy, combined with petrographic and geochemical data, can be powerful tools in targeting emerald ore. In fact, reflectance spectroscopy has been applied on different scales to unravel propitious mining sites, ore controls and/or spectral mineral footprint in several deposits (e.g., Thompson et al. 2009, Ramakrishnan et al. 2013, Turner et al. 2017, Medina et al. 2021, Zhou et al. 2022). The interaction of electromagnetic radiation with matter provides information on chemical composition and, hence, mineralogical assemblage. The reflected energy is marked as spectral features, recording electronic transition processes related to transition metals in the end of ultraviolet to visible-near infrared range (VNIR: 350-1000 nm) and molecular vibrational processes in the short-wave infrared range (SWIR: 1000-2500 nm) (Hunt 1977, Clark 1999, Thompson et al. 1999).

Unlike geochemistry, in the VNIR and SWIR spectroscopy, quartz, alkali feldspar, and plagioclase have a significantly lower or null influence on the outcome since they do not show diagnostical spectral features in this wavelength region (Clark 1999, Hecker et al. 2010). Leaving, in terms of rock-forming minerals, to amphibole, mica, and calcite, for example, the spotlights of reflectance spectroscopy in the range of 350-2500 nm. This is particularly useful

when tracking the emerald ore, as phlogopite schists and other common paragenesis associated with emerald mineralized zones (*e.g.,* actinolite, chlorite, talc, and carbonates) will have a distinctive spectral signature derived from vibrational absorption features in this region (Pontual et al. 2008).

However, while this spectral range is almost insensitive to feldspars, it is a well-established procedure for the identification of clay minerals and sericite (Thompson et al. 1999, Swayze et al. 2014), a common alteration product of the alkali feldspars vastly observed in exposed surficial and fluid-affected rocks. Thus, allowing a clearer distinction between felsic/quartz-feldspathic compositions and mafic/ultramafic rocks (see Araújo Neto et al. 2021a).

Imaging spectroscopy, on the other hand, employs the principles of reflectance spectroscopy in a high-detailed dimension as a hyperspectral scanner, acquiring images in hundreds of spectral bands, with each pixel containing its own spectral signature (Kruse 1994, Goetz 2009). In conjunction with statistical techniques, this method allows rapid identification and mapping of different materials. Thus, the applications are vast: from mineral mapping in drill cores (Kruse 1996, Lypaczewski et al. 2019, Naleto et al. 2019, Moura et al. 2022) to orbital or airborne imaging of hydrothermal alteration in ground targets (Crósta et al. 1998, Laukamp et al. 2011).

In this paper, we propose the use of point and imaging spectroscopy to propose a spectral footprint of the Paraná deposit, investigating the emerald ore and other potential mineralized rocks in drill core and handpicked samples. We expect to unveil how this method applies to emerald exploration by answering the prime questions: (i) is it possible to identify the emerald spectral signature within the host rock? (ii) Does it allow a distinction between sterile and potentially mineralized rocks? (iii) And how to apply the method in the light of emerald prospecting?

GEOLOGICAL BACKGROUND

The Borborema Province represents the northeastern portion of the South American platform. This complex mosaic-like structured Precambrian tectonic province covers most of the Northeast Region of Brazil (Almeida et al. 1981) (Figure 4.1a). The province is divided into three subprovinces by two major E-W strike-slip shear zones: Northern (NOS), north of the Patos shear zone, Transversal/Central (TRS), between the Patos and Pernambuco shear zones, and Southern (SOS), on the south of the Pernambuco shear zone (Van Schmus et al. 2011;

Figure 4.1b). In this scenario, emerald occurrences are found exclusively in the NOS, a crustal block composed dominantly of Paleoproterozoic gneisses and migmatites extensively reworked during the Brasiliano/Pan-African orogenic collage (800-500 Ma; Brito Neves et al. 2014).

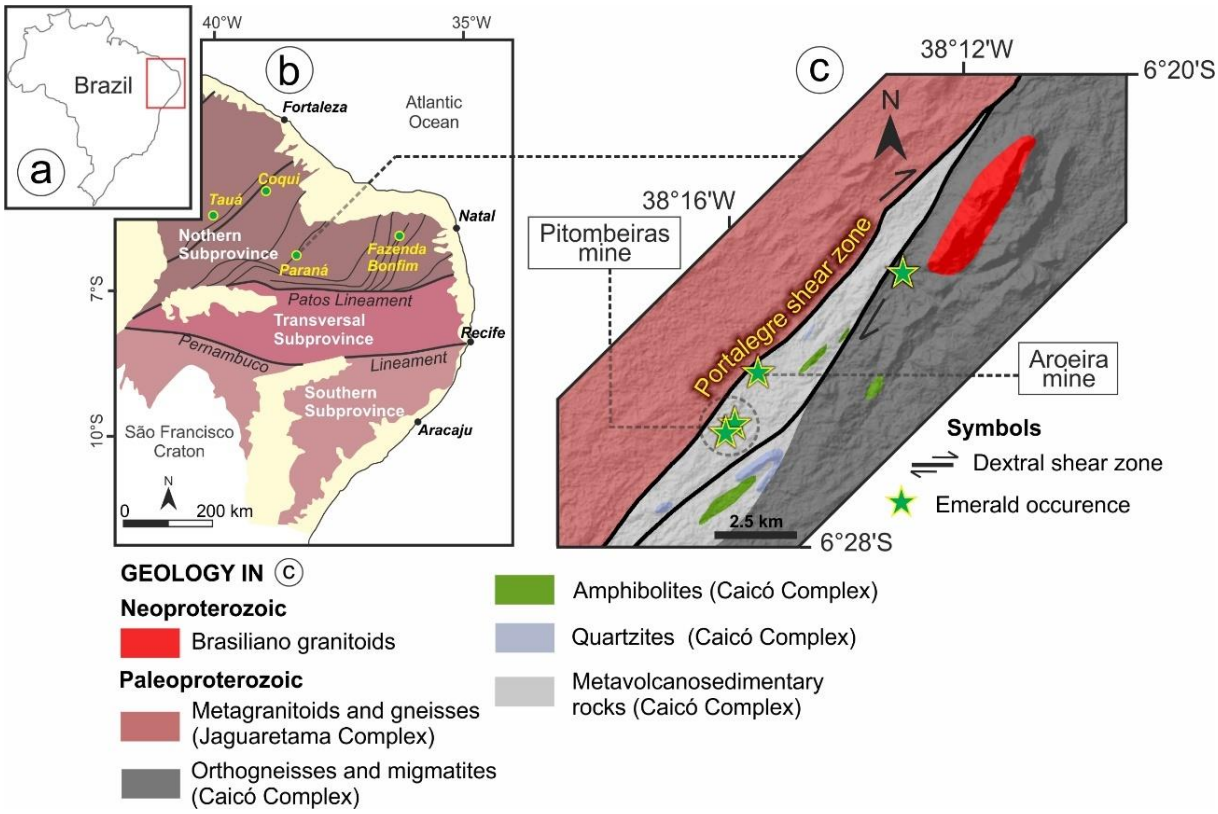

Figure 4.1. Geological setting of the study area. (a) Geographic location of the Borborema Province in Brazil. (b) Schematic geotectonic subdivision of the Borborema Province illustrating main structures of the Northern Subprovince and known emerald mineralizations (Modified from Santos et al. 2014). (c) Simplified geologic map of the Paraná emerald deposit with main emerald occurrences and location of the Pitombeiras and Aroeira mines.

Standing on strongly deformed areas of the NOS, four emerald mineralization are reported from west to east: the Tauá and Coqui occurrences and the Paraná and Fazenda Bonfim deposits. Despite punctual distinctions, they are all classified as “tectonic magmatic-related, hosted in mafic/ultramafic”, where the emerald-bearing host is a biotite/phlogopite schist formed after metasomatic reactions between granitic pegmatites and Cr-V-Fe-rich mafic-ultramafic rocks. Also, in those areas, there is a clear connection between the presence of emerald ore and aquamarine-bearing pegmatite fields affected by Brasiliano shear zones (Araújo Neto et al. 2021b). The extensive transcurrent shear system in the NOS is assumed to

be responsible for channeling hydrothermal fluids and mobilizing, from different rock sources, the elements involved in the emerald crystallization.

In central NOS, the Paraná emerald deposit lies in a gneiss-migmatite domain that represents the Paleoproterozoic basement of the subprovince (Figure 4.1c), together with amphibolite lenses, quartzites, and other undifferentiated metavolcanosedimentary rocks, all grouped as the Caicó Complex (Medeiros 2008, Araújo Neto et al. 2018). During the Brasiliano orogeny, deformation and magmatism defined the ultimate geological framework of the deposit and surrounding areas. The development of extensive transcurrent shear zones and the injection of large granitic bodies, as well as several quartz-feldspar pegmatite dykes and veins (Figure 4.2a), established the ideal setting for ore-forming processes to take place (Araújo Neto et al. 2021a). Hydrothermalism and metasomatism between mafic rocks and Be-bearing pegmatites led to the formation of emerald-bearing schists (Figure 4.2b). The emerald ore occurs as lens-shaped bodies interleaved with mylonitic gneisses in a NE-SW trend within the Portalegre shear zone (Figure 4.2c). Emerald crystals can be found in phlogopite-, actinolite-phlogopite schists, and schist-hosted granitic lenses or veins (Figure 4.2d).

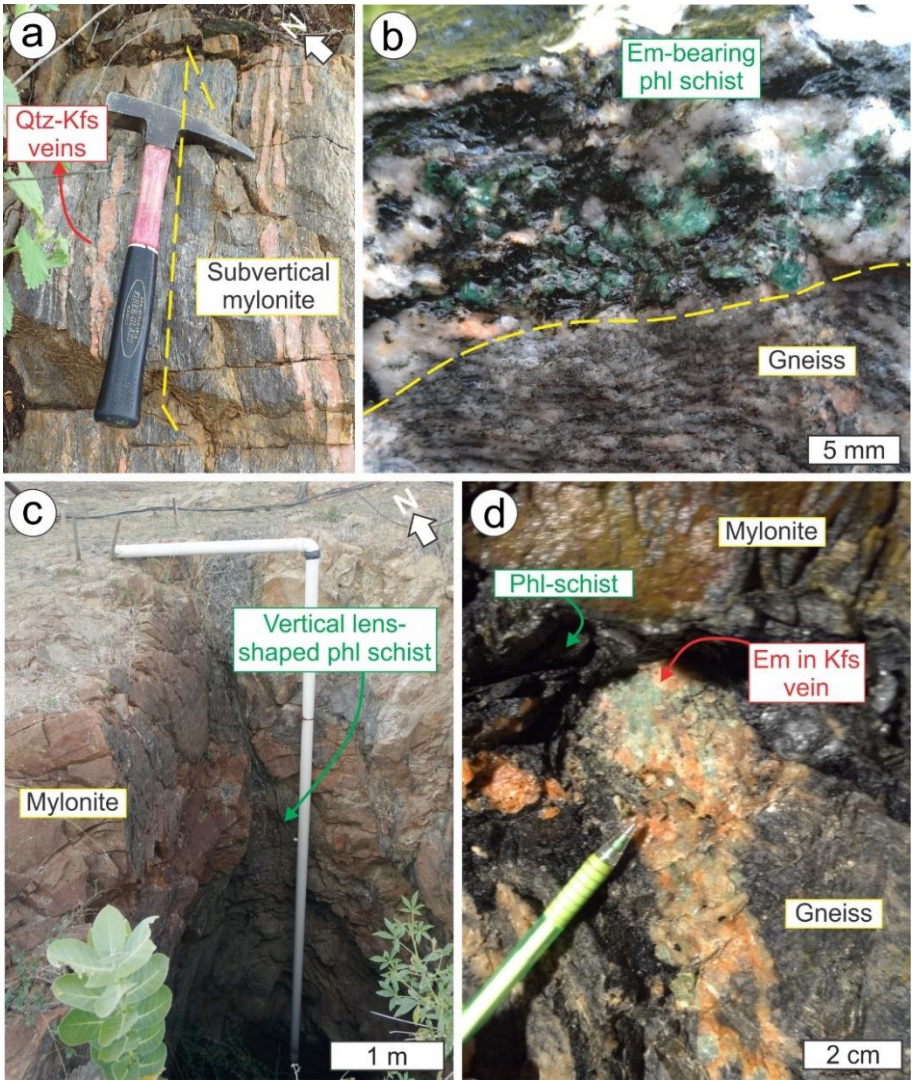

Figure 4.2. Geological features of the Paraná emerald deposit. (a) Quartz-feldspar veins concordant with the mylonitic foliation of a biotite gneiss of the Caicó Complex. Horizontal view. (b) Emerald-bearing phlogopite schist at the contact zone with a biotite gneiss. (c) Lens-shaped phlogopite schist inserted in mylonitic gneisses within the Portalegre shear zone. Vertical view of a mine shaft in the Pitombeiras region. (d) Phlogopite schist hosting emerald-bearing K-feldspar veins in a mine gallery front (Aroeira mine). Em = emerald; Kfs = K-feldspar; Phl = phlogopite; Qtz = quartz.

MATERIAL AND ANALYTICAL METHODS

Sampling

For geochemistry and spectral measurements, we focused on 103 samples from four different drill cores of the Paraná emerald deposit provided by the mining company “Mineração

Limeira Comércio Exportação e Importação Ltda". Saprolites and rocks decomposed into soil were not considered in this study. Drillholes FTA 01 and FTA 02 are from the Aroeira mine and drillholes MLL F01 and MLL F02 are from the Pitombeiras mine. Geological descriptions of the drill cores were done during field campaigns. Subsequently, petrographic studies were performed in the Laboratory of Gemology at the Federal University of Pernambuco (UFPE), Brazil, using an Olympus BX51 microscope coupled with an Olympus DP26 camera. Whole-rock geochemistry was carried out in 40 representative samples covering the highest number of lithotypes along the drillhole, whereas reflectance spectroscopy was performed in all 103 samples. Four handpicked samples containing emeralds were selected for point spectral measurements and one sample for imaging spectroscopy, since none of the potential host rocks recovered from the drillholes was emerald bearing.

Lithogeochemistry

Physical preparation for the 40 drill core samples was performed in the Stable Isotope Laboratory of the Nucleus of Geochemical Studies (NEG-LABISE) at the UFPE. The samples were crushed, split, milled, and then sent to the ALS laboratory for chemical analysis. Whole-rock samples were analyzed for major oxides by fusion/X-ray fluorescence (ALS code ME-XRF26) and trace elements (in ppm) by four acid digestion with inductively coupled plasma-atomic emission spectrometry (ICP-AES) (ALS code ME-ICP61). Loss on ignition was obtained using the WST-SEQ instrument at 500ºC after the sample was pre-dried at 105ºC (ALS code OA-GRA05x). Chemical data were imputed as an Excel spreadsheet file (Microsoft Office®) in the Orange Data Mining software (v. 3.32) for statistics and graphic presentation.

A principal component analysis (PCA) was applied to the geochemistry data aiming to group and represent the many chemical variables of the 40 samples. The PCA was applied, using Orange Data Mining software, on a covariance matrix of the original data (sixteen analyzed elements – Al, Ba, Ca, Cr, Fe, K, Mg, Mn, Na, P, S, Si, Sr, Ti, V and Be) after normalization to adjust the values to a common scale, dividing the columns of element concentration by its standard deviation (Orange Visual Programming 2022). The results are sixteen new uncorrelatable variables (principal components or PCs), each one comprehending a linear combination of the original variables (eigenvector) and characterized by an eigenvalue that measures the concentration of variability in the data (Mather 2004). The highest eigenvalue (higher variance) is calculated for the first principal component (PC1) and then decreases with the higher order of the PCs (Mather 2004).

Reflectance spectroscopy

Reflectance measurements on 103 drill cores and 04 handpicked samples were performed at the Laboratory of Reflection Spectroscopy of the Institute of Geoscience, University of Campinas (UNICAMP), Brazil. The samples were analyzed using a FieldSpec®4 Standard Resolution spectroradiometer (Analytical Spectral Devices), marked by 2151 channels from the ultraviolet to short-wave infrared wavelengths (350-2500 nm). Spectral sampling (bandwidth) is 1.4 nm for the 350-1000 nm range and 1.1 nm for the 1001-2500 nm range (Malvern Panalytical 2022). A contact probe (20 mm spot size) with an internal light source was used to perform the measurements, and the instrument was calibrated using a Spectralon® white reference plate.

A total of 348 measured spectra were later interpreted by visual examination, determining shape and wavelength position, using the software Hyperspectral Python (HypPy; Hecker et al. 2019). Electronic transitional and vibrational process related to mineral chemistry were interpreted by comparison with specialized references (*e.g.*, Clark 1999, Pontual et al. 2008) and previous studies on the Paraná emerald deposit (Araújo Neto et al. 2019, Araújo Neto et al. 2021a).

Imaging spectroscopy

Hyperspectral data were obtained for 06 drill core samples and 01 handpicked sample using two HySpex hyperspectral imaging cameras from Senai/Cimatec at Salvador (Bahia). The VNIR-1800 camera is marked by 186 channels in the range of 400-1000 nm, whereas the SWIR-384 camera has 288 channels registering reflected radiation in 930-2500 nm. Imaging spectroscopy was performed with a sensor height of 30 cm and sight fields of 16-17°, resulting in images with ~1mm-sized pixels.

Reference measurements were made on a Spectralon® white plate for the empirical transformation of raw data (radiance, L) to reflectance values. This correction was performed based on the ratio between radiance values of the images and the radiance value from the average of pixels of the reference plate ($\rho = L_{image}/L_{Spectralon}$), resulting in a spectral reflectance image. Data processing was performed on Envi® software (v.5.5), licensed by the Instituto Tecnológico Vale. A Savitzky-Golay filter was applied to the final products in order to smooth the noise inherent to hyperspectral images (Schafer 2011). Empirical tests resulted in the

selection of the following parameters: window size of 4 and degree of smoothing polynomial of 2 for both VNIR and SWIR spectral intervals.

These filtered reflectance images were classified using the Spectral Angle Mapper (SAM) supervised classification algorithm (Kruse et al. 1993) as a test for automatic identification of mineral composition in selected rocks of the Paraná deposit. As a result, a thematic digital product is generated, showing different classes for chosen minerals or mineral assemblages in each analyzed rock, enabling fast analysis of minerals and textures in given lithotypes.

RESULTS AND DISCUSSION

Drill core and petrographic characterization

Four main groups of lithologies were categorized after drill core descriptions (Figure 4.3): (i) “basement gneiss”, covering a wide range of textures, structures, and composition but still exceptionally different from the other groups; (ii) “pegmatite”, mostly quartz-feldspar injections with minor biotite; (iii) “mafic schist”, encompassing phlogopite-, actinolite-phlogopite-, and phengite-phlogopite schists; and (iv) “breccia”, late-stage hydrothermal breccia with massive calcite matrix.

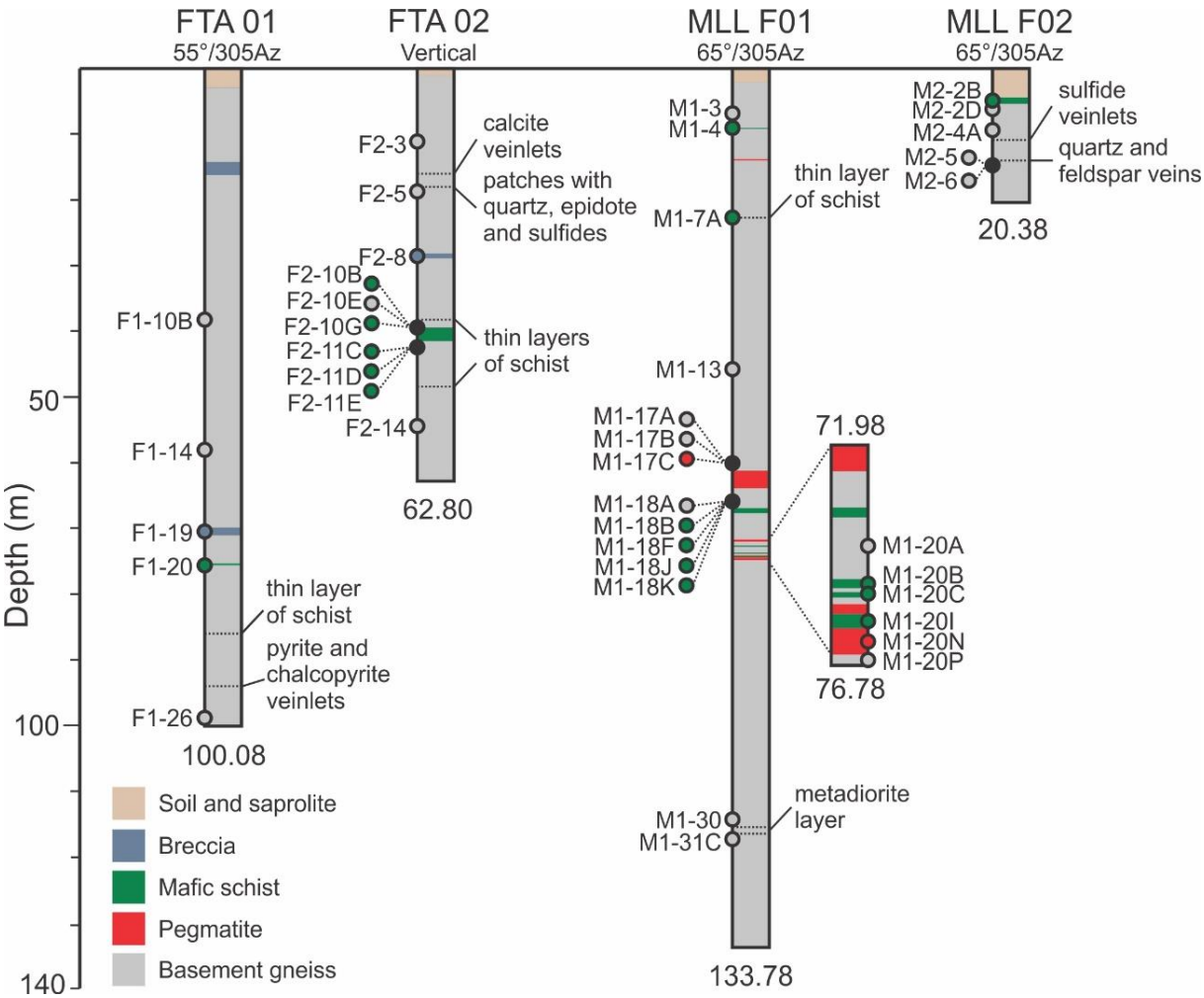

Figure 4.3. Stratigraphy in the Paraná emerald deposit from studied drillholes. Labeled circles mark the location of sampled rocks for whole-rock geochemistry (n = 40). Total depth for each hole is given in meters at the bottom of the profile. See Appendix for full chemical analysis and descriptive statistics.

The basement gneiss is by far the dominant lithology in the drill cores (Figure 4.3, 4.4a). Compositionally, it usually varies from granodiorite to syenogranite, as banded gneisses or without the banding structure (metagranitoids). Diorite compositions are also found in the cores, although less frequently. Biotite is the main mafic mineral (Figure 4.4b), and it is constantly found as the only mafic essential mineral phase, except in a few samples of hornblende gneisses (or metadiorites), where hornblende is followed by biotite in the modal composition (Figure 4.4c). Titanite, epidote, allanite, and zircon are common accessory mineral phases. Some samples may show protomylonitic to mylonitic textures. In the most developed mylonites, muscovite plays an important role in the mineral assemblage (Figure 4.4d).

Alteration of alkali feldspar to clay minerals and/or sericite (sericitization) is a common feature for the whole group despite individual composition.

Pegmatites are usually homogenous meter- to centimeter-sized dykes, basically composed of quartz and alkali feldspar, with or without biotite. Deformed crystals and signs of dynamic recrystallization (formation of subgrains and recrystallized grains) give them an aspect of “sheared pegmatite”. Sericitization of K-feldspar crystals is very common.

The “mafic schist” group comprises the potential emerald-hosting phlogopite schist and actinolite-phlogopite schist (Figure 4.4e), as well as phengite-phlogopite schist (Figure 4.4f), which is considered sterile and less important as emerald ore. Unlike the gneiss samples, the compositional variations of the schists were considered separately for analytical purposes due to their importance for the emerald deposit, with each type constrained by petrographic, chemical, and spectral characteristics. Although very similar at first, by naked-eye observations, their mineral assemblages are easily distinguishable by petrographic studies, mostly controlled by different proportions of mica (phlogopite and phengite) and amphibole (actinolite). Quartz and alkali feldspar are the common felsic phases, and apatite is an accessory mineral found in most of the samples.

The last group is also the last lithotype formed in the deposit. Hydrothermal calcite veins crosscut both schists and gneisses, occasionally forming hydrothermal breccias with angular pieces of gneisses (or mylonites) cemented by white and red calcite and silica (Figures 4.4g and 4.4h).

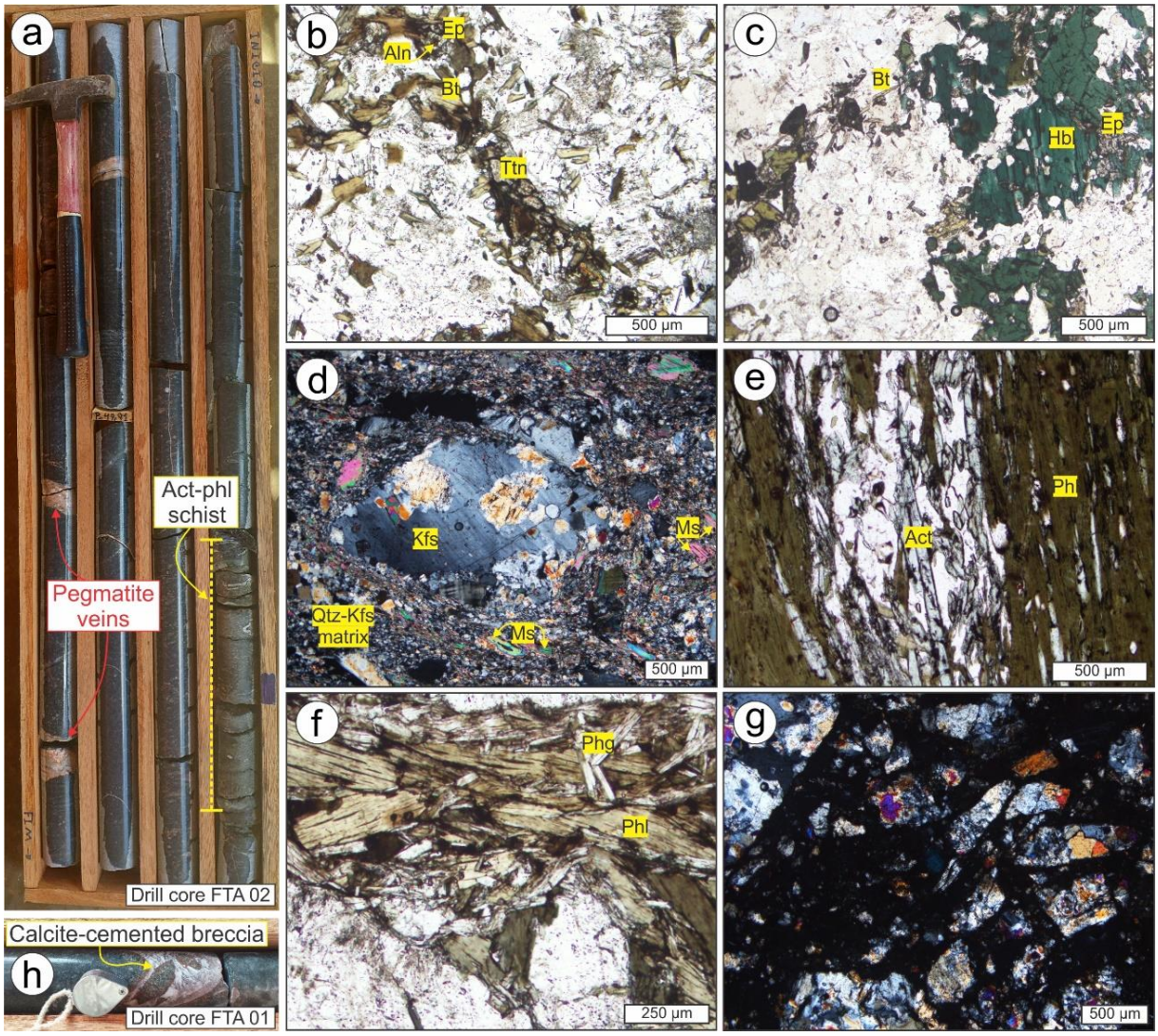

Figure 4.4. Geologic characteristics of the main lithotypes in the drill cores. (a) Drill core image of FTA 02. Thin section photomicrographs of (b) biotite gneiss with altered K-feldspar in parallel light, (c) biotite-hornblende gneiss in parallel light, (d) K-feldspar porphyroclast surrounded by muscovite and quartz-feldspar matrix in a mylonite in crossed nicols, (e) actinolite-phlogopite schist in parallel light, (f) phengite-phlogopite schist in parallel light and (g) hydrothermal breccia with angular pieces of gneissic mylonite in crossed nicols (the cement in black is red calcite and silica). (h) Example of calcite-cemented breccia in drill core image of FTA 01. Act = actinolite; Aln = allanite; Bt = biotite; Ep = epidote; Hbl = hornblende; Kfs = K-feldspar; Ms = muscovite; Phg = phengite; Phl = phlogopite; Qtz = quartz; Ttn = titanite.

Geochemical signature of drill core samples

The chemical data of eighteen gneiss and two mylonite samples display the felsic character of these rocks, with an average silica content of ~66 wt% and ~72 wt%, respectively

(see Appendix for full chemical analysis). Two exceptions are samples F1-10B and M1-31C which are metadiorites with more intermediate values of SiO_2 (54.55 wt% and 58.76 wt%). Relatively low MgO (1.39 wt% and 0.68 wt% mean) and Cr_2O_3 (0.03 wt% mean for both gneiss and mylonite) and relatively high Al_2O_3 (15.33 wt% and 13.62 wt% mean) and Na_2O (3.72 wt% and 1.59 wt%) are the most representative chemical features of these gneissic rocks (Figure 4.5). The two pegmatite samples show high content of SiO_2 and Al_2O_3 (average of 69.32 and 16.75 wt%, respectively), with very low CaO, Cr_2O_3 and MgO. They can be chemically distinguished from other felsic rocks because of their very low concentration of Fe_2O_3 (0.34 wt% mean) and high K_2O content (8.18 wt% mean).

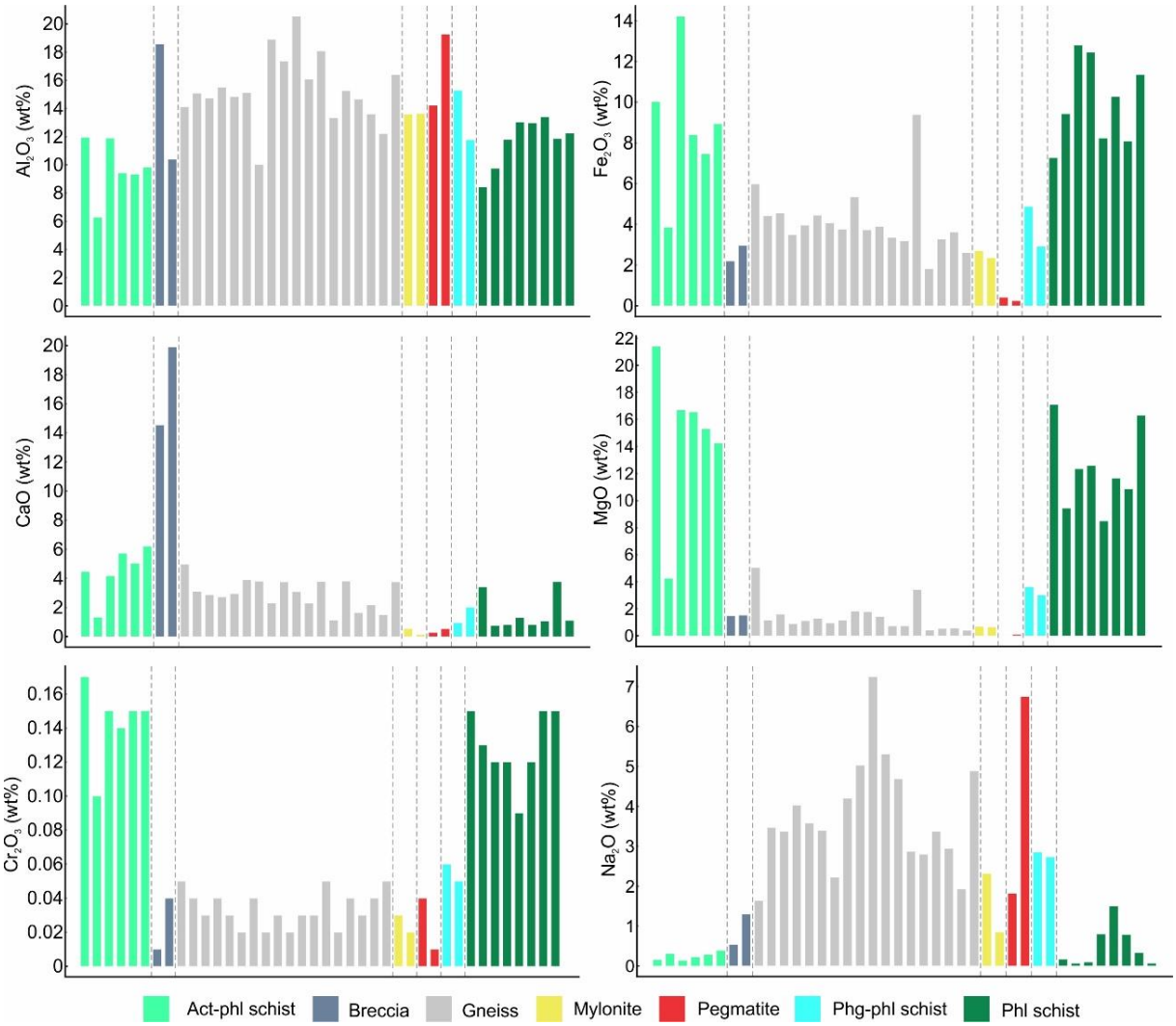

Figure 4.5. Bar diagrams of element concentration for important oxides. See appendix for full chemical analysis. Act = actinolite; Phg = phengite; Phl = phlogopite.

The schists have an intermediate to mafic character. The silica content decreases from phengite-phlogopite- (65.72 wt% mean, n = 2), actinolite-phlogopite- (51.35 wt% mean, n = 6) to phlogopite-schist (50.96 wt% mean, n = 8) (Figure 4.5). Yet, the higher value of SiO_2 in phengite-phlogopite schists is attributed more to the presence of several quartz-feldspar veinlets into these rocks than to the mica compositional variation. For that reason, phengite-phlogopite schists show intermediate values of Al_2O_3, Fe_2O_3, MgO, and Cr_2O_3, between those of felsic rocks and mafic schists (Figure 4.5). The geochemistry of the actinolite-phlogopite- and phlogopite-schists are very similar, marked by the highest contents of Fe_2O_3 (8.82 wt% and 9.99 wt% mean, respectively), MgO (14.74 wt% and 12.35 wt% mean) and Cr_2O_3 (0.14 wt% and 0.13 wt% mean). The most striking difference between both schists is the CaO content almost 3x higher in the actinolite-phlogopite- (4.49 wt% mean) in comparison with those where phlogopite is the only mafic phase (1.63 wt% mean). Calcium is also determinant in the two analyzed breccia samples, averaging 17.23 wt% of CaO. These breccias also stand out for their high values of loss on ignition (16.48 wt% mean), typical of carbonate-rich rocks.

In a primary approach, a MgO x Al_2O_3 diagram can be used to discriminate potential host rocks from the others. The samples were grouped in three different sections (A, B and C) for description purposes (Figure 4.6). Magnesium is more common in intermediate to mafic rocks and is concentrated in the phlogopite- and actinolite-phlogopite-bearing, ranging from 8.49 to 21.40 wt% of MgO, while Al_2O_3 content is no more than 14 wt%. These two schists are mostly confined in section A, with Cr_2O_3 following the same enrichment trend of MgO – larger circles represent high chromium content. The only exception is the actinolite-phlogopite schist (sample F2-10G) in section B, which has low MgO and the lowest Al_2O_3 value due to massive quantities of quartz veins interleaved within the schist foliation, increasing its amount of SiO_2 to 77.82 wt%, thus being unrepresentative of actinolite-bearing schist. In fact, the actinolite-bearing has a tendency to be Mg-richer, because actinolite in the Paraná deposit has ~20 wt% of MgO, while phlogopite has ~17 wt% and phengite ~4 wt% (Araújo Neto et al. 2021a).

Section B delimits an intermediate chemistry between the host schists and the most felsic rocks. Metadiorites and phengite-phlogopite schists are represented in this field, with MgO content between 2 and 6 wt%. Other gneisses, mylonites, pegmatites and breccias are grouped in section C, with the lowest values of MgO (0-2 wt%) but with plots scattered in the Al_2O_3 axis (concentrations ranging from 10.01 to 20.54 wt%).

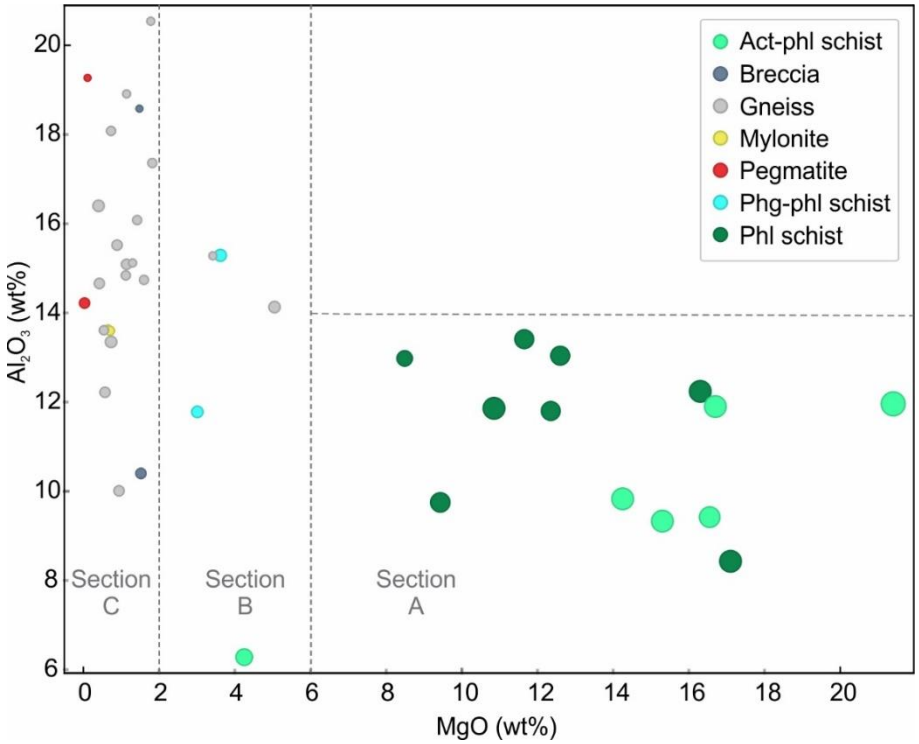

Figure 4.6. MgO vs Al_2O_3 diagram. Larger circles represent higher values of Cr_2O_3. Act = actinolite; Phg = phengite; Phl = phlogopite.

Although magnesium itself is very useful for the discrimination of potential host rocks, either for its natural enrichment in mafic rocks or for being the main substituent in emerald crystals (Groat et al. 2008, Aurisicchio et al. 2018), it is not enough to group all different rocks associated with the deposit nor understanding their chemical particularities. One way to represent many chemical variables is to apply the principal component analysis (PCA), simplifying their information into new uncorrelatable variables (Pearson 1901).

A combination of PC1 and PC3 was empirically chosen to graphically represent the chemical variation of the 40 drill core samples (Figure 4.7), since PC2 allowed less group distinction (no distinctive field for breccia samples, for example). The negative correlation between Si, Al, Na versus Mg, Cr, Fe, Mn, V, and P is represented in PC1, while PC3 registers the variance between Ca (high positive values) and K, Na (high negative values) leading to distinct compositional fields individualized by the PC1 x PC3 plot. Five lithochemical groups were defined using the PCA technique. Groups I, II, and III are well distinguished for laying in very distinct fields, while groups IV and V are less representative due to overlapping and small sampling.

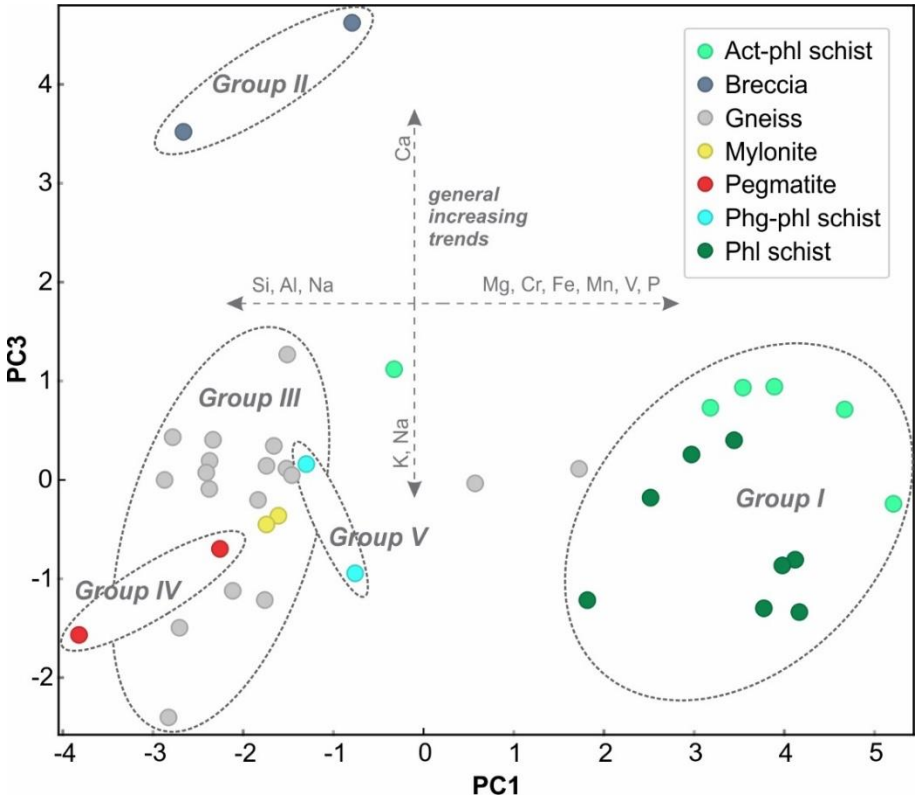

Figure 4.7. PC1 and PC3 eigenvector plot and representation of the five lithotypes groups. Act = actinolite; Phg = phengite; Phl = phlogopite.

Group I is clustering the mafic host rocks, reflecting their higher concentration of Mg, P, and transition metals. It is arguable that this group can be still subdivided into two different fields due to the slight increase of the PC3 eigenvectors in the actinolite-phlogopite schists, probably because of their higher Ca content.

The breccia samples of group II are plotted in a very separate field, representative of the presence of calcite and thus, the highest Ca concentrations.

Gneisses and mylonites were clustered in group III, with a stronger influence of higher concentrations of Si, Al, Na, and K. The same is observed for groups IV and V, representatives of pegmatites and phengite-phlogopite schists, respectively, whose patterns are not well-established due to a large intersection with group III and a small number of samples.

The few ungrouped samples were outliers of the actinolite-phlogopite schist and gneiss. The first is sample F2-10G, previously mentioned for its high quantity of quartz veins. The others are metadiorites with an intermediate composition, leading their chemistry to constantly be found between those of mafic schists and other gneissic samples.

Reflectance spectroscopy of drill core samples

Reflectance spectra of biotite gneisses are characterized by a broad Fe^{2+} absorption feature of biotite in the VNIR range followed by weak OH and H_2O vibrational asymmetrical features centered at ~1392 and ~1910 nm (Dyar 1990, Clark 1999, Pontual et al. 2008). In the SWIR region, these gneisses show a distinct ~2200 nm feature, typically associated with Al-OH vibrational process in dioctahedral mica (Scott and Yang 1997, Pontual et al. 2008). This feature has been frequently linked to the presence of fine-grained muscovite crystals (sericite) as a result of alkali feldspar alteration (Araújo Neto et al. 2021a, Moura et al. 2022). Biotite absorption features are representative of this lithotype, with a diagnostic Fe-OH feature centered at ~2250 nm, a deeper and sharper Mg-OH absorption at ~2330 nm, and a secondary Mg-OH absorption at ~2388 nm (Figure 4.8), typical for most Mg-minerals (Pontual et al. 2008). The shift of the secondary Mg-OH absorption towards 2392-2394 nm can be an indication that hornblende is present in the mineral assemblage (Figure 4.8). In this case, the primary Mg-OH absorption in shorter wavelengths (~2320 nm) should also be expected, but this apparently does not persist in mixed spectra.

Mylonite samples are muscovite-rich and, therefore, marked by the presence of deep OH and water absorptions at ~1413 and ~1910 nm, Al-OH features at ~2212 nm, and two diagnostic absorptions of white mica at ~2350 and ~2439 nm (Scott and Yang 1997, Pontual et al. 2008). The absence of well-marked and sharp biotite Fe-OH feature at 2250 nm is also distinctive, usually appearing as a shoulder near the deep ~2200 nm absorption (Figure 4.8). Pegmatites are mostly marked by OH and water absorptions. Weak Al-OH features are present, probably derived from alteration minerals such as clay minerals and sericite (Pontual et al. 2008). Breccias are distinguished by well-marked calcite absorptions features. A large band with features at ~1876 and ~1992 nm and a weak feature at ~2155 nm are representatives of carbonate absorptions. The presence of sharp and deep asymmetric absorption feature at ~2338 nm, with a shoulder at ~2297 nm is diagnostic of calcite.

The schist compositional variation can be distinguished by the spectral signature of phlogopite, phengite and actinolite in the SWIR region (see Araújo Neto et al. 2021a). Spectral analysis of all forty-one schist samples in the drill cores endorses the importance of a phlogopite Fe-OH absorption at ~2250 nm as a diagnostic feature of the schist host. Despite the presence of phengite and actinolite, the Fe-OH absorption preserves its sharp and deep shape (Figure 4.8). In “pure” phlogopite schists, when no other mica or amphibole is present, this feature is followed by two Mg-OH absorptions at ~2330 and ~2388 nm. The presence of phengite, on the

other hand, is marked by ~2216 nm Al-OH absorption, at a slightly longer wavelength compared to "normal" muscovite compositions. Like most white micas, phengite has also two diagnostics absorptions at ~2348 and ~2440 nm, consistently at lower depths in comparison with the Al-OH feature (Scott and Yang 1997, Pontual et al. 2008). When actinolite is in the mineral assemblage, a shoulder at ~2296 nm is recorded, and the Mg-OH absorption feature at ~2330 nm is usually found at shorter wavelengths (~2315 nm) (Pontual et al. 2008).

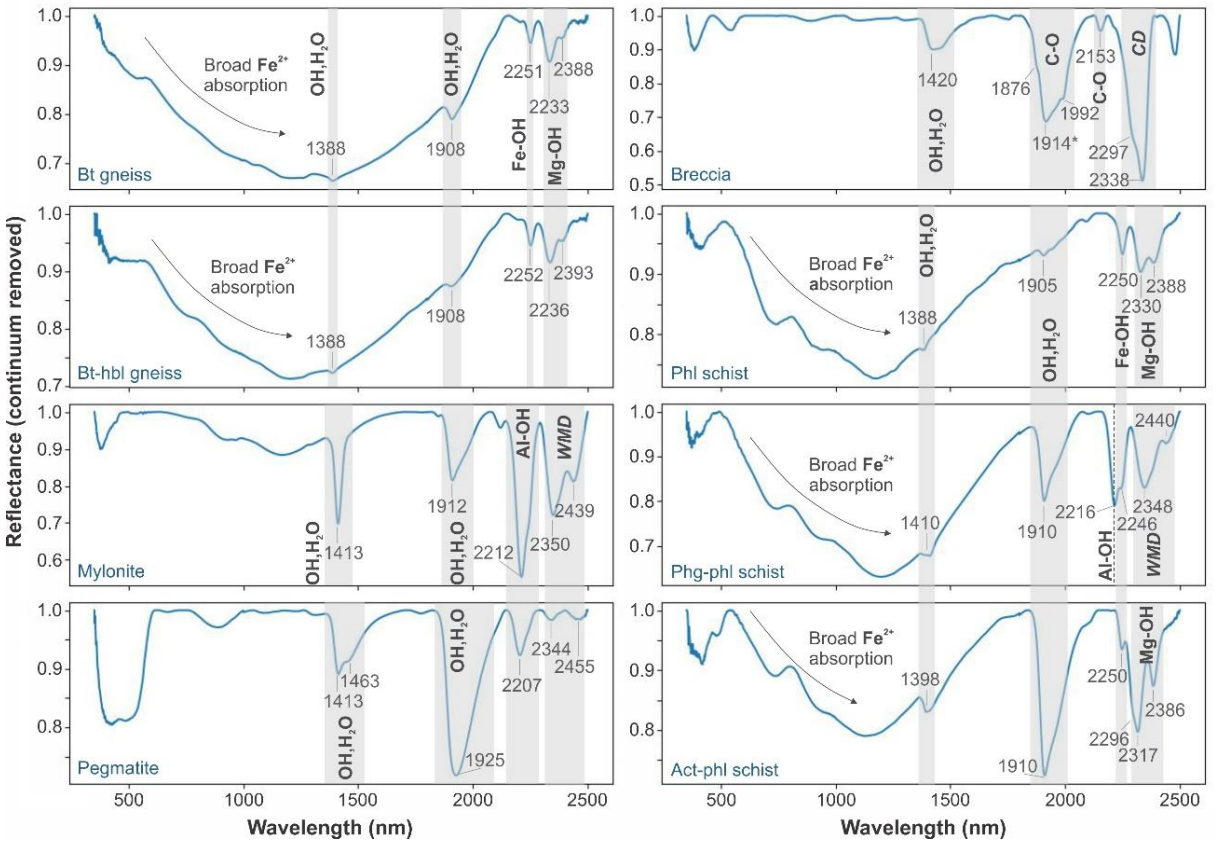

Figure 4.8. Interpreted representative spectra for main lithotypes of the Paraná emerald deposit. *WMD* and *CD* stands for "white mica diagnostic" and "calcite diagnostic" respectively. Act = actinolite; Bt = biotite; Hbl = hornblende; Phg = phengite; Phl = phlogopite.

Point reflectance spectroscopy of emerald in a mixed spectrum

In emerald-bearing phlogopite schist, the strong Fe^{2+} absorption in phlogopite masks the main distinctive features of emerald in the VNIR range (i.e., Cr-related absorptions at 430 and 630-640 nm; Wood and Nassau 1968, Rondeau et al. 2008). Yet, emerald is also distinguished from mica and amphibole by its symmetrical water absorptions centered at ~1410

and ~1900 nm and, while the first one can be attenuated by the presence of iron-rich minerals, the second one can still be detected in a mixed spectrum. In the SWIR range, other characteristic absorption features of the Paraná emerald are observed at ~2070, ~2150, ~2200 and ~2330 nm (see Araújo Neto et al. 2021).

How much of the emerald spectral signature is preserved in a mixture with the schist is certainly dependent on the proportion of emerald and mica in the area measured by the contact probe. Virtual simulations of a mixture can be made using the raw continuum-removed reflectance data of pure emerald and pure phlogopite schist, by summing their reflectance values multiplied by their proportion in each wavelength. Figure 4.9 contains several absorption spectra for different proportions of emerald and schist. In a 5%-emerald and 95%-schist mixture, there are at least two absorption features still recognizable for the diagnosis of emerald at ~1150 (H_2O absorption) and ~2155 nm. The emerald spectral footprint is clearer after 20% of emerald in the mixture, when sharp and deep symmetrical absorption features derived from the channel water (~1410 and ~1900 nm) become well-defined, as well as other diagnostic features at ~1460, ~2020, and ~2070 nm. The Cr absorption in the VNIR region is only marked after 50% of emerald in the mixture. Thus, investigations on emerald color in mixed spectra are probably uncertain for surfaces with less than 50% of emerald in a phlogopite schist matrix.

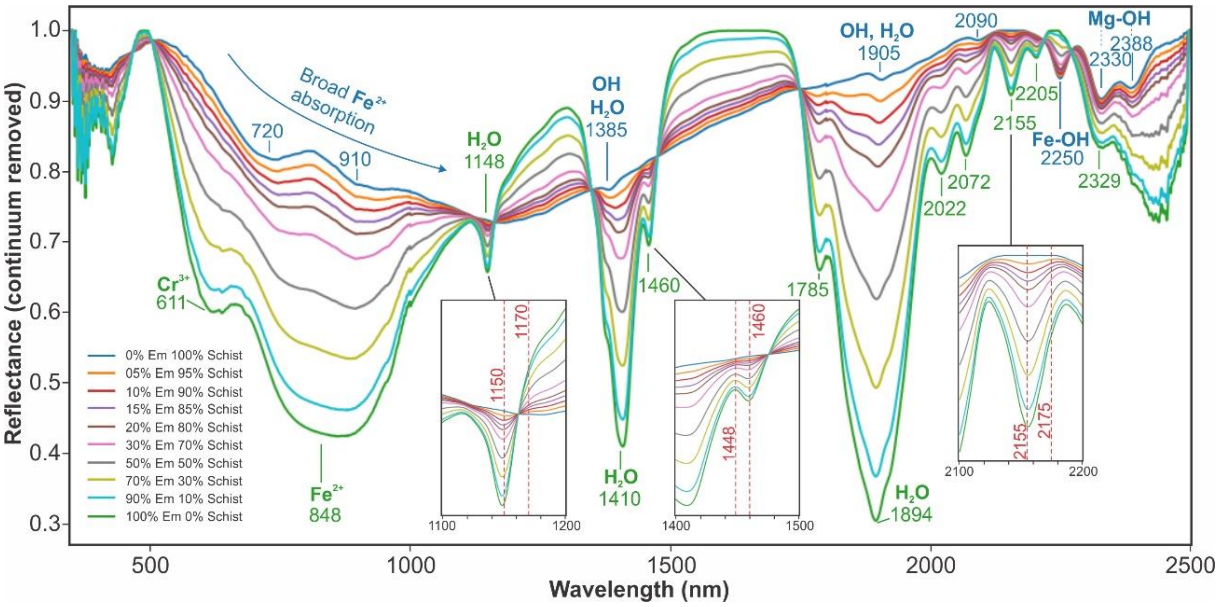

Figure 4.9. Simulation of mixed spectra with different proportions of emerald and phlogopite schist. The boxes show in detail the selected absorption features for emerald spectral indices. Em = emerald.

Spectral metrics applied to emerald exploration

Although precise, visual interpretations can take a long time to analyze and identify hundreds of samples – a common sampling number if the method is used in an exploratory context. To speed up the process, an automatized method can be employed based on spectral indices, *i.e.*, reflectance gradient in specific wavelengths diagnostic of a chosen target. They can be calculated in normalized spectra (hull quotient) using the depth of the diagnostic absorption feature or by spectral math (*e.g.*, reflectance ratio ρ/ρ). Examples of successful case studies in exploration geology are given by Tappert et al. (2011), Prado et al. (2016), Mesquita et al. (2019), Silva et al. (2022).

For the Paraná emerald deposit, three emerald indices (EI) were tested for automatized spectral identification (see details in Figure 4.9). EI1, EI2, and EI3 were selected based on emerald absorption features in the SWIR range, since the VNIR region of the spectrum is highly affected by iron absorption features of mafic minerals in the host rock. Hence, discarding the use of depth of chromium and iron absorptions in emerald as potential indices. A plot of EI1 versus EI2 using Orange Data Mining software is proposed in Figure 4.10 to quickly target emerald and emerald-bearing samples.

The EI1 was chosen based on the water absorption feature of emerald at ~1150 nm, creating a gradient with the higher reflectance values at 1170 nm that persists even in mixed spectra with only 10% of emerald (Figure 4.10). Other rock samples show decreasing reflectance values towards 1170 nm or present just a slightly increase in the range of 1150-1170 nm, thus the reflectance ratio ρ1170/ρ1150 > 1.01 should be indicative of emerald. However, if the emerald water feature at ~1150 nm is subtle, it may overlap other lithotypes that lie in 1.00 < EI1 < 1.01 (*e.g.*, ML-04 in Figure 4.10).

The secondary absorption feature at ~1460 nm, following the main water absorption at ~1410 nm, was chosen for the EI2. These secondary features are typical for the Paraná emerald, producing lower reflectance values in higher wavelengths in the range of 1448-1460 nm. This is considered the best emerald index for the Paraná deposit because do not overlap with other rock samples. For instance, measured emerald samples have ρ1448/ρ1460 > 1.00 while all other lithotypes of the 103 drill core samples showed ρ1448/ρ1460 < 1.00 (Figure 4.10).

The EI3 considered the emerald deep diagnostic absorption feature at ~2155 nm in the ρ2175/ρ2155 reflectance ratio. This index can distinguish emerald and emerald-bearing schists from schists without emerald. Most normalized schist spectra will show a flat line in the range of 2155-2175; thus, EI3 = 1.00. In the presence of emerald, even subtle absorptions will take

these values to EI3 >1.00 (see the detail in Figure 4.9). However, this index shows a large overlap with calcite-bearing samples because of the carbonate diagnostic feature centered at the same position of ~2155 nm. Therefore, for automatized investigations, EI3 must be used with caution or integrated with another EI when carbonate minerals are present in the context of the mineralization.

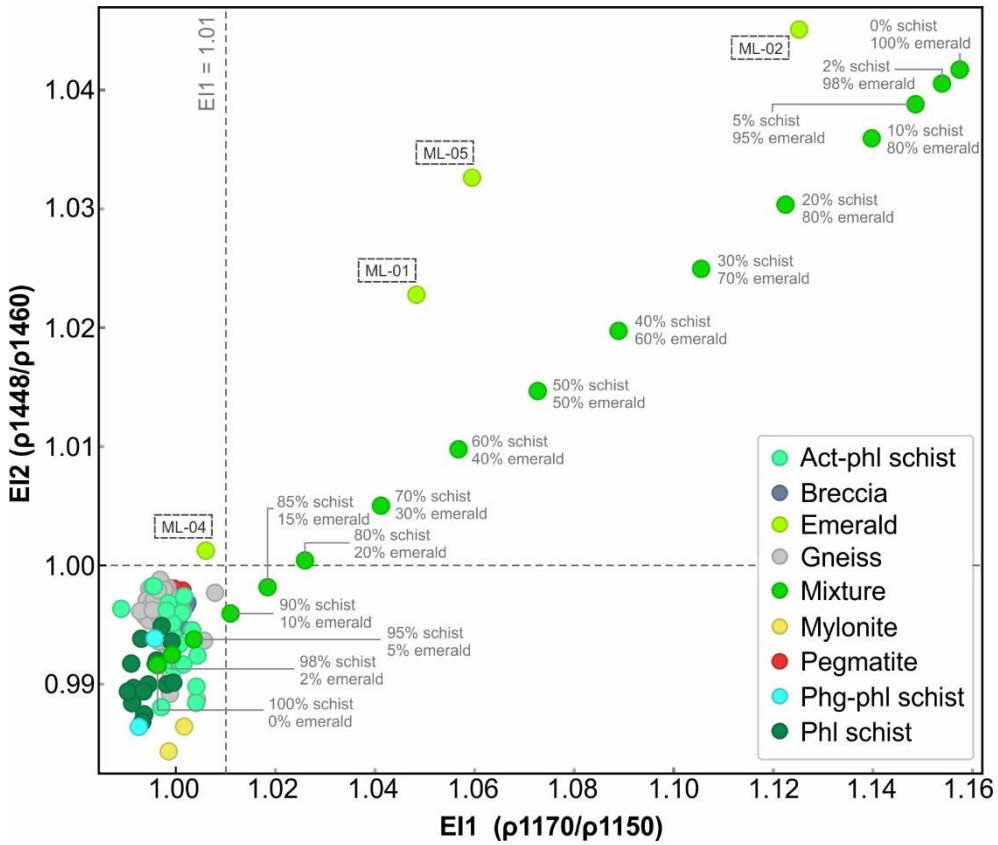

Figure 4.10. Diagram of emerald indices EI1 x EI2. The dashed line represents the lower limit of distinction for emeralds in each index (n = 123). Act = actinolite; Phg = phengite; Phl = phlogopite.

Host rock spectral metrics and validation through geochemical data

In the outcrop scale, but especially in local and regional approaches, the volume of emerald crystals is too small to be relevant for this spectral method. In this case, exploration spectroscopy should focus on the host rocks, *i.e.*, mafic schists. The purpose is to identify potentially mineralized horizons in drill cores and, even though schists can be rapidly distinguished from other rocks by naked-eye observations in this scale, the results can be extrapolated to airborne and orbital spectroscopy to target unexplored potential areas. However,

once this study was carried out on fresh drill core samples, one must proceed carefully if working with saprolite and soils. Different minerals resulting from weathering may influence the spectral outcome.

The most striking geochemical difference between the host and other rocks of the Paraná deposit is the MgO content. Also, Mg-OH vibrational processes are responsible for major absorption features in the main mafic minerals that comprise the host rock paragenesis: phlogopite and actinolite. Consequently, the proposed indices are based on the depth (MI_{depth}) and gradient (MI_{ratio}) of the Mg-OH feature centered around 2388 nm. An actinolite index (ACI) based on the Mg-OH absorption centered at ~2315 nm is proposed and even more precise for actinolite-bearing samples. The main target and limitations of each individual index are discussed below.

The MI_{depth} considers the depth of the 2388 nm feature in comparison to the convex hull (MI_{depth} = 1- ρ2388). Although also present in the biotite signature of the biotite gneisses, this feature is consistently deeper in Mg-richer minerals. Thus, breccias and pegmatites will show MI_{depth} values closer to zero, while gneisses can have higher values but still no more than 0.08, which would be attributed to mafic schists. However, samples with white mica have wide and deep absorption feature at ~2350 nm, and despite the difference in the wavelength position, this feature is deep enough to overlap MI_{depth} values of muscovite- and phengite-bearing rocks with those of phlogopite- and actinolite-bearing (Figure 4.11). Another limitation is that if the 2388 nm feature is too subtle (measurements on actinolite-bearing samples with too many quartz-feldspar veins, for example), they may overlap with some biotite gneiss spectral signature (see drill core FTA 02 in Figure 4.11).

To avoid overlapping with white mica, a MI_{ratio} is proposed. The MI_{ratio} does not only consider the depth of the 2388 nm feature but the gradient with the reflectance value at 2360 nm in the ρ2360/ρ2388 ratio. As reflectance in white mica shows increasing values towards 2388 nm, the ρ2360/ρ2388 ratio should always be less than 1.00 (Figure 4.11). Still, once MI_{ratio} is more of a wavelength position-driven than a depth-driven index, it may bring the values of biotite gneisses closer to those of mafic schists.

The ACI relies on the shift of the Mg-OH feature to ~2315 nm when actinolite is in the paragenesis. The index is based on the reflectance ratio ρ2340/ρ2315 and can be used to identify actinolite-phlogopite schists even when other indices have not (Figure 4.11). When using this index, one should be careful because ACI values >1.00 are also expected for other amphibole-rich rocks such as amphibolite and hornblende gneiss. The best setting is to integrate different indices when targeting host rocks. If more lithotypes are of economic interest, other indices can

be included. For instance, the marble index (ρ2414/ρ2475) of Silva et al. (2022) targets calcite-rich rocks and should be able to individualize calcite-rich breccias. A summary of all indices proposed in this work is presented in Table 4.1.

Table 4.1. Main characteristics of spectral indices proposed for emerald exploration in the Paraná deposit using ASD-FieldSpec.

Spectral index	Main target or lithotype	Diagnostic absorption feature	Spectral metric	Observed limitations
EI1	Emerald and emerald-bearing rocks	Emerald H_2O absorption feature at ~1150 nm.	ρ1170/ρ1150	Subtle water feature may overlap other sterile samples
EI2	Emerald and emerald-bearing rocks	Emerald secondary absorption feature at ~1460 nm.	ρ1448/ρ1460	In an emerald-schist mixture situation, needs at least 20% of emerald
EI3	Emerald and emerald-bearing rocks	Emerald diagnostic absorption feature at ~2155 nm.	ρ2175/ρ2155	Overlap with calcite-bearing samples
MI_{depth}	Phlogopite schist and actinolite-phlogopite schist	Phlogopite and actinolite Mg-OH absorption feature at ~2388 nm.	1- ρ2388	Overlap with white mica-rich samples. Sensible to subtle absorptions.
MI_{ratio}	Phlogopite schist and actinolite-phlogopite schist	Phlogopite and actinolite Mg-OH absorption feature at ~2388 nm.	ρ2360/ρ2388	Less effective separability with biotite-rich rocks
ACI	Actinolite-phlogopite schist	Actinolite Mg-OH absorption feature at ~2315 nm.	ρ2340/ρ2315	Overlap with other amphibole-rich rocks.

The direct correlation between MgO content and the depth of the Mg-OH absorption feature at ~2388 nm is poorly observed. The Pearson correlation coefficient is 0.64. This low value is coherent once there is an overlap of the Mg-OH feature with the deep Al-OH absorption of white mica-rich rocks, *i.e.*, samples with low MgO wt%. Besides, the presence of quartz and feldspar has a strong influence on the whole-rock geochemistry, but this influence is less effective in reflectance spectroscopic data. For instance, a schist sample with several quartz-feldspar veinlets will show a decrease in the total MgO wt%, but not necessarily a decrease in the depth of the Mg-OH feature. The latter will also be affected by the main paragenesis covered

by the area of the contact probe. Therefore, an improved study on the correlation between spectral reflectance and chemistry should be expected using mineral chemistry data of the main active minerals in the visible to shortwave infrared range (*e.g.*, phlogopite, actinolite, phengite, etc.).

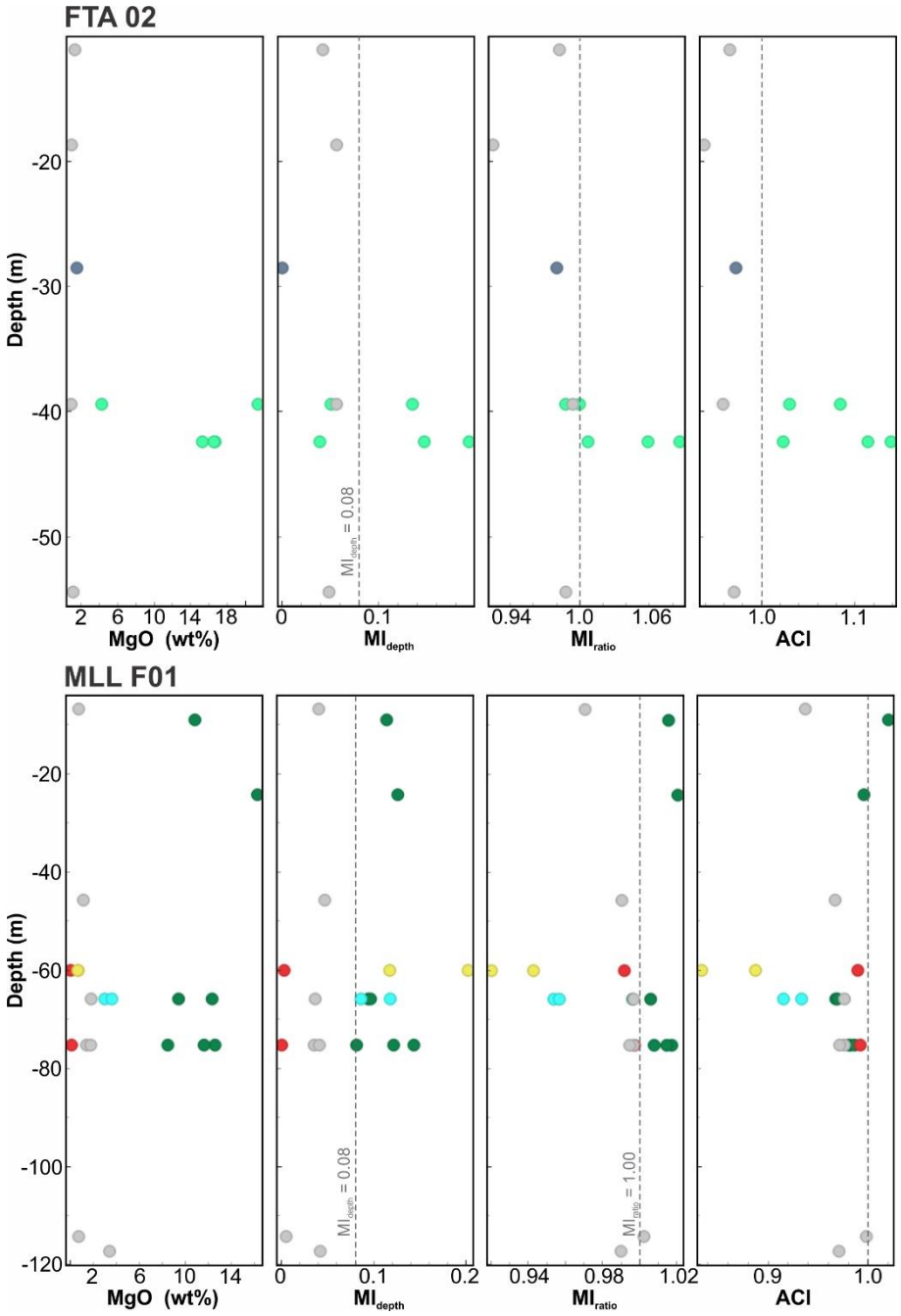

Figure 4.11. Integration of geochemistry (MgO wt%) and spectral indices of drill core samples in the most representative drill holes (FTA 02 and MLL F01). The color legend is the same as in Figure 4.10.

Imaging spectroscopy: a high-resolution procedure for exploration

The most advanced product for emerald exploration using reflectance data is a mineralogical map obtained through the SAM algorithm in HySpex images. In this case, each pixel registers spectral information that can be compared with a reference spectrum (endmember), by calculating the angle between their vectors in a D-dimensional space (Kruse et al. 1993). Thus, the final thematic map is dependent on the number of selected endmembers and the empirical maximum angle accepted (radians). Through this method, one can quickly analyze mineral assemblage in a rock log and track the schist mineralogical variation. For an actinolite-phlogopite schist, SAM was applied using phlogopite (0.04 rad) and actinolite (0.03 rad) endmembers in the SWIR region (2200-2450 nm), since the distinctive spectral absorptions of these minerals are present in this wavelength range. Figure 4.12a shows the distribution of classified phlogopite and actinolite in sample M2-2A.

Most important for the emerald exploration is the automatic identification of emerald crystals in pixels of ~1 mm. The SAM classifier was applied in the VNIR range (400-1000 nm), as emerald has a unique absorption signature in this region of the spectrum in comparison with those of phlogopite and other rock-forming minerals. A classification map is presented in Figure 4.12b after selecting the following endmembers and respective maximum angle: emerald (0.09 rad), phlogopite (0.70 rad), and a mixture of K-feldspar, quartz, and minor sericite (0.04 rad). Emerald stands out by its Cr^{3+} absorption features at 435, 467, and 627 nm, and Fe^{2+} absorption around 830 nm. Phlogopite has a broad iron absorption in the VNIR range, while quartz, K-feldspar, and sericite do not show relevant diagnostic absorptions in this wavelength region. Hence, the emerald class in sample ARO-SH01 was precisely mapped in the contact zone between the biotite gneiss and the phlogopite schist. Unclassified pixels are shown in black and occur mostly where there is a higher mixture of phlogopite/biotite with quartz and K-feldspar.

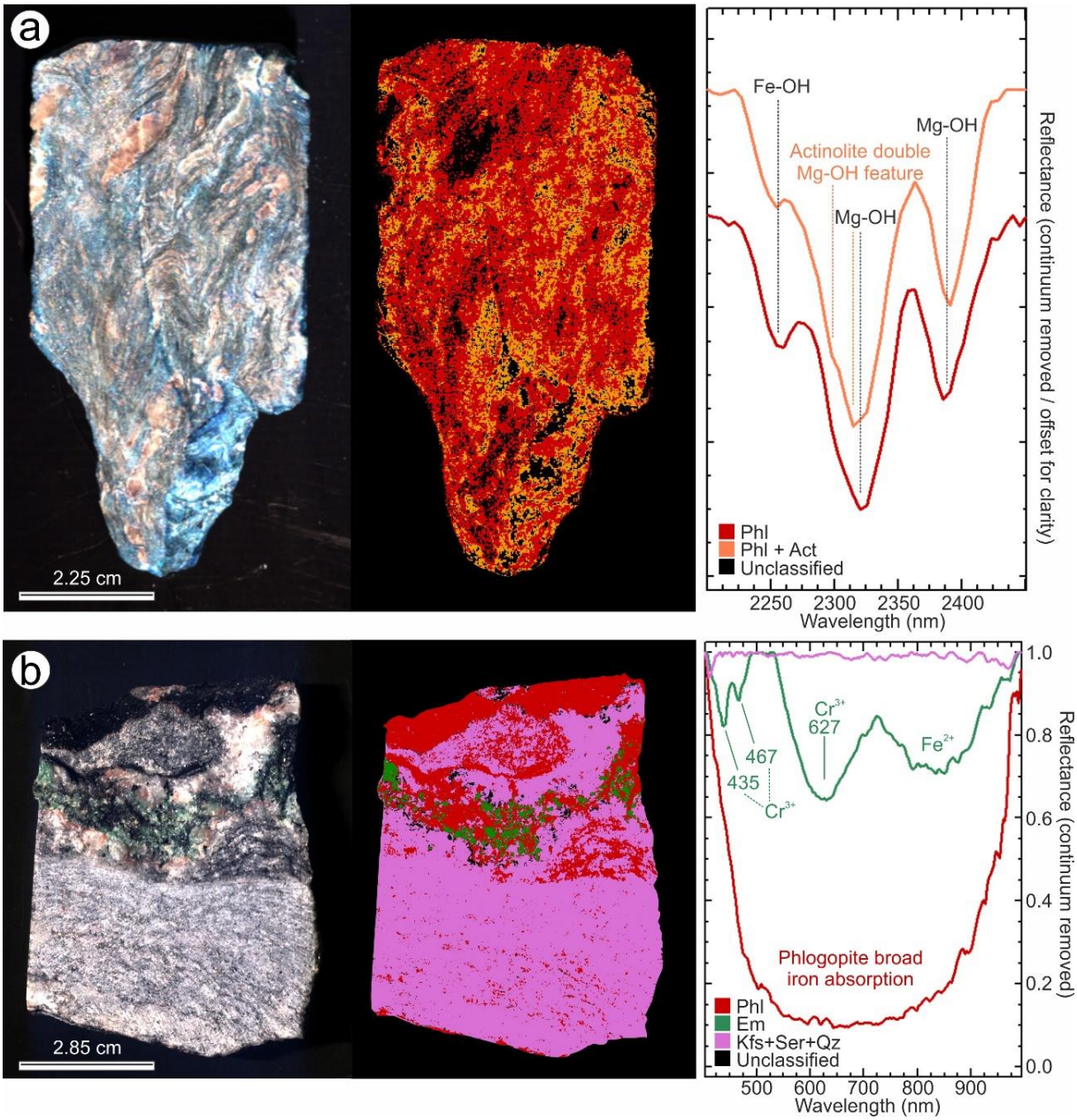

Figure 4.12. Classified mineralogical maps for samples of the Paraná emerald deposit using SAM algorithm in HySpex images. (a) Major mafic phases of an actinolite-phlogopite schist classified by SAM algorithm in the range of 2200-2450 nm. (b) Emerald crystals mapped in the contact zone between biotite gneiss and phlogopite schist after SAM algorithm in the range of 400-1000 nm. Act = actinolite; Em = emerald; Kfs = K-feldspar; Phl = phlogopite; Qtz = quartz; Ser = sericite.

CONCLUDING REMARKS

Spectral footprint determination is a prominent tool for emerald exploration. Point spectral reflectance can be used as a first investigative approach to unravel the host rock and

emerald mineralization relationship. In routine analysis, these spectral investigations can be applied to drill cores and other collected samples, directly on field campaigns or in laboratory measurements. The spectral indices proposed in this paper (EI1, EI2, and EI3) are able to identify the emerald spectral signal even in mixture situations. Each spectral index has its own application and limitations that should be taken into consideration. Therefore, the integration of different indices is recommended.

When emerald is not present or it is not relevant to the work scale, one may target potential mineralized host rocks by individualizing the phlogopite schist and actinolite-phlogopite schist signatures. For instance, so far, no emerald crystals have been found in phengite-phlogopite schists in the Paraná deposit. These differences in the schist's mineralogical composition although difficult to observe with naked-eye, can be quickly tracked using Mg-OH derived spectral indices (MI_{depth}, MI_{ratio}, ACI). These indices are also efficient into separate the host schists from other associated rocks in the Paraná deposit (gneisses, mylonites, breccias, etc.).

Furthermore, this method is applicable to most of the common emerald deposits worldwide, as they are associated with mafic-ultramafic schists (Giuliani et al. 2019), and it can be adapted to include new important mineral assemblages. For example, talc is a common mineral associated with the emerald mineralization process in other deposits (Alexandrov et al. 2001, Seifert et al. 2004, Santiago et al. 2019). In this case, diagnostic talc absorptions at 2288, 2310, and 2390 nm (Pontual et al. 2008) should be considered.

The spectral library provided in this work can also be used for detailed mineralogical and textural discriminating analysis, as high-resolution spectral images can highlight emerald crystals in a pixel scale of ~1 mm, allowing the distinction of different mineral classes through supervised classification routines. Future investigations for the applications of reflectance spectroscopy on emerald exploration should focus on the viability of this method to target potential host rocks in orbital and/or airborne spectral images.

ACKNOWLEDGMENTS

We would like to express our gratitude to Mr. Luis Amorim and all the crew of Mineração Limeira Comércio, Exportação e Importação for providing access to drill core samples and support to our research through geochemistry analysis. J.F.A. Neto thanks the Coordenação de Aperfeiçoamento de Pessoal de Nível Superior (CAPES) for his doctoral scholarship. We would also like to thank the Institute of Geosciences of UNICAMP, especially

Prof. Carlos R. de Souza Filho and Dr. Rebecca Scafutto for the assistance with ASD-FieldSpec data acquisition.

REFERENCES

Alexandrov, P., Guiliani, G., Zimmerman, J.L. (2001). Mineralogy, age and fluid geochemistry of the Rila Emerald deposits, Bulgaria. *Economic Geology*, 96:1469-1476. https://doi.org/10.2113/gsecongeo.96.6.1469

Almeida, F.F.M., Hasui, Y., Brito Neves, B.B., Fuck, R.A. (1981). Brazilian structural provinces: an introduction. *Earth Science Reviews*, 17(1-2), 1-29. https://doi.org/10.1016/0012-8252(81)90003-9

Araújo Neto, J.F., Barreto, S.B., Carrino, T.A., Müller, A., Santos, L.C.M.L. (2019). Mineralogical and gemological characterization of emerald crystals from Paraná deposit, NE Brazil: a study of mineral chemistry, absorption and reflectance spectroscopy and thermal analysis. *Brazilian Journal of Geology*, 49(3), 1-15. https://doi.org/10.1590/2317-4889201920190014

Araújo Neto, J.F., Barreto, S.B., Carrino, T.A., Souza, I.M.B.A., Santos, G.L. (2021a). Geochemical and reflectance spectroscopy data integration to characterize emerald deposits: the case of the Paraná deposit, Brazil. *Anais da Academia Brasileira de Ciências*, 93(1), e20200236. https://doi.org/10.1590/0001-3765202120200236

Araújo Neto, J.F., Lira Santos, G., Souza, I.M.B.A., Barreto, S.B., Santos, L.C.M.L., Bezerra, J.P.S., Carrino, T.A. (2018). Integration of remote sensing, airborne geophysics and structural analysis to geological mapping: a case study of the Vieirópolis region, Borborema Province, NE Brazil. *Geologia USP. Série Científica*, 18(3), 89-103. https://doi.org/10.11606/issn.2316-9095.v18-140834

Araújo Neto, J.F., Santos, L.C.M.L., Santos, G.L. (2021b). Geologia e aspectos genéticos de depósitos de esmeralda em zonas de cisalhamento: um olhar sobre os depósitos esmeraldíferos da Província Borborema, Nordeste do Brasil. *Geologia USP. Série Científica*, 21(2), 19-39. https://doi.org/10.11606/issn.2316-9095.v21-180467

Aurisicchio, C., Conte, A.M., Medeghini, L., Ottolini, L., De Vito, C. (2018) Major and trace element geochemistry of emerald from several deposits: Implications for genetic models and classification schemes. *Ore Geology Reviews*, 94, 351–366. https://doi.org/10.1016/j.oregeorev.2018.02.001

Brito Neves, B.B., Fuck, R.A., Pimentel, M.M. (2014). The Brasiliano collage in South America: a review. *Brazilian Journal of Geology*, 44(3), 493-518. https://doi.org/10.5327/Z2317-4889201400030010

Clark, R.N. (1999). Spectroscopy of rocks and minerals, and principles of spectroscopy. In: Rencz, A.N. (ed). *Manual of remote sensing*. Remote Sensing for the Earth Science, 3, New York, John Wiley and Sons, p. 3-58.

Crósta, A.P., Sabine, C., Taranik, J.V., (1998). Hydrothermal alteration mapping at Bodie, California, using AVIRIS hyperspectral data. *Remote Sensing of Environment*, 65, 309–319. https://doi.org/10.1016/S0034-4257(98)00040-6

Dyar, M.D. (1990). Mossbauer spectra of biotite from metapelites. *American Mineralogist*, 75, 656-666.

Giuliani, G., Groat, L.A., Marshall, D., Fallick, A.E., Branquet, Y. (2019). Emerald Deposits: A Review and Enhanced Classification. *Minerals*, 9(2), 105. https://doi.org/10.3390/min9020105

Groat, L.A., Giuliani, G., Marshall, D.D., Turner, D. (2008). Emerald deposits and occurrences: A review. *Ore Geology Reviews*, 34, 87-112. https://doi.org/10.1016/j.oregeorev.2007.09.003

Hecker, C., Van Ruitenbeek, F.J.A, van der Werff, H.M.A, Bakker, W.H., Hewson, R.D, van der Meer, F.D. (2019). Spectral absorption feature analysis for finding ore. A tutorial on using the method in geological remote sensing. *IEEE Geoscience and Remote Sensing Magazine*, 7, 51-71. Doi: 10.1109/MGRS.2019.2899193

Hecker, C., van der Meijde, M., van der Meer, F.D. (2010). Thermal infrared spectroscopy on feldspars — Successes, limitations and their implications for remote sensing, *Earth-Science Reviews*, 103, 60-70. https://doi.org/10.1016/j.earscirev.2010.07.005

Hunt, G.R. (1977). Spectral Signatures of Particulate Minerals in the Visible and near Infrared. Geophysics, 42, 501-513. https://doi.org/10.1190/1.1440721

HypPy. (2022). Hyperspectral Python. Available at: <http://hyppy.byethost18.com/index.html>. Accessed on: oct. 02, 2022.

Kruse, F.A. (1996). Identification and mapping of minerals in drill core using hyperspectral image analysis of infrared reflectance spectra. *International Journal of Remote Sensing*, 17(9), 1623-1632. https://doi.org/10.1080/01431169608948728

Kruse, F.A., Lefkoff, A.B., Boardman, J.B., Heidebrecht, K.B., Shapiro, A.T., Barloon, P.J., Goetz, A.F.H. (1993). The Spectral Image Processing System (SIPS) - Interactive Visualization and Analysis of Imaging spectrometer Data. *Remote Sensing of the Environment*, 44(2-3), 145-163. https://doi.org/10.1016/0034-4257(93)90013-N

Laukamp, C., Cudahy, T., Cleverley, J.S., Oliver, N.H.S., Hewson, R. (2011). Airborne hyperspectral imaging of hydrothermal alteration zones in granitoids of the Eastern Fold Belt, Mount Isa Inlier, Australia. *Geochemistry: Exploration, Environment, Analysis*, 11, 3-24. https://doi.org/10.1144/1467-7873/09-231

Lypaczewski, P., Rivard, B., Gaillard, N., Perrouty, S., Piette-Lauzière, N., Bérubé, C.L., Linnen, R.L. (2019). Using hyperspectral imaging to vector towards mineralization at the Canadian Malartic gold deposit, Québec, Canada. *Ore Geology Reviews*, 111, 102945. https://doi.org/10.1016/j.oregeorev.2019.102945

Malvern Panalytical. (2022). ASD FieldSpec 4 Standard-Res Spectroradiometer. Malvern Panalytical. Available at: <https://www.asdi.com/productsand-services/fieldspec-spectroradiometers/fieldspec-4-standard-res/>. Accessed on: oct. 02, 2022.

Mather, P.M. (2004). Image transforms. In: Mather, P.M. (Ed.), Computer processing of remotely-sensed images. An introduction. John Wiley & Sons Ltd., Chichester, pp. 136-79.

Medina, C.M., Ducart, D.F., Passos, J.S., Oliveira, L.R. (2021). Exploration vectoring from the white mica spectral footprint in the atypical auriferous Lavra Velha deposit, San Francisco Craton, Brazil. *Ore Geology Reviews*, 139, 104438. https://doi.org/10.1016/j.oregeorev.2021.104438

Medeiros, V.C. (Ed.). (2008). *Geologia e Recursos Minerais da Folha Sousa SB.24-Z-A*. Escala 1:250.000. Recife: CPRM – Serviço Geológico do Brasil.

Mesquita, N.M., Carrino, T.A., Souza Neto, J.A. (2019). The use of reflectance spectroscopy and the prehnite spectral index to target gold mineralization at the Bonfim polymetallic skarn deposit, Seridó Mobile Belt, Borborema Province, Brazil. *Ore Geology Reviews*, 115, 103192. https://doi.org/10.1016/j.oregeorev.2019.103192

Moura, W.A.L., Carrino, T.A., Pabón, R.E.C., Lima Filho, M., Souza Neto, J.A. (2022). Applying spectral tools in a mixed siliciclastic-carbonate environment: An integrative sedimentological case study from the Estiva Formation, Pernambuco Basin, Northeast Brazil. *Journal of South American Earth Sciences*, 116, 103831. https://doi.org/10.1016/j.jsames.2022.103831

Naleto, J.L.C., Perrotta, M.M., Costa, F.G., Souza Filho, C.R. (2019). Point and imaging spectroscopy investigations on the Pedra Branca orogenic gold deposit, Troia Massif, Northeast Brazil: Implications for mineral exploration in amphibolite metamorphic-grade terrains. *Ore Geology Reviews*, 107, 283-309. https://doi.org/10.1016/j.oregeorev.2019.02.019

Orange Visual Programming. (2022). PCA. Available at: <https://orange3.readthedocs.io/projects/orange-visual-programming/en/latest/widgets/unsupervised/PCA.html>. Accessed on: nov. 15, 2022.

Pearson, K. (1901). On lines and planes of closest fit to systems of points in space. *Philosophical Magazine Series*, 2(11), 559-572. https://doi.org/10.1080/14786440109462720

Pontual, S., Merry, N., Gamson, P. (2008). Spectral Interpretation - Field Manual. GMEX. Spectral Analysis Guides for Mineral Exploration: Victoria. AusSpec International Pty. Ltd., p. 189

Prado, E.M.G., Silva, A.M., Ducart, D.F., Toledo, C.L.B., Assis, L.M. (2016). Reflectance spectroradiometry applied to a semi-quantitative analysis of the mineralogy of the N4ws deposit, Carajás Mineral Province, Pará, Brazil. *Ore Geology Reviews*, 78, 101-119. https://doi.org/10.1016/j.oregeorev.2016.03.007

Ramakrishnan, D., Nithya, M., Singh, K. D. and Bharti, R. (2013). A field technique for rapid lithological discrimination and ore mineral identification: results from Mamandur polymetal

deposit, India. *Journal of Earth System Science*, 122, 93-106. https://doi.org/10.1007/s12040-012-0255-x

Rondeau, B., Fritsch, E., Peucat, J., Nordrum, F.S., Groat, L.A. (2008). Characterization of Emeralds from a historical deposit: Byrud (Eidsvoll), Norway. *Gems and Gemology*, 44(2),108-122. Doi: 10.5741/GEMS.44.2.108

Santiago, J.S., Souza, V.S., Dantas, E.L., Oliveira, C.G. (2019). Ediacaran emerald mineralization in Northeastern Brazil: the case of the Fazenda Bonfim Deposit. *Brazilian Journal of Geology*, 49(4), 1-14. https://doi.org/10.1590/2317-4889201920190081

Santos, E.J., Souza Neto, J.A., Silva, M.R.R., Beurlen, H., Cavalcanti, J.A.D., Silva, M.G., Dias, V.M., Costa, A.F., Santos, L.C.M.L., Santos, R.B. (2014). Metalogênese das porções norte e central da Província Borborema. In: Silva, M.G., Rocha Neto, M.B., Jost, H., Kuyumijan, R.M. *Metalogênese das províncias tectônicas brasileiras*. 343-388. Belo Horizonte: CPRM.

Schafer, R.W. (2011). What is a Savitzky-Golay filter? *IEEE Signal Processing Magazine*, 28(4), 111-117. doi: 10.1109/MSP.2011.941097
Schwarz, D., Giuliani, G. (2001). Emerald deposits a review. *Australian Gemmologist*, 21, 17-23.

Scott, K.M., Yang K. (1997). Spectral reflectance studies of white micas. Commonwealth Scientific and Industrial Research Organisation, Exploration and Mining Report 439R, p. 35.

Seifert, A.V., Žáček, V., Vrána, S., Pecina, V., Zachariáš, J., Zwaan, J.C. (2004). Emerald Mineralization in the Kafubu area, Zambia. *Bulletin of Geosciences*, 79, 1-40.

Silva, L.A., Carrino, T.A., Santos, L.C.M.L., Pabón, R.E.C. (2022). Spectral characterization of the Umbuzeiro Doce skarn target (Brazil): insights for the exploration of a W-Mo-gemological vesuvianite system. *Brazilian Journal of Geology*, 52(4), e20220035. https://doi.org/10.1590/2317-4889202220220035

Simandl, G.J., Paradis, S. and Birkett, T. (1999). Schist-hosted Emeralds. In: G.J. Simandl, Z.D. Hora and D.V. Lefebure (eds.), *Selected British Columbia Mineral Deposit Profiles*, Volume 3, Industrial Minerals, British Columbia Ministry of Energy and Mines, Open File 1999-10.

Swayze, G.A. et al. 2014. Mapping advanced argillic alteration at Cuprite, Nevada, using imaging spectroscopy. *Economic Geology*, 109, 1179-1221. https://doi.org/10.2113/econgeo.109.5.1179

Tappert, M., Rivard, B., Giles, D., Tappert, R., Mauger, A. (2011). Automated drill core logging using visible and near-infrared reflectance spectroscopy: a case study from the Olympic Dam IOCG deposit, South Australia. *Economic Geology*, 106(2), 289-296. https://doi.org/10.2113/econgeo.106.2.289

Thompson, A.J.B., Hauff, P.L., Robitaille, A.J. (1999). Alteration mapping in exploration: application of short-wave infrared (SWIR) spectroscopy. *Society of Economic Geologist Newsletter*, 39, 15-17.

Thompson, A., Scott, K., Huntington, J., Yang, K. (2009). Mapping Mineralogy with Reflectance Spectroscopy: Examples from Volcanogenic Massive Sulfide Deposits. In: R. Bedell, A.P. Crósta, E. Grunsky (eds.). *Remote Sensing and Spectral Geology*. Reviews in Economic Geology, 2009.

Turner, D., Groat, L.A., Rivard, B., Belley, P.M. (2017). Reflectance Spectroscopy and Hyperspectral Imaging of Sapphire-bearing Marble from the Beluga Occurrence, Baffin Island, Nunavut. *The Canadian Mineralogist*, 55(4), 787-797. https://doi.org/10.3749/canmin.1700023

Van Schmus, W.R., Kozuch, M., Brito Neves, B.B. (2011). Precambrian history of the Zona Transversal of the Borborema Province, NE Brazil: Insights from Sm-Nd and U-Pb geochronology. *Journal of South American Earth Sciences*, 31(2-3), 227-252. https://doi.org/10.1016/j.jsames.2011.02.010

Walton, L. (2004). *Exploration criteria for coloured gemstone deposits in the Yukon*. Yukon: Yukon Geological Survey.

Wood, D.L., Nassau, K. (1968). The characterization of beryl and emerald by visible and infrared absorption spectroscopy. *American Mineralogist*, 53(5-6), 777-800.

Zhou, Y., Wang, T., Fan, F., Chen, S., Guo, W., Xing, G., Sun, J., Xiao, F. (2022). Advances on Exploration Indicators of Mineral VNIR-SWIR Spectroscopy and Chemistry: A Review. *Minerals*, 12, 958. https://doi.org/10.3390/min12080958

Zwaan, J.C. (2006). Gemmology, geology and origin of the Sandawana emerald deposits, Zimbabwe. *Scripta Geologica*, 131, 1-211.

APPENDIX 1

Whole-rock geochemistry of drill core samples of the Paraná emerald deposit.

Sample	Class	Depth*	Al_2O_3	BaO_	CaO	Cr_2O_3	Fe_2O_3	K_2O	MgO	MnO	Na_2O	P_2O_5	SO_3	SiO_2	SrO	TiO_2	Total	LOI	V	Be
		m	wt.%	wt.%	wt.%	wt.%	wt.%	wt.%	wt.%	wt.%	wt.%	wt.%	wt.%	wt.%	wt.%	wt.%	wt.%	wt.%	ppm	ppm
F1-10B	Gneiss	38.22	14.13	0.32	4.97	0.05	5.99	7.45	5.05	0.09	1.64	1.01	0.01	54.55	0.11	1.57	99.28	2.23	102	2.9
F1-14	Gneiss	54.41	15.09	0.11	3.09	0.04	4.42	3.87	1.14	0.06	3.47	0.2	0.01	67.31	0.05	0.59	100.7	1.17	43	2.2
F1-19	Breccia	70.46	18.58	0.02	14.55	0.01	2.2	1.03	1.48	0.03	0.54	0.01	0.02	45.75	0.08	0.06	100.05	15.68	9	4
F1-20	Phl schist	75.92	8.43	0.16	3.41	0.15	7.27	6.47	17.1	0.12	0.17	0.82	0.01	50.96	0.01	0.54	99.06	3.27	77	17.6
F1-26	Gneiss	98.83	14.74	0.12	2.87	0.03	4.55	3.65	1.6	0.07	3.37	0.18	0.01	66.95	0.05	0.58	100.3	1.48	47	4.8
F2-3	Gneiss	11.10	15.12	0.12	3.9	0.02	4.45	3.26	1.3	0.07	3.4	0.19	0.03	67.73	0.06	0.58	101.15	0.83	51	2.1
F2-5	Gneiss	18.70	10.01	0.05	3.8	0.04	4.07	1.18	0.94	0.07	2.22	0.12	0.12	76.94	0.03	0.4	101	0.96	48	1.8
F2-8	Breccia	28.53	10.4	0.07	19.9	0.04	2.96	2.92	1.52	0.06	1.3	0.11	0.03	43.64	0.03	0.33	100.65	17.28	23	2.1
F2-10B	Act-phl schist	39.41	11.96	0.05	4.47	0.17	10.03	3.33	21.4	0.22	0.16	0.81	0.01	40.27	0.02	0.78	101.75	7.8	101	10
F2-10E	Gneiss	39.41	15.52	0.24	2.72	0.04	3.49	3.91	0.89	0.03	4.03	0.13	0.14	68.03	0.1	0.63	100.9	0.86	36	4
F2-10G	Act-phl schist	39.41	6.28	0.21	1.33	0.1	3.86	3.46	4.25	0.07	0.31	0.3	0.01	77.82	0.05	0.35	100.6	2.11	36	4.7
F2-11C	Act-phl schist	42.41	11.9	0.07	4.18	0.15	14.22	5.64	16.7	0.21	0.14	0.49	0.02	41.14	0.01	1.29	101.8	5.42	130	15.6
F2-11D	Act-phl schist	42.41	9.42	0.18	5.72	0.14	8.4	5.07	16.55	0.15	0.23	0.89	0.01	48.69	0.03	0.63	100.5	4.22	85	15.2
F2-11E	Act-phl schist	42.41	9.33	0.24	5.04	0.15	7.47	5.9	15.3	0.13	0.29	0.86	0.01	52.11	0.04	0.58	100.4	2.75	84	15.3
F2-14	Gneiss	54.41	14.84	0.12	2.95	0.03	3.96	3.53	1.12	0.06	3.58	0.17	0.02	67.49	0.05	0.56	99.35	0.81	41	3
M1-03	Gneiss	6.82	18.08	0.11	3.78	0.03	3.35	3.09	0.73	0.05	4.69	0.12	0.01	64.01	0.04	0.43	99.63	1.08	32	4.9
M1-04	Gneiss	9.03	11.86	0.21	3.77	0.15	8.09	5.93	10.85	0.12	0.34	0.97	0.01	53.77	0.03	0.69	99.57	2.63	83	12.2
M1-7A	Phl schist	24.28	12.24	0.17	1.1	0.15	11.36	8.79	16.3	0.19	0.07	0.59	0.01	45.34	0.01	0.58	99.44	2.35	90	7.7
M1-13	Gneiss	45.75	18.91	1.79	2.3	0.02	3.76	6.26	1.14	0.06	4.2	0.1	0.38	59.08	0.08	0.33	99.54	1.06	30	1.9
M1-17A	Mylonite	60.06	13.6	0.12	0.54	0.03	2.71	5.17	0.7	0.08	2.32	0.08	0.01	72.12	0.02	0.31	99.43	1.56	25	8.9

M1-17B	Mylonite	60.06	13.64	0.09	0.14	0.02	2.36	5.43	0.65	0.08	0.85	0.05	0.01	72.72	0.01	0.28	98.75	2.37	25	9.9
M1-17C	Pegmatite	60.06	14.22	0.04	0.28	0.04	0.42	9.83	0.03	0.02	1.82	0.01	0.01	73.27	0.01	0.02	101	0.96	3	2.7
M1-18A	Gneiss	65.88	17.36	0.08	3.76	0.03	5.34	1.96	1.82	0.07	5.03	0.23	0.01	62.89	0.06	0.65	100.75	1.41	52	50.8
M1-18B	Phl schist	65.88	9.75	0.09	0.75	0.13	9.43	6.67	9.43	0.17	0.07	0.38	0.01	59.02	0.01	0.39	99.15	2.73	78	5
M1-18F	Phl schist	65.88	11.8	0.1	0.81	0.12	12.8	8.21	12.35	0.24	0.1	0.53	0.01	49.14	0.01	0.53	99.61	2.66	101	4.7
M1-18J	Phg-phl schist	65.88	15.29	0.13	0.95	0.06	4.88	7.47	3.62	0.1	2.85	0.14	0.01	62.02	0.04	0.31	100.5	2.57	39	8.8
M1-18K	Phg-phl schist	65.88	11.78	0.09	2	0.05	2.92	4.48	3.01	0.08	2.73	0.21	0.01	69.41	0.02	0.21	100.4	3.33	26	7.5
M1-20A	Gneiss	75.28	20.54	0.06	3.08	0.02	3.73	2.02	1.78	0.06	7.25	0.17	0.01	59.96	0.07	0.57	101.2	1.8	39	72.5
M1-20B	Phl schist	75.28	13.04	0.09	1.3	0.12	12.46	8.11	12.6	0.26	0.8	0.61	0.01	46.01	0.01	0.73	98.87	2.56	102	16.4
M1-20C	Phl schist	75.28	12.98	0.12	0.81	0.09	8.24	7.93	8.49	0.21	1.5	0.38	0.01	56.16	0.02	0.42	100.35	2.85	65	16.5
M1-20I	Phl schist	75.28	13.41	0.1	1.05	0.12	10.28	8.98	11.65	0.29	0.79	0.64	0.01	47.31	0.01	0.57	98.31	2.95	83	9.5
M1-20N	Pegmatite	75.28	19.27	0.08	0.53	0.01	0.25	6.53	0.11	0.01	6.75	0.01	0.01	65.37	0.03	0.03	99.55	0.55	1	12.6
M1-20P	Gneiss	75.28	16.08	0.14	2.28	0.03	3.9	2.88	1.42	0.06	5.31	0.18	0.01	65.93	0.04	0.51	100.15	1.36	35	34.7
M1-30	Gneiss	114.28	13.35	0.18	1.14	0.05	3.18	5.56	0.73	0.03	2.87	0.09	0.01	72.18	0.03	0.38	101.05	1.22	25	2.4
M1-31C	Gneiss	117.28	15.28	0.11	3.81	0.02	9.39	3.7	3.42	0.12	2.8	0.51	0.02	58.76	0.05	0.86	100.4	1.49	96	2.4
M2-2B	Act-phl schist	4.87	9.83	0.21	6.21	0.15	8.94	6.25	14.25	0.15	0.39	1.02	0.01	48.08	0.04	0.81	99.11	2.61	95	7
M2-2D	Gneiss	5.86	14.66	0.17	1.64	0.04	1.82	5.58	0.42	0.02	3.37	0.07	0.09	71.48	0.08	0.23	100.4	0.68	12	2.6
M2-4A	Gneiss	9.36	13.61	0.13	2.18	0.03	3.28	4.19	0.54	0.03	2.94	0.09	0.51	71.28	0.04	0.35	99.9	0.66	25	6.8
M2-5	Gneiss	14.71	12.22	0.15	1.5	0.04	3.62	5.05	0.57	0.04	1.93	0.08	1.45	73.52	0.03	0.35	101.85	1.25	21	2.3
M2-6	Gneiss	14.71	16.4	0.07	3.76	0.05	2.61	1.51	0.4	0.04	4.89	0.17	0.33	68.36	0.04	0.38	100.3	1.22	18	4.2

LOI = loss on ignition at 1000 °C; *mean depth value for a drill core segment

5 CONSIDERAÇÕES FINAIS

O depósito de esmeralda de Paraná, bem como alguns dos principais depósitos brasileiros (*e.g.* Itabira-Nova Era, Carnaíba) e demais mineralizações de esmeralda encontradas na Província Borborema (Coqui, Fazenda Bonfim), apresenta uma forte conexão com fontes magmáticas de berílio e uma estruturação tectônica que estabelece a configuração litoestrutural final do depósito, caracterizando-o como depósito do tipo *tectonic-magmatic-related*, hospedado em rochas máficas/ultramáficas (tipo IA; Giuliani et al., 2019).

O desenvolvimento de extensas zonas de cisalhamento nos estágios finais da Orogênese Brasiliana (*ca.* 600-500 Ma) facilitou a migração de fluidos pegmatíticos de idade Neoproterozoica/Cambriana e a interação desses fluidos com rochas máficas e ultramáficas mais antigas, além de fornecer as condições de temperatura e alojamento necessárias para formação do minério na Província Borborema. Registros de mineralização de esmeralda limitados à Subprovíncia Setentrional demonstra a ligação destas ocorrências à presença de campos e distritos pegmatíticos berilíferos em áreas intensamente deformadas.

Na região de Paraná, um forte controle estrutural da mineralização pela zona de cisalhamento Portalegre é observado em diferentes escalas. A esmeralda é encontrada em flogopita xistos e actinolita-flogopita xistos inseridos em corredores miloníticos da ZCPA. Essa estrutura é representada por uma assinatura magnética intensa e de profundidade mais elevada, alinhada na direção NE-SW. Nesse contexto, interpretação de imagens aeromagnéticas associadas a soluções de profundidade por deconvolução Euler são ferramentas eficazes na delimitação desta estrutura na escala regional.

Estudos estruturais nas escalas meso- e microscópicas apontam para uma formação sin-cinemática dos cristais de esmeralda e do xisto hospedeiro. Temperaturas de 390-550 °C restringidas por análise microestrutural estão de acordo com a faixa de temperatura usual para formação de esmeralda. Adicionalmente, idades $^{40}Ar/^{39}Ar$ em flogopita de aproximadamente 524-528 Ma fortalecem o suporte a uma origem do depósito durante os estágios finais da orogênese Brasiliana. Zircões de idade Riaciana (2.20-2.21 Ga) encontrados em *boudins* e demais corpos deformados de composição granítica no interior dos xistos apontam para um retrabalhamento de gnaisses do Complexo Caicó durante o alojamento do xisto hidrotermal.

O desenvolvimento do minério teria se dado após interações metassomáticas entre uma fonte pegmatítica de berílio e uma fonte máfica rica em elementos cromóforos (possíveis lentes de anfibolito do Complexo Caicó), resultando em pegmatitos dessilicados e flogopita xistos contendo esmeralda, respectivamente.

O flogopita xisto mineralizado, bem como as demais rochas associadas ao depósito, pode ser classificado de forma automatizada através de sua assinatura espectral. Utilizando espectroscopia de reflectância pontual é possível distinguir a mineralogia dos xistos máficos e identificar amostras potencialmente mineralizadas. A utilização integrada dos três índices espectrais de esmeralda propostos nesse trabalho (EI1, EI2 e EI3) mostraram-se eficaz em identificar a presença espectral de esmeralda tanto em simulações de mistura esmeralda-xisto quanto em amostras reais, com plotagem dos valores de EI1 versus EI2 despontando como método mais eficiente.

As rochas hospedeiras (*i.e.*, flogopita xisto e actinolita-flogopita xisto) podem ser identificadas por um índice espectral derivado de feições de absorção Mg-OH (MI_{depth}, MI_{ratio}, ACI). Esses índices são particularmente importantes quando não há esmeralda ou quando a escala de trabalho não é apropriada para detecção de pequenos cristais de berilo. Adicionalmente, há uma grande aplicabilidade desses índices para outros depósitos do tipo *tectonic-magmatic-related* hospedados em rochas máficas-ultramáficas, uma vez que flogopita e actinolita são assembleias minerais importantes na maioria desses depósitos.

Usando classificação supervisionada em imagens hiperespectrais de alta resolução pode-se chegar ao detalhe de mapear cristais de esmeralda em amostras de mão ou de furo de sonda em pixels de aproximadamente 1 mm utilizando espectros de referência (endmembers). Nesse sentido, a biblioteca espectral produzida por este trabalho pode ser utilizada por outras abordagens espectrais destinadas à exploração de esmeralda ou outros minerais raros, e futuras investigações devem ser voltadas à aplicabilidade de técnicas espectrais para exploração de esmeralda por imagens orbitais ou de aerolevantamentos.

REFERÊNCIAS

ABDALLA, H.M.; MOHAMED, F.H. Mineralogical and geochemical investigations of beryl mineralizations, Pan-African belt of Egypt: Genetic and exploration aspects. **Journal of African Earth Sciences**, v. 28, p. 581-598, 1999. https://doi.org/10.1016/S0899-5362(99)00033-0

ALEXANDROV, P.; GUILIANI, G.; ZIMMERMAN, J. L. Mineralogy, age and fluid geochemistry of the Rila Emerald deposits, Bulgaria. **Economic Geology**, v. 96, p. 1469-1476, 2001. DOI: https://doi.org/10.2113/gsecongeo.96.6.1469

ALMEIDA, A. F.; PARENTE, C. V.; ARTHAUD, M. H. (Eds.). **Quixeramobim - SB.24-V-D-III**. Escala 1:100.000: nota explicativa integrada com Boa Viagem e Itatira. Ceará: UFC/CPRM, p. 196, 2007.

ALMEIDA, F. F. M.; HASUI, Y.; BRITO NEVES, B. B.; FUCK, R. A. Brazilian structural provinces: an introduction. **Earth Science Reviews**, v. 17, n. 1-2, p. 1-29, 1981. DOI: https://doi.org/10.1016/0012-8252(81)90003-9

ALMEIDA, G. M.; FUCK, R. A.; DANTAS, E. L.; LIMA, S. S. Oblique collision and accretionary processes in the South Borborema Province: Insights from structural geology and geophysical data. **Tectonophysics**, v. 844, 229607, 2022. DOI: https://doi.org/10.1016/j.tecto.2022.229607

ALMEIDA, G.M.; FUCK, R.A.; LIMA, D.P.D.; DANTAS, E.L. Accretion tectonics in Western Gondwana highlighted by the aeromagnetic signature of the Sergipano Belt, NE Brazil. **Tectonophysics**, v. 802, p. 228742, 2021. DOI: https://doi.org/10.1016/j.tecto.2021.228742

ARAÚJO, M. N. C.; ALVES DA SILVA, F. C.; JARDIM DE SÁ, E. F. Pegmatite emplacement in the Seridó Belt, Northeastern Brazil: Late stage kinematics of the Brasiliano orogen. **Gondwana Research**, v. 4, n. 1, p. 75-85, 2001. DOI: https://doi.org/10.1016/S1342-937X(05)70656-0

ARAÚJO, M. N. C.; VASCONCELOS, P. M.; ALVES DA SILVA, F. C.; JARDIM DE SÁ, E.; SÁ, J. M. $^{40}Ar/^{39}Ar$ geochronology of gold mineralization in Brasiliano strike-slip shear zone in the Borborema Province, NE Brazil. **Journal of South American Earth Sciences**, v. 19, p. 445-460, 2005. DOI: https://doi.org/10.1016/j.jsames.2005.06.009

ARAÚJO NETO, J. F. **Caracterização da esmeralda do município de Paraná, estado do Rio Grande do Norte, Brasil**. Dissertação (Mestrado em Geociências). Centro de Tecnologia e Geociências, Universidade Federal de Pernambuco, 2018.

ARAÚJO NETO, J. F.; BARRETO, S. B.; CARRINO, T. A.; MÜLLER, A.; SANTOS, L.C.M.L. Mineralogical and gemological characterization of emerald crystals from Paraná deposit, NE Brazil: a study of mineral chemistry, absorption and reflectance spectroscopy and thermal analysis. **Brazilian Journal of Geology**, v. 49, n. 3, p. 1-15, 2019. DOI: https://doi.org/10.1590/2317-4889201920190014

ARAÚJO NETO, J. F.; BARRETO, S. B.; CARRINO, T. A.; SOUZA, I. M. B. A.; SANTOS, G. L. Geochemical and reflectance spectroscopy data integration to characterize emerald deposits: the case of the Paraná deposit, Brazil. **Anais da Academia Brasileira de Ciências**, v. 93, n. 1, e20200236, 2021a. DOI: https://doi.org/10.1590/0001-3765202120200236

ARAÚJO NETO, J. F.; LIRA SANTOS, G.; SOUZA, I. M. B. A.; BARRETO, S. B., SANTOS, L. C. M. L.; BEZERRA, J. P. S.; CARRINO, T. A. Integration of remote sensing, airborne geophysics and structural analysis to geological mapping: a case study of the Vieirópolis region, Borborema Province, NE Brazil. **Geologia USP. Série Científica**, v. 18, n. 3, p. 89-103, 2018. DOI: https://doi.org/10.11606/issn.2316-9095.v18-140834

ARAÚJO NETO, J. F.; SANTOS, L. C. M. L. O papel da Zona de Cisalhamento Portalegre no controle das mineralizações de esmeralda do sudoeste do Rio Grande do Norte: considerações preliminares. **XXVIII Simpósio de Geologia do Nordeste**, 505. Aracajú: SBG - Núcleo Nordeste, 2019.

ARAÚJO NETO, J. F.; SANTOS, L. C. M. L.; SANTOS, G. L. Geologia e aspectos genéticos de depósitos de esmeralda em zonas de cisalhamento: um olhar sobre os depósitos esmeraldíferos da Província Borborema, Nordeste do Brasil. **Geologia USP. Série Científica**, v. 21, n. 2, p. 19-39, 2021b. DOI: https://doi.org/10.11606/issn.2316-9095.v21-180467

ARCHANJO, C. J.; HOLLANDA, M. H. B. M.; RODRIGUES, S. W. O.; BRITO NEVES, B. B.; ARMSTRONG, R. Fabrics of pre- and syntectonic granite plutons and chronology of shear zones in the Eastern Borborema Province, NE Brazil. **Journal of Structural Geology**, v. 30, n. 3, p. 310-326, 2008. DOI: https://doi.org/10.1016/j.jsg.2007.11.011

AURISICCHIO, C.; CONTE, A. M.; MEDEGHINI, L.; OTTOLINI, L.; DE VITO, C. Major and trace element geochemistry of emerald from several deposits: Implications for genetic models and classification schemes. **Ore Geology Reviews**, v. 94, p. 351-366, 2018. DOI: https://doi.org/10.1016/j.oregeorev.2018.02.001

BARRETO, S. B. **Caracterização químico-mineralógica dos berilos de Tenente Ananias – RN**. Dissertação (Mestrado em Geociências). Instituto de Geociências, Universidade Federal de Pernambuco, Recife, 1991.

BARRETO, S. B.; BITTAR, S. M. B. The gemstone deposits of Brazil: occurrences, production and economic impact. **Boletín de la Sociedad Geológica Mexicana**, v. 62, n. 1, p. 123-140, 2010.

BARTON, M. D.; YOUNG, S. Non-pegmatitic deposits of beryllium: mineralogy, geology, phase equilibria and origin. In: Grew, E.S. (Ed.). Beryllium: Mineralogy, Petrology, and Geochemistry. **Reviews in Mineralogy and Geochemistry**, v. 50, n. 1, p. 591-691, 2002. DOI: https://doi.org/10.2138/rmg.2002.50.14

BAUMGARTNER, R.; ROMER, R. L.; MORITZ, R.; SALLET, R.; CHIARADIA, M. Columbite–tantalite-bearing granitic pegmatites from the Seridó Belt, northeastern Brazil: genetic constraints from U–Pb dating and Pb isotopes. **The Canadian Mineralogist**, v. 44, n. 1, p. 69-86, 2006. DOI: https://doi.org/10.2113/gscanmin.44.1.69

BEURLEN, H.; BARRETO, S. B.; MARTIN, R.; MELGAREJO, J.; DA SILVA, M. R. R.; SOUZA NETO, J. A. The Borborema Pegmatite Province, NE-Brazil revisited. **Estudos**

Geológicos, v. 19, n. 2, p. 62-66, 2009. DOI: http://dx.doi.org/10.18190/1980-8208/estudosgeologicos.v19n2p62-66

BEURLEN, H.; MOURA, O. J. M.; SOARES, D. R.; DA SILVA, M. R. R.; RHEDE, D. Geochemical and geological controls on the genesis of gem-quality "Paraíba Tourmaline" in granitic pegmatites from northeastern Brazil. **The Canadian Mineralogist**, v. 49, n. 1, p. 277-300, 2011. DOI: https://doi.org/10.3749/canmin.49.1.277

BLENKINSOP, T. G.; TRELOAR, P. J. Geometry, classification and kinematics of S-C and S-C′ fabrics in the Mushandike area, Zimbabwe. **Journal of Structural Geology**, v. 17, n. 3, p. 397-408, 1995. https://doi.org/10.1016/0191-8141(94)00063-6

BIONDI, J. C. Depósitos de esmeralda de Santa Terezinha (GO). **Revista Brasileira de Geociências**, v. 20, p. 7-24, 1990.

BRITO NEVES, B. B.; FUCK, R. A.; PIMENTEL, M. M. The Brasiliano collage in South America: a review. **Brazilian Journal of Geology**, v. 44, n. 3, p. 493-518, 2014. DOI: https://doi.org/10.5327/Z2317-4889201400030010

BRITO NEVES, B. B.; SANTOS, E. J.; FUCK, R. A.; SANTOS, L. C. M. L. A preserved early Ediacaran magmatic arc at the northernmost portion of the Transversal Zone central subprovince of the Borborema Province, Northeastern South America. **Brazilian Journal of Geology**, v. 46, n. 4, p. 491-508, 2016. https://doi.org/10.1590/2317-4889201620160004

BRITO NEVES, B. B.; SANTOS, E. J.; VAN SCHMUS, W. R. Q. Tectonic history of the Borborema Province. In: CORDANI, U. G.; MILANI E. J.; THOMAZ FILHO A.; CAMPOS D. A. (Org.). Tectonic Evolution of South America. Rio de Janeiro, **31st International Geological Congress Special Publication**, p. 151-182, 2000.

BÜHN, B. M.; PIMENTEL, M. M.; MATTEINI, M.; DANTAS, E. L. High spatial resolution analysis of Pb and U isotopes for geochronology by laser ablation multicollector inductively coupled plasma mass spectrometry (LA-MC-ICP-MS). **Anais da Academia Brasileira de Geociências**, Rio de Janeiro, v. 81, p. 1-16, 2009. DOI: https://doi.org/10.1590/S0001-37652009000100011

CALLIGARO, T.; DRAN, J. C.; POIROT, J. P.; QUERRÉ, G.; SALOMON, J.; ZWAAN, J. C. PIXE/PIGE characterisation of emeralds using an external micro-beam. **Nuclear Instruments and Methods in Physics Research Section B**, v. 161-163, p. 769-774, 2000. DOI: https://doi.org/10.1016/S0168-583X(99)00974-X

CAMPELO, R.C. **Análise de terrenos na porção setentrional da Província Borborema, NE do Brasil: integração de dados geológicos e gravimétricos**. Dissertação (Mestrado). Natal: Centro de Ciências Exatas e da Terra, Universidade Federal do Rio Grande do Norte, 1999.

CASSEDANNE, J. P.; CASSEDANNE, J. O.; MELLO, Z. F. As esmeraldas de Tauá e Pilão Arcado. **Mineração Metalúrgica**, v. 43, n. 410, p. 50-58, 1979.

CASTELO BRANCO, R. M. G.; GIULIANI, G.; CHEILLETZ, A.; CLEMENTEILE, L. Os berilos verdes da região de Coqui, município de Quixeramobim: novas ocorrências de esmeraldas no estado do Ceará. **XXXV Congresso Brasileiro de Geologia**. Belém: SBG, 1988.

CAVALCANTE, J. C.; VASCONCELOS, A. M.; GOMES, F. E. M.; MEDEIROS, M. F.; PAIVA, I. G. **Atlas digital de geologia e recursos minerais do Ceará**. Escala 1:500.000. Fortaleza: CPRM, 2003.

CAVALCANTI, J. A. D. (Ed.). **Geologia e recursos minerais da Folha Várzea do Boi SB.24-V-B-IV: estado do Ceará**. Fortaleza: CPRM, 2015.

CAVALCANTI NETO, M. T. O.; BARBOSA, R. V. N. As esmeraldas de Lajes, Caiçara do Rio dos Ventos e São Tomé/RN. **Holos**, v. 2, p. 92-104, 2007. DOI: https://doi.org/10.15628/holos.2007.103

CAWOOD, P. A.; HAWKESWORTH, C. J. Temporal relations between mineral deposits and global tectonic cycles. **Geological Society, London, Special Publications**, v. 393, n. 1, p. 9-21, 2015. DOI: https://doi.org/10.1144/SP393.1

CAXITO, F. A.; SANTOS, L. C. M. L.; GANADE, C. E.; BENDAOUD, A.; FETTOUS, E-H.; BOUYO, M. H. Toward an integrated model of geological evolution for NE Brazil-NW Africa: The Borborema Province and its connections to the Trans-Saharan (Benino-Nigerian and Tuareg shields) and Central African orogens. **Brazilian Journal of Geology**, v. 50, n. 2, e20190122, 2020. DOI: https://doi.org/10.1590/2317-4889202020190122

CLARK, R.N. Spectroscopy of rocks and minerals, and principles of spectroscopy. In: RENCZ, A.N. (ED.). **Manual of remote sensing**. Remote Sensing for the Earth Science, 3, New York, John Wiley and Sons, p. 3-58, 1999.

CORNEJO, C., BARTORELLI, A. **Minerais e pedras preciosas do Brasil**. São Paulo: Solaris Edições Culturais, 2010.

COUTO, P. A. A. **Mapa Gemológico do Estado da Bahia: Texto Explicativo.** Salvador: CPRM, 2000.

CPRM – SERVIÇO GEOLÓGICO DO BRASIL. **Projetos Aerogeofísicos: Paraíba - Rio Grande do Norte; Pernambuco - Paraíba. Relatório final do levantamento e processamento dos dados magnetométricos e gamaespectrométricos**. Relatório técnico. Lasa Engenharia e Prospecções, Prospectors Aerolevantamentos e Sistemas, 2010.

CRÓSTA, A. P.; SABINE, C.; TARANIK, J. V. Hydrothermal alteration mapping at Bodie, California, using AVIRIS hyperspectral data. **Remote Sensing of Environment**, v. 65, p. 309–319, 1998. DOI: https://doi.org/10.1016/S0034-4257(98)00040-6

D'EL-REY SILVA, L. J. H.; GIULIANI, G. Controle estrutural da jazida de esmeraldas de Santa Terezinha de Goiás: Implicações na gênese, na têctonica regional e no planajamento de lavra. **XXXV Congresso Brasileiro de Geologia**, v. 1, p. 413-427. Belém: SBG, 1988.

D'EL-REY SILVA, L. J. H.; BARROS NETO, L. S. The Santa Terezinha-Campos Verdes emerald district, central Brazil: structural and Sm-Nd data to constrain the tectonic evolution of the Neoproterozoic Brasília belt. **Journal of South American Earth Sciences**, v. 15, n. 6, p. 693-708, 2002. DOI: https://doi.org/10.1016/S0895-9811(02)00087-1

DA NÓBREGA, M. A.; SÁ, J. M.; BEZERRA, F. H. R.; HADLER NETO, J. C.; IUNES, P. J.; GUEDES, S.; TELLO SAENZ, C. A.; HACKSPACHER, P. C.; LIMA-FILHO, F. P. The use of apatite fission track thermochronology to constrain fault movements and sedimentary basin evolution in northeastern Brazil. **Radiation Measurements**, v. 39, p. 627-633, 2005. DOI: https://doi.org/10.1016/j.radmeas.2004.12.006

DA SILVA, M. R. R.; HÖLL, R; BEURLEN, H. Borborema Pegmatitic Province: geological and geochemical characteristics. **Journal of South American Earth Sciences**, v. 8, p. 355-364, 1995. DOI: https://doi.org/10.1016/0895-9811(95)00019-C

DANTAS, E.L.; SOUZA, Z.S.; WERNICK, E.; HACKSPACHER, P.C.; MARTIN, H.; XIAODONG, D.; LI, J.-W. Crustal growth in the 3.4–2.7 Ga São José de Campestre Massif, Borborema Province, NE Brazil. **Precambrian Research**, v. 227, p. 120-156, 2013. DOI: https://doi.org/10.1016/j.precamres.2012.08.006

DANTAS, E.L.; VAN SCHMUS, W.R.; HACKSPACHER, P.C.; FETTER, A.H.; BRITO NEVES, B.B.; CORDANI, U.; NUTMAN, A.P.; WILLIAMS, I.S. The 3.4-3.5 Ga São José do Campestre massif, NE Brazil: remnants of the oldest crust in South America. **Precambrian Research**, v. 130, n. 1-4, p. 113-137, 2004. DOI: https://doi.org/10.1016/j.precamres.2003.11.002

DELGADO, I. M.; SOUZA, J. D.; SILVA, L. C.; SILVEIRA FILHO, N. C.; DOS SANTOS, R. A.; PEDREIRA, A. J.; GUIMARÃES, J. T.; ANGELIM, L. A. A.; VASCONCELOS, A. M.; GOMES, I. P.; LACERDA FILHO, J. V.; VALENTE, C. R.; PEROTTA, M. M.; HEINECK, C. A. Geotectônica do Escudo Atlântico. In: BIZZI, L.A. (ed.) et al. Geologia, tectônica e recursos minerais do Brasil: texto, mapas & SIG. **Geology, tectonics and mineral resources of Brazil: text, maps & GIS**. Brasília: CPRM, p. 227-334, 2003.

DEMARTIS, M; PINOTTI, L. P.; CONIGLIO, J. E.; D'ERAMO, F. J.; TUBÍA, J. M.; ARAGÓN, E.; INSÚA, L. A. A. Ascent and emplacement of pegmatitic melts in a major reverse shear zone (Sierras de Córdoba, Argentina). **Journal of Structural Geology**, v. 33, n. 9, p. 1334-1346, 2011. DOI: https://doi.org/10.1016/j.jsg.2011.06.008

DEREPPE, J. M.; MOREAUX, C.; CHAUVAUX, B.; SCHWARZ, D. Classification of emeralds by artificial neural networks. **Journal of Gemmology**, v. 27, p. 93-105, 2000. DOI: https://doi.org/10.15506/JOG.2000.27.2.93

DYAR, M. D. Mossbauer spectra of biotite from metapelites. **American Mineralogist**, v. 75, p. 656-666, 1990.

EBERT, H. The Precambrian geology of the Borborema Belt (State of Paraíba and Rio Grande do Norte, northeastern Brazil) and the origin of its mineral provinces. **Geologische Rundschau**, v. 59, p. 1299-1326, 1970.

FALEIROS, F. M.; CAMPANHA, G. A. C.; MARIA, R.; FUZIKAWA, K. Quartz recrystallizations regimes, c-axis texture transition and fluid inclusion reequilibration in a prograde greenschist to amphibolite facies mylonite zone (Ribeira Shear Zone, SE Brazil). **Tectonophysics**, v. 485, p. 193-214, 2010. DOI: https://doi.org/10.1016/j.tecto.2009.12.014

FERREIRA, A. C. D.; DANTAS, E. L.; FUCK, R. A.; NEDEL, I. M. Arc accretion and crustal reworking from late Archean to Neoproterozoic in Northeast Brazil. **Scientific Reports**, v. 10, p. 7855, 2020. DOI: https://doi.org/10.1038/s41598-020-64688-9

FERSMANN, A. Geochemische Migration der Elemente. **Abhandlungen zur praktishen Geologie und Bergwirtschaftslenhre**, v. 18, p. 74-118, 1929.

FETTER, A. H.; VAN SCHMUS, W. R.; SANTOS, T. J. S.; NOGUEIRA NETO, J. A.; ARTHAUD, M. H. U-Pb and Sm-Nd geochronological constraints on the crustal evolution and basement architecture of Ceará State, NW Borborema Province, NE Brazil: implications for the existence of the Paleoproterozoic supercontinent "Atlantica". **Revista Brasileira de Geociências**, v. 30, p. 102-106, 2000.

FITZ GERALD, J. D.; STÜNITZ, H. Deformation of granitoids at low metamorphic grade. I: Reactions and grain size reduction. **Tectonophysics**, v. 221, n. 3-4, p. 269-297, 1993. DOI: https://doi.org/10.1016/0040-1951(93)90163-E

FUCK, R. A.; DANTAS, E. L.; DE SORDI, D. A.; CHIARINI, M. F. N.; OLIVEIRA, C. G. **Santa Terezinha de Goiás - SD.22-Z-A-III**. Escala 1:100.000: nota explicativa. Goiás: UnB/CPRM, 2007.

GANADE DE ARAÚJO, C.; RUBATTO, D.; HERMANN, J.; CORDANI, U. G.; CABY, R.; BASEI, M. A. S. Ediacaran 2,500-km-long synchronous deep continental subduction in the West Gondwana Orogen. **Nature Communications**, v. 5, 5198, 2014. DOI: https://doi.org/10.1038/ncomms6198

GIULIANI, G.; CHEILLETZ, A.; ARBOLEDA, C.; CARRILLO, V.; RUEDA, F.; BAKER, J. H. An evaporitic origin of the parent brines of Colombian emeralds: fluid inclusion and sulphur isotope evidence. **European Journal of Mineralogy**, v. 7, p. 151-165, 1995.

GIULIANI, G.; FRANCE-LANORD, C.; ZIMMERMANN, J. L.; CHEILLETZ, A.; ARBOLEDA, C.; CHAROY, B.; COGET, P.; FONTAN, F.; GIARD, D. Fluid composition, δD of channel H_2O, and $\delta^{18}O$ of lattice oxygen in beryls: genetic implications for Brazilian, Colombian, and Afghanistani emerald deposits. **International Geology Reviews**, v. 39, p. 400-424, 1997. DOI: https://doi.org/10.1080/00206819709465280

GIULIANI, G.; GROAT, L. A.; MARSHALL, D.; FALLICK, A. E.; BRANQUET, Y. Emerald Deposits: A Review and Enhanced Classification. **Minerals**, v. 9, n. 2, p. 105, 2019. DOI: https://doi.org/10.3390/min9020105

GIULIANI, G.; SILVA, L. J. H. D.; COUTO, P. Origin of emerald deposits of Brazil. **Mineralium Deposita**, v. 25, p. 57-64, 1990. DOI: https://doi.org/10.1007/BF03326384

GRIFFON, J. C.; KREMER, M. R.; MISI, A. Estudo estrutural e genético da Jazida de Esmeralda de Carnaíba-BA. **Anais da Academia Brasileira de Ciências**, v. 39, p. 150-161, 1967.

GROAT, L. A.; GIULIANI, G.; MARSHALL, D. D.; TURNER, D. Emerald deposits and occurrences: A review. **Ore Geology Reviews**, v. 34, p. 87-112, 2008. DOI: https://doi.org/10.1016/j.oregeorev.2007.09.003

GROAT, L.; GIULIANI, G.; MARSHALL, D.; TURNER, D. Emerald. In: RAESIDE, E. R. (Ed.). Geology of Gem Deposits, **Mineralogical Association of Canada, Short Course Series**, v. 44, p. 135-174, 2014.

GRUNDMANN, G.; MORTEANI, G. Emerald mineralisation during regional metamorphism: the Habachtal (Austria) and Leydsdorp (Transvaal, South Africa) deposits. **Economic Geology**, v. 84, p. 1835-1849, 1989. DOI: https://doi.org/10.2113/gsecongeo.84.7.1835

HACKSPACHER, P. C.; LEGRAND, J. M. Microstructural and metamorphic evolution of the Portalegre shear zone, northeastern Brazil. **Revista Brasileira de Geociências**, v. 19, p. 63-75, 1989.

HACKSPACHER P. C.; VAN SCHMUS W. R.; DANTAS E. L. Um embasamento Transamazônico na Provincia Borborema. **36° Congresso Brasileiro de Geologia**, Natal, Anais, v. 6, p. 2683-2696, 1990.

HALDAR, S. K. Chapter 3 - Exploration Geology. In: **Mineral Exploration Principles and Applications**, p. 41-53, 2013. DOI: https://doi.org/10.1016/B978-0-12-416005-7.00003-9

HECKER, C.; VAN RUITENBEEK, F. J. A; VAN DER WERFF, H. M. A; BAKKER, W. H.; HEWSON, R. D.; VAN DER MEER, F. D. Spectral absorption feature analysis for finding ore. A tutorial on using the method in geological remote sensing. **IEEE Geoscience and Remote Sensing Magazine**, v. 7, p. 51-71, 2019. DOI: 10.1109/MGRS.2019.2899193

HECKER, C.; VAN DER MEIJDE, M.; VAN DER MEER, F. D. Thermal infrared spectroscopy on feldspars — Successes, limitations and their implications for remote sensing, **Earth-Science Reviews**, v. 103, p. 60-70, 2010. DOI: https://doi.org/10.1016/j.earscirev.2010.07.005

HOLLANDA, M. H. B. M.; ARCHANJO, C. J.; SOUZA, L. C.; DUNYI, L.; ARMSTRONG, R. Long-lived Paleoproterozoic granitic magmatism in the Seridó-Jaguaribe domain, Borborema Province–NE Brazil. **Journal of South American Earth Sciences**, v. 32, n. 4, p. 287-300, 2011. DOI: https://doi.org/10.1016/j.jsames.2011.02.008

HOLLANDA, M. H. B. M.; SOUZA NETO, J. A.; ARCHANJO, C. J.; STEIN, H.; MAIA, A. C. S. AGE OF the granitic magmatism and the W-Mo mineralization in skarns of the Seridó belt (NE Brazil) based on zircon U-Pb (SHRIMP) and molybdenite Re-Os dating. **Journal of South American Earth Sciences**, v. 79, p. 1-11, 2017. DOI: https://doi.org/10.1016/j.jsames.2017.07.011

HRONSKY, J. M. A.; GROVES, D. I. Science of targeting: definition, strategies, targeting and performance measurement. **Australian Journal of Earth Sciences**, v. 55, n. 1, p. 3-12, 2008. DOI: http://dx.doi.org/10.1080/08120090701581356

HUNT, G. R. Spectral Signatures of Particulate Minerals in the Visible and near Infrared. **Geophysics**, v. 42, p. 501-513, 1977. DOI: https://doi.org/10.1190/1.1440721

HYPPY. **Hyperspectral Python**. Disponível em: <http://hyppy.byethost18.com/index.html>. Acesso em: 02 de outubro de 2022.

JACKSON, S. E.; PEARSON, N. J.; GRIFFIN, W. L.; BELOUSOVA, E. A. The application of laser ablation-inductively coupled plasma-mass spectrometry to in situ U–Pb zircon geochronology. **Chemical Geology**, v. 211, n. 1-2, p. 47-69, 2004. DOI: https://doi.org/10.1016/j.chemgeo.2004.06.017

JARDIM DE SÁ, E. F.; FUCK, R. A.; MACEDO, M. H. F.; PEUCAT, J. J.; KAWASHITA, K.; SOUZA, Z. S.; BERTRAND, J. M. Pre-brasiliano orogenic evolution in the Seridó belt, NE Brazil: Conflicting geochronological and structural data. **Revista Brasileira de Geociências**, v. 25, n. 4, p. 307-314, 1995.

JARDIM DE SÁ, E. F.; MEDEIROS, W. E.; CASTRO, D. L. Contribuição da gravimetria aos modelos de estruturação crustal da Província Borborema, Nordeste do Brasil. **Atas XVII Simpósio de Geologia do Nordeste**, p. 352-357, Fortaleza, CE, 1997.

KITT, S.; KISTERS, A.; STEVEN, N.; MAIDEN, K.; HARTMANN, K. Shear-zone hosted copper mineralisation of the Omitiomire deposit — Structural controls of fluid flow and mineralisation during subduction accretion in the Pan-African Damara Belt of Namibia. **Ore Geology Reviews**, v. 75, p. 1-15, 2016. DOI: https://doi.org/10.1016/j.oregeorev.2015.10.035

KAZMI, A. H.; SNEE, L. W. Geology of the world emerald deposits: a brief review. In: KAZMI, A. H.; SNEE, L. W. (Eds.) **Emeralds of Pakistan – Geology, Gemology and Genesis, Geological Survey of Pakistan**. p. 13-38. New York: Elite Publishers Limited, Karachi, Pakistan and Van Nostrand Reinhold Company, 1989.

KOPPERS, A. A. ArArCALC—Software for $^{40}Ar/^{39}Ar$ age calculations. **Computers & Geosciences**, v. 28, n. 5, p. 605-619, 2002. DOI: https://doi.org/10.1016/S0098-3004(01)00095-4

KOPPERS, A. A. P.; STAUDIGEL, H.; DUNCAN, R. A. High-resolution $^{40}Ar/^{39}Ar$ dating of the oldest oceanic basement basalts in the western Pacific basin. **Geochemistry Geophysics Geosystems**, v. 4, n. 11, p. 1-20, 2003. DOI: https://doi.org/10.1029/2003GC000574

KORPERSHOEK, H. R. **Report on the Boa Esperança emerald showing, Tauá, State of Ceará, Northeast Brazil.** Relatório Interno. Mineração São Pedro Ltda./MBL - Mineração Brasileira Ltda, 1983.

KRUSE, F. A. Identification and mapping of minerals in drill core using hyperspectral image analysis of infrared reflectance spectra. **International Journal of Remote Sensing**, v. 17, n. 9, p. 1623-1632, 1996. DOI: https://doi.org/10.1080/01431169608948728

KRUSE, F. A.; LEFKOFF, A. B.; BOARDMAN, J. B.; HEIDEBRECHT, K. B.; SHAPIRO, A. T.; BARLOON, P. J.; GOETZ, A. F. H. The Spectral Image Processing System (SIPS) - Interactive Visualization and Analysis of Imaging spectrometer Data. **Remote Sensing of the Environment**, v. 44, n. 2-3, p. 145-163, 1993. DOI: https://doi.org/10.1016/0034-4257(93)90013-N

KUIPER, K.; DEINO, A.; HILGEN, F. J.; KRIJGSMAN, W.; RENNE, P. R.; WIJBRANS, J. R. Synchronizing rock clocks of Earth history. **Science**, v. 320, n. 5875, p. 500-504, 2008. DOI: https://doi.org/10.1126/science.1154339

LAUKAMP, C.; CUDAHY, T.; CLEVERLEY, J. S.; OLIVER, N. H. S.; HEWSON, R. Airborne hyperspectral imaging of hydrothermal alteration zones in granitoids of the Eastern Fold Belt, Mount Isa Inlier, Australia. **Geochemistry: Exploration, Environment, Analysis**, v. 11, p. 3-24, 2011. DOI: https://doi.org/10.1144/1467-7873/09-231

LIMA, H. M.; PIMENTEL, M. M.; FUCK, R. A.; SANTOS, L. C. M. L.; DANTAS, E. L. Geochemical and detrital zircon geochronological investigation of the metavolcanosedimentary Araticum complex, sergipano fold belt: Implications for the evolution of the Borborema Province, NE Brazil. **Journal of South American Earth Sciences**, v. 86, p. 176-192, 2018. DOI: https://doi.org/10.1016/j.jsames.2018.06.013

LIRA SANTOS, G.; SOUZA, I. M. B. A.; BARRETO, S. B.; ARAÚJO NETO, J. F.; MÜLLER, A. The Serra Branca amazonite pegmatite of the Vieirópolis pegmatite field, Paraíba, Brazil: a new and unusual megacrystic amazonite deposit. **The Canadian Mineralogist**, canmin.1900095, 2020. DOI: https://doi.org/10.3749/canmin.1900095

LUDWIG, K. R. User's manual for Isoplot 3.75. **Berkeley Geochronological Center Special Publication No. 5.**, 2012.

LYPACZEWSKI, P.; RIVARD, B.; GAILLARD, N.; PERROUTY, S.; PIETTE-LAUZIÈRE, N.; BÉRUBÉ, C. L.; LINNEN, R. L. Using hyperspectral imaging to vector towards mineralization at the Canadian Malartic gold deposit, Québec, Canada. **Ore Geology Reviews**, v. 111, 102945, 2019. DOI: https://doi.org/10.1016/j.oregeorev.2019.102945

MALVERN PANALYTICAL. **ASD FieldSpec 4 Standard-Res Spectroradiometer. Malvern Panalytical.** Disponível em: <https://www.asdi.com/productsand-services/fieldspec-spectroradiometers/fieldspec-4-standard-res/>. Acesso em: 02 de outubro de 2022.

MATHER, P. M. Image transforms. In: MATHER, P. M. (ED.), **Computer processing of remotely-sensed images. An introduction.** John Wiley & Sons Ltd., Chichester, pp. 136-79, 2004.

MATTEINNI, M.; JUNGES, S. L.; DANTAS, E. L.; PIMENTEL, M. M.; BÜHN, B. M. In situ zircon U-Pb and Lu-Hf isotope systematic on magmatic rocks: Insights on the crustal evolution of the Neoproterozoic Goiás Magmatic Arc, Brasília belt, Central Brazil. **Gondwana Research**, v. 17, n. 1, p. 1-12, 2010. DOI: https://doi.org/10.1016/j.gr.2009.05.008

MEDINA, C. M.; DUCART, D. F.; PASSOS, J. S.; OLIVEIRA, L. R. Exploration vectoring from the white mica spectral footprint in the atypical auriferous Lavra Velha deposit, San Francisco Craton, Brazil. **Ore Geology Reviews**, v. 139, 104438, 2021. DOI: https://doi.org/10.1016/j.oregeorev.2021.104438

MEDEIROS, V. C. (ED.). **Geologia e Recursos Minerais da Folha Sousa SB.24-Z-A.** Escala 1:250.000. Recife: CPRM – Serviço Geológico do Brasil, 2008.

MEDEIROS, V. C.; NASCIMENTO, M. A. L.; GALINDO, A. C.; DANTAS, E. L. Augen gnaisses riacianos no Domínio Rio Piranhas-Seridó - Província Borborema, Nordeste do Brasil. **Geologia USP. Série Científica**, v. 12, n. 2, p. 3-14, 2012. DOI: https://doi.org/10.5327/Z1519-874X2012000200001

MEERT, J. G.; LIEBERMAN, B. S. The Neoproterozoic assembly of Gondwana and its relationship to the Ediacaran–Cambrian radiation. **Gondwana Research**, v. 14, n. 1-2, p. 5-21, 2008. DOI: https://doi.org/10.1016/j.gr.2007.06.007

MESQUITA, N. M.; CARRINO, T. A.; SOUZA NETO, J. A. The use of reflectance spectroscopy and the prehnite spectral index to target gold mineralization at the Bonfim polymetallic skarn deposit, Seridó Mobile Belt, Borborema Province, Brazil. **Ore Geology Reviews**, v. 115, 103192, 2019. DOI: https://doi.org/10.1016/j.oregeorev.2019.103192

MIN, K.; MUNDIL, R.; RENNE, P. R.; LUDWIG, K. R. A test for systematic errors in 40Ar/39Ar geochronology through comparison with U/Pb analysis of a 1.1-Ga rhyolite. **Geochimica et Cosmochimica Acta**, v. 64, n. 1, p. 73-98, 2000. DOI: https://doi.org/10.1016/S0016-7037(99)00204-5

MORAES, J. F. S. **Gemas do Estado do Rio Grande do Norte. Recife**. Relatório Técnico. CPRM – Serviço Geológico do Brasil, 1999.

MORAES, J. F. S. As ocorrências de esmeraldas do Estado do Rio Grande do Norte: uma nova tipologia de depósito. **XVIII Simpósio de Geologia do Nordeste**. Recife: SBG: Núcleo Nordeste, 2000.

MOURA, W. A. L.; CARRINO, T. A.; PABÓN, R. E. C.; LIMA FILHO, M.; SOUZA NETO, J. A. Applying spectral tools in a mixed siliciclastic-carbonate environment: An integrative sedimentological case study from the Estiva Formation, Pernambuco Basin, Northeast Brazil. **Journal of South American Earth Sciences**, v. 116, 103831, 2022. DOI: https://doi.org/10.1016/j.jsames.2022.103831

NALETO, J. L. C.; PERROTTA, M. M.; COSTA, F. G.; SOUZA FILHO, C. R. Point and imaging spectroscopy investigations on the Pedra Branca orogenic gold deposit, Troia Massif, Northeast Brazil: Implications for mineral exploration in amphibolite metamorphic-grade terrains. **Ore Geology Reviews**, v. 107, p. 283-309, 2019. DOI: https://doi.org/10.1016/j.oregeorev.2019.02.019

NASCIMENTO, M. A. L.; GALINDO, A. C.; MEDEIROS, V. C. Ediacaran to Cambrian magmatic suites in the Rio Grande do Norte domain, extreme Northeastern Borborema Province (NE of Brazil): Current knowledge. **Journal of South American Earth Sciences**, v. 58, p. 281-299, 2015. DOI: https://doi.org/10.1016/j.jsames.2014.09.008

OLIVEIRA, R. G., MEDEIROS, W. E. Deep crustal framework of the Borborema Province, NE Brazil, derived from gravity and magnetic data. **Precambrian Research**, v. 315, p. 45-65, 2018. DOI: https://doi.org/10.1016/j.precamres.2018.07.004

ORANGE VISUAL PROGRAMMING. **PCA**. Disponível em: <https://orange3.readthedocs.io/projects/orange-visual-

programming/en/latest/widgets/unsupervised/PCA.html>. Acesso em: 15 de novembro de 2022.

OTTAWAY, T. L.; WICKS, F. J.; BRYNDZIA, L. T.; KEYSER, T. K.; SPOONER, E. T. C. Formation of the Muzo hydrothermal emerald deposit in Colombia. **Nature**, v. 369, p. 552-554, 1994. DOI: https://doi.org/10.1038/369552a0

PEARSON, K. On lines and planes of closest fit to systems of points in space. **Philosophical Magazine Series**, v. 2, n. 11, p. 559-572, 1901. DOI: https://doi.org/10.1080/14786440109462720

PEREIRA, L. C. L.; SANTOS, L. C. M. L.; CARRINO, T. A. The role of airborne geophysics in the investigation of gold occurrences in the Itapetim Region, Borborema Province, Northeast Brazil. **Brazilian Journal of Geology**, v. 49, n. 3, e20190028, 2019. DOI: https://doi.org/10.1590/2317-4889201920190028.

PONTUAL, S.; MERRY, N.; GAMSON, P. **Spectral Interpretation - Field Manual. GMEX. Spectral Analysis Guides for Mineral Exploration: Victoria**. AusSpec International Pty. Ltd., 189 pp., 2008.

PRADO, E. M. G.; SILVA, A. M.; DUCART, D. F.; TOLEDO, C. L. B.; ASSIS, L. M. Reflectance spectroradiometry applied to a semi-quantitative analysis of the mineralogy of the N4ws deposit, Carajás Mineral Province, Pará, Brazil. **Ore Geology Reviews**, v. 78, p. 101-119, 2016. DOI: https://doi.org/10.1016/j.oregeorev.2016.03.007

RAMAKRISHNAN, D.; NITHYA, M.; SINGH, K. D.; BHARTI, R. A field technique for rapid lithological discrimination and ore mineral identification: results from Mamandur polymetal deposit, India. **Journal of Earth System Science**, v. 122, p. 93-106, 2013. DOI: https://doi.org/10.1007/s12040-012-0255-x

REID, A. B.; ALLSON, J. M.; GRANSER, H.; MIETT, A. J.; SOMERTON, I. W. Magnetic interpretation in three dimensions using Euler deconvolution. **Geophysics**, v. 55, p. 80-91, 1990. DOI: https://doi.org/10.1190/1.1442774

RIBEIRO-ALTHOFF, A. M.; CHEILLETZ, A.; GIULIANI, G.; FÉRAUD, G.; BARBOSA CAMACHO, G.; ZIMMERMANN, J. L. $^{40}Ar/^{39}Ar$ and K-Ar Geochronological Evidence for Two Periods (~2 Ga and 650 to 500 Ma) of Emerald Formation in Brazil. **International Geology Review**, v. 39, n. 10, p. 924-937, 1997. DOI: https://doi.org/10.1080/00206819709465310

RONDEAU, B.; NOTARI, F.; GIULIANI, G.; MICHELOU, J.-C.; MARTINS, S.; FRITSCH, E.; RESPINGER, A. La mine de Piteiras, Minas Gerais, nouvelle source d'émeraude de belle qualité au Brésil**. Revue de Gemmologie**, v. 148, p. 9-25, 2003.

RONDEAU, B.; FRITSCH, E.; PEUCAT, J.; NORDRUM, F. S.; GROAT, L. A. Characterization of Emeralds from a historical deposit: Byrud (Eidsvoll), Norway. **Gems and Gemology**, v. 44, n. 2, p. 108-122, 2008. DOI: 10.5741/GEMS.44.2.108

RUDOWSKI, L. **Pétrologie et géochimie des granites transamazoniens de Campo Formoso et Carnaíba (Bahia, Brésil) et des phlogopitites à émeraude associées**. Tese (Doutorado). Université Paris, Paris, 1989.

SANTANA, A. J.; MOREIRA, M. D.; COUTO, P. A. A. **Esmeralda de Carnaíba e Socotó, Bahia: geologia e potencialidade econômica**. Salvador: CBPM, 1995.

SANTIAGO, J.S.; SOUZA, V. S.; DANTAS, E. L.; OLIVEIRA, C. G. Ediacaran emerald mineralization in Northeastern Brazil: the case of the Fazenda Bonfim Deposit. **Brazilian Journal of Geology**, v. 49, n. 4, p. 1-14, 2019. DOI: https://doi.org/10.1590/2317-4889201920190081

SANTOS, E. J., MEDEIROS, V. C. Constraints from granitic plutonism on proterozoic crustal growth of the Transverse Zone, Borborema Province, NE-Brazil. **Revista Brasileira de Geociências**, v. 29, p. 73-84, 1999.

SANTOS, E. J., SOUZA NETO, J. A., SILVA, M. R. R., BEURLEN, H., CAVALCANTI, J. A. D., SILVA, M. G., DIAS, V. M., COSTA, A. F., SANTOS, L. C. M. L., SANTOS, R. B. Metalogênese das porções norte e central da Província Borborema. In: SILVA, M. G., ROCHA NETO, M. B., JOST, H., KUYUMIJAN, R. M. **Metalogênese das províncias tectônicas brasileiras**. p. 343-388, 2014. Belo Horizonte: CPRM.

SANTOS, E. J.; VAN SCHMUS, W. R.; KOZUCH, M.; BRITO NEVES, B. B. The Cariris Velhos tectonic event in northeast Brazil. **Journal of South American Earth Sciences**, v. 29, n. 1, p. 61-76, 2010. DOI: https://doi.org/10.1016/j.jsames.2009.07.003

SANTOS, G. L.; SOUZA, I.M.B.A.; BARRETO, S.B.; ARAÚJO NETO, J.F.; MÜLLER, A. The Serra Branca amazonite pegmatite of the Vieirópolis pegmatite field, Paraíba, Brazil: A new and unusual megacrystic amazonite deposit. **The Canadian Mineralogist**, v. 58, n. 6, p. 679-702, 2020. DOI: https://doi.org/10.3749/canmin.1900095

SANTOS, L. C. M. L., CAXITO, F. A., BOUYO, M. H., OUADAHI, S., ARAÏBIA, K., LAGES, G. A., SANTOS, G. L., PITOMBEIRA, J. P. A., CAWOOD, P. A. Relics of ophiolite-bearing accretionary wedges in NE Brazil and NW Africa: connecting threads of western Gondwana´s ocean during Neoproterozoic times. **Geosystems and Geoenvironment**, p. 100148, 2023. DOI: https://doi.org/10.1016/j.geogeo.2022.100148

SANTOS, L. C. M. L.; DANTAS, E. L.; CAWOOD, P. A.; LAGES, G. A.; LIMA, H. M.; SANTOS, E. J. Accretion tectonics in western Gondwana deduced from Sm-Nd isotope mapping of terranes in the Borborema Province, NE Brazil. **Tectonics**, v. 37, p. 2727-2743, 2018. DOI: https://doi.org/10.1029/2018TC005130

SANTOS, L. C. M. L., DANTAS, E. L., CAWOOD., P. A., LAGES, G. A., LIMA., H. M., SANTOS, E. J., CAXITO, F. A. Early to late Neoproterozoic subduction-accretion episodes in the Cariris Velhos Belt of the Borborema Province, Brazil: Insights from isotope and whole-rock geochemical data of supracrustal and granitic rocks. **Journal of South American Earth Sciences**, v. 96, p. 102384, 2019. DOI: https://doi.org/10.1016/j.jsames.2019.102384

SANTOS, L. C. M. L.; DANTAS, E. L.; VIDOTTI, R. M.; CAWOOD, P. A.; SANTOS, E. J.; FUCK, R. A.; LIMA, H. M. Two-stage terrane assembly in Western Gondwana: Insights from

structural geology and geophysical data of central Borborema Province, NE Brazil**. Journal of Structural Geology**, v. 103, p. 167-184, 2017. DOI: https://doi.org/10.1016/j.jsg.2017.09.012

SANTOS, L. C. M. L.; LAGES, G. A.; LIMA, H. M.; ARAÚJO NETO, J. F.; SANTOS, G. L.; PAIXÃO, M. S. An overview on the Rhyacian–Orosirian (ca. 2.1–2.0 Ga) granitic magmatism of the Alto Moxotó Terrane and its implications for the crustal evolution of the Borborema Province, NE Brazil. **Journal of Iberian Geology**, v. 48, p. 225-239, 2022. DOI: https://doi.org/10.1007/s41513-022-00191-6

SANTOS, L. C. M. L., OLIVEIRA, R. G., LAGES, G. A., DANTAS, E. L., CAXITO, F., CAWOOD, P. A., FUCK, R. A., LIMA, H. M., SANTOS, G. L., ARAÚJO NETO, J. F. Evidence for Neoproterozoic terrane accretion in the central Borborema Province, West Gondwana deduced by isotopic and geophysical data compilation. **International Geology Review**, v. 64, n. 11, p. 1574-1593, 2021. DOI: https://doi.org/10.1080/00206814.2021.1944332

SANTOS, T. J. S., FETTER, A. H., NETO, J. A. N. Comparisons between the Northwestern Borborema Province, NE Brazil, and the Southwestern Pharusian Dahomey Belt, SW Central Africa. **Geological Society, London, Special Publication**, v. 294, p. 101-119, 2008.

SATIR, M. Rb-Sr-Altersbestimmungen and Glimmern der westlichen Hohen Tauern: interpretation und geologische Bedeutung. **Schweizerische Mineralogische und Petrographische Mitteilungen**, v. 54, p. 214-228, 1974.

SCHAFER, R. W. What is a Savitzky-Golay filter? **IEEE Signal Processing Magazine**, v. 28, n. 4, p. 111-117, 2011. DOI: 10.1109/MSP.2011.941097

SCHOLZ, R., ROMANO, A. W., BELOTTI, F. M., CHAVES, M. L. S. C. Prospecção geoquímica de berilo variedade esmeralda na região da Fazenda Bonfim (Lajes, RN). **Geociências**, v. 29, n. 4, p. 613-621, 2010.

SCHULZ, B.; SIEGESMUND, S.; STEENKEN, A.; SCHOENHOFER, R.; HEINRICHS, T. Geologie des ostalpinen Kristallins südlich des Tauernfensters zwischen Virgental und Pustertal. **Zeitschrift der Deutschen Geologischen Gesellschaft**, v. 152, p. 261-307, 2001. DOI: https://doi.org/10.1127/zdgg/152/2001/261

SCHWARZ, D. **Esmeraldas: inclusões em gemas**. Ouro Preto: Universidade Federal de Ouro Preto (UFOP), Imprensa Universitária, 1987.

SCHWARZ, D., GIULIANI, G. Emerald deposits a review. **Australian Gemmologist**, v. 21, p. 17-23, 2001.

SCHWARZ, D., GIULIANI, G., GRUNDMANN, G., GLAS, M. Die Entstehung der Smaragde, ein vieldisskutiertes Thema. In: SCHWARZ, D., HOCHLITNER, R. (Eds.) Smaragd, der kostbarste Beryll, der teuerste Edelstein. **Extra Lapis**, v. 21, p. 68-73, 2001.

SCHWARZ, D.; GIULIANI, G.; GRUNDMANN, G.; GLAS, M. The origin of emerald - A controversial topic**. Extra Lapis English**, v. 2, p. 18-21, 2002.

SCOTT, K. M.; YANG, K. **Spectral reflectance studies of white micas.** Commonwealth Scientific and Industrial Research Organisation, Exploration and Mining Report 439R, p. 35, 1997.

SEIFERT, A. V.; ŽÁČEK, V.; VRÁNA, S.; PECINA, V.; ZACHARIÁŠ, J.; ZWAAN, J. C. Emerald Mineralization in the Kafubu area, Zambia. **Bulletin of Geosciences**, v. 79, p. 1-40, 2004.

SIAL, A. N.; FERREIRA, V. P. Magma associations in Ediacaran granitoids of the Cachoeirinha–Salgueiro and Alto Pajeú terranes, northeastern Brazil: Forty years of studies. **Journal of South American Earth Sciences**, v. 68, p. 113-133, 2016. DOI: https://doi.org/10.1016/j.jsames.2015.10.005

SILVA, L. A.; CARRINO, T. A.; SANTOS, L. C. M. L.; PABÓN, R. E. C. Spectral characterization of the Umbuzeiro Doce skarn target (Brazil): insights for the exploration of a W-Mo-gemological vesuvianite system. **Brazilian Journal of Geology**, v. 52, n. 4, e20220035, 2022. DOI: https://doi.org/10.1590/2317-4889202220220035

SIMANDL, G. J.; PARADIS, S.; BIRKETT, T. Schist-hosted Emeralds. In: G.J. SIMANDL, Z.D. HORA AND D.V. LEFEBURE (EDS.) **Selected British Columbia Mineral Deposit Profiles**, Volume 3, Industrial Minerals, British Columbia Ministry of Energy and Mines, Open File 1999-10, 1999.

SINKANKAS, J. **Emerald and other beryls**. Prescott: Geoscience Press. 665p, 1989.

SOUZA, L. C. (ED.). **Geologia e Recursos Minerais da Folha Pau dos Ferros SB.24-Z-A-II**. Escala 1:100.000. Recife: CPRM - Serviço Geológico do Brasil / Universidade Federal do Rio Grande do Norte, 2017.

SOUZA NETO, J. A.; LEGRAND, J. M.; VOLFINGER, M.; PASCAL, M.-L.; SONNET, P. W–Au skarns in the Neo-Proterozoic Seridó Belt, Borborema Province in northeastern Brazil: an overview with emphasis on the Bonfim deposit. **Mineralium Deposita**, v. 43, p. 185-205, 2008. DOI: https://doi.org/10.1007/s00126-007-0155-1

STEIGER, R. H.; JÄGER, E. Subcommission on geochronology: Convention on the use of decay constant in geo- and cosmochronology, **Earth and Planetary Science Letters**, v. 36, n. 3, p. 359–362, 1977. DOI: https://doi.org/10.1016/0012-821X(77)90060-7

STIPP, M.; STÜNITZ, H.; HEILBRONNER, R.; SCHMID, S. M. The eastern Tonale fault zone: a “natural laboratory” for crystal plastic deformation of quartz over a temperature range from 250 to 700°C. **Journal of Structural Geology**, v. 24, p. 1861–1884, 2002. DOI: https://doi.org/10.1016/s0191-8141(02)00035-4

SWAYZE, G. A. et al. Mapping advanced argillic alteration at Cuprite, Nevada, using imaging spectroscopy. **Economic Geology**, v. 109, p. 1179-1221, 2014. DOI: https://doi.org/10.2113/econgeo.109.5.1179

TALUKDAR, M.; CHATTOPADHYAY, N.; SANYAL, S. Shear controlled Fe-mineralization from parts of South Purulia Shear Zone. **Journal of Applied Geochemistry**, v. 14, n. 4, p. 496-508, 2012.

TAPPERT, M.; RIVARD, B.; GILES, D.; TAPPERT, R.; MAUGER, A. Automated drill core logging using visible and near-infrared reflectance spectroscopy: a case study from the Olympic Dam IOCG deposit, South Australia. **Economic Geology**, v. 106, n. 2, p. 289-296, 2011. DOI: https://doi.org/10.2113/econgeo.106.2.289

TAYLOR, J. R. **An Introduction to Error Analysis: The Study of Uncertainties in Physical Measurements**, 327 pp., University Science Books, Mill Valley, California, 1997.

THOMPSON, A. J. B.; HAUFF, P. L.; ROBITAILLE, A. J. Alteration mapping in exploration: application of short-wave infrared (SWIR) spectroscopy. **Society of Economic Geologist Newsletter**, v. 39, p. 15-17, 1999.

THOMPSON, A.; SCOTT, K.; HUNTINGTON, J.; YANG, K. Mapping Mineralogy with Reflectance Spectroscopy: Examples from Volcanogenic Massive Sulfide Deposits. In: BEDELL, R.; CRÓSTA, A.P., GRUNSKY, E. (EDS.). **Remote Sensing and Spectral Geology. Reviews in Economic Geology**, 2009.

TULLIS, J. Deformation of granitic rocks: experimental studies and natural examples. In: KARATO, S-I.; WENK, H-R. (EDS.) Plastic deformation of minerals and rocks. **Reviews in Mineralogy and Geochemistry**, v. 51, n. 1, p. 51–95, 2002. DOI: https://doi.org/10.2138/gsrmg.51.1.51

TURNER, D.; GROAT, L. A.; RIVARD, B.; BELLEY, P. M. Reflectance Spectroscopy and Hyperspectral Imaging of Sapphire-bearing Marble from the Beluga Occurrence, Baffin Island, Nunavut. **The Canadian Mineralogist**, v. 55, n. 4, p. 787-797, 2017. DOI: https://doi.org/10.3749/canmin.1700023

VAN SCHMUS, W. R.; BRITO NEVES, B. B.; HACKSPACHER, P. C.; BABINSKI, M. U-Pb and Sm-Nd geochronological studies of the Eastern Borborema Province, Northeastern Brazil, initial conclusions. **Journal of South American Earth Sciences**, v. 8, n. 3-4, p. 267-288, 1995. DOI: https://doi.org/10.1016/0895-9811(95)00013-6

VAN SCHMUS, W. R., KOZUCH, M., BRITO NEVES, B. B. Precambrian history of the Zona Transversal of the Borborema Province, NE Brazil: Insights from Sm-Nd and U-Pb geochronology. **Journal of South American Earth Sciences**, v. 31, n. 2-3, p. 227-252, 2011. DOI: https://doi.org/10.1016/j.jsames.2011.02.010

VAN SCHMUS, W. R., OLIVEIRA, E. P., SILVA FILHO, A. F., TOTEU, F., PENAYE, J., GUIMARÃES, I. P. Proterozoic Links between the Borborema Province, NE Brazil, and the Central African Fold Belt. **Geological Society, London, Special Publications**, v. 294, n. 1, p. 69-99, 2008. DOI: https://doi.org/10.1144/SP294.5

VAPNIK, Y.; MOROZ, I.; ELIEZRI, I. Formation of emeralds at pegmatite-ultramafic contacts based on fluid inclusions in Kianjavato emerald, Mananjary deposits, Madagascar. **Mineralogical Magazine**, v. 70, n. 2, p. 141–158, 2006. DOI: https://doi.org/10.1180/0026461067020320

VAPNIK, Y.; SABOT, B.; MOROZ, I. Fluid inclusions in Ianapera emerald, Southern Madagascar. **International Geology Review**, v. 47, p. 647–662, 2005. DOI: https://doi.org/10.2747/0020-6814.47.6.647

VASCONCELOS, F. J. C. **Ocorrência de esmeralda em Pitombeiras, município de Paraná, Estado do Rio Grande do Norte**. Especialização em Gemologia. Belo Horizonte: Instituto de Geociências – UFMG, 1984.

VAUCHEZ, A.; NEVES, S. P.; CABY, R.; CORSINI, M.; EGYDIO-SILVA, M.; ARTHAUD, M. H.; AMARO, V. The Borborema shear zone system, NE Brazil. **Journal of South American Earth Sciences**, v. 8, p. 247-266, 1995. DOI: https://doi.org/10.1016/0895-9811(95)00012-5

VIEGAS, L. G. F.; ARCHANJO, C. J.; HOLLANDA, M. H. B. M.; VAUCHEZ, A. Microfabrics and zircon U–Pb (SHRIMP) chronology of mylonites from the Patos shear zone (Borborema Province, NE Brazil). **Precambrian Research**, v. 243, p. 1-17, 2014. DOI: https://doi.org/10.1016/j.precamres.2013.12.020

VITORINO, A. L. A.; FIGUEIREDO E SILVA, R. C.; LOBATO, L. M. Shear-zone-related gold mineralization in quartz-carbonate veins from metamafic rocks of the BIF-hosted world-class Cuiabá deposit, Rio das Velhas greenstone belt, Quadrilátero Ferrífero, Brazil: Vein classification and structural control. **Ore Geology Reviews**, v. 127, 103789, 2020. DOI: https://doi.org/10.1016/j.oregeorev.2020.103789

WALTON, L. **Exploration criteria for coloured gemstone deposits in the Yukon**. Yukon: Yukon Geological Survey, 2004.

WIEDENBECK, M. et al. Further Characterisation of the 91500 Zircon Crystal. **Geostandards and Geoananalytical Research**, v. 28, n. 1, p. 9-39, 2004.

WOOD, D. L., NASSAU, K. The characterization of beryl and emerald by visible and infrared absorption spectroscopy. **American Mineralogist**, v. 53, n. 5-6, p. 777-800, 1968.

YORK, D. Least squares fitting of a straight line with correlated errors. **Earth and Planetary Science Letters**, v. 5, p. 320–324, 1968. DOI: https://doi.org/10.1016/S0012-821X(68)80059-7

ZHOU, Y.; WANG, T.; FAN, F.; CHEN, S.; GUO, W.; XING, G.; SUN, J.; XIAO, F. Advances on Exploration Indicators of Mineral VNIR-SWIR Spectroscopy and Chemistry: A Review. **Minerals**, v. 12, n. 8, p. 958, 2022. DOI: https://doi.org/10.3390/min12080958

ZWAAN, J. C. Gemmology, geology and origin of the Sandawana emerald deposits, Zimbabwe. **Scripta Geologica**, v. 131, p. 1-211, 2006.

ZWAAN, J. C., JACOB, D. E., HAEGER, T., CAVALCANTI NETO, M. T. O., KANIS, J. Emeralds from the Fazenda Bonfim Region, Rio Grande do Norte, Brazil. **Gems & Gemology**, v. 48, n. 1, p. 2-17, 2012.

ANEXO A – COMPROVANTE DE SUBMISSÃO DO ARTIGO CIENTÍFICO II

UNIVERSIDADE FEDERAL DE PERNAMBUCO

JOSE FERREIRA DE ARAUJO NETO <ferreira.araujo2@ufpe.br>

SG-D-23-00020 - Confirming your submission to Journal of Structural Geology

1 mensagem

Journal of Structural Geology <em@editorialmanager.com> 23 de janeiro de 2023 às 19:16
Responder a: Journal of Structural Geology <support@elsevier.com>
Para: José Ferreira de Araújo Neto <ferreira.araujo2@ufpe.br>

ELSEVIER

This is an automated message.

Structural and geochronological constraints on the Portalegre shear zone: implications for emerald mineralization in the Borborema Province, Brazil

Dear Mr. Araújo Neto,

We have received the above referenced manuscript you submitted to Journal of Structural Geology. It has been assigned the following manuscript number: SG-D-23-00020.

To track the status of your manuscript, please log in as an author at https://www.editorialmanager.com/sg/, and navigate to the "Submissions Being Processed" folder.

Thank you for submitting your work to this journal.

Kind regards,
Journal of Structural Geology

More information and support

You will find information relevant for you as an author on Elsevier's Author Hub: https://www.elsevier.com/authors

FAQ: How can I reset a forgotten password?
https://service.elsevier.com/app/answers/detail/a_id/28452/supporthub/publishing/kw/editorial+manager/

For further assistance, please visit our customer service site: https://service.elsevier.com/app/home/supporthub/publishing/. Here you can search for solutions on a range of topics, find answers to frequently asked questions, and learn more about Editorial Manager via interactive tutorials. You can also talk 24/7 to our customer support team by phone and 24/7 by live chat and email.

This journal uses the Elsevier Article Transfer Service. This means that if an editor feels your manuscript is more suitable for an alternative journal, then you might be asked to consider transferring the manuscript to such a journal. The recommendation might be provided by a Journal Editor, a dedicated Scientific Managing Editor, a tool assisted recommendation, or a combination. For more details see the journal guide for authors.

#AU_SG#

To ensure this email reaches the intended recipient, please do not delete the above code

ELSEVIER

RELX™

In compliance with data protection regulations, you may request that we remove your personal registration details at any time. (Remove my information/details). Please contact the publication office if you have any questions.

← **Submissions Being Processed for Author**

Page: 1 of 1 (1 total submissions) Results per page 10

Action	Manuscript Number	Title	Initial Date Submitted	Status Date	Current Status
Action Links	SG-D-23-00020	Structural and geochronological constraints on the Portalegre shear zone: implications for emerald mineralization in the Borborema Province, Brazil	Jan 23, 2023	Jan 23, 2023	Submitted to Journal

Page: 1 of 1 (1 total submissions) Results per page 10